DRAFT

BMI-2104
Volume II

Radionuclide Release Under Specific LWR Accident Conditions

Volume II
BWR, MARK I Design

Prepared by
J. A. Gieseke, P. Cybulskis, R. S. Denning,
M. R. Kuhlman, K. W. Lee, H. Chen

Battelle Columbus Laboratories
Columbus, Ohio 43201

July 1984

DRAFT

BMI-2104
Volume II

Radionuclide Release Under Specific LWR Accident Conditions

Volume II
BWR, MARK I Design

Prepared by
J. A. Gieseke, P. Cybulskis, R. S. Denning,
M. R. Kuhlman, K. W. Lee, H. Chen

Battelle Columbus Laboratories
Columbus, Ohio 43201

July 1984

Prepared for
Office of Nuclear Regulatory Research
U.S. Nuclear Regulatory Commission
Washington, D.C. 20555

ACKNOWLEDGMENTS

Battelle's Columbus Laboratories wishes to acknowledge and express appreciation for the computer codes made available for this program by Sandia National Laboratory, Battelle's Pacific Northwest Laboratories, and the Kernforschungszentrum Karlsruhe, and for the computations and consultation provided by Sandia and the Oak Ridge National Laboratories. Further, members of the Peer Review Group have contributed significantly to this effort by providing comments, suggestions, and information on various reactor systems design.

The support of the U.S. Nuclear Regulatory Commission is gratefully acknowledged, and is the untiring leadership of the NRC staff, particularly Mel Silberberg and Mike Jankowski.

The diligent efforts of many Battelle staff members contributed to the preparation of this report. The following list identifies those staff making major contributions:

RJ Avers
GT Brooks
EP Bryant
R Freeman-Kelly
CS Jarrett
H Jordan
RG Jung
DJ Lehmicke
MB Neher
DR Rhodes
PM Schumacher
RO Wooton.

TABLE OF CONTENTS

TABLE OF CONTENTS
(Continued)

1. EXECUTIVE SUMMARY

This is Volume 2, dealing with the Peach Bottom nuclear power plant, of a seven-volume report of work done at Battelle's Columbus Laboratories to estimate the amount of radioactive material that could be released from light water reactor (LWR) power plants under specific, hypothetical accident conditions. To make these estimates, five power plants were selected that represent the major categories of LWRs: three pressurized water reactors (PWRs) and two boiling water reactors (BWRs). Specifications and data from these plants, along with data from laboratory experiments, were input to computer codes designed to describe various conditions prevailing inside an operating reactor. Ultimately, these computer codes provide an estimate of how much radioactive material would be able to escape to the environment if a specific series of events (an "accident sequence") took place.

Volume 2 of this report deals with the Peach Bottom 2 Power station, a General Electric BWR, Mark I containment design. The specific accident sequences investigated for the Peach Bottom plant were selected to represent cases of high risk, severe consequences, and most importantly, a wide range of physical conditions. The computer codes used to analyze the accident sequences were the best available, including the new MARCH 2 code. Other power plants included in the study are Surry PWR (Volumes 1 and 5); Grand Gulf BWR (Volume 3); Sequoyah PWR (Volume 4); and Zion PWR (Volume 6). The seventh volume will address technical questions raised during the peer review of this effort.

The possibility of radioactive material being released to the environment has long been the focus of considerable public concern about the safety of nuclear power plants. Since 1962, several major reports have addressed that concern by using computer codes to estimate the release of fission products (radioactive material produced during reactor operations) to the reactor containment building, and thence to the environment, during a hypothetical severe accident. Although these analyses have improved over the years, in terms of how realistically they describe what happens during a hypothetical accident, it has not previously been possible to apply the various codes consistently to follow the transport of fission products along their flow path

from the core to the environment. This limitation resulted in piecemeal, parametric estimates of release.

The research results reported here are intended to provide a systematic, sequential application of the codes as well as to present analyses performed with improved computational procedures. It is to be recognized that this report describes an analytical approach for estimating radionuclide transport and deposition which incorporates individual physical and chemical processes or mechanisms. This approach is being evaluated for use in predicting the amount fission product release (the "source term") to the environment for specific reactors and accident sequences. When verified, these prediction techniques are expected to be more specific and perhaps to supersede generic tables of release fractions provided by previous analyses.

The purpose of this report is then to:

(1) Develop updated release-from-plant fission product source terms for four types of nuclear power plants and for accident sequences giving a range of conditions. The estimated source terms are to be based on consistent step-by-step analyses using improved computational tools for predicting radionuclide release from the fuel and radionuclide transport and deposition.

(2) Determine the effects on fission product releases associated with major differences in plant design and accident sequences.

(3) Provide in-plant time- and location-dependent distributions of fission product mass for use in equipment qualification.

Approach

This study was conducted by selecting specific plants and accident sequences and then using consistent and improved analyses of fission product release from fuel and radionuclide transport and deposition to predict fission product release to the environment for these specific cases. The approach comprises a sequence of steps; in the combined analysis, the results are specific to a particular set of accident conditions, and each step is based on results from analyses of the previous step.

The Peach Bottom Plant

Peach Bottom Unit 2 was selected to characterize BWR Mark I designs. The containment of Peach Bottom 2 is typical of BWR Mark I designs: its drywell is shaped like a light bulb (with the "bulb" pointing down) and is connected to a toroidal wetwell that encircles the "bulb". As in most BWR Mark I designs, the Peach Bottom 2 drywell and wetwell are made of steel, with an internal design pressure of 56 psig (0.38 MPa).

Accident Sequences Chosen for Study

The following accident sequences were selected because they represent high-risk situations with potentially severe consequences and because they involve a considerable range in physical conditions:

AE Sequence:

- Large break Loss-of-Coolant Accident (LOCA), Failure of Emergency Core Cooling System.
- Break occurs in a recirculation line.
- Suppression pool remains subcooled throughout the accident.
- Containment is assumed to fail by overpressurization from non-condensible gases produced by steam-cladding reactions and core-concrete interactions.

TC Sequence:

- Transient, failure of control rod insertion (failure to scram).
- Emergency Core Cooling Systems operate.
- Containment failure results from the imbalance in heat generation and heat removal due to the continued high power level of the reactor.

TW Sequence:

- Transient, loss of decay heat removal

- Emergency Core Cooling Systems operate.
- Containment failure by overpressurization precedes core melting
- It is assumed that operators will depressurize the primary coolant system before core melting occurs.

Computer Codes Used in the Study

The present efforts built on previous computer modeling work performed at Battelle-Columbus, at Sandia, and in the Federal Republic of Germany, and on experimental and model evaluation studies performed at Oak Ridge, EG&G Idaho, Sandia, and Pacific Northwest Laboratories. In addition to the calculations performed at Battelle-Columbus, calculations of thermal-hydraulic behavior and fission product release related to molten core-concrete interactions were performed by Sandia. Research efforts specifically directed toward increasing our understanding of fission product release and transport under severe accident conditions are under way at the laboratories listed above, as well as at other research installations around the world. Over the next few years, it is expected that considerable progress will be made in this area. Therefore, this report must be considered as an expression of current knowledge, with the expectation of future validation or modification of the calculated fission product releases.

The first step in analyzing accident sequences was to collect plant design data and perform thermal-hydraulic calculations. Thermal-hydraulic conditions in the reactor over time were estimated with the MARCH 2 code, and detailed thermal-hydraulic conditions for the reactor's primary coolant system were estimated with the MERGE code, developed specifically for this program.

The time-dependent core temperatures from the MARCH 2 code were used as input to another code developed for this program, CORSOR, which predicts time- and temperature-dependent releases of radionuclides from the fuel inside the reactor pressure vessel. Releases of radionuclides from the interaction of the melted reactor core with the concrete outside the reactor vessel were estimated by Sandia National Laboratories using their computer code, VANESA.

Using the MARCH/MERGE-predicted thermal-hydraulic conditions and the CORSOR-predicted radionuclide release rates as input, a newly developed

version of the TRAP-MELT code was used to predict vapor and particulate transport in the primary coolant circuit. Transport and deposition of radionuclides in the containment were calculated using the NAUA-4 code. For flow through a pressure suppression pool, scrubbing of radionuclides in particulate form was calculated using the SPARC code.

The calculations performed in this study were of a "best estimate" type. Whenever possible, input was derived from experimental measurements. Data employed in these analyses include vapor deposition velocities, aerosol deposition rates, aerosol agglomeration rates, fission product release rates from fuel, particle sizes formed from vaporizing/condensing fuel materials, engineering correlations for heat and mass transfer, and physical properties of various fuel, fission product, and structural materials.

Summary of Results

The results for the release of fission products from the fuel during the period of fuel heatup and melting in-vessel and during ex-vessel attack of the concrete in the present study are generally consistent with the results of analyses previously reported in the literature. Essentially all of the volatile fission products are predicted to be released from the fuel during initial core melting in all cases. The release of tellurium was found to have some dependence on the details of the accident scenario, and its predicted total releases are somewhat lower than previous estimates.

The retention of fission product aerosols during their transport through the reactor coolant system in the present study was found to be on the order of 10-20 percent of that released from the fuel. Primary system retention of tellurium was found to be quite high, but since only a fraction of the total tellurium release occurred during the in-vessel phase of the accidents, the effect on the overall tellurium release from the plant was not great. In general, the predicted retention for Peach Bottom is not as high as for some of the PWR sequences considered in the other volumes of this study; the differences in the predicted primary system retention are associated with differences in accident thermal-hydraulics for the two types of designs. The prediction of primary system retention of the released fission products was found to be

sensitive to the details of accident thermal-hydraulics although a wide variety of modeling assumptions were not considered for this plant alone. Further, the ultimate fate of fission products deposited on primary system surfaces is quite uncertain. Follow-on analyses which include the heating of these surfaces by the decaying fission products may show significant fission product reevolution.

Fission product aerosol removal by the BWR pressure suppression pool has been found to be sensitive to the aerosol particle size distribution, the nature of the flows through the pool, and the thermodynamic state of the pool. For accident sequences such as AE, in which the suppression pool remains subcooled, quite high pool decontamination factors are predicted. Due to the timing and location of the predicted containment failure in this sequence, however, not all of the released fissin products pass through the pool, thus limiting overall decontamination and resulting in substantial releases to the environment. In sequences such as TC and TW, all of the melt releases are discharged to the suppression pool, but here the pool is boiling or saturated at the time of core melting, greatly reducing its effectiveness for fission product retention. Overall approximately one-half of the aerosol releases were predicted to have been retained in the suppression pool for the accident sequences considered here.

In the accident sequences evaluated here for the Peach Bottom reactor, the failure of the primary containment was assumed to lead to the failure or bypass of the secondary containment (reactor building). The potential effectiveness of the secondary containment and the Standby Gas Treatment System (SGTS) were explicitly considered for one of the accident sequences. The potential for retention in the reactor building and removal by the SGTS was found to be limited by outleakage from the reactor building, as the gas and vapor inputs carrying the fission products exceeded the flow capacity of the SGTS. The inclusion of the secondary containment was found to result in only a fractional reduction in the predicted fission product source term to the environment. The overall fission product releases to the environment in the present study were generally found to be somewhat lower than those reported in WASH-1400 although in some cases they were predicted to be somewhat higher. The primary system retention and removal by saturated pools included in this

study tend to reduce the predicted releases to the environment. The containment failure pressure and the location of the assumed failure used in the present study tend in some cases to significantly increase the predicted releases compared to the WASH-1400 assumptions.

In viewing the results presented in this report, it should be recognzied that uncertainties could be quite large. The prediction of fission product release to the environment has been shown to be sensitive to accident thermal-hydraulics, the mechanisms of fission product release and transport, as well as the structural behavior of the containment. It should also be recognized that prediction of the course and consequences of the low probability hypothetical situations considered here is inherently uncertain; at best, the small number of potential accident scenarios considered here can only be representative of a wide spectrum of possible outcomes in the event such accidents do take place.

2. INTRODUCTION

The possibility of radioactive material being released to the environment from LWRs has long been the impetus for considerable concern and research. Most reactors in the United States were designed, and their sites were chosen, on the basis of research report TID-14844.(2.1) Published in 1962, TID-14844 makes certain assumptions about the release of fission products (radioactive material produced during reactor operations) to the reactor containment area during a hypothetical severe accident. Although these assumptions are representative of the state of knowledge at the time, the behavior of fission products has become better understood in the intervening years. Accordingly, the Nuclear Regulatory Commission conducted the Reactor Safety Study to reassess the accident risks in U.S. commercial nuclear power plants. The report of that study, known as WASH-1400,(2.2) was published in 1975 are provided a more comprehensive and physically accurate description of fission product behavior. The amount of fission product release (the "source term") estimated in WASH-1400 has since been used extensively in planning and evaluating reactor operations.

The WASH-1400 source term to the environment for accident sequences has had broad implications for operating LWRs--in licensing, emergency planning, safety goals, and indemnification policy. However, additional research continued to provide even better methods for estimating fission product release and transport. In 1981, the Nuclear Regulatory Commission issued the report "Technical Bases for Estimating Fission Product Behavior During LWR Accidents",(2.3) a review of the state of knowledge at the time. As part of the Technical Bases report, the assumptions, analytical procedures, and available data were evaluated, and new estimates were made. One advantage of the new estimates was that they took into account the fact that some radioactive material would be deposited inside the reactor primary system during an accident and would therefore not be available to escape to the containment and from there to the environment. On the other hand, because of the limitations of the computer codes available at that time, the new estimates could not follow the transport of fission products along their flow path from the core to the environment by applying the various codes consistently. This resulted in piecemeal, parametric estimates of release.

The research results reported here are intended to provide this systematic, sequential application of the codes as well as to present analyses performed with computational procedures improved since the "Technical Bases" report. It is to be recognized that in this study, an analytical approach was developed for estimating radionuclide transport and deposition which incorporates individual physical and chemical processes or mechanisms. This approach is being evaluated for use in predicting fission product source terms for release to the environment for specific reactors and accident sequences. When verified, predictions made with the approach used here are expected to replace the generic tabular release fractions such as those in Table 6, Appendix V of WASH-1400, where release fractions are given for broad classes of accidents.

The purpose of this report is then to:

(1) Develop analytical procedures and use them to predict updated release-from-plant fission product source terms for four types of nuclear power plants and for accident sequences giving a range of conditions. The estimated source terms are to be based on consistent step-by-step analyses using improved computational tools for predicting radionuclide release from the fuel and radionuclide transport and deposition.

(2) Determine the effects on fission product releases associated with major differences in plant design and accident sequences.

(3) Provide in-plant time- and location-dependent distributions of fission product mass for use in equipment qualification.

It is not necessarily the intent of this work to produce an all-encompassing definition of source terms, but rather to make best estimates of source terms for a range of typical plants and several risk-significant sequences covering a wide range of conditions. These analyses are to be made with the best available techniques, in a consistent manner, following along release pathways for fission products, and at a level of detail consistent with current knowledge of pertinent physical processes. Based on state-of-the-art techniques, these best-estimate analyses should provide an indication of the conservatisms inherent in current source term assumptions and guidance for the development of new source terms. The analytical methods and corresponding predictions presented here are based on currently available information and are subject to revision and improvement as better analytical procedures are developed and as a more extensive experimental base evolves.

The preparation of this report, therefore, is an evolutionary process which will be carried out over a period of time, with verification and possibly revision of the procedures continuing over several years.

As a part of this evolutionary process, it should be noted that this report is to be revised using improved analytical procedures and incorporating comments and suggestions from participants at a series of NRC sponsored "Peer Review Meetings".

2.1 References

(2.1) DiNunno, J. J., et al, "Calculation of Distance Factors for Power and Test Reactors Sites", TID-14844 (March 23, 1962).

(2.2) "Reactor Safety Study--An Assessment of Accident Risks in U.S. Commercial Nuclear Power Plants", WASH-1400, NUREG-75/014 (October, 1975).

(2.3) "Technical Bases for Estimating Fission Product Behavior During LWR Accidents", NUREG-0772 (June, 1981).

3. GENERAL APPROACH

The general philosophy behind this study is that mechanistic predictions of radionuclide release and transport are possible if proper modeling is performed to represent the physical and chemical processes occurring during LWR accidents. The study, then, represents an attempt to describe in a reasonably complete but tractable fashion the processes influencing radionuclide release to the environment for selected plants and accident conditions.

The objectives of this study originally called for a consistent analysis of radionuclide behavior by following fission product transport along flow paths, starting with release into the core region and ending with final release to the environment. To meet these objectives, numerous decisions and assumptions were required for the analyses: selection of plants and sequences for consideration; choice of analytical tools to be used or upgraded; evaluation and incorporation of experimental data; and determination of major physical effects which would be considered on a parametric variation basis to determine the sensitivity of calculations to such variations. Some of the major considerations will be reviewed and discussed in this section.

The general approach in this study was to select specific plants and accident sequences for consideration and then to use consistent and improved analyses of fission product release from fuel, transport, and deposition to predict fission product release to the environment for these specific cases. The approach consists of a series of steps performed in sequence such that in the combined analysis, the results are specific to an individual set of accident conditions, and each step is based on results from analyses of the previous step.

3.1 Plant Selection

The first major step in the process was the selection of types of nuclear power plant designs to be considered and a specific plant to represent each type. The types to be considered were: large, dry PWRs; Mark I BWRs; Mark III BWRs; and ice-condenser containment PWR designs. The specific plants chosen to represent each type, respectively, are the Surry and Zion, Peach Bottom, Grand Gulf, and Sequoyah plants. These selections were made on a

combined basis of typicality of design and availability of design details needed for analysis.

3.2 Selection of Accident Sequences

Accident sequences were chosen for each plant such that significant contributions to risk and a wide range of physical conditions were represented in the analyses. The selected plants and accident sequences are listed below:

PWR: Large Dry Containment (Surry-Volumes 1 and 5)	PWR: Large Dry Containment (Zion-Volume 6)	BWR: Mark I (Peach Bottom-Volume 2)
AB	TMLB'	TC
S_2D	S_2D	AE
V		TW
TMLB'		

BWR: Mark III (Grand Gulf-Volume 3)	PWR: Ice Condenser Containment (Sequoyah-Volume 4)
TPI	S_2HF
TQUV	TMLB'
TC	TML
S_2E	

The accident sequences for each plant are described in detail in Section 4.2 of the volume of the report dealing with that plant.

3.3 Computer Codes Used in the Study

Following the selection of plants and sequences, the required plant design data were collected and thermal-hydraulic analyses performed for each accident sequence. Overall thermal-hydraulic conditions on a time-dependent basis were estimated with the MARCH code,[3.1] and detailed thermal-hydraulic conditions for the primary system were estimated with the MERGE[3.2] code developed specifically for this program.

The time-dependent core temperatures were used as input to another code developed for this program, CORSOR[3.3], which predicts time- and temperature-dependent mass releases of radionuclides from the fuel within the

pressure vessel. Releases during core-concrete interactions of radionuclides remaining with the melt were provided by Sandia National Laboratories using their newly developed model, VANESA[3.4].

Using the MARCH/MERGE-predicted thermal-hydraulic conditions and the CORSOR-predicted radionuclide release rates as input, a newly developed version of the TRAP-MELT code (TRAP-MELT 2)[3.5] was used to predict vapor and particulate transport in the primary coolant circuit.

Retention of aerosols in suppression pools was calculated using the SPARC[3.6] code and transport and deposition of radionuclides in the containment were calculated using the NAUA-4[3.7] code.

The basic stepwise procedure described above is illustrated in Figure 3.1, which shows the relationships among the computational models. The calculations were of a "best estimate" type using input derived from experimental measurements whenever possible. Types of data employed in the analyses include vapor deposition velocities, aerosol deposition rates, aerosol agglomeration rates, fission product release rates from fuel, particle sizes formed from vaporizing/condensing fuel materials, engineering correlations for heat and mass transfer, and physical properties of various fuel, fission product and structural materials.

3.3.1 Assumptions

In preparation for performing calculations of thermal-hydraulic conditions and radionuclide transport and deposition, it was necessary to make a number of assumptions or to select conditions from among several options. Major assumptions used in this study of the Peach Bottom plant are listed below in the categories of geometry, thermal hydraulics, and mechanisms.

Geometry

(1) Surfaces within the containment building available for radionuclide deposition include only the major geometrical features of the building.

(2) There is no attenuation of radionuclides as they pass through leak paths in the containment shell.

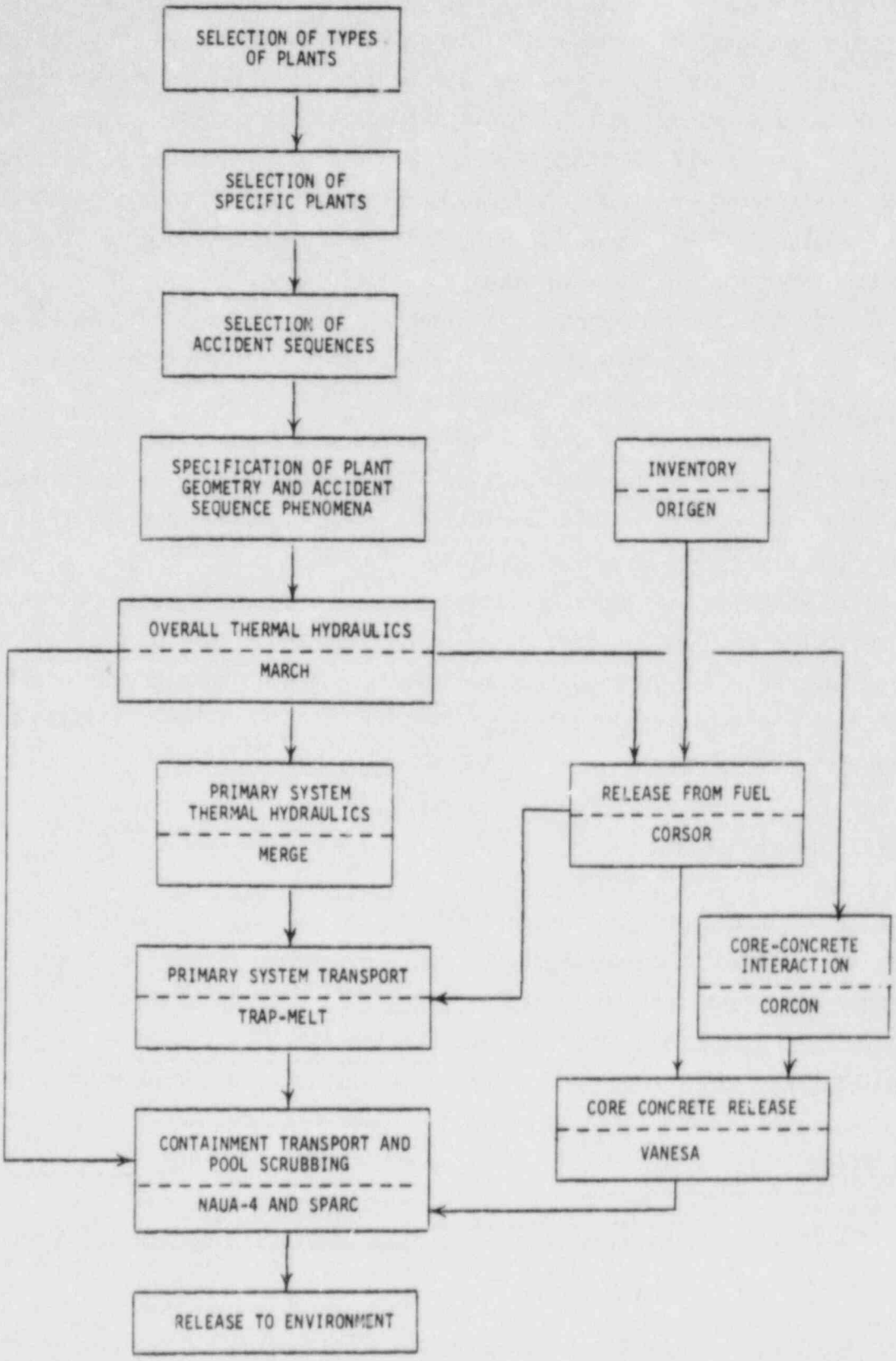

FIGURE 3.1. INFORMATION FLOW FOR RELEASE, TRANSPORT AND DEPOSITION CALCULATION

Thermal Hydraulics

(3) Before pressure vessel failure, flow from the primary coolant system is restricted to direct leak paths.

(4) The upper plenum geometry is modeled in terms of surface areas, steel thickness, and compartment heights rather than with exact geometries.

(5) Decay heating of surfaces by deposited fission products is neglected in the calculations.

Mechanisms

(7) Neither deposition nor resuspension of radionuclides occurs during rector coolant system depressurization at the time of pressure vessel melt-through.

(8) In the long term (after pressure vessel failure), deposited radionuclides remain in the primary system indefinitely.

(9) No change in fission product physical or chemical properties results from radioactive decay.

Some of the above assumptions have been relaxed or changed to accommodate best estimates of conditions and occurrences in specific cases. These are discussed in greater detail for each plant in Section 6.1 of the volume of the report dealing with that plant.

3.3.2 Uncertainty Considerations

The computation of radionuclide release and transport using mechanistic models is subject to many uncertainties of various magnitudes and importance. Quantitative estimates of uncertainties in individual parameters, and hence the overall importance of such uncertainties, has been outside the scope of this study. Where practical, however, qualitative (and in some cases quantitative) estimates of uncertainties have been noted.

Some of the uncertainties in the analyses and procedures can be identified that are currently considered significant. The following is a list of some uncertainties that are believed significant and warrant further evaluation through more detailed analyses:

(1) The simplified fuel melting model in MARCH (i.e., a single melting temperature) could bias the predicted release of material from overheated fuel, particularly regarding the source of inert and low volatility fission product aerosols.

(2) The rate coefficients for the release of fission products from overheated fuel are empirical, rather than mechanistically based, and rely largely on scaled, simulant experiments.

(3) The model for the release of fission products and inert materials during the attack of concrete has a very limited experimental basis.

(4) The flow patterns in the reactor coolant system are uncertain. The adequacy of the simple thermal-hydraulic models used in this study will require experimental verification.

(5) Primary system transport models used in these analyses have not been validated against integral experiments.

(6) The mode and timing of containment failure in severe accident sequences can have a major influence on fission product behavior but are subject to large uncertainty.

(7) The calculation methods for water condensation in the containment are based on limited, small-scale experiments and require verification at larger scales.

(8) Deposition velocities for vapor species used in the TRAP-MELT calculations were taken as a mid-points in order-of-magnitude ranges of experimental data. More accurate data would reduce the uncertainty in these parameters and in the resulting rates for deposition by sorption.

3.4 References

(3.1) Wooton, R. O. and Avci, H. I., "MARCH (Meltdown Accident Response Characteristics) Code Description and User's Manual", NUREG/CR-1711, BMI-2064 (October, 1980).

(3.2) Freeman-Kelly, R. G. and Jung, R. G., "A User's Guide for MERGE" (February 10, 1984).

(3.3) CORSOR Manual.

(3.4) VANESA Manual.

(3.5) TRAP-MELT 2.1 User's Manual.

(3.6) Owczarski, P. C., Postma, A. K., and Schreck, R. I., "Technical Bases and User's Manual for SPARC -- Suppression Pool Aerosol Removal Code", report to the U.S. NRC, NUREG/CR-3317 (May, 1983).

(3.7) Bunz, H., Koyro, M., and Schock, W., "A Code for Calculating Aerosol Behavior in LWR Core Melt Accidents Code Description and User's Manual".

4. PLANT SELECTION AND ACCIDENT SEQUENCES

4.1 General Plant Description

The Peach Bottom 2 reactor was selected here, and in the Reactor Safety Study, to characterize the boiling water reactor Mark I plant designs. The basic BWR Mark I design, referred to as an inverted light bulb and torus, is illustrated in Figure 4.1. In the Peach Bottom unit, the drywell and torus are made of steel, with an internal design pressure of 56 psig (0.38 MPa). This construction is typical of Mark I designs, although two reactors of this class are reinforced concrete with a steel liner. The reactor coolant system design is referred to as BWR/4. The thermal power is 3293 MW(t) and the net electrical output is 1065 MW(e). The free volume in the Mark I BWR containment varies substantially from the large dry PWR containment. The gas volumes in the drywell and wetwell are 159,000 ft^3 (4503 m^3) and 119,000 ft^3 (3370 m^3), respectively, in comparison with a volume of 1.8×10^6 ft^3 (50,970 m^3) in the large dry containment (Surry) previously investigated.

The primary containment structure in the Peach Bottom 2 design is enclosed by a reactor building. Leakage from the primary containment may be filtered by the Standby Gas Treatment System (SGTS) in the reactor building before being released to the environment. The response of the reactor building and Standby Gas Treatment System to severe accident conditions, particularly following failure of the primary containment, could significantly affect the consequences of accidents.

4.2 Selection Basis and General Description of Accident Sequences

Three accident sequences were selected for analyzing the Mark I design: AE, TW, and TC. (Table 4.1 relates the letters used to identify the accident sequence with the systems that failed during the accident.) The TW and TC sequences were found to dominate the predicted risk in the Reactor Safety Study.(4.1) They have also been identified as important sequences in the Accident Sequence Evaluation Program(4.2). Both sequences have similar

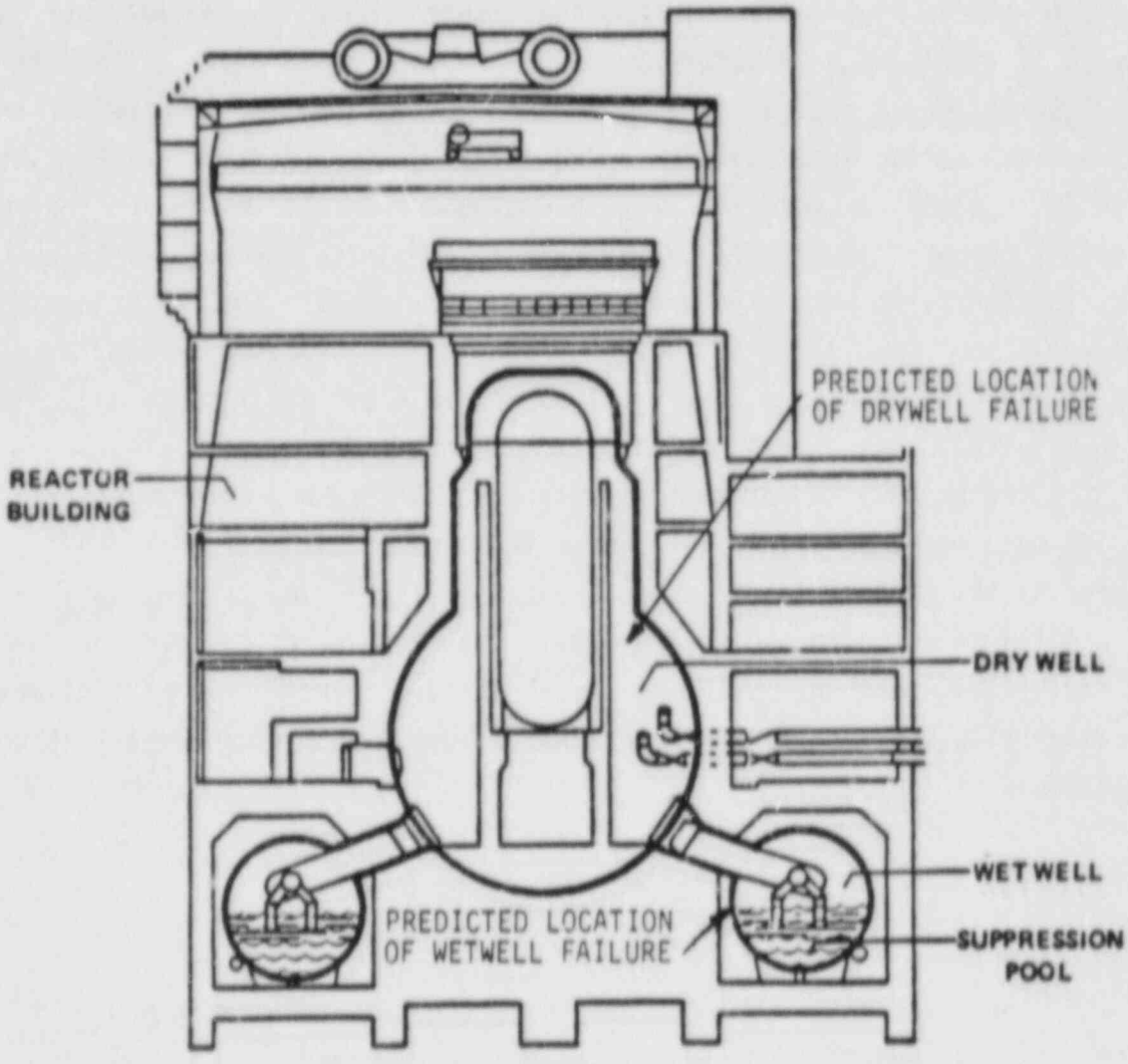

FIGURE 4.1 BWR MARK I CONTAINMENT DESIGN

TABLE 4.1. KEY TO BWR ACCIDENT SEQUENCE SYMBOLS

A - Rupture of reactor coolant boundary with an equivalent diameter of greater than six inches.

B - Failure of electric power to engineered safety features.

C - Failure of the reactor protection system.

D - Failure of vapor suppression.

E - Failure of emergency core cooling injection.

F - Failure of emergency core cooling functionability.

G - Failure of containment isolation to limit leakage to less than 100 volume percent per day.

H - Failure of core spray recirculation system.

I - Failure of low pressure recirculation system.

J - Failure of high pressure service water system.

M - Failure of safety/relief valves to open.

P - Failure of safety/relief valves to reclose after opening.

Q - Failure of normal feedwater system to provide core makeup water.

S_1 - Small pipe break with an equivalent diameter of about 2" - 6"

S_2 - Small pipe break with an equivalent diameter of about 1/2"-2".

T - Transient event.

U - Failure of high pressure coolant injection or reactor core isolation cooling system to provide core makeup water.

V - Failure of low pressure emergency core cooling system to provide core makeup water.

W - Failure to remove residual core heat.

Containment Failure Modes.

α = steam explosion in reactor vessel.

β = steam explosion in containment.

γ = containment failure due to overpressure; release through reactor building.

γ' = containment failure due to overpressure; release direct to atmosphere.

δ = containment isolation failure in drywell.

ϵ = containment isolation failure in wetwell.

ζ = containment leakage greater than 2400 volume percent per day.

η = reactor building isolation failure.

θ = Standby Gas Treatment System failure.

behavior in that containment failure precedes core damage, and the pathway for release of fission products during core heatup is through safety/relief valves to the suppression pool. To examine a broader range of accident conditions, the AE sequence, which involves a release pathway from the drywell to the suppression pool, was also selected for analysis.

In the Reactor Safety Study, analyses indicated that the most likely location of containment failure due to overpressurization would be in the torus region containing the suppression pool (see Figure 4.1). Thus, for accident sequences such as TW and TC, in which the containment is predicted to fail before the core begins to heat up, there is more question as to whether water would actually be in the pool when fission products were being released. The torus forming the suppression pool could fail, with resulting spillage of the water, and the pool water would flash after containment failure. Furthermore, part of the ceiling of the room containing the torus is near the periphery of the plant, and if that part of the ceiling failed because of loads induced by rupture of the torus, a direct release pathway would be opened to the environment. The large release fractions of volatile fission products predicted for some accident sequences in the Reactor Safety Study all involved this combination of failures: failure of the torus preceding fuel melting, bypass of the suppression pool, and failure of the reactor building to make a direct pathway to the environment.

More recent analyses of the Mark I containment indicate that the location of failure under high overpressure conditions may be the drywell rather than the wetwell.[4.3] Failure was predicted at approximately 117 psig (0.8 MPa) at the knuckle where the spherical lower region of the drywell joins the upper section (see Figure 4.1). It should be noted, however, that the criteria used to define failure in the later study were not the same as that for the WASH-1400 analyses. The potential for fission product retention in the reactor building after release from the primary containment, as well as the potential effectiveness of the SGTS, is very sensitive to the location and mode of primary containment failure. At one extreme, the reactor building could fail, rendering the SGTS ineffective; on the other extreme, a relatively small opening in the primary containment may limit gas flows into the reactor building to rates that can be completely accommodated by the SGTS.

4.2.1 Sequence AE (Loss of Coolant Accident, Failure of ECC System)

In this accident sequence, a break occurs in a recirculation line. The reactor blows down into the drywell, which relieves through vertical vents into the suppression pool. The ECC systems (sprays and flooding) are assumed not to operate. Following blowdown, residual water remains in the lower plenum of the reactor, but the core is dry. During heatup and melting, gases flow from the core, through the steam separators, down the outer annulus, out the intake of the broken loop, and out the break. This flow is driven by gas expansion and by generation of steam from thermal radiation in the core. Gas flows from the drywell through vents into the pool. The pool remains subcooled throughout the accident.

The buildup of noncondensible gases from the reaction of the cladding with steam and from molten core-concrete interaction is predicted to fail the containment by overpressurization. The predicted consequences could be sensitive to both the timing and the location of the primary containment failure. In the Reactor Safety Study, the failure was assumed to be in the wetwell, and failure was predicted to take place after reactor vessel melt-through. Thus the AE sequence in the Reactor Safety Study analyses included significant scrubbing of the melt release. However, current analyses, based on more recent but lower containment failure pressure, indicate that containment failure could take place before reactor vessel melt-through. Also, if the containment fails in the drywell, much of the melt release would not pass through the suppression pool in this sequence.

After the core melts through the lower head of the vessel and begins to attack the concrete, fission products are released to the drywell as the result of sparging of the melt by gases released from the concrete. In addition, fission products could continue to be released to the drywell from fuel remaining in the reactor vessel or from reevolution of fission products from surfaces inside the vessel. If the primary containment fails in the drywell prior to pressure vessel failure, the pathway for the release of fission products would not include the suppression pool during this phase of the accident.

Figures 4.2 and 4.3 illustrate the flow paths for release to the environment during the different phases of the accident with containment failure preceding (Figure 4.2) or following (Figure 4.3) pressure vessel melt-through. In each case, the failure in primary containment was assumed to occur in the drywell. If failure were to occur in the wetwell, the flow pathway would look like Phase 1 and Phase 2 in Figure 4.3 but would continue from the wetwell with branches to the environment and reactor building following failure of the primary containment. The cases analyzed in this report involved the pathways indicated in Figure 4.2.

4.2.2 Sequence TC (Transient, Failure to Scram)

In this transient, the control rods fail to insert and shut down the reactor, but the emergency core cooling systems function. The reactor power equilibrates at a level that is balanced by the coolant makeup rate. Heat is removed from the primary system by releasing steam to the suppression pool. Since the power level of the reactor (approximately 30 percent) exceeds the heat removal capability for cooling the pool, the temperature of the pool rises, and the pressure in the containment increases to the failure level. After the containment fails, the system depressurizes, the suppression pool boils, and the makeup pumps stop delivering coolant to the vessel. As the core heats and melts, fission products flow with the gases through the steam separators. The flow splits, with a major fraction (85 percent) going through the steam dryers and the balance (15 percent) bypassing the dryers through the outer annulus. The split flows merge at the steam line and pass through relief lines to the suppression pool. With an assumed failure in the drywell, some suppression pool water would flash at the time of primary containment failure. Unless the forces generated by depressurization resulted in structural failure in the torus, some water would be in the suppression pool during fission product release; however, this water would either be boiling or saturated. From the top of the suppression pool, gases and entrained aerosols would be transported through vacuum breakers back into the drywell before leaking through the break in containment to the reactor building or directly to the environment.

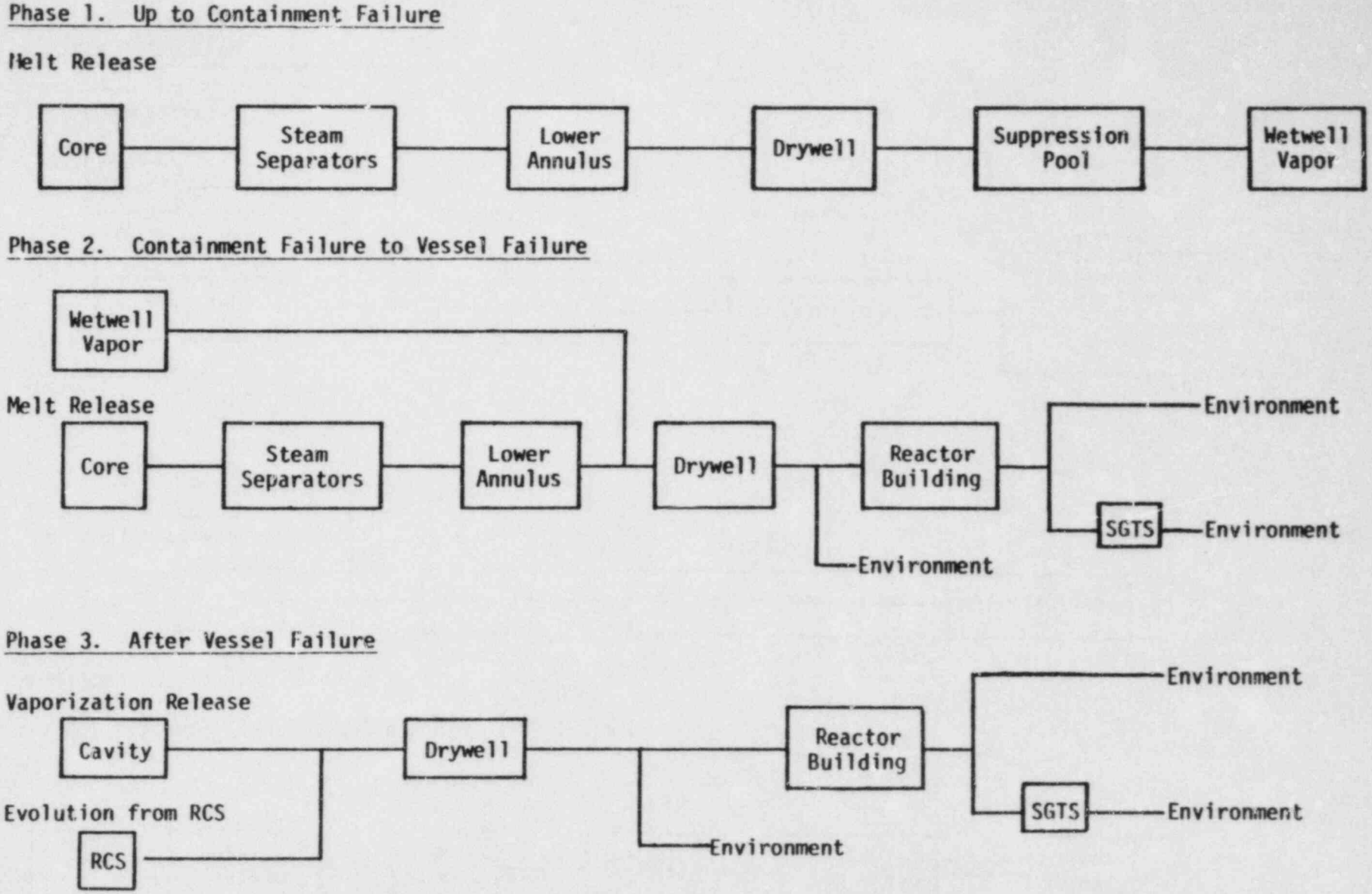

FIGURE 4.2. FLOW PATH FOR FISSION PRODUCT RELEASE IN SEQUENCE AE WHEN CONTAINMENT FAILURE PRECEDES VESSEL FAILURE

Phase 1. Up to Vessel Penetration

Melt Release

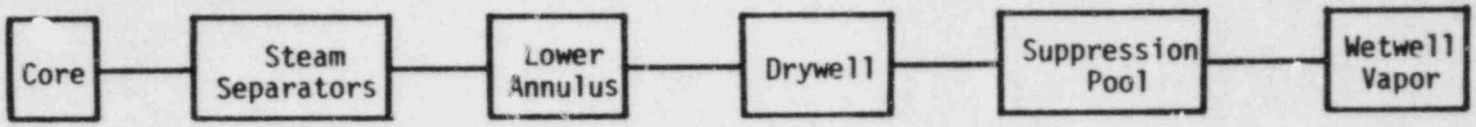

Phase 2. Vessel Penetration to Containment Failure

Vaporization Release

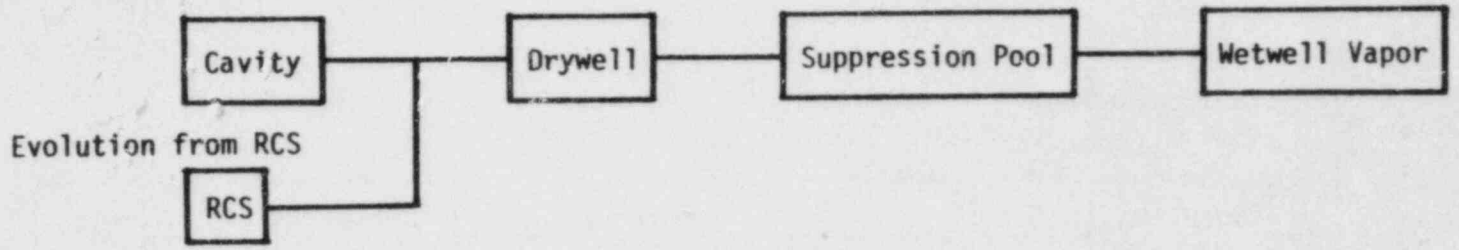

Phase 3. After Containment Failure

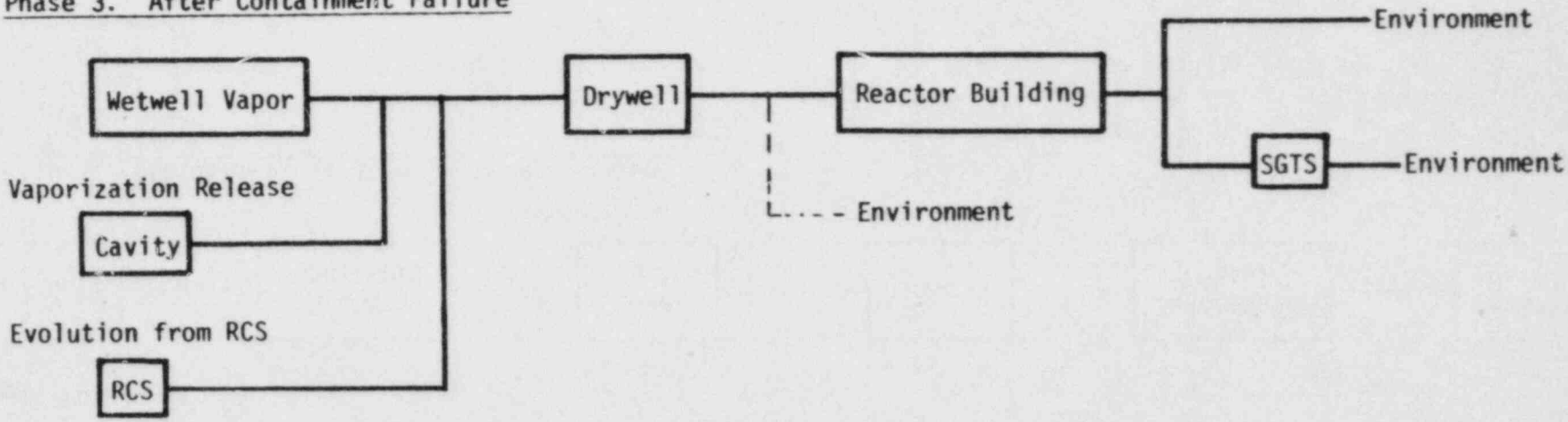

FIGURE 4.3. FLOW PATH FOR FISSION PRODUCT RELEASE IN SEQUENCE AE WHEN CONTAINMENT FAILURE FOLLOWS VESSEL PENETRATION

Following reactor vessel melt-through, the airborne fission products in the vessel flow directly to the containment. Fission products released from RCS surfaces and from attack of the concrete by the molten core also contribute to the source term to the containment and, through the break in containment, to the environment.

The flow paths for fission product transport during different phases of the accident in the TC sequence are illustrated in Figure 4.4. If the containment were to fail in the wetwell rather than the drywell, the pathway through the drywell would be bypassed during Phase 1 (up to vessel penetration) and the flow would also pass into the wetwell regions from the drywell during Phase 2 (after vessel penetration), Under these conditions, however, the pathway might not pass through a water pool.

4.2.3 Sequence TW (Transient, Loss of Decay Heat Removal)

In this sequence the reactor shuts down and the emergency core cooling systems operate, but the suppression pool heat removal system fails, so that the suppression pool overheats and the containment pressure rises. As in the TC sequence, the containment fails prior to core melting, but since the core is at decay heat power level, the time to failure is substantially longer. The flow paths to the environment are the same as described for the TC sequence. In the analysis of sequence TW, it was assumed that the operators would depressurize the reactor coolant system prior to core meltdown.

4.3 Containment Failure Mode and Reactor Building Response

In the Mark I containment design, the steel walls of the drywell and wetwell provide the high pressure leak-tight boundary that assures the containment of the pressure surge and confinement of fission products released in the design basis accidents. The reactor building that surrounds the primary containment also has some potential for the attenuation of the fission product source term to the environment in an accident. This building is not designed to withstand high internal pressures. It does, however, have a filtered exhaust

Phase 1. Up to Vessel Penetration (Containment failed prior to core melt).

Melt Release

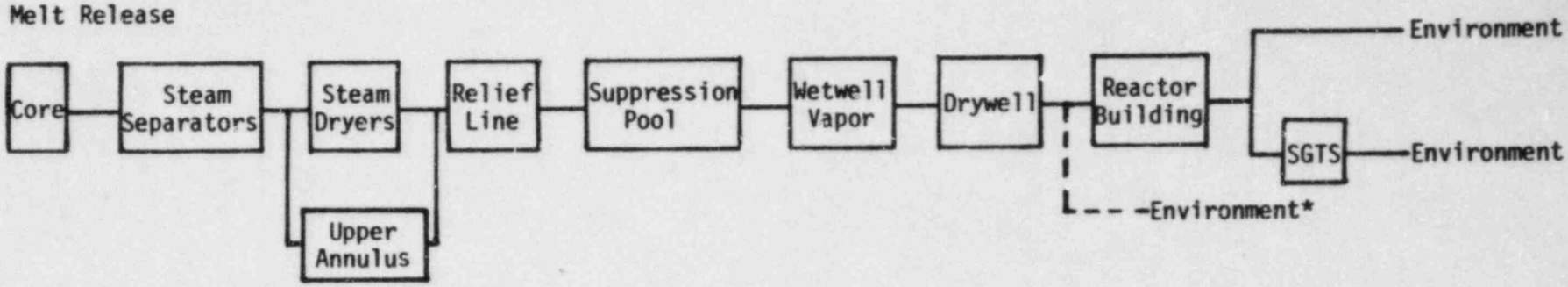

Phase 2. After Vessel penetration.

Vaporization Release and RCS Evolution

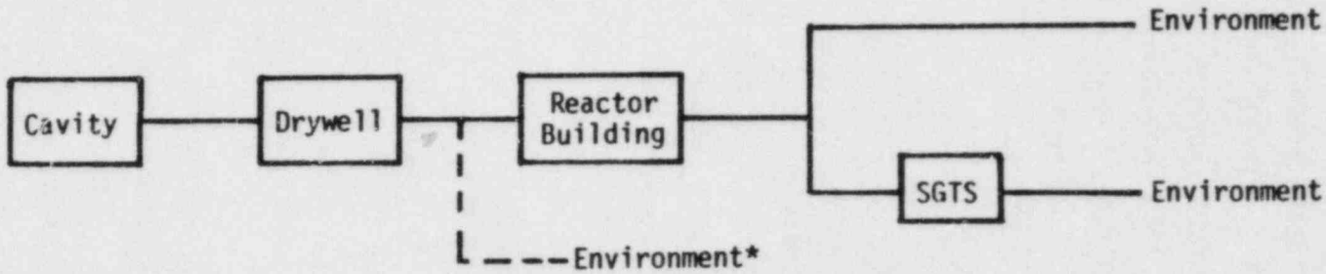

* Global failure of RB.

FIGURE 4.4. FLOW PATH FOR FISSION PRODUCT RELEASE IN SEQUENCES TC AND TW

system called the Standby Gas Treatment System which would be effective in controlling limited leakages from the primary containment. Following containment failure, the survival of the reactor building and the subsequent effectiveness of the reactor building in attenuating the source term is uncertain. If the primary containment depressurizes from high pressure (e.g., 132 psia), the resulting pressure in the lower portion of the reactor building would exceed the level at which blowout panels would fail internally and relieve to the refueling floor. If the reactor building were to remain intact following the blowdown, the Standby Gas Treatment System would be available in limiting direct outleakage through the walls of the building, leading to plateout in the building, retention in the charcoal and HEPA filters, and an elevated release. In addition, if the fire protection sprinkler system in the lower portion of the reactor building were activated by the hot steam, washout of fission products could also occur. Thus, a number of mechanisms could be effective in the reactor building, if the building is able to withstand the loads induced by primary containment failure. The expected performance of the SGTS under accident conditions is described in Appendix A.

4.3.1 Containment Failure -- Mode and Pressure Level

In the Reactor Safety Study, nonlinear elastic analyses were performed with the MONSAS code for the Peach Bottom primary containment design. The analyses indicated several potential failure locations; these included the inner diameter of the toroidal suppression chamber, the knuckle region between the cylindrical and spherical portions of the drywell, the expansion joints on the vents between the drywell and the suppression pool, and the drywell supports. Reaction forces from surrounding structures or attached equipment were not included in the analysis. Some of the design details were not available for the analyses and were estimated. Burst pressures of about 250 psig were indicated based on the development of the ultimiate strength of the material. The actual failure pressure that was adopted was 175 $\pm$ 25 psia, with the most likely location of failure being the inner diameter of the toroidal suppression

chamber. The uncertainties in the pressure at which failure was predicted and the location of failure were therefore large.

More recently, analyses were performed at Ames Laboratory for a number of steel containment designs.(4.3) In this study, the predicted failure pressure for the Browns Ferry Mark I design was 117 psig with failure predicted to occur at the intersection of the cylindrical and hemispherical segments of the drywell. The computer code ANSYS was used in the analysis. Failure was assumed to occur at two times the yield strain. If consideration is given to strength beyond yield and plastic strain, it is likely that the actual failure would be at higher pressure and might occur at a different location. The importance of the assumed failure criterion should be recognized. The failure pressure developed in the above study and that developed in the Reactor Safety Study are based on different failure criteria.

The analyses described above examined the structural failure of the wall material under high internal pressure. Other failure mechanisms must also be considered such as failure of penetration seals subjected to high temperature, failure of penetrations under pressure, blowout of hatch seals, and failure of valves. These mechanisms have only recently received attention by the NRC for conditions exceeding design levels. A number of related research programs are currently being performed at Sandia National Laboratories.(4.4)

The mode and location of containment failure can have major effects on the predicted subsequent release of fission products to the environment. In the Reactor Safety Study, it was assumed that failure of the containment in the suppression pool region would result in displacement of the pool water and that no subsequent scrubbing of fission products by the pool would occur. After release into the suppression pool room, it was assumed that fission products would either be transported through subcompartments of the reactor building, through the blowout panels and to the environment, or would be released directly to the environment, if the walls were to fail in a quadrant of the room with direct access to the outside. In WASH-1400, the failure mode of the first type was referred to as and the second type was referred to as γ'. The most severe releases predicted were all of the latter type (e.g., TC-γ' and TW-γ'). In these sequences, containment failure preceded core meltdown, no scrubbing of fission products by the remaining saturated water was assumed

to occur, and the fission products were released directly to the environment from the suppression pool room.

4.3.2 Analysis of Reactor Building Response

In order to evaluate the likelihood of different levels of performance of the reactor building following containment failure, a number of analyses were performed with the MARCH 2 code. Specifically, analyses were made to determine under what set of conditions the reactor building would:

(1) Remain intact -- where the SGTS is effective in keeping the reactor building pressure below the point at which the refueling floor blowout panels would fail.

(2) Retain long-term integrity -- in which blowout panels relieve to the refueling floor and from the refueling floor to the atmosphere, but continued operation of the SGTS results in leakage to both the refueling floor and the lower portion of the reactor building, mixing and deposition of fission products, some filtering of fission products, and an elevated release.

(3) Undergo major structural failure -- in which it would be questionable that any retention mechanisms should be considered effective.

The principal variable changed in the analyses was the hole size at the time of containment failure. For the TW and TC sequences, in which the potential for retention in the reactor building is particularly important, a minimum leak rate can be identified for the primary containment following failure which corresponds to the steam production rate. If the leak rate were smaller than this value, the pressure would rise until the leakage area increased to match this rate. For TW and TC, these areas are approximately 1/4 ft^2 and 5 ft^2, respectively. In either of these cases, the steam leakage rate into the reactor building is greater than the capacity of SGTS and, at a minimium, both sets of blowout panels would be expected to fail prior to core meltdown.

There is very little basis for the prediction of the hole size in the primary containment structure following failure. In a steel containment

structure, however, if a region of the shell is loaded to near the ultimate strength or undergoes large deformations before failure, a very large leakage area can be expected following failure. If a localized weak element exists such as failure of a hatch seal at lower pressure, the subsequent leak area would be limited.

For the purposes of examining the response of the reactor building to a large leak area following failure, the AE sequence was analyzed with a 10 ft^2 hole. In the analysis, a leakage in the lower portion of the reactor building associated with the operation of two trains of the SGTS was employed up to a pressure of 15.047 psia (50 lb/ft^2 differential) at which point the opening was increased to 300 ft^2 to correspond to failure of the blowout panels. A peak pressure of 16.0 psia (1.3 psig) was obtained at approximately 20 seconds following failure.

In the TC sequence, a peak pressure of 16.4 psia (1.7 psig) lasting a longer time was seen, since the primary containment pressure did not decrease as rapidly due to flashing of the suppression pool water. The above calculated maximum pressure is based on the use of the entire volume of the lower portion of the reactor building and does not account for pressure differentials that would exist between subcompartments. The design pressure of the lower portion of the containment is 3 psig to withstand tornado loads. Thus, if leakage from the annulus is confined to the lower portion of the reactor building and the flow areas between subcompartments are large enough, the lower portion of the containment would relieve through blowout panels to the refueling floor area, but the structure of the lower part of the building would remain intact.

Within the uncertainties associated with the mode of failure of the primary containment and the subsequent blowdown in the reactor building, we have concluded that a significant potential exists for a direct leak path into the refueling floor area of the building (e.g., by lifting the plug above the primary containment) or for exceeding the pressure capability of a subcompartment of the lower portion of the reactor building (e.g., the torus room that is in direct communication with the annulus). Either of these modes of failure could lead to a direct pathway to the environment with very limited potential for additional fission product retention. Resolution of this issue

is beyond the scope of the current effort. Both scenarios will be examined to determine the effect on accident source terms.

In sequences such as TC and TW, failure of the primary containment is followed by the release of large amounts of steam. The steam release would continue following initial containment depressurization due to the flashing of the suppression pool and continued boiloff from the primary system. If the reactor building were to survive primary containment failure, the SGTS would be subjected to this continued steam input; the ability of the SGTS to handle a large steam throughput without losing its effectiveness is not clear.

A separate consideration involved the possibility of a major hydrogen deflagration event in the reactor building following core meltdown. In the AE accident sequence, flammable mixtures of hydrogen and air are predicted to exist in the building shortly after containment failure which would produce pressures in the neighborhood of 50 psig if ignited. In the TC and TW sequences, air would be depleted in the reactor building following blowdown of the steam in the primary containment. Whether the fire protection spray system operates or not could have a major influence on the amount of air available to mix with hydrogen and the potential for steam inerting preventing deflagration.

To summarize the above discussion of reactor building response, it is to be concluded that the likelihood of severe structural damage in the reactor building as the result of blowdown loads appears to be significant, and if the building survives blowdown of the primary containment, subsequent failure as the result of hydrogen deflagration is also possible. Because of the expected importance of building integrity on source term attenuation and within the uncertainties in our current understanding of the involved phenomena, sequences in which there would be little attenuation of the source term within the reactor building appear to be credible. The quantification of this effect follows from calculations discussed in the remainder of this volume.

References

(4.1) "Reactor Safety Study: An Assessment of Accident Risks in U.S. Commercial Nuclear Power Plants", WASH-1400 (1975).

(4.2) Kolaczkowski, A. M., et al, "Interim Report on Accident Sequence Likelihood Reassessment (Accident Sequence Evaluation Program), Draft (February, 1983).

(4.3) Greimann, L. G., et al, "Reliability Analysis of Steel Containment Strength", NUREG/CR-2442 (June, 1982).

(4.4) Larkins, J. T. and Cunningham, M. A., "Nuclear Power Plant Severe Accident Research Plan", NUREG-0900 (January, 1983).

5. ANALYTICAL METHODS

This section describes the analytical methods used in assessing the source term to the environment for the Peach Bottom plant, a BWR Mark I design. The methods employed here differ significantly from those used to analyze the Surry plant, as described in Volume 1 of this report[5.1]. The Surry plant has been reevaluated using these revised methods; the results of the Surry reevaluation are reported in Volume 5[5.2].

The first major difference between the methods used here and those described in Volume 1 is that the MARCH 2 code is used here for the overall thermal-hydraulic calculations, replacing the MARCH 1.1 code used for Volume 1. MARCH 2 incorporates a number of improvements in the treatment of accident thermal-hydraulics over the earlier version of the code. The second major change is that in the present analysis, an accounting is made for the effect of Zircaloy cladding oxidation on the release rate for tellurium. Finally, a new code called SPARC is used here to predict the retention of aerosols in suppression pools.

Some other, less significant changes have been made as well. These are discussed in the text.

5.1 Thermal Hydraulic Behavior

This section describes the computer code MARCH 2, which, along with the MERGE code, was used to analyze the thermal-hydraulic response of the reactor core, the primary coolant system, and the containment system for the selected accident sequences.

5.1.1 Overall System Thermal Hydraulics: MARCH 2

The MARCH 2[5.3] (Meltdown Accident Response CHaracteristics) computer code describes the physical processes involved in severe fuel-damage accidents in light water reactors. Version 2 of the code replaces Version 1.1.[5.4] The differences between the two versions include changes in models, code structure, and programming language. The new models in MARCH 2 were developed at a

number of institutions, including Battelle, Sandia National Laboratories, Oak Ridge National Laboratories, Brookhaven National Laboratory, and the Tennessee Valley Authority. In many cases, these models are provided as options to existing models. The changes in MARCH were largely undertaken to address recognized deficiencies in the early version related to modeling approximations, time-step control, and transportability of the code to other installations.

The MARCH 2 code was developed primarily for use in probabilistic risk assessment. The uncertainties in many of the MARCH 2 models are large, and in many cases the extent to which the models have been validated against experiments is limited. More mechanistic codes are being developed by the NRC, such as SCDAP and HECTR, but they were not available for use in this program.

The MARCH 2 code examines the behavior of a large variety of accident processes including depressurization or leakage from the reactor coolant system, core uncovery, core heatup, oxidation of Zircaloy cladding, fuel melting, fuel slumping, fuel-coolant interaction in the lower vessel head, vessel head failure, fuel-coolant interaction in the reactor cavity, debris bed coolability, core-concrete interactions, production of combustible gases, gas combustion in the containment, containment heat transfer, intercompartment flows, and the effect of engineered safety features on containment thermal hydraulic behavior. Some of the principal modeling improvements in Version 2 of the MARCH code are described below.

5.1.1.1 Containment Response. The containment response modeling in MARCH 2 includes the following principal changes: provision for expanded blowdown input via subroutine INITIAL, the ability to accept two input terms from the primary system, completely revised treatment of burning of combustibles, addition of a heat sink for radiation heat transfer from the debris in the reactor cavity, and removal of a number of restrictions in the earlier code.

The expanded blowdown table input capability is intended to facilitate the interfacing of the MARCH code with more detailed thermal-hydraulic codes that may be used to describe the initial portion of the accident sequence.

The containment response subroutine, MACE, has been changed to accommodate simultaneous break and relief/safety valve flows from the primary system. The two inputs can be directed to different compartments if desired, e.g.,

break flow to the drywell and relief/safety valve flow to the suppression pool of a BWR.

5.1.1.2 Primary System Response. The MARCH 2 treatment of the primary system includes both improvements in the treatment of initial (early) primary system response and the addition of several phenomenological models to treat the processes following core collapse into the bottom head. Included are changes in the steam generator model to remove some of the restrictions and limitations of the earlier version, improved break flow models, changes in the flashing model in response to primary system pressure changes, provisions for simultaneous break and relief/safety valve flow, changes in the treatment of heat transfer to structures, and consideration of the transport of fission products within the primary system.

5.1.1.3 Water and Steam Properties. The representation of the properties of water and steam has been improved in MARCH 2. This has included expansion of the property tables and correlations incorporated in the code as well as inclusion of additional properties required by the new phenomenological models. The input parameters are based on the ASME steam tables.

5.1.1.4 Decay Heat. MARCH 2 incorporates the current American National Standard[5.5] for evaluating fission product decay heating as a function of time after shutdown and time at power, including the contributions from heavy element decay. This replaces the earlier, simplified version incorporated in MARCH 1.1. Alternatively, decay heat as a function of time may be input in tabular form; this approach would be particularly appropriate for transients with failure to scram, where the power history would be provided by more detailed system codes.

5.1.1.5 Core Heat Transfer. MARCH 2 retains the basic model of the core as developed for the earlier version, but incorporates additional models for a more detailed treatment of heat transfer processes. Heat transfer between the fuel rods and the steam-hydrogen gas mixture is now calculated using either the full Dittus-Boelter correlation[5.6] for turbulent flow or a laminar flow correlation. A subroutine has also been added to approximate axial conduction

heat transfer in the fuel rods using the Fourier law of heat conduction and the BOIL-calculated node temperatures. The effect of axial and radial thermal radiation heat transfer within the core, as well as between the core and surrounding structures and water surfaces, can now be calculated. The heatup of the core support barrel by thermal radiation is included. Additional changes include corrections in the heat transfer analysis of partially covered core nodes and improvements in the metal-water reaction model.

5.1.1.6 Core Debris. A number of phenomenological models have been added for the treatment of the core debris in the reactor vessel bottom head. These include a flat plate critical heat flux model, a fragmented debris-to-water heat transfer correlation, and several options that consider formation of debris beds within the vessel head while water is still in the vessel. The bottom head heatup model utilizes a calculated heat transfer coefficient between the molten debris and the vessel head.

A major area of concern and controversy in the analysis of core meltdown accidents has been the behavior of core and structural debris upon contact with water in the reactor cavity. The highly simplified models of MARCH 1.1 have been supplemented with a flat plate critical heat flux model, a particulate heat transfer model with more mechanistic heat transfer coefficients, and several debris bed heat transfer correlations. If desired, the switchover from one model to another can be based on calculated conditions, e.g., debris temperature. The production of hydrogen from steel-water reactions has been incorporated into these models in addition to the zirconium-water reaction previously available. Also included are the heating of the evolved gases by the debris beds and the effect of hydrogen flow on bed floodings.

A heat sink has been provided for the thermal radiation from the top of the core debris as calculated by the INTER subroutine. The decomposition of concrete due to radiated heat flux is treated by an ablation-type model with the resulting gases added to the containment atmosphere. Also, the geometry of the corium-concrete mixture is fixed following solidification of the melt.

5.1.1.7 Burning in Containment. The treatment of combustible gases now includes consideration of the burning of hydrogen and carbon monoxide if

their concentrations exceed flammability limits. Included are explicit considerations of inerting due to high steam concentrations and oxygen depletion, direction-dependent compositions for flame propagation between compartments, and burn velocities as functions of composition. Various options are available to explore the effects of assumptions about the burning of hydrogen and carbon monoxide.

5.1.2 Primary System Thermal Hydraulics: MERGE

When the MERGE[5.7] code was written, the existing computer codes describing the thermal-hydraulic behavior of a core meltdown accident were not capable of analyzing the flow and temperatures in the individual volumes of the reactor coolant system downstream of the core in the pathway for release to the containment. The report "Technical Bases for Estimating Fission Product Behavior During LWR Accidents"[5.8], published by the NRC in 1981, indicated that in at least some accident sequences, the retention of fission products in the reactor coolant system (RCS) could be significant. To support more realistic analyses of fission product retention with the TRAP-MELT code discussed in Section 5.3.1, an effort was undertaken to write a simple stand-alone code, MERGE, to predict gas temperature, surface temperature, and flow within the reactor coolant system.

MERGE calculations are based on the output of MARCH, and the output of MERGE is input to the TRAP-MELT code. The MARCH results used by MERGE are: the primary system pressure, the flow rate of hydrogen leaving the core, the flow rate of steam leaving the core, and the average temperature of gases leaving the core. The MERGE analysis accounts for conservation of energy and conservation of mass by species. It is assumed that the gases within a volume are well mixed and have the same temperature, and that the pressure differential between volumes is negligible.

In MERGE, the equations are solved with an explicit time difference scheme. At a particular time step, conditions within the first volume downstream of the core are calculated first, and the solution proceeds from each volume to the next downstream volume. Knowing the initial and inlet flow conditions for each volume, MERGE solves for the value of the outlet flow from

the volume that yields the known pressure. Heat transfer from flowing gas to structures is accounted for. Forced laminar, forced turbulent, and natural convection heat transfer coefficients are utilized as appropriate, with a radiative term added to the coefficient. In addition, the MERGE-calculated radiation heating of the first structure is calculated based on a MARCH-calculated radiative flux.

The MERGE code involves certain approximations and limitations. In the MERGE analysis, the flow of gases in the upper plenum is assumed to be one-dimensional; in reality, circulation patterns could probably be established in this region due to the strong temperature gradients. Whether a more detailed analysis is required for this region must be determined by the results of sensitivity studies with the TRAP-MELT code. The need for validation experiments must also be evaluated.

5.2 Radionuclide Release from Fuel

5.2.1 Source Within Pressure Vessel: CORSOR

CORSOR[5.9] is a simple correlative code which estimates aerosol and fission product release rates from the core during the period of core melting in a light water reactor. Quantifying the aerosol and fission product release from the core region is an important first step in determining the radionuclide source term to the containment during a hypothetical severe core damage accident. The timing of the release of various materials influences their retention in the reactor coolant system because it determines which species emanating from the core will be able to interact. The timing also determines the residence time of the released materials and the temperatures in the reactor coolant system, since these are both dynamic parameters. Simplistic source terms, such as constant or linearly increasing release rates with concurrent releases for all radionuclides, may therefore lead to unrealistic estimates of radionuclide transport behavior.

For the present analysis, the core has been divided into 240 nodes, 10 radial and 24 axial, which have distinct temperatures as predicted by MARCH. The core inventory, determined from the program ORIGEN[5.10], has been divided

equally among the nodes. In an actual reactor, the distribution would vary both axially and radially and would change with time. Typically, fuel is shifted between three radial zones during its irradiation history. To flatten the power distribution across the core, the freshest fuel is placed in the outside zone of the core and the most highly burned-up fuel is placed in the central region. Thus, an abrupt change in the spatial distribution of radionuclides occurs at the time of refueling but then continues to shift during the cycle as the fissile inventory is preferentially depleted in the regions of higher flux.

Alternative distributions of fission products can be used in the CORSOR program, and the effect on fission product release rates of the "flat-flux" assumption can be quantitatively assessed by examining the results of parametric studies such as those described in Appendix B of Volume 1[5.1]. Uncertainties in the release rate coefficients are expected to have a more significant effect on release rates than will the assumptions regarding fission product distribution among core regions.

Temperatures at each of the nodes are obtained from the MARCH code for each of a number of time steps, beginning at the start of the accident and continuing to a user-specified time. An average temperature is computed over each time span during core heatup and melting, and if the temperature is less than 900 C for any node, no release will occur from that node. The average temperature for failure of the cladding of a fuel rod is taken to be 900 C.[5.8] The sensitivity of CORSOR release estimates to the temperature set for cladding failure was also discussed in Appendix B of Volume 1.[5.1] When any axial position in a fuel bundle achieves a temperature of 900 C, CORSOR calculates a gap release of certain volatile fission products for all fuel rods in that radial zone. This is intended to simulate the gap release accompanying the bursting of individual fuel rods. This release occurs because certain fission products accumulate in the fuel-cladding gap because of migration within the fuel. The amount of the gap release is taken to be 5 percent of the initial amount present for cesium, 1.7 percent for iodine, 3 percent for the noble fission gases, 0.01 percent for tellurium and antimony, and 0.0001 percent for barium and strontium. Since this emission is very small in comparison with the melt release, and is concurrent with the melt release, it is not treated separately in any of the transport analyses. Clearly, the gap release would

require more careful analysis if less severe hypothetical accident conditions were considered.

Subsequent mass release as the nodes progress toward melting is calculated on a nodal basis as the product of the amount of each species remaining, the release rate coefficient, and the time interval of integration. The mass released is then summed over all the nodes in the core for each species to give the total mass released during the time step. It should be noted that the MARCH code predictions for core temperatures do not take into account the heat of vaporization of materials released from the core.

The computation of the fractional release rate coefficients for fission products is based on empirical correlations derived from experiments performed by Lorenz, Parker, Albrecht, and others.[5.11-5.17] The data from these experiments were graphed and curves developed for the releases. A fractional release rate coefficient, K(T), is derived for species by fitting an equation of the form

$$K(T) = Ae^{BT}$$

to each of these curves. The resulting values of A and B for three different temperature regions of the graph are basically the same as those defined in Appendix B of the "Technical Bases Report"[5.8] but have, in many cases, been adjusted to account for updated evaluations.[5.18] It should be noted that the fractional release rate is a function of temperature and elemental species only, and any effects of pressure and specific surface area of the melt on the release rate are not considered. Additionally, details of complex phase interactions of various components within the melting core are, for the most part, not known quantitatively; hence the release rates are valid only to the extent that the experiments upon which the release rates are based adequately modeled a core meltdown situation.

The release rate coefficients used in CORSOR are the same as those used in Volume I of this report, with the following exception. Tellurium release from the fuel elements appears to be strongly dependent on the extent of oxidation of the zirconium cladding. At this time the effect of zirconium oxidation on the tellurium release rate is not well quantified, nor is it known with any certainty whether this phenomenon is exhibited in the release rates of other metals' releases. In an attempt to factor into these the inhibition

of tellurium release caused by the presence of unoxidized zirconium, the following sets of release rate coefficients[5.19] were employed for calculation of the fractional release rate for tellurium according to the usual equation, $K(T) = Ae^{BT}$:

Zirconium Oxidation:	<90%		≥90%	
	A	B	A	B
T < 1600 °C	1.65 E-11	0.01061	6.50 E-10	0.01061
T ≥ 1600 °C	9.04 E-8	0.00522	3.62 E-6	0.00522

This is obviously not an ideal approach to the problem at hand, but much remains to be learned about releases from molten core materials.

Several uncertainties associated with the CORSOR predictions must be mentioned. These uncertainties most strongly impact the predicted release rates for aerosols, rather than for the more volatile materials. One difficulty in predicting aerosol release is that as core melting progresses, the temperatures increase throughout the core until, eventually, a loss of geometry would be expected to occur. In the BWR analyses, core slumping occurs in such a way as to remove radial regions from the core in an incremental fashion. Thus, the emission of fission products from the fuel rods which have fallen to the lower structures is included in the calculations of the source to the primary system. This represents a change from the PWR analysis reported in Volume 1, in which emission into the primary system was halted at the time of core slumping. A further difference between the two sets of analyses is that for the BWR sequences, significant periods of time elapse between vessel dryout and bottom head failure. Thus, during a portion of the melt period, the core is emitting fission products into an essentially stagnant volume.

The behavior of the control rods during core melting is also a source of uncertainty with respect to aerosol generation. In the sequences modeled here, the rods are fully inserted into the core, and it is assumed that these rods are at the same temperatures as the core nodes in which they reside. Thus the release of control rod materials is simulated in CORSOR by the addition of the tin and steel to the inventory of materials available for release. The burnable poison rods are not considered as a source of aerosol material though it is understood that the boron in them may play a role in aerosol formation.

5.2.2 Source from Melt-Concrete Interactions: VANESA

The release of fission products and nonradioactive aerosols during the interaction of molten core materials with concrete plays an important role in determining the risk of severe reactor accidents and is modeled with the VANESA code. Aerosol production and fission product release from core debris outside the reactor vessel can persist for many hours. The aerosols produced in this way do not usually have to traverse a convoluted pathway before they enter the reactor containment as do aerosols produced in the reactor vessel. The increased inventory of aerosols in the reactor containment brought on by ex-vessel core-debris interactions could lead to rapid agglomeration and settling of the condensed fission products released during the in-vessel phases of an accident. If containment failure is delayed, the primary source of radioactivity released to the environment would come from ex-vessel sources.

Release of fission products from core-concrete interactions can compensate for any inhibition in the release of volatile species during the in-vessel phase of an accident because gases from the thermal decomposition of concrete sparge through the melt and drive the release processes. Ex-vessel processes can also lead to the release of fission product elements that are ordinarily quite refractory. This, again, is because of the strong driving force produced by gas sparging and the unusual melt chemistry that arises during ex-vessel interactions of core debris with concrete.

Also of importance is the generation of aerosols from nonradioactive materials, such as concrete and steel, during ex-vessel interactions. The additional concentrations of suspended particulates in the containment brought on by these aerosols naturally mitigate the inventory of radioactivity released from the fuel that would then be available for release to the environment. This additional material, on the other hand, poses yet another threat to equipment in the containment whose performance is degraded by the presence of aerosols.

VANESA is a mechanistic model of fission product release and aerosol generation during core-concrete interactions. This model was based on observation from experiments involving high-temperature melts on concrete and information from analogous industrial processes. Two broad mechanisms of aerosol

formation are considered in the model:vaporization of melt species accentuated by gas sparging, and mechanical formation of aerosols by violent agitation of the molten debris sparged with decomposition gases. Vaporization processes produce the most intense aerosol generation during ex-vessel core debris interactions, while mechanical processes provide a mechanism for aerosol formation that persists even when debris temperatures are so low that little vaporization of species in the debris can occur.

Input to this model includes melt temperature, concrete erosion rate, and gas generation rate predicted by the CORCON model of melt-concrete interactions. It computes the thermochemical limits of vaporization from the melt, and then compares the extent of vaporization recognizing kinetic barriers, such as mass transport, to the approach to the thermochemical limits for vaporization. Mechanical aerosol generation is estimated by analogy to experimental data with simulant systems.

More complete descriptions of the model are provided in the users' manual[5.20] and its uncertainties are discussed further in Appendix C of Volume 1.[5.1]

5.3 Radionuclide Transport and Deposition

5.3.1 Transport in Reactor Coolant System: TRAP-MELT

The TRAP-MELT code that was used for the primary system radionuclide transport analyses of this study was developed from the published TRAP-MELT code[5.21] used for the "Technical Bases" report[5.8]. Major changes were made in the treatment of aerosol particle transport and behavior and in radionuclide condensation on and evaporation from particles. In addition, the internal data base of the code was increased to include physical property data for tellurium and cesium hydroxide. An outline of the code, highlighting these changes, is given below. A more detailed description is given in the TRAP-MELT Users' Manual[5.22].

The TRAP-MELT model is designed to treat radionuclide transport in an arbitrary flow system whose thermal-hydraulic conditions are given as functions of time. For this study, the data needed by TRAP-MELT to define the

thermal-hydraulic conditions of the primary system were generated by MERGE. In addition, TRAP-MELT requires the definition of source terms for each radionuclide; these terms were developed by CORSOR.

Once the flow system is defined, it is subdivided into a series of control volumes that can, in principle, be arbitrary in number and flow connections and that are chosen on the basis of characteristic geometry, thermal-hydraulic conditions, and suspected significant radionuclide behavior such as change of phase, agglomeration, or deposition. Radionuclides in each control volume are assigned, with uniform distribution, to one of two carriers: the wall surfaces and the gas phase. Each radionuclide is allowed to reside on these carriers in either particulate (liquid or solid) or vapor form so that by combining carrier with form in the concept of "state", the condition of a radionuclide in a given control volume is completely determined by its state. TRAP-MELT thus considers five states:

- Radionuclide vapor carried by gas
- Radionuclide particle carried by gas
- Radionuclide vapor carried on wall surface
- Radionuclide particle carried on wall surface
- Radionuclide vapor reacted with wall surface.

This list of states is not exhaustive (for instance, in two-phase flow, the carrier water must be considered) and the logic of the code has been chosen to accept an arbitrary number of states readily .

Radionuclide transport can occur among the five states of an individual control volume or between certain states of different control volumes connected by fluid flow. The former types of transport are modeled or correlated in the code itself. The latter are assumed to occur in phase with the fluid flow (as developed by codes such as MERGE) and are imposed on the system. Sources of radionuclides to the system may occur in any volume and any state, and they must be input to the code as mass rate functions of time.

At present, the intravolume transport mechanisms contained in TRAP-MELT are:

- Competitive condensation on, or evaporation from, wall surfaces and particles of cesium iodide, cesium hydroxide, and tellurium

- Irreversible reaction of molecular iodine, cesium hydroxide, and tellurium with stainless steel surfaces

- Particle deposition on surfaces due to
  - Settling
  - Diffusion from laminar and turbulent flow
  - Inertial impaction from turbulent flow
  - Thermophoresis.

Particle transport (and evaporation or condensation from or on particles) depends on particle size. TRAP-MELT takes this into account by considering a discretized particle size distribution that is subject to change, in each volume, by the deposition processes themselves, by possible particle sources, by flow of particles from other volumes, by flow of particles out of the volume in question, and by agglomeration. The last can be due to many mechanisms. TRAP-MELT considers the following agglomeration mechanisms:

- Brownian
- Gravitational
- Turbulent (shear and inertial).

Considerations of stiffness and linearity split the system of first-order differential equations resulting from the above-listed transport mechanisms into three classes. Most of the deposition mechanisms (transfer from gas to wall surface) are taken as first order in the concentration of radionuclide species on the carrier (gas, particle, or wall) from which the transfer occurs. They constitute the first class, whose transport scheme can be written in the form:

$$\frac{dC}{dt} = S + MC, \tag{5.1}$$

where C is the concentration vector of the species in question for each state and volume, S is the source rate vector for each state and volume, and M is the transport matrix between all states and volumes. Because the deposition terms are taken as first order, M is independent of C and depends, with S, on time only. It is thus possible to solve Equation (5.1) as a set of first-order differential equations with constant coefficients by standard techniques. This is done in TRAP-MELT for the class of linear mechanisms. Condensation

and evaporation, which have a much shorter time constant than the linear processes, constitute the second class and are treated outside this framework but parallel to it, as is particle agglomeration, which constitutes the third class of mechanisms in the TRAP-MELT code.

The approach to this parallel treatment is as follows: Equation (5.1) is taken as the master time-translation operation of the radionuclide system. Time steps are adjusted so that S and M change little over a time step and so that the time step does not exceed one-third of the smallest flow residence time for any control volume. The latter assures that the system does not translate excessively between couplings to the other two classes of mechanisms. In addition, the characteristic coagulation time for the aerosol in each volume is evaluated and compared to the master time step. If the former is short compared to the latter, the master time step is appropriately reduced.

At the beginning of each time step, phase transitions of radionuclides are modeled by examining each control volume in turn and solving the molecular mass transport equations for vapor transport among the gas phase, particles, and wall surfaces. Because of the low heats of vaporization of the radionuclides in question, this transport is assumed to be isothermal. Transfer to the walls assumes the Dittus-Boelter correlation[5.6] for pipe flow and transfer to the particles occurs by diffusion based on the size distribution at the beginning of the time step. Redistribution of the vapor phase occurs in a time that is small compared to the master time step; therefore, this redistribution is essentially decoupled from the other processes considered which justifies the use of a time parallel solution treatment.

Once redistribution of the vapor phase has been effected, its effect on the existing particle size distribution (in the volume in question) is calculated by assuming that each size class gains (or loses) mass in proportion to the rate of vapor transfer to (or from) that size class. Conservation of number for each size class then dictates redistribution between, in general, two new contiguous size classes, the number in each size class being determined by mass conservation.

At the end of a time step, the particle size distribution in each volume is reevaluated over that time step to account for possible particle agglomeration, sources, and flow terms. The agglomeration algorithm has been

excerpted from the QUICK aerosol behavior code[5.23], which is based on a size discretization scheme.

The approximations inherent in this parallel treatment are minimized by relegating mass redistribution and conservation to the master Equation (5.1), except for redistribution due to radionuclide phase change. Agglomeration and particle evaporation/condensation serve only to modify the particle size distribution and therefore affect particle deposition indirectly through mass-distribution-averaged deposition velocities. Thus the aerosol aspect is solved (over a master time step) completely in parallel to Equation (5.1), using all sources, flow terms, and particle removal terms evaluated for each size class considered. The resultant distribution is used to evaluate average particle deposition terms for use in the master equation only. Similarly, reevaluation of the particle size distribution due to radionuclide phase change affects these average deposition terms only.

In addition to the time-dependent thermal-hydraulic conditions and mass input rates by species, the TRAP-MELT code requires input information on the initial particle size distribution of the source, the control volume geometry, and the physical properties of species (including deposition velocities on surface materials). The code provides output in terms of time- and location-dependent mass by species and state, as well as size distribution of suspended particulate material.

There are a number of uncertainties which affect the TRAP-MELT code predictions of primary system retention of materials. Any errors or imprecisions in the input to the code will clearly affect the quality of the results, both for the primary system thermal-hydraulics provided by MERGE and for the core release rates determined by CORSOR. The extent of interaction among the materials released from the melting core is determined largely by the timing of their releases, and this represents a less straightforward, but no less important, potential effect on the code's results due to input inaccuracies.

The experimentally determined vapor deposition velocities for Te, CsOH and I_2 on hot surfaces may not represent an accurate description of the process as it occurs in the reactor coolant system (RCS) because of the imprecision in the available data and because the experimental systems may differ from the actual RCS conditions. Nevertheless, what data are available have been incorporated, since these analyses are intended to reflect the state of

the art. Additional uncertainties affecting vapor and aerosol deposition arise from possibly inadequate specifications of primary system geometry and flow patterns.

The disposition of materials suspended in the coolant system at the time of core slumping or at depressurization of the pressure vessel can have significant impact on retention calculated for some of the sequences analyzed. This is because some fission products and aerosols emitted from the core have not escaped the RCS at the time of core slumping and are still available for injection into the containment. The large burst of steam which accompanies core slumping or depressurization when the pressure vessel fails will rapidly sweep out the coolant system, and the very short transit time to the containment is expected to lead to minimal retention of these materials. Thus, in the analyses in this document, the material suspended in the RCS at the time of core slump or pressure vessel failure is assumed to be injected into the containment as a "puff" release, with no further retention in the primary system.

The analyses in the main body of this document are subject to some uncertainties which may overpredict retention in the primary system. One mechanism not included in the current analysis is the structure heatup due to decay heat from the deposited fission products. Heatup of surfaces where species of intermediate volatility (e.g., CsI and CsOH) are deposited would lead to reevolution and transport of the previously deposited materials through the reactor coolant system to regions of lower surface temperature or to the containment. Thus, the deposition of these species may be self-limiting to some extent.

5.3.2 Transport in Containment: SPARC

Many BWR accident sequences involve a fission-product flow path which passes through a suppression pool. Although the importance of the suppression pool in removing fission products has long been recognized, comprehensive analytical models that consider all pertinent parameters (such as particle size, bubble size, pool dimensions, and pressure and temperature conditions) have not been available. The SPARC code was written specifically for the

analysis reported here and was used to calculate removal of particulate matter by a suppression pool.

The SPARC code was developed by Owczarski, et al[5.24]. The model includes particulate removal due to steam condensation, gravitational settling, inertial impaction both inside the gas bubbles and in the gas injection regime, diffusion deposition, and mechanical entrainment of pool liquid at the pool surface. In addition, a mechanism which retards particle deposition due to evaporation of steam is considered. Details of the model are provided in the SPARC Users' Manual[5.24]. The bubble shape in the SPARC code is assumed as an oblate spheroid. For all calculations of pool scrubbing in this study, the ratio of minor to major axes (aspect ratio) for the bubble was taken as 1:3. The bubble diameter based on a spherical shape was taken as 0.75 cm in all cases.

Recognizing that the role of the suppression pool in removing particulates was neglected in the past, or a fixed removal efficiency or decontamination factor was arbitrarily assumed, use of the SPARC code in this program represents an improvement over previous source term analyses by accounting mechanistically for the effects of the suppression pool.

5.3.3 Transport in Containment: NAUA 4

The NAUA code was developed at the Kernforschungszentrum Karlsruhe, West Germany, for calculating aerosol behavior in LWR core melt accidents.[5.25] It is based on mechanistic modeling of aerosol agglomeration and deposition within a containment vessel where a condensing steam atmosphere may exist. The model for steam condensation on particles was validated by small-scale experimental measurements[5.26], and larger-scale validation is being planned.

The NAUA code calculates physical processes, excluding chemical changes and radioactive decay. The removal processes considered include gravitational settling and diffusional plateout. Interactive processes include Brownian and gravitational agglomeration and steam condensation. Aerosol sources and leakage are also included. Compositional changes resulting from time-dependent compositions for the input aerosol are tracked by the code.

The particle size distribution is defined by a number of monodisperse fractions. In this approach, the governing integro-differential equation is

transformed into a system of coupled first-order differential equations. In effect, the particle size fractions interact and deposit according to the included mechanisms, generating a time-dependent distribution of mass among the various size fractions. Steam condensation is handled in a separate integration. Output from the code includes mass concentrations of condensed water and dry aerosol materials (airborne and on surfaces), as well as particle size distributions at various times throughout the calculation.

Since the original version of the NAUA code has no provision for engineered safeguards, calculations were made to account for removal of aerosol particles by sprays, as follows:

$$\frac{dn}{dt} = -\varepsilon\pi R^2 N\,(V_g - v_g)n, \tag{5.2}$$

where

n is the aerosol particle concentration,

ε is the collision efficiency,

V_g and v_g are settling velocities of the spray drops and aerosol particles, respectively,

R is the radius of the spray drop, and

N is the water drop concentration.

Due to hydrodynamic interaction between a falling water drop and airborne particles, only a small fraction of the particles within the cross-sectional area of the water drop is removed by spraying. To account for this hydrodynamic effect, the collision mechanisms due to inertial impaction, interception, and Brownian diffusion of aerosol particles were used by defining ε in Equation (5.2) as:

$$\varepsilon = \varepsilon_I + \varepsilon_R + \varepsilon_D, \tag{5.3}$$

where ε_I, ε_R and ε_D are the collision efficiencies due to intertial impaction, interception, and Brownian diffusion, respectively. The following collision efficiency models were utilized for the three mechanisms:

$$\varepsilon_I = \frac{Stk^2}{(Stk + 0.35)2} \tag{5.4}$$

$$\varepsilon_R = \frac{1.5(r/R)^2}{(1+r/R)^{1/3}} \tag{5.5}$$

$$\varepsilon_D = 3.5\ Pe^{-2/3}, \tag{5.6}$$

where Stk is the Stokes number for aerosol particles based on a characteristic length of water drop with radius R; r is the particle radius; and Pe is the Peclet number. The Stokes number and the Peclet number are defined as

$$Stk = \frac{2\ r^2 \rho_p V_g C}{9\mu R} \text{ and} \tag{5.7}$$

$$Pe = \frac{2V_g R}{\bar{D}} \tag{5.8}$$

where $\bar{D}$ is the diffusion coefficient of aerosol particle
V_g is the settling velocity of water drop
C is the Cunningham slip correction factor
ρ_p is the particle density
μ is the gas viscosity.

In general, for relatively large particles, the inertial effects on the overall collision efficiency are larger than the interception term because the water drops are much larger than the aerosol particles. As particle size becomes smaller, the Brownian diffusion term will become increasingly important. It should also be mentioned that Equation (5.4) is given by Hetsroni[5.27] and Equations (5.5) and (5.6) are based on the work of Lee and Gieseke[5.28, 5.29].

Another particle deposition mechanism, diffusiophoresis, was added to the NAUA code. Diffusiophoresis results from steam condensation onto containment walls and involves two mechanisms: a net flow of gas toward the wall surface (known as Stefan flow), and a molecular weight gradient caused by the steam concentration gradient. In general, the effects of Stefan flow are much larger than those of the molecular weight gradient and result in deposition of particles on the wall surface. The condensation rate toward wall surfaces calculated by the MARCH code has been used to calculate deposition due to diffusiophoresis.

In utilizing the NAUA computer code for calculating aerosol behavior during various accident sequences, it was noted that in certain cases the code requires a long computing time to calculate the rate of condensation of water vapor onto particles. This type of problem takes place when a large amount of condensible water vapor was used as an input. It was noted that a saturation ratio of much greater than 1.0 was frequently encountered even after the condensation calculation was completed.

Some literature suggests that pure water vapor at 20 C will spontaneously form water droplets in the absence of condensation nuclei when the saturation ratio exceeds 3.5, and at 0 C a saturation ratio of 4.3 is required for homogeneous nucleation. This mechanism has been implemented in NAUA in addition to the existing condensation calculation. As the critical supersaturation for the homogeneous nucleation, the following correlation equation given by Green and Lane[5.30] was used:

$$S = \exp(0.557 \cdot (\sigma/T)^{3/2} \cdot M),$$

where

S is the critical supersaturation
σ is surface tension
T is the temperature in °K
M is the molecular weight of water.

No nucleation or self-condensation rates are calculated in the code. Rather, if critical supersaturation is realized at a given time, the excess water vapor is assumed to form water particles of a uniform size spontaneously. Of course, these small pure water droplets are subsequently subject to NAUA's usual condensation and coagulation processes both among themselves and with other particles containing solids. Although the effects of this mechanism on the overall aerosol concentration change are insignificant, the computational time is reduced considerably by this implementation.

References

(5.1) Gieseke, J. A., et al, "Radionuclide Release Under Specific LWR Accident Conditions, Volume 1", BMI-2104 (July, 1983).

(5.2) Gieseke, J. A., et al, "Radionuclide Release Under Specific LWR Accident Conditions, Volume 5", BMI-2104 (July, 1984).

(5.3) Wooton, R. O., et al, "MARCH 2 Code Description and Users' Manual", Draft (December, 1982).

(5.4) Wooton, R. O. and Avci, H. I., "MARCH (Meltdown Accident Response Characteristics) Code Description and Users' Manual", NUREG/CR-1711, BMI-2064 (October, 1980).

(5.5) "American National Standard for Decay Heat Power in Light Water Reactors", ANSI/ANS-5.1-1979.

(5.6) Geankoplis, C. J., "Mass Transport Phenomena", Holt, Rinehart, and Winston (1972).

(5.7) Freeman-Kelly, R., "A Users' Guide for MERGE", Battelle's Columbus Laboratories, October, 1982.

(5.8) "Technical Basis for Estimating Fission Product Behavior During LWR Accidents", NUREG-0772 (June, 1981).

(5.9) CORSOR Manual.

(5.10) Bell, M. J., "ORIGEN, The ORNL Isotope Generation and Depletion Code", ORNL-4628 (1973).

(5.11) Lorenz, R. A., et al, "Fission Product Release from Highly Irradiated LWR Fuel", NUREG/CR-0722 (1980).

(5.12) Lorenz, R. A., Collins, J. L., and Malinauskas, A. P., "Fission Product Source Terms for the LWR Loss-of-Coolant Accident", NUREG/CR-1288 (1980).

(5.13) Lorenz, R. A., et al, "Fission Product Release from Highly Irradiated LWR Fuel Heated to 1300-1600 C in Steam", NUREG/CR-1386 (1980).

(5.14) Lorenz, R. A., "Fission Product Release from BWR Fuel Under LOCA Conditions", NUREG/CR-1773 (1981).

(5.15) Parker, G. W., Martin, W. J., and Creek, G. E., "Effect of Time and Gas Velocity of Distribution of Fission Products from UO_2 Melted in a Tungsten Crucible in Helium", Nuclear Safety Program Semi-Annual Report for period ending June 30, 1963, ORNL-3483, 19-20 (1967).

(5.16) Albrecht, H., Matschoss, V., and Wild, H., "Experimental Investigation of Fission and Activation Product Release from LWR Fuel Rods at Temperatures Ranging from 1500-2800 C", proceedings of the Specialists' Meeting on the Behavior of Defected Zirconium Alloy Clad Ceramic Fuel in Water Cooled Reactors, 141-146 (September, 1979).

(5.17) Albrecht, H., Matschoss, V., and Wild, H., "Release of Fission and Activation Products During Light Water Reactor Core Meltdown", Nuclear Technology, 46, 559-565 (1979).

(5.18) Niemczyk, S. J. and McDowell-Boyer, L. M., "Technical Considerations Related to Interim Source Term Assumptions for Emergency Planning and Equipment Qualification", ORNL/TM-8275 (1982).

(5.19) Lorenz, R. A., Beahm, E. C., and Wichner, R. P., "Review of Tellurium Release Rates from LWR Fuel Elements and Aerosol Formation from Silver Control Rod Materials", ORNL, letter report, February 28, 1983.

(5.20) VANESA Manual.

(5.21) Jordan, H., Gieseke, J. A., and Baybutt, P., "TRAP-MELT Users' Manual", NUREG/CR-0632, BMI-2017 (February, 1979).

(5.22) TRAP-MELT 2.1 User's Manual.

(5.23) Jordan, H., Schumacher, P. M., and Gieseke, J. A., "QUICK Users' Manual", NUREG/CR-2105, BMI-2082 (April, 1981).

(5.24) Owczarski, P. C., Postma, A. K., and Schreck, R. I., "Technical Bases and Users' Manual for SPARC -- Suppression Pool Aerosol Removal Code", report to the U.S. NRC, NUREG/CR-3317 (May, 1983).

(5.25) Bunz, H., Koyro, M., and Schock, W., "A Code for Calculating Aerosol Behavior in LWR Core Melt Accidents Code Description and Users' Manual".

(5.26) Schock, W., Bunz, H., and Koyro, M., "Messungen der Wasserdampfkondensation an Aerosolen unter LWR-un-falltypischen Bedingungen", KfK 3153 (August, 1981).

(5.27) Hetsroni, G., "Handbook of Multiphase Systems", McGraw Hill Book Company and Hemisphere Pub. Co. (1982).

(5.28) Lee, K. W. and Gieseke, J. A., J. Aerosol Science, 11, 335 (1980).

(5.29) Lee, K. W. and Gieseke, J. A., Environ. Sci. & Technol., 13, 446 (1979).

(5.30) Green, H. L. and Lane, W. R., Particulate Clouds: Dust, Smokes and Mists, D. Van Nostrand Co., Princeton, New Jersey (1957).

6. BASES FOR TRANSPORT CALCULATIONS

6.1 Plant Geometry and Thermal Hydraulic Conditions

The MARCH 2 code* was operated for each of the three accident sequences analyzed. The results of the MARCH analyses are used as inputs for the fission product release and transport calculations. A summary of important reactor characteristics, containment parameters, and MARCH options is presented in Table 6.1.** The values of parameters used to describe the reactor coolant system such as the masses, surface areas, volumes, etc., were primarily obtained through information provided by the General Electric Company and are not reproduced here due to their proprietary nature.

In the following sections of the report, the results obtained with the MARCH and MERCE codes are described for each of the accident sequences.

6.1.1 Sequence AE

A large break in the piping of the recirculation loop with failure of the standby core cooling system would result in loss of reactor coolant and uncovery of the core. Since core uncovery occurs early in the accident, the decay heat level is high and a rapid core meltdown would be expected. Table 6.2 indicates the times of key events as predicted by the MARCH 2 code. Table 6.3 presents details of the core and primary system response at key times during the sequence. Core uncovery, heatup, and melting occur at low primary system pressure. The temperatures of selected fuel regions are illustrated as a function of time in Figure 6.1.

In the MARCH analyses for the Peach Bottom accident sequences, fuel slumping (movement of molten fuel from the core region to the support structures) was assumed to take place when the lowest mode in a core region was fully molten. As can be seen from the event times in Table 6.2, initial slumping of the highest power (hottest) regions in the core was predicted

---

* A description of this version of MARCH can be found in 5.1.1.

** All tables in this section of the report have been placed at the end of the section.

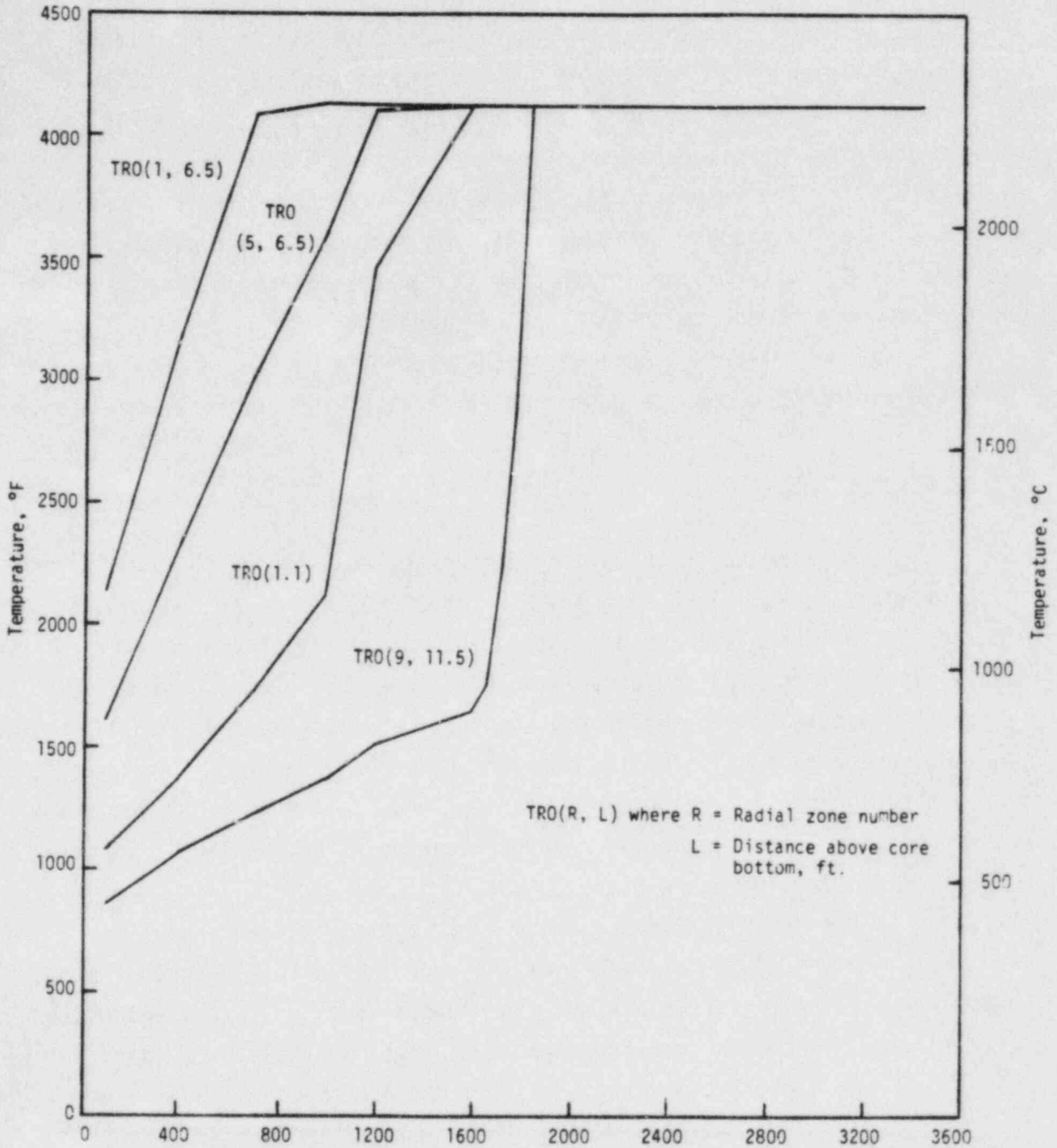

FIGURE 6.1 TEMPERATURES OF SELECTED FUEL REGIONS AS A FUNCTION OF TIME -- PEACH BOTTOM AE SEQUENCE

relatively early in the sequence. Collapse of the entire core into the bottom head was assumed when 75 percent of the core was molten or when the structures supporting the core reached their melting temperature. The support structures would be heated by the core debris that have fallen out of the core region. Since the outer portions of the core operate at lower power levels than the central region, they experience slower heatup and thus require a longer time to reach melting. The molten fuel that falls into the vessel head will evaporate the residual water there and will be partially quenched. In the AE sequence, the primary system and containment are at the same pressure, thus there is no stress on the bottom head other than the weight of the core debris; vessel failure in this case takes place by melt-through of the bottom head. Under the conditions assumed, melt-through of the vessel head is predicted about an hour after the collapse of the core into the bottom of the vessel.

The prediction of the onset and progression of core slumping with the model described above can be sensitive to core power distribution, core nodalization, and assumptions regarding metal-water reactions after the onset of melting. The core power distribution used in the Peach Bottom analyses was more peaked than would be typical of a core with high burnup.

Prior to the accident, the piping and structures in the reactor coolant system would be in the temperature range of 290 to 300 C. Heatup of the fuel and the release of fission products occur at approximately 210 kPa (30 psia). Thus, at the time of fission product release the structures are expected to be heated above steam saturation temperature. The flow path for fission product release within the reactor coolant system is illustrated in Figure 6.2. Figure 6.3 is a schematic of the breakdown of control volumes used in the MERGE analysis. Predicted gas and structure temperatures for each volume are illustrated in Figures 6.4 and 6.5, respectively. It should be noted that time zero in Figures 6.4 and 6.5 is the start of core melting or 11.5 minutes into the accident. The decrease in temperatures occurring at the later stages of the accident results from cooling by the large amount of steam generated as the core is predicted to slump into the lower head of the vessel.

The flow path from the vessel to the suppression pool is illustrated in Figure 6.6 for the time period prior to containment failure. Figures 6.7 and 6.8 describe the temperature and pressure in the drywell and wetwell vapor space throughout the accident. Key event times for each of the sequences are

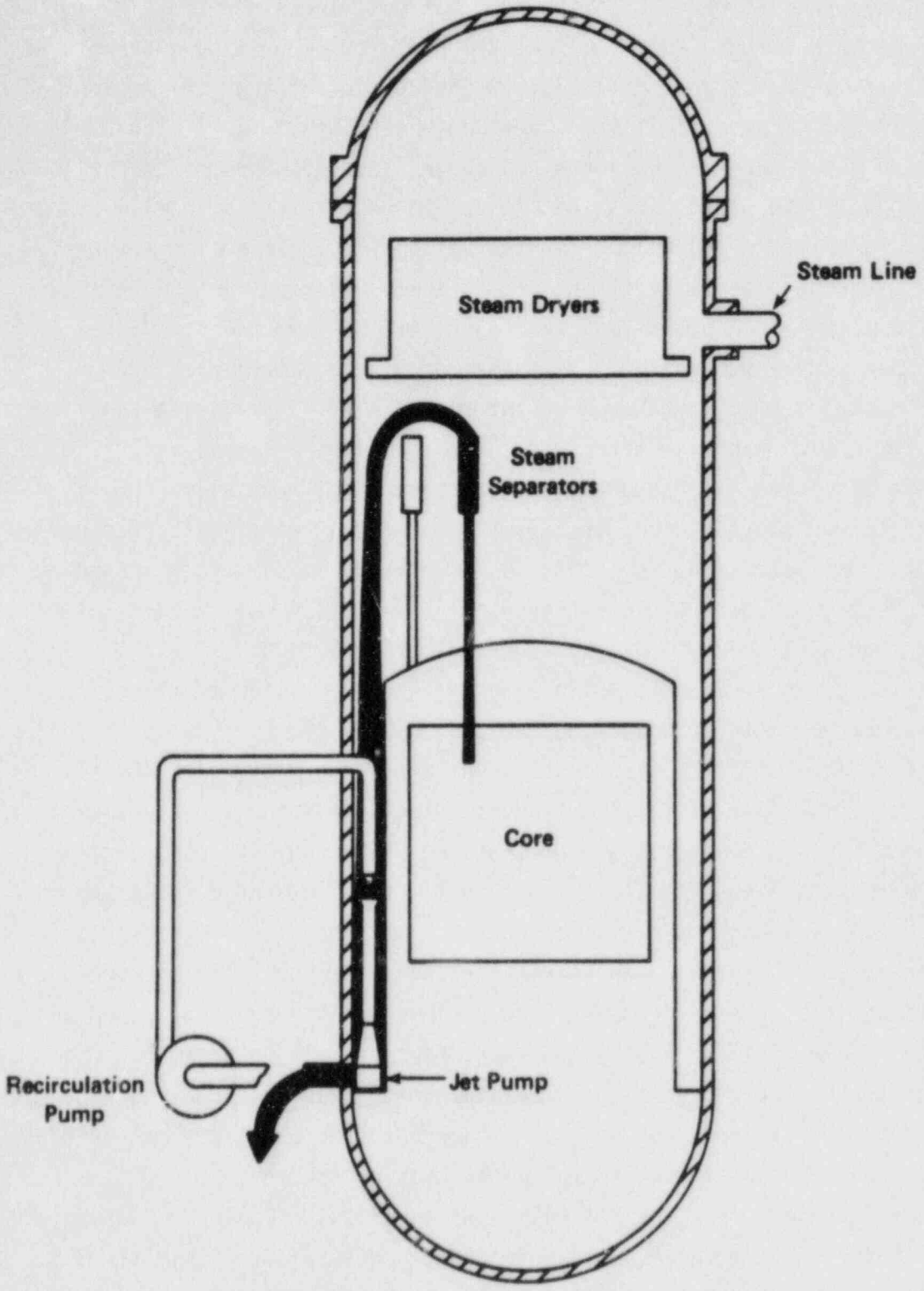

FIGURE 6.2 FLOWPATH FOR FISSION PRODUCT TRANSPORT IN THE RCS - SEQUENCE AE

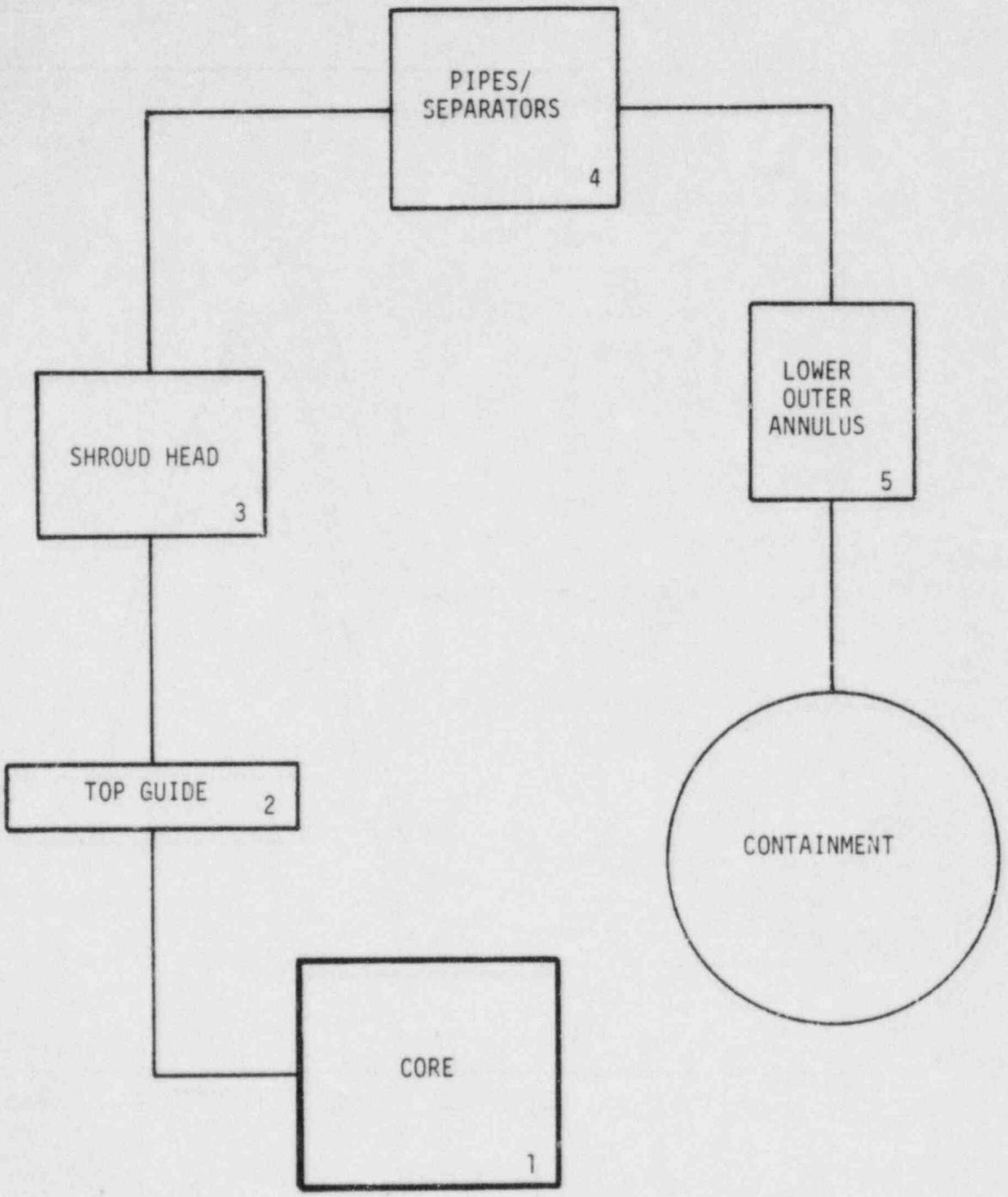

FIGURE 6.3 SCHEMATIC OF CONTROL VOLUMES FOR THE PEACH BOTTOM AE SEQUENCE

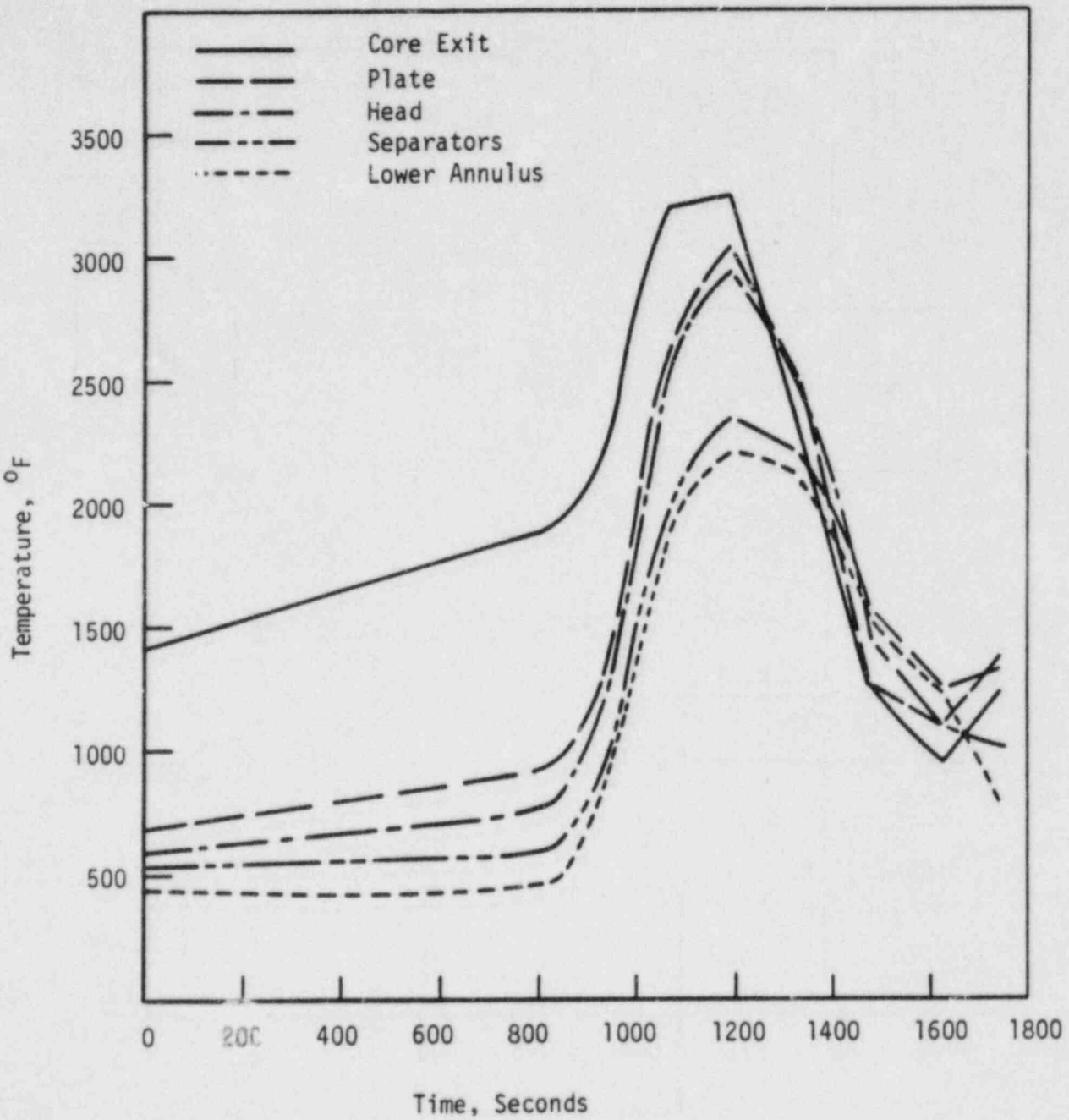

FIGURE 6.4 GAS TEMPERATURES IN RCS VOLUMES - SEQUENCE AE

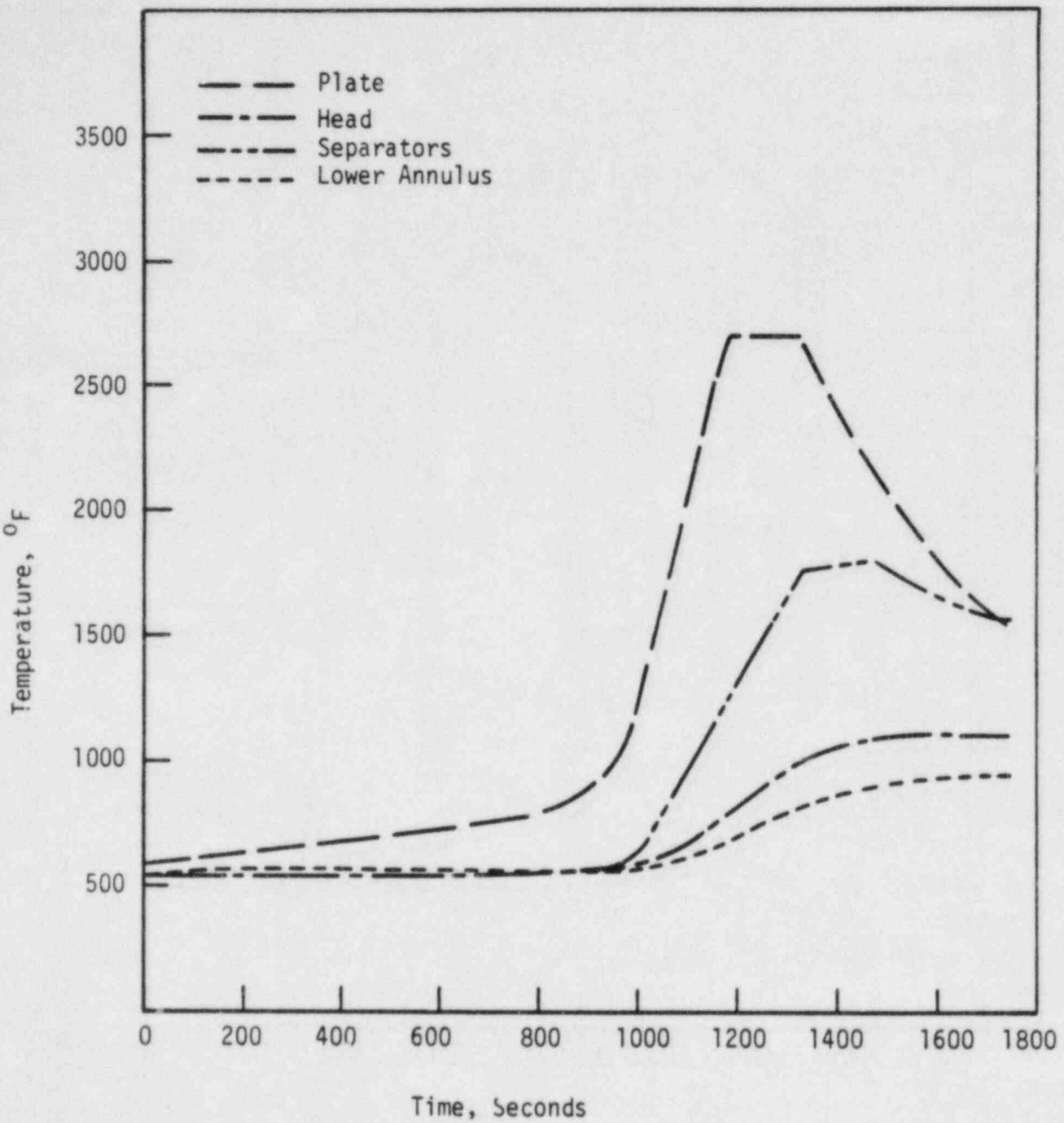

FIGURE 6.5 STRUCTURE TEMPERATURES IN RCS VOLUMES - SEQUENCE AE

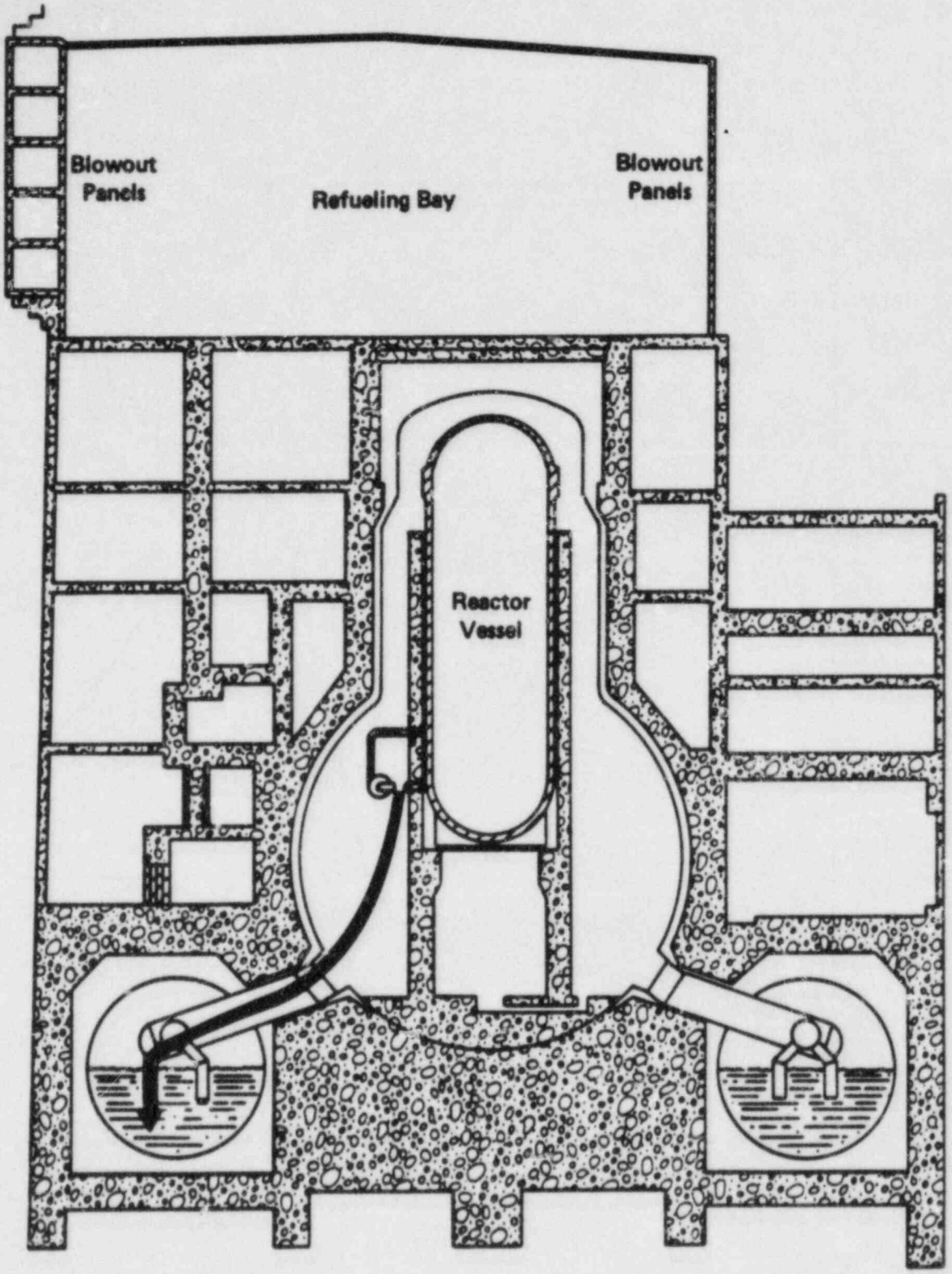

FIGURE 6.6 FLOWPATH FOR FISSION PRODUCT TRANSPORT BEFORE CONTAINMENT FAILURE - SEQUENCE AE

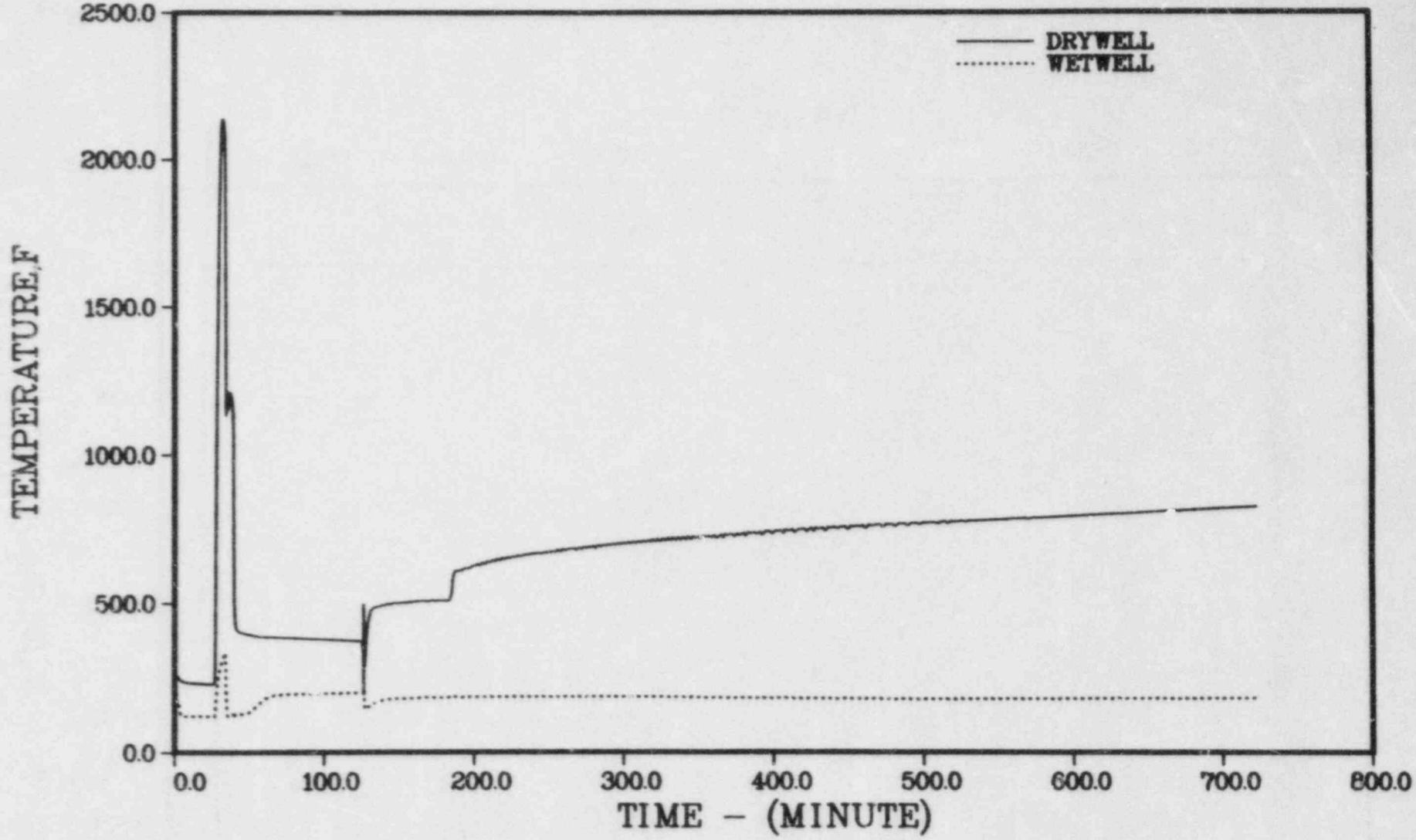

FIGURE 6.7 TEMPERATURES IN CONTAINMENT VOLUMES - SEQUENCE AE

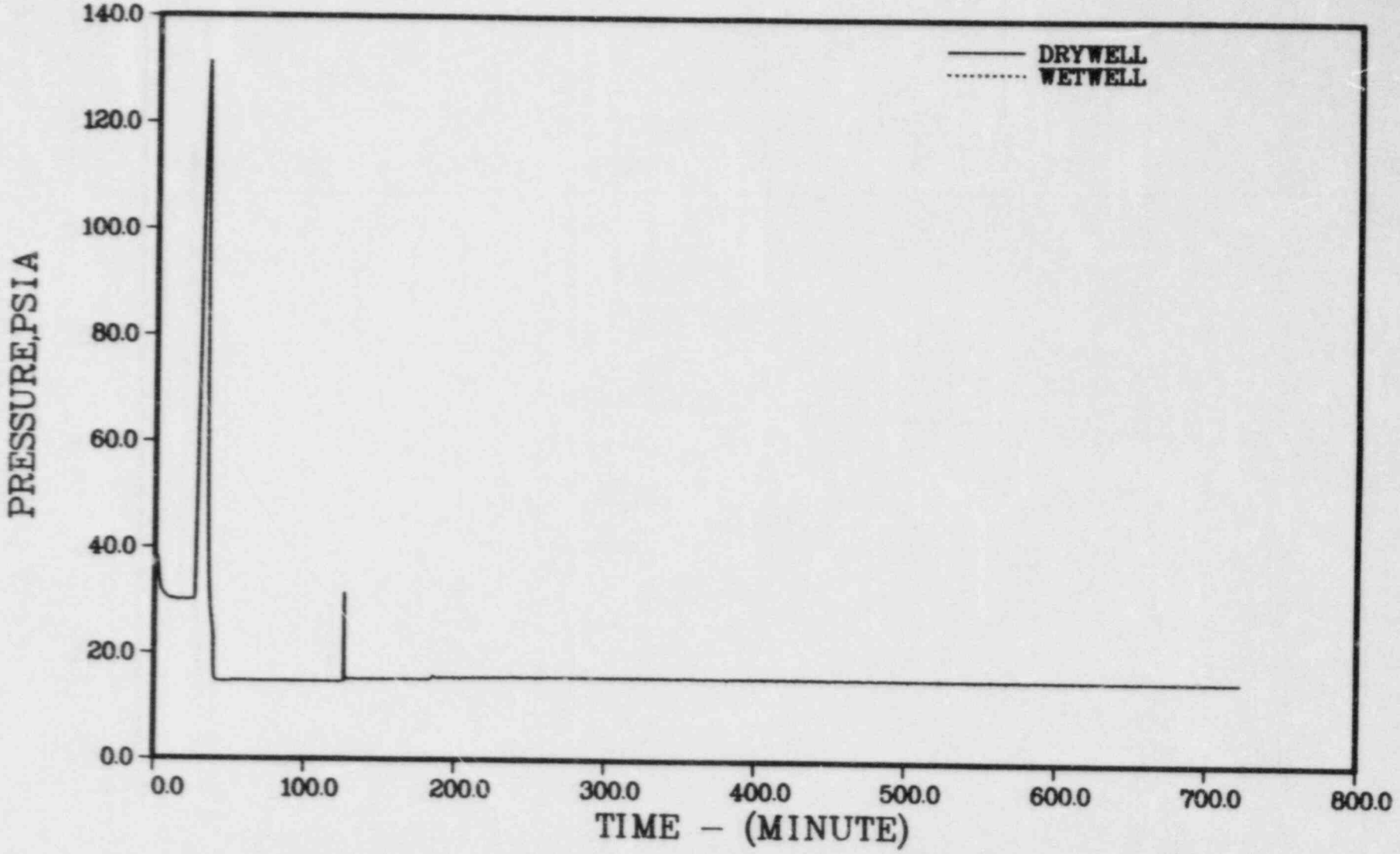

FIGURE 6.8 PRESSURES IN CONTAINMENT VOLUMES - SEQUENCE AE

provided in Table 6.2. Table 6.4 gives details of the containment conditions at key times during the sequence. Prior to containment failure the flow passes from the drywell into the suppression pool after leaving the vessel. Temperatures in the drywell are nominal and in the wetwell are cool because of the cold suppression pool.

After the start of core slumping, the pressure in the containment volumes rises rapidly due to the production of hydrogen and the transport of the noncondensibles into the wetwell. At 132 psia, a leak area of 7 ft^2 is assumed to open in the drywell. The prediction of the occurrence of containment failure at this point in the accident sequence is sensitive to the failure pressure as well as the core slumping scenario assumed. Figure 6.9 illustrates the subsequent flow paths for the fission products. Fission products airborne in the vapor space of the wetwell would flow back through the vacuum breaker into the drywell and then out the break into the annulus surrounding the steel shell of the containment. As discussed in Section 4.3, the fission products may then follow a number of possible pathways depending on the response of the reactor building to failure of the primary containment shell. Fission products released to the drywell after containment failure would flow out the break in the primary containment shell without passing through the suppression pool. The predicted consequences of this accident sequence will therefore be very sensitive to the estimated time of containment failure. After vessel failure, the vaporization release of fission products will be to the drywell. Again, the flow path does not include the suppression pool. The temperatures in the drywell atmosphere are predicted to become very hot in this phase. The question of the overheating and failure of penetrations is not a significant issue, however, because the integrity of the primary containment has already been breached.

Table 6.5 summarizes the leak rates derived from the MARCH analyses that were used in the analysis of fission product release to the environment.

6.1.2 Sequence TC

In the transient sequence TC, the reactor power level equilibrates with the primary coolant makeup provided by the emergency core cooling system. A nominal power level of 30 percent of full power was assumed, but the actual

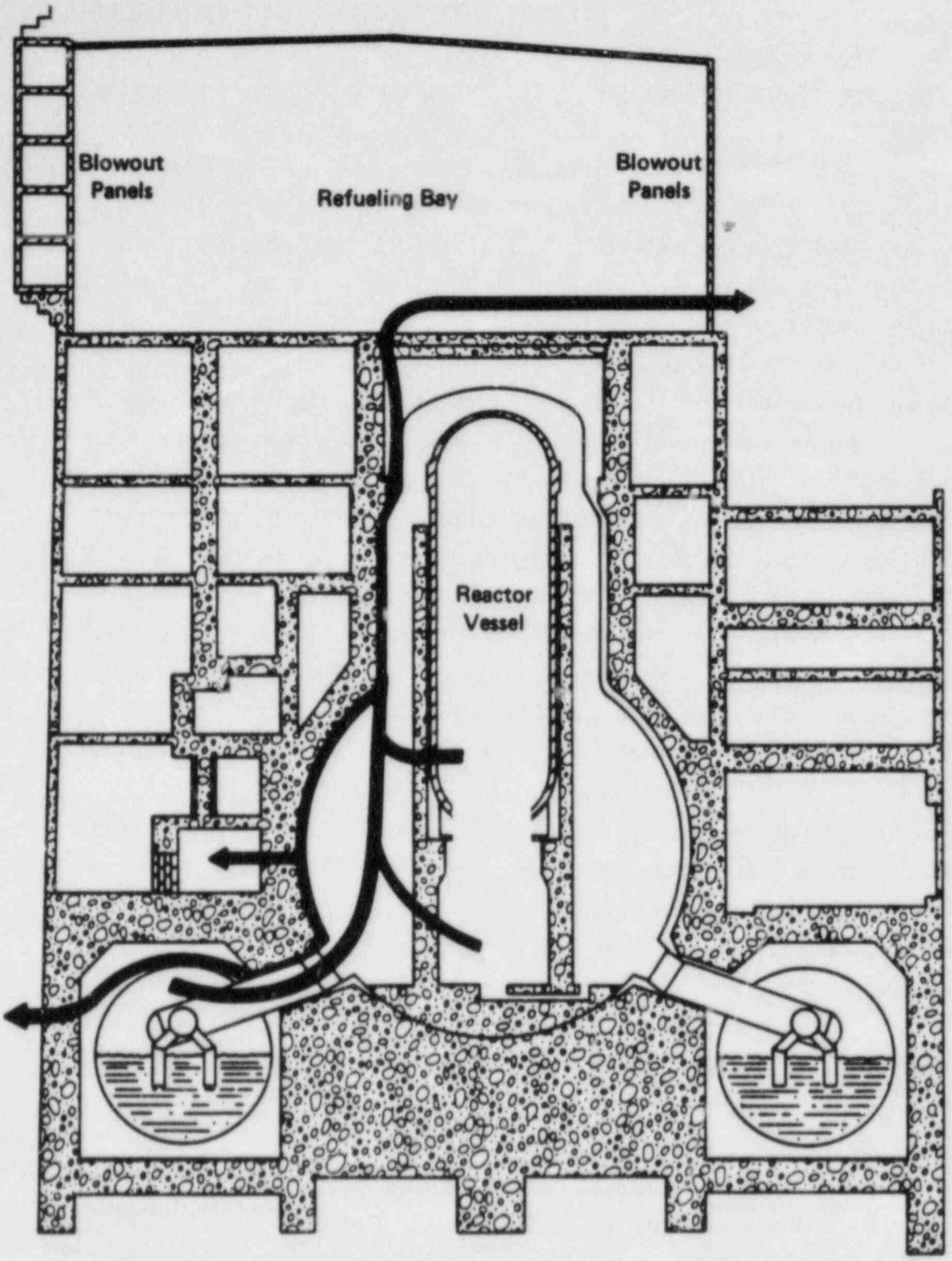

FIGURE 6.9 FLOWPATHS FOR FISSION PRODUCT TRANSPORT AFTER CONTAINMENT FAILURE - SEQUENCE AE

power level in the analyses would vary with the water level in the reactor vessel. Heat was removed from the primary system via steam flow through the safety/relief valves into the suppression pool. Since the core power level is considerably above the capacity of the residual heat removal system, the temperature of the pool rises and the pressure in the containment increases to the failure point. At the time of predicted containment failure, the emergency core cooling system is drawing water from the condensate storage tank. For the purpose of this analysis, the operation of the emergency core cooling system is not affected by the failure of the containment. As the inventory of the condensate storage tank is depleted, the emergency core cooling system is switched to take suction from the suppression pool. The water in the suppression pool has been heated to a high temperature and would be boiling or at saturation following containment failure. Since the emergency core cooling system pumps are not designed to operate under these conditions, they are assumed to fail due to cavitation. Core uncovery and melting follow. Table 6.2 indicates times of key events as predicted by the MARCH 2 code. Table 6.3 gives core and primary system conditions at key times in the sequence. The temperature transient of selected fuel regions is illustrated in Figure 6.10. Core uncovery, heatup, and melting occur with the primary system at approximately 7.93 MPa (1150 psia). While the core power level is substantial during the time to containment failure, it drops rapidly as the core begins to uncover. At the start of core melting as well as thereafter the power is down to decay heat levels.

The flow path for fission product transport within the reactor vessel is illustrated in Figure 6.11. After passing through the steam separators, the flow splits with the greater fraction (85 percent) passing through the steam dryers and a smaller fraction (15 percent) bypassing the steam dryers. The flow then exits the vessel through the steam lines and safety/relief lines to the suppression pool. A schematic of the control volumes used in the MERGE analysis is provided in Figure 6.12. Gas and structure temperatures are shown in Figures 6.13 and 6.14, respectively. Time zero in Figures 6.13 and 6.14 corresponds to 97 minutes (5820 seconds) into the accident. As in the AE sequence, temperatures near the end of the core melting phase drop following slumping of the fuel. The peak gas temperature in the relief line to the suppression pool is approximately 1900 F (1040 C). The predicted temperatures

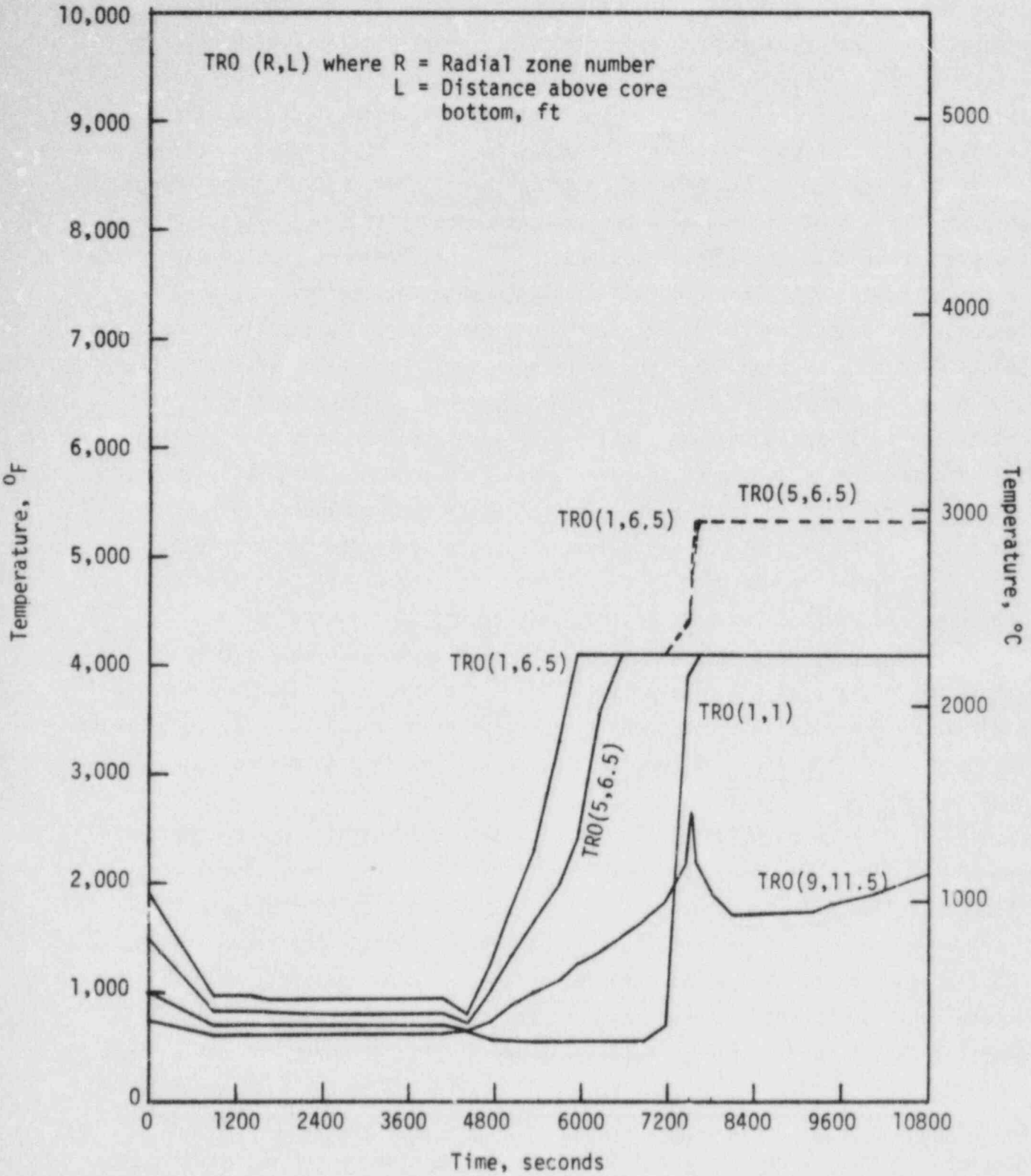

FIGURE 6.10 TEMPERATURES OF SELECTED FUEL REGIONS AS A FUNCTION OF TIME - SEQUENCE TC

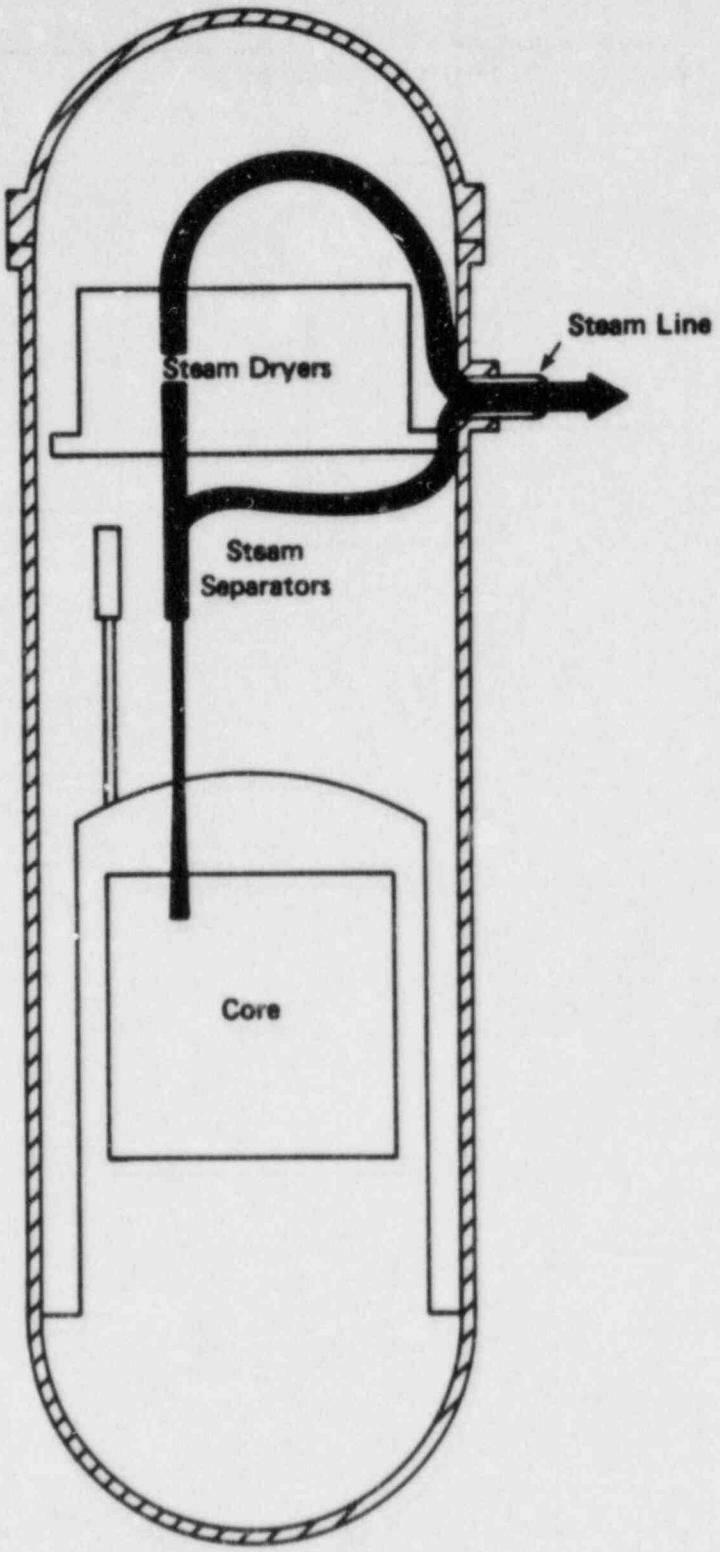

FIGURE 6.11 FLOWPATHS FOR FISSION PRODUCT TRANSPORT IN RCS - SEQUENCES TC AND TW

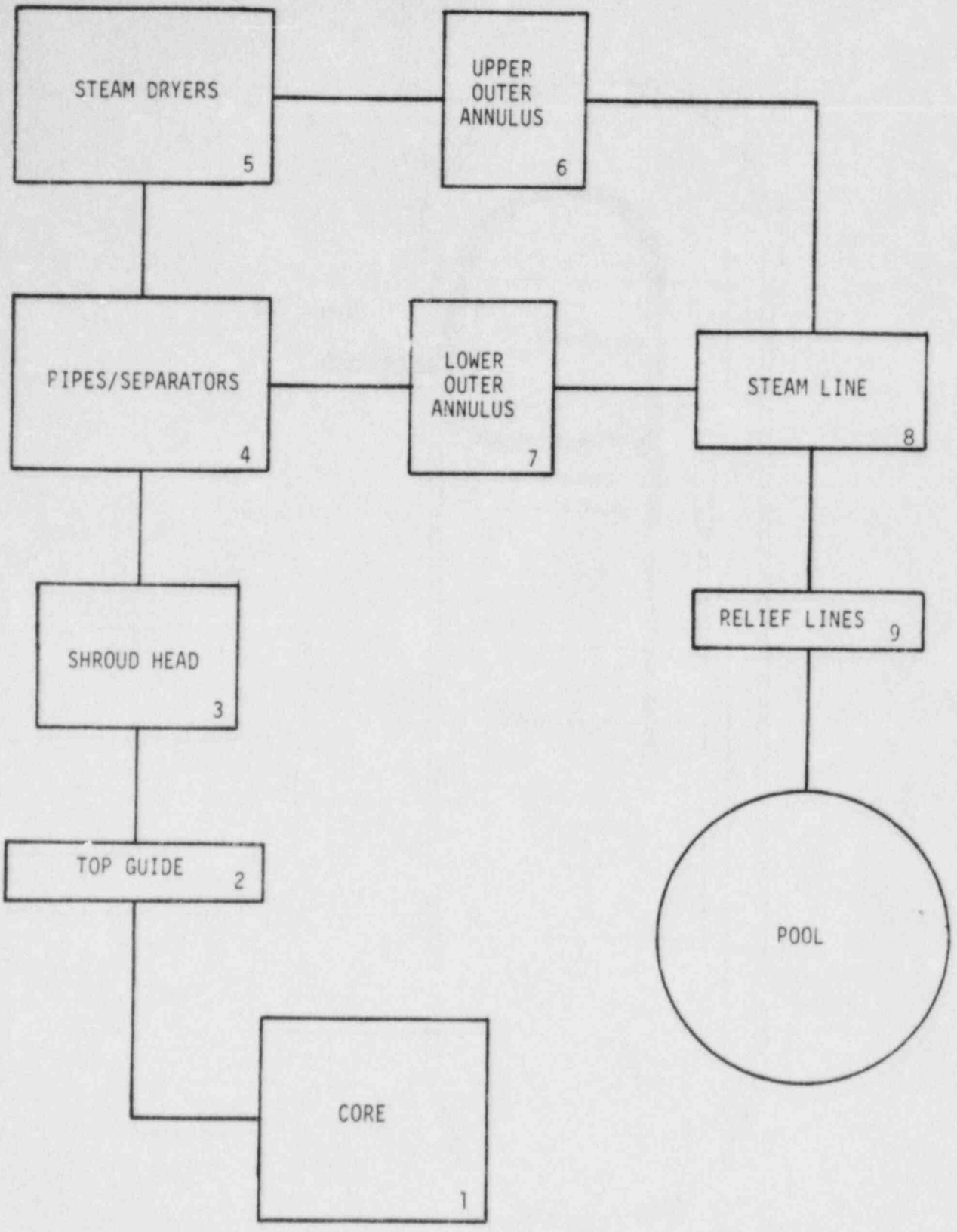

FIGURE 6.12 SCHEMATIC OF CONTROL VOLUMES FOR THE PEACH BOTTOM TC AND TW ACCIDENT SEQUENCES

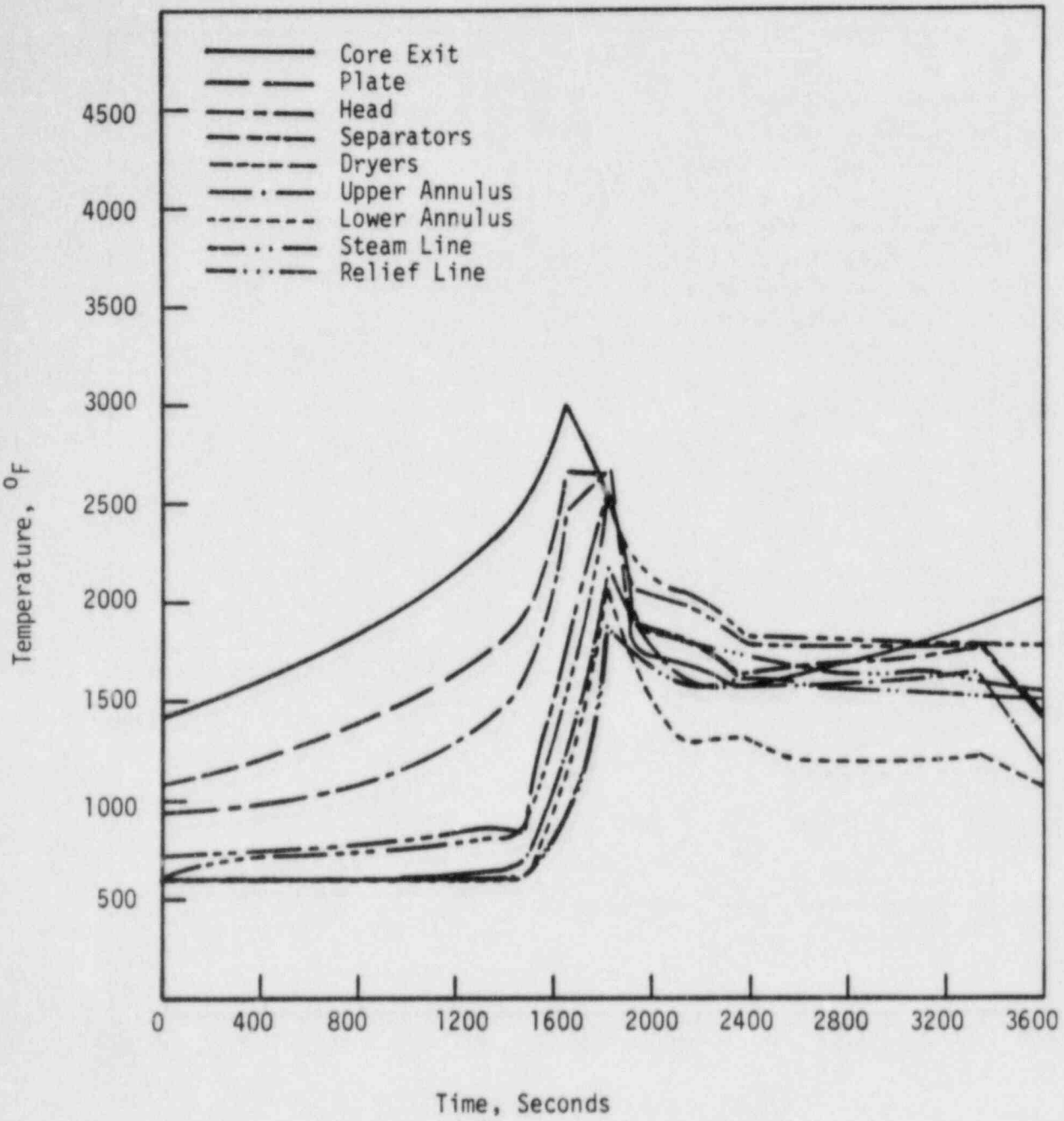

FIGURE 6.13 GAS TEMPERATURES IN RCS VOLUMES - SEQUENCE TC

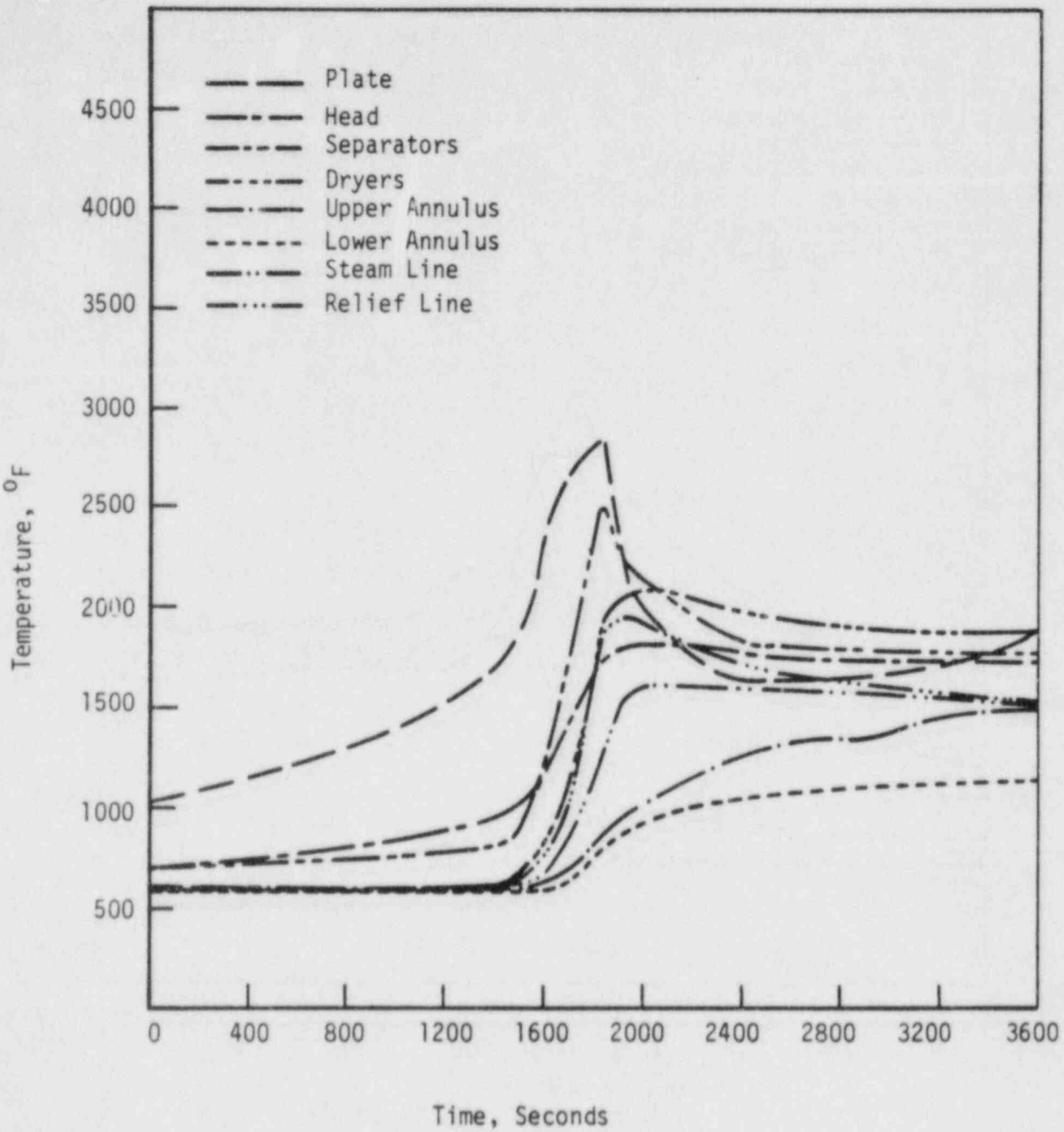

FIGURE 6.14 STRUCTURE TEMPERATURES IN RCS VOLUMES - SEQUENCE TC

are high enough to prevent significant retention of cesium hydroxide and cesium iodide on the reactor coolant system surfaces.

The flow path from the vessel to the suppression pool is illustrated in Figure 6.15. The flow path is then from the vapor space of the wetwell through vacuum breakers into the drywell and then into the reactor building through the break. Figures 6.16 and 6.17 show the temperatures and pressures in the containment volumes in the accident. Table 6.4 gives the containment conditions at key times during the sequence. Containment failure precedes core melt and the subsequent thermodynamic condition of the suppression pool is boiling or saturated.

Figure 6.18 illustrates the flow paths from the vessel and reactor cavity after reactor vessel failure. The vaporization release of fission products does not pass through the suppression pool prior to exiting the drywell. In the TC_{γ}' sequence, the fission products are assumed to be released from the drywell to the environment without further attenuation in the reactor building. In the TC_{γ} sequence, the reactor building is assumed to remain intact following failure of the primary containment.

Table 6.5 summarizes the leak rate data derived from the MARCH analyses and used for the evaluation of the fission product release to the environment.

Reactor Building Response

Following blowdown of the primary containment, the blowout panels between the lower portion of the reactor building and the refueling floor region were assumed to fail, connecting the two volumes. The pressure in the reactor building subsequently was calculated to rise to 0.25 psig, resulting in failure of the blowout panels in the upper region of the reactor building with a corresponding leak area of 3000 ft^2 to the environment. MARCH calculations (Figure 6.19) indicate a peak reactor building pressure of about 1.0 psig. Because of the continuing large steam input to the suppression pool with the core at a power level of about 30 percent, the drywell depressurization (Figure 6.20) requires about 20 minutes. At about 75 minutes, the containment pressure begins to fall more rapidly. At this time, the ECC makeup switches from the condensate storage tank to the boiling suppression pool and the pumps

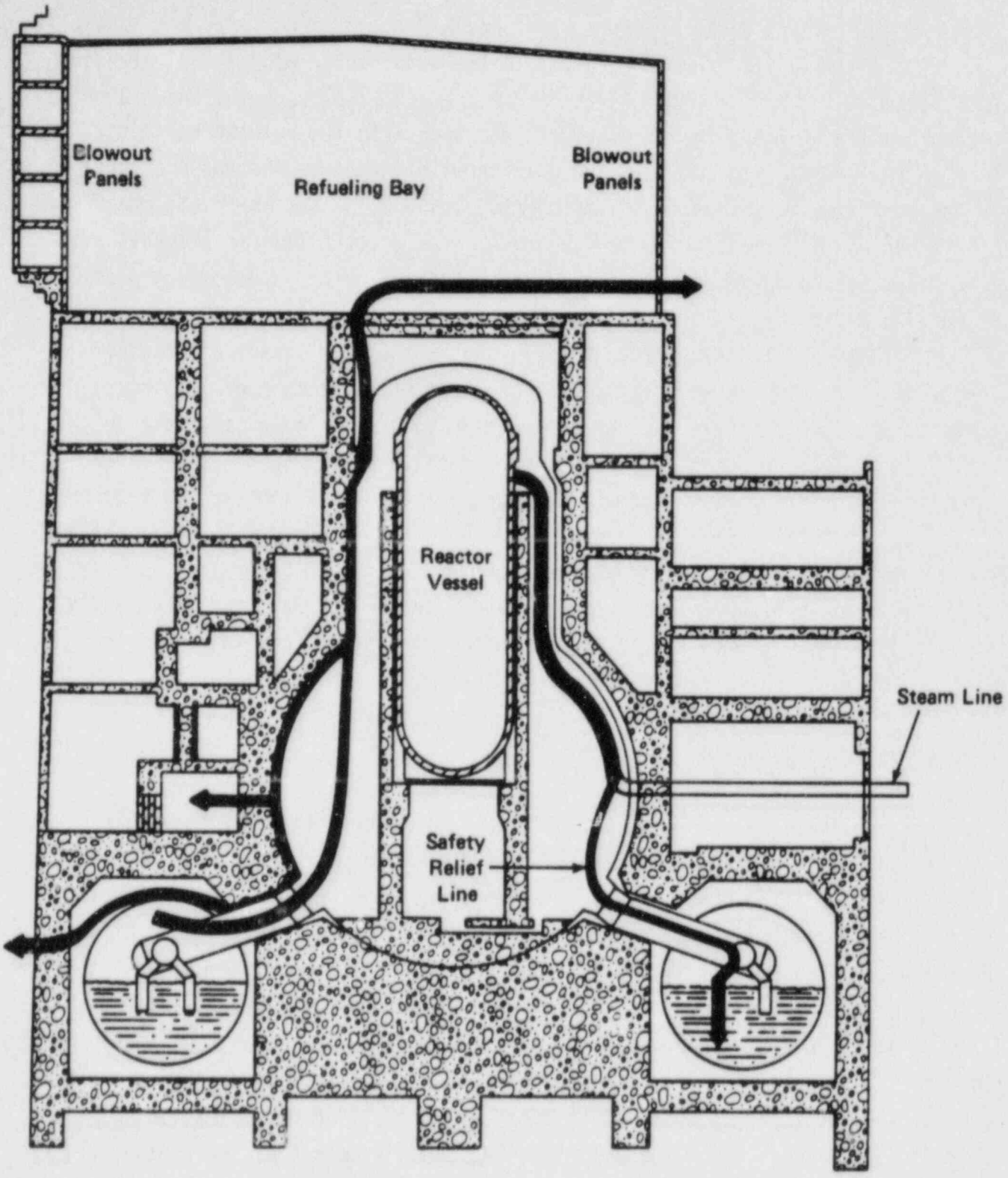

FIGURE 6.15 FLOWPATH FOR FISSION PRODUCT TRANSPORT BEFORE VESSEL FAILURE - SEQUENCES TC AND TW

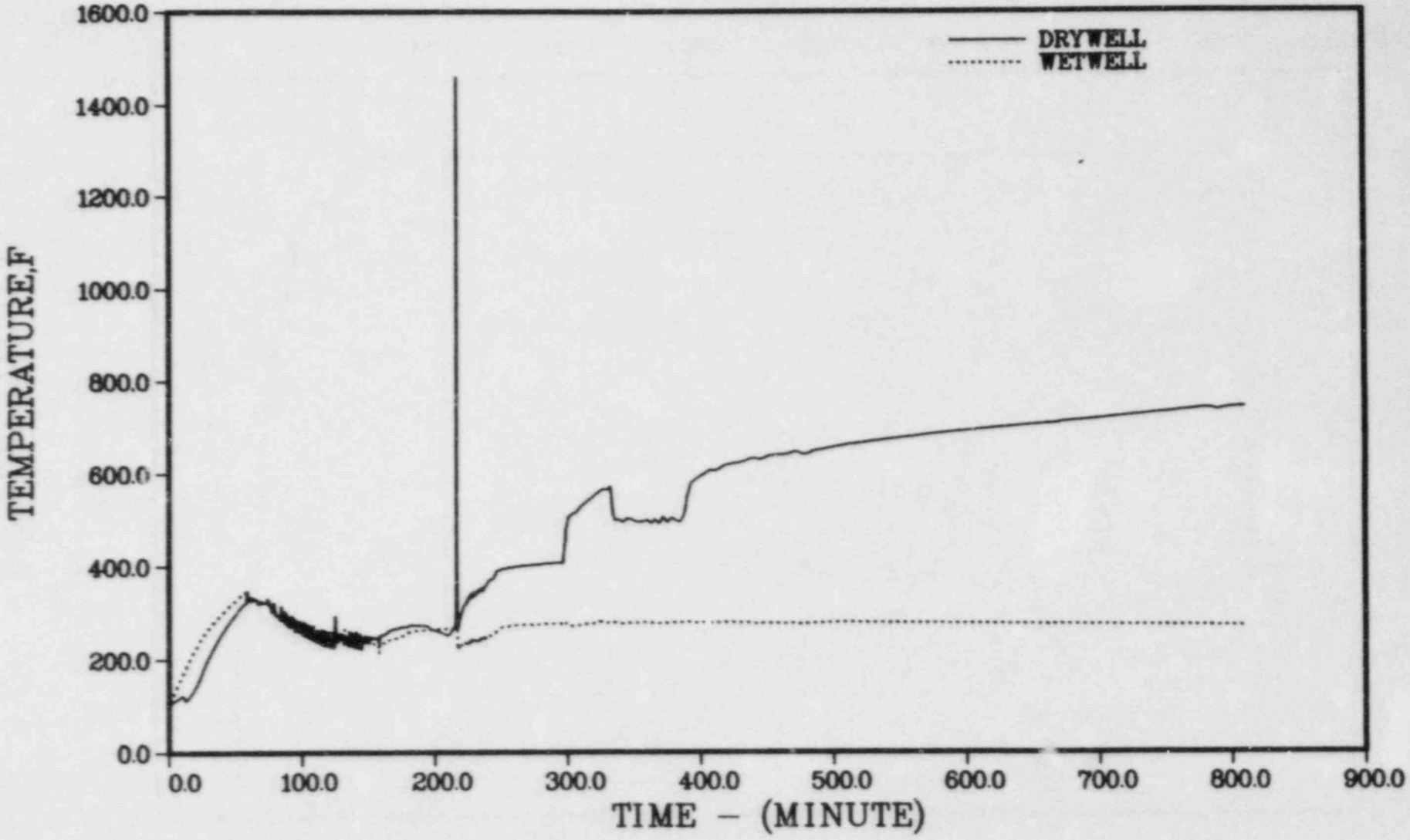

FIGURE 6.16 GAS TEMPERATURES IN CONTAINMENT VOLUMES - SEQUENCE TC

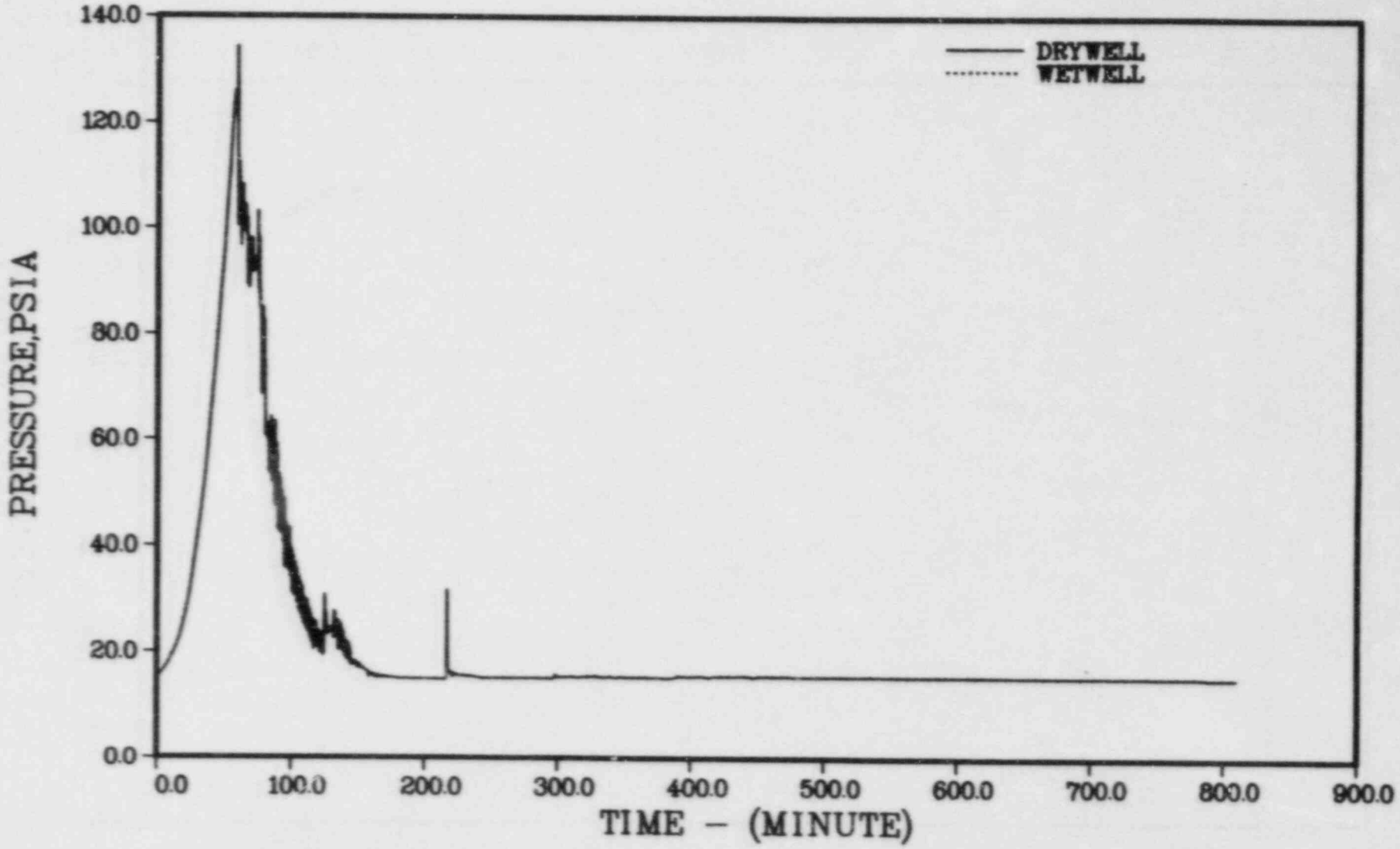

FIGURE 6.17 PRESSURES IN CONTAINMENT VOLUMES - SEQUENCE TC

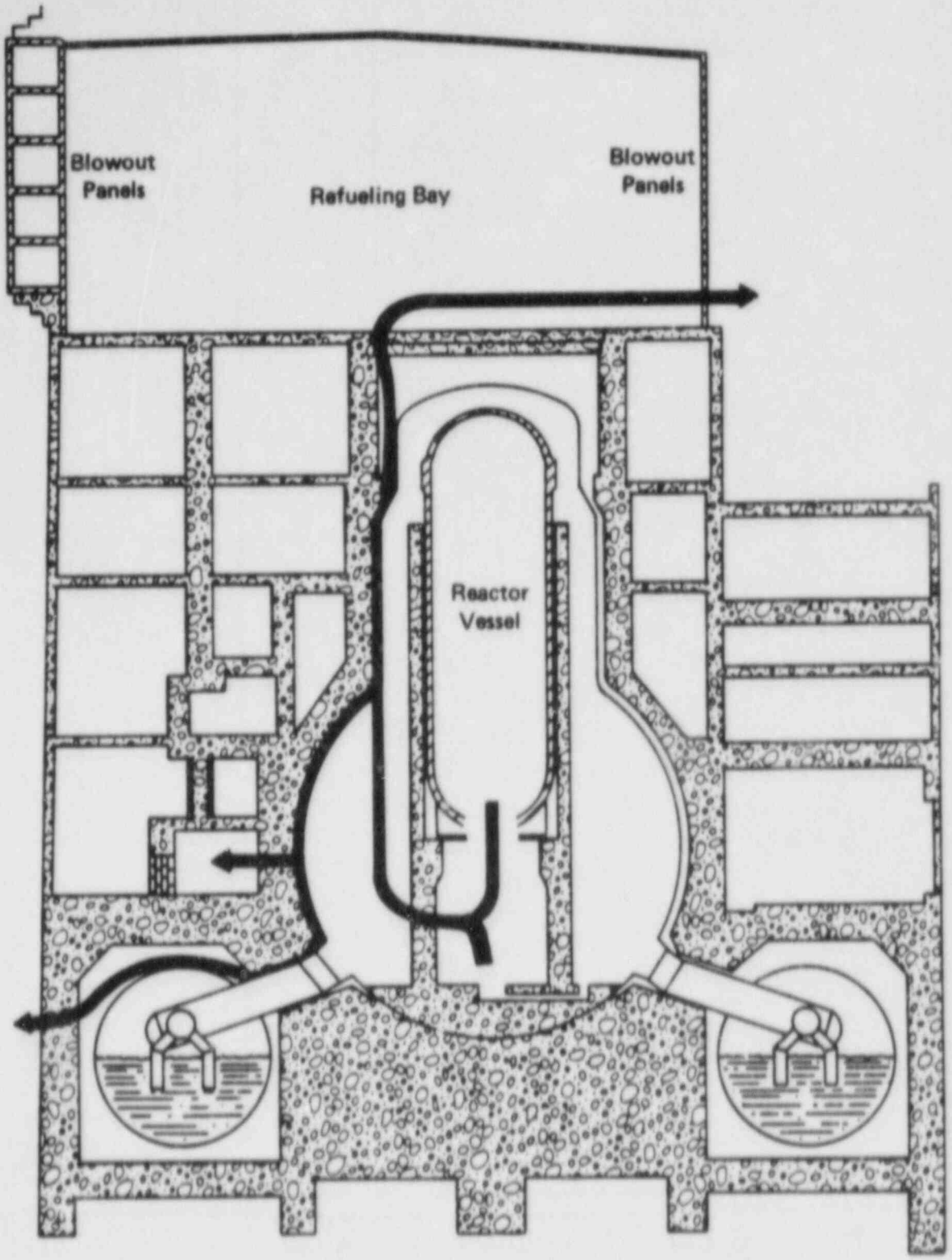

FIGURE 6.18 FLOWPATH FOR FISSION PRODUCT TRANSPORT AFTER VESSEL FAILURE - SEQUENCES TC AND TW

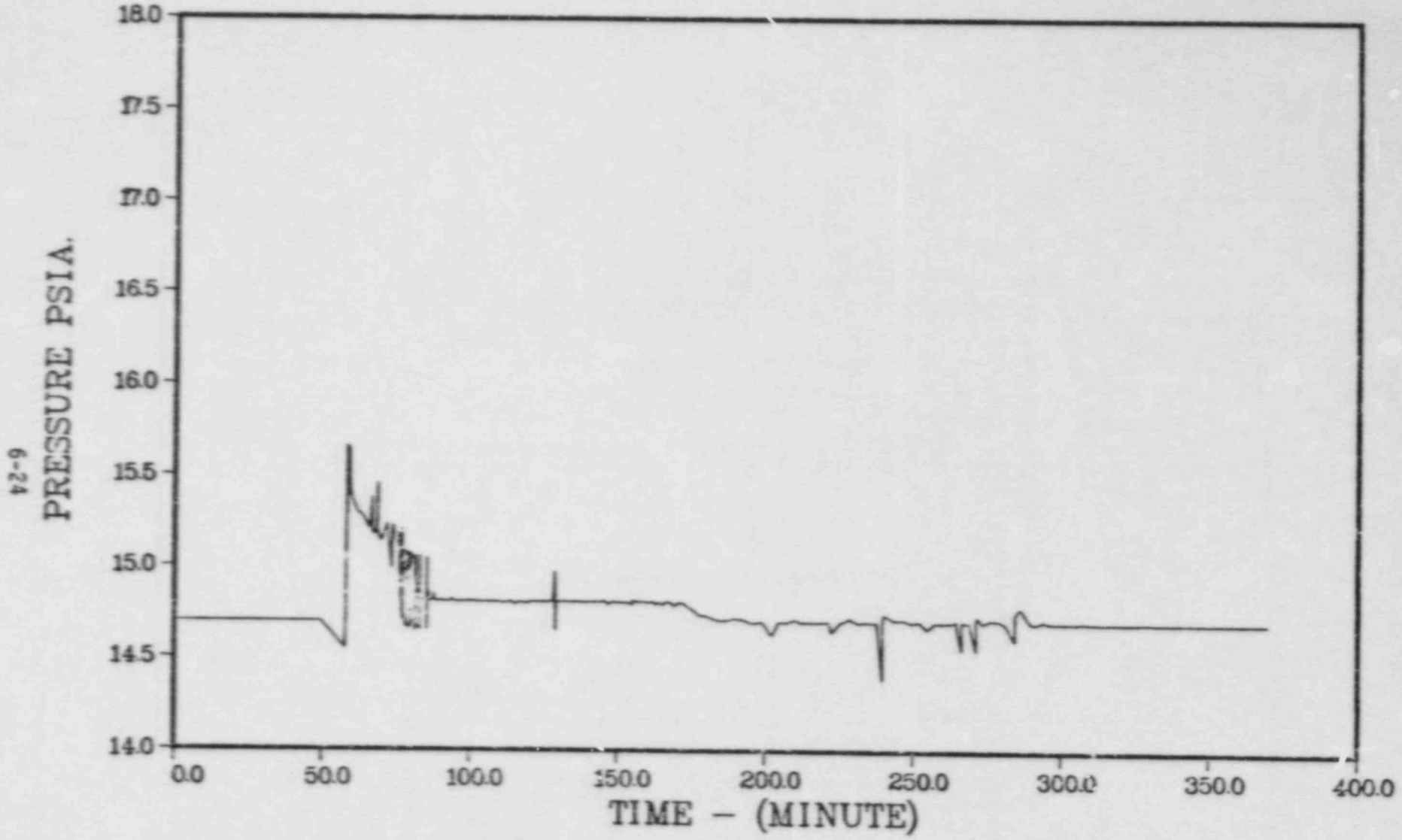

FIGURE 6.19. REACTOR BUILDING PRESSURE DURING TCY SEQUENCE

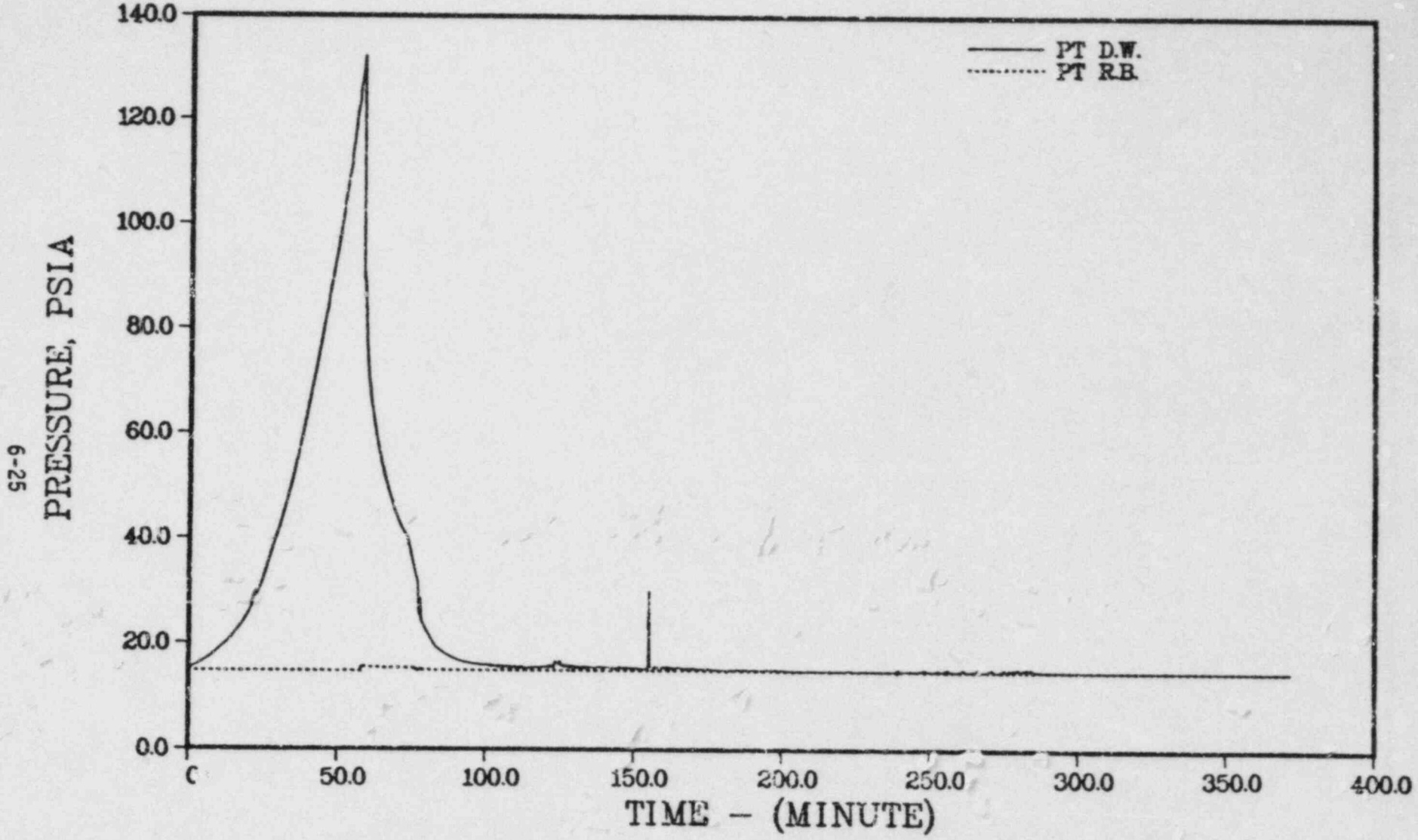

FIGURE 6.20. DRYWELL (DW) AND REACTOR BUILDING (RB) PRESSURE DURING TCY SEQUENCE

fail. The steam release rate to the containment decreases substantially as the core uncovers and the power level drops to decay levels.

The ventilation system in the reactor building was assumed to continue to operate after drywell failure, exhausting gases up the stack at a constant rate of 25,000 ft^3/minute. It is important to note that the reactor building stays at a positive pressure for a prolonged period of time even with the very large leak area; this will result in significant leakage out of the building in addition to the flow up the stack. When the pressure falls below atmospheric pressure, the fans begin to draw outside air into the reactor building. Figure 6.21 shows the concentration of oxygen in the reactor building. Following containment failure, essentially all of the air (and oxygen) is exhausted from the building. Continued operation of the fans has little effect on the air (oxygen) concentration until about 175 minutes. After 175 minutes, the relatively low gas generation rates during the concrete decomposition phase of the sequence allow the reactor building pressure to fall below atmospheric pressure. The combination of steam condensation on walls and the operation of the fans subsequently draws outside air into the building.

Note in Figure 6.21 that no flammable hydrogen-air mixtures are predicted in the reactor building for the TC sequence. When the hydrogen concentration peaks at about 14 percent, there is essentially no oxygen in the building. When the oxygen concentration increases above 5 to 6 percent, the hydrogen is generally below 3 to 4 percent. Such mixtures are marginally, but not generally, considered flammable. If the fire protection system in the reactor building had been assumed to operate, inflow of air would have occurred earlier in the sequence resulting in flammable mixtures.

In the analysis of the reactor building response the entire volume of the building was considered to be available for the expansion of the gases and vapors released from the primary containment. Obviously a variety of paths for gas (and fission product) release from the primary containment, through the reactor building, and out to the environment can be postulated in addition to the one explicitly considered in this study. Alternate paths that are more direct than the one considered will likely involve higher local pressures and shorter residence times within the building. The assumed availability of the entire reactor building volume for gas expansion tends to enhance the potential for fission product deposition.

6.1.3 Sequence TW

In the TW sequence, the reactor shuts down, the emergency core cooling system operates, but the heat removal system for the suppression pool fails. This sequence is similar to TC in that the flow paths for fission product transport are the same. The time scale for the TW sequence is much more protracted, however, due to the substantially lower power levels involved. As in TC, the suppression pool heats up and the containment fails prior to core meltdown. Containment failure is not predicted to occur until 28 hours, however, as opposed to 1 hour in the TC sequence. In addition, it was assumed in the analysis of the TW sequence that the operators would depressurize the primary system prior to core meltdown. Table 6.2 gives the timing of the key events and Table 6.3 presents core and primary system conditions at key times for this sequence. Because of the low decay heat level, the emergency core cooling system is able to keep the primary system filled; this extends the time of core uncovery when the emergency core cooling system fails.
Figure 6.22 illustrates the heatup of selected regions of the core. The same control volume setup was used in the MERGE analysis as described previously for the TC sequence. Figures 6.23 and 6.24 show the gas and structure temperatures in the control volumes as a function of time. In Figures 6.23 and 6.24, time zero corresponds to 2,622.3 minutes into the accident. Flow paths in the containment are also the same as for the TC sequence. Figures 6.25 and 6.26 illustrate the time-dependent behavior of the pressure and temperature in the wetwell and drywell throughout the accident. Table 6.4 gives the containment conditions at key times and Table 6.5 summarizes the leak rates used in the fission product release calculations.

6.2 Radionuclide Sources

6.2.1 Source Within Pressure Vessel

Inventory

The fission product inventories used in the analyses in this report are based on results of the ORIGEN 2[6.1] code for the Browns Ferry Unit 1

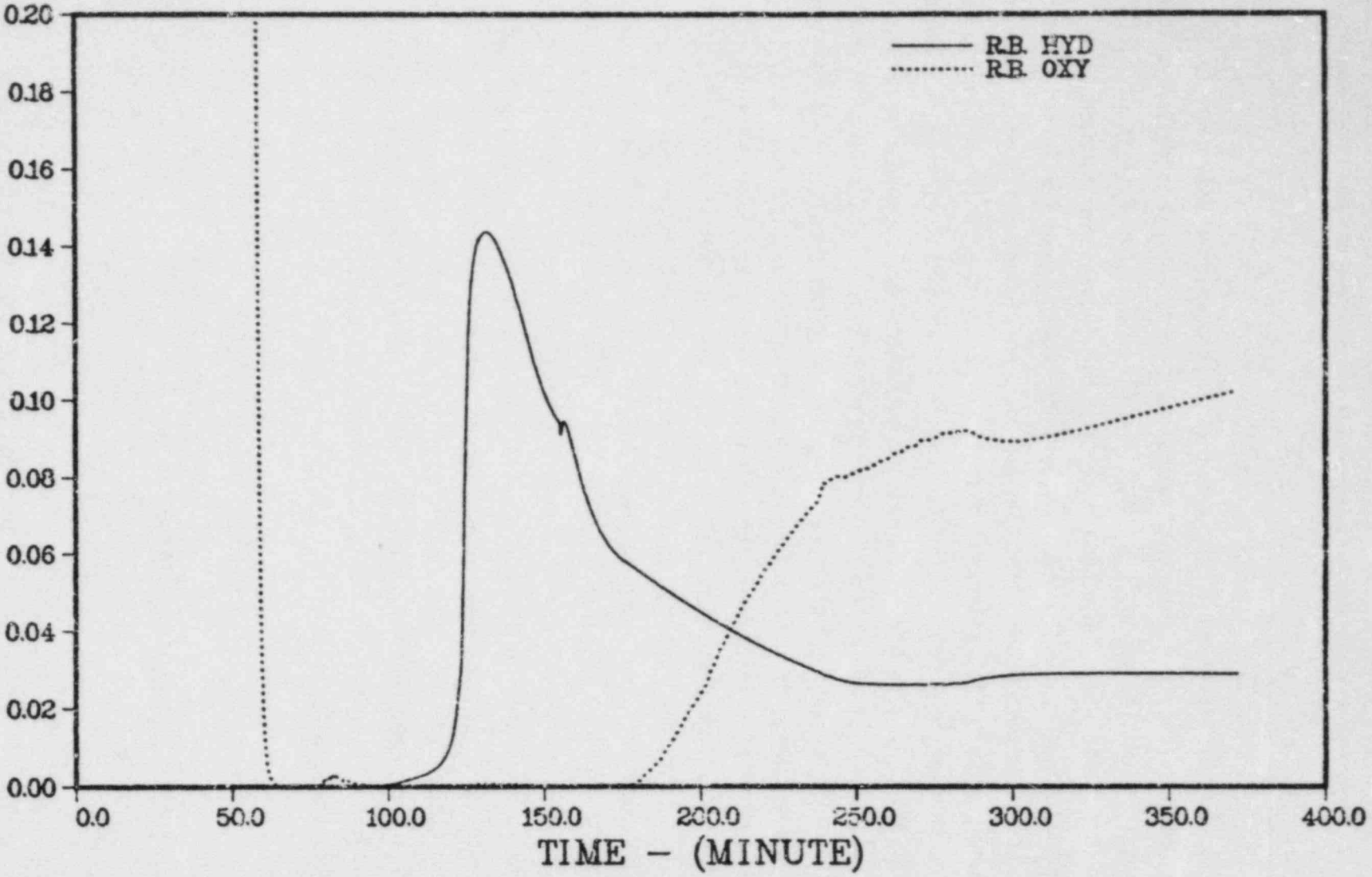

FIGURE 6.21. MOLE FRACTIONS OXYGEN (OXY) AND HYDROGEN (HYD) IN REACTOR BUILDING DURING TCY SEQUENCE

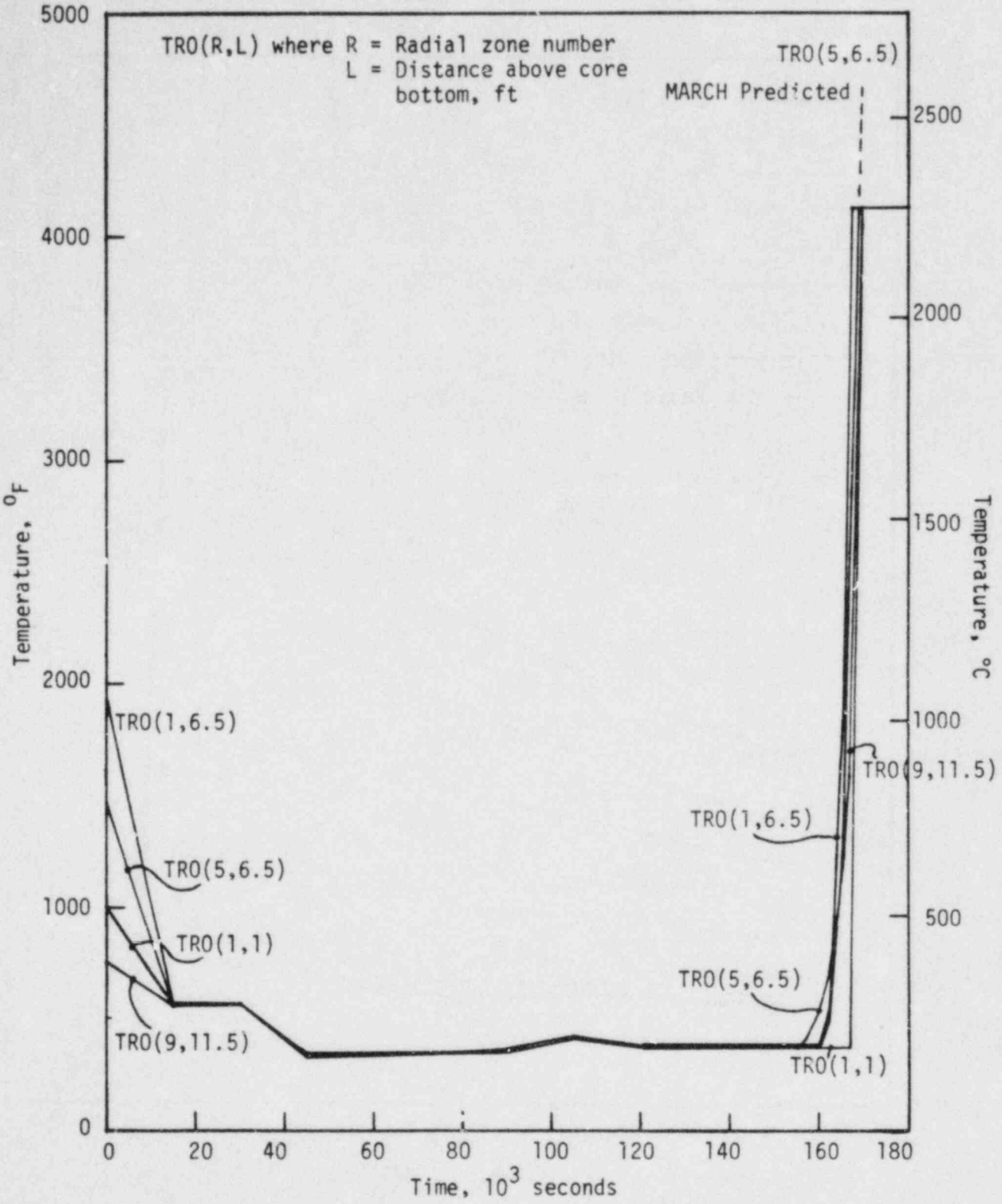

FIGURE 6.22. TEMPERATURE OF SELECTED FUEL REGIONS AS A FUNCTION OF TIME - SEQUENCE TW

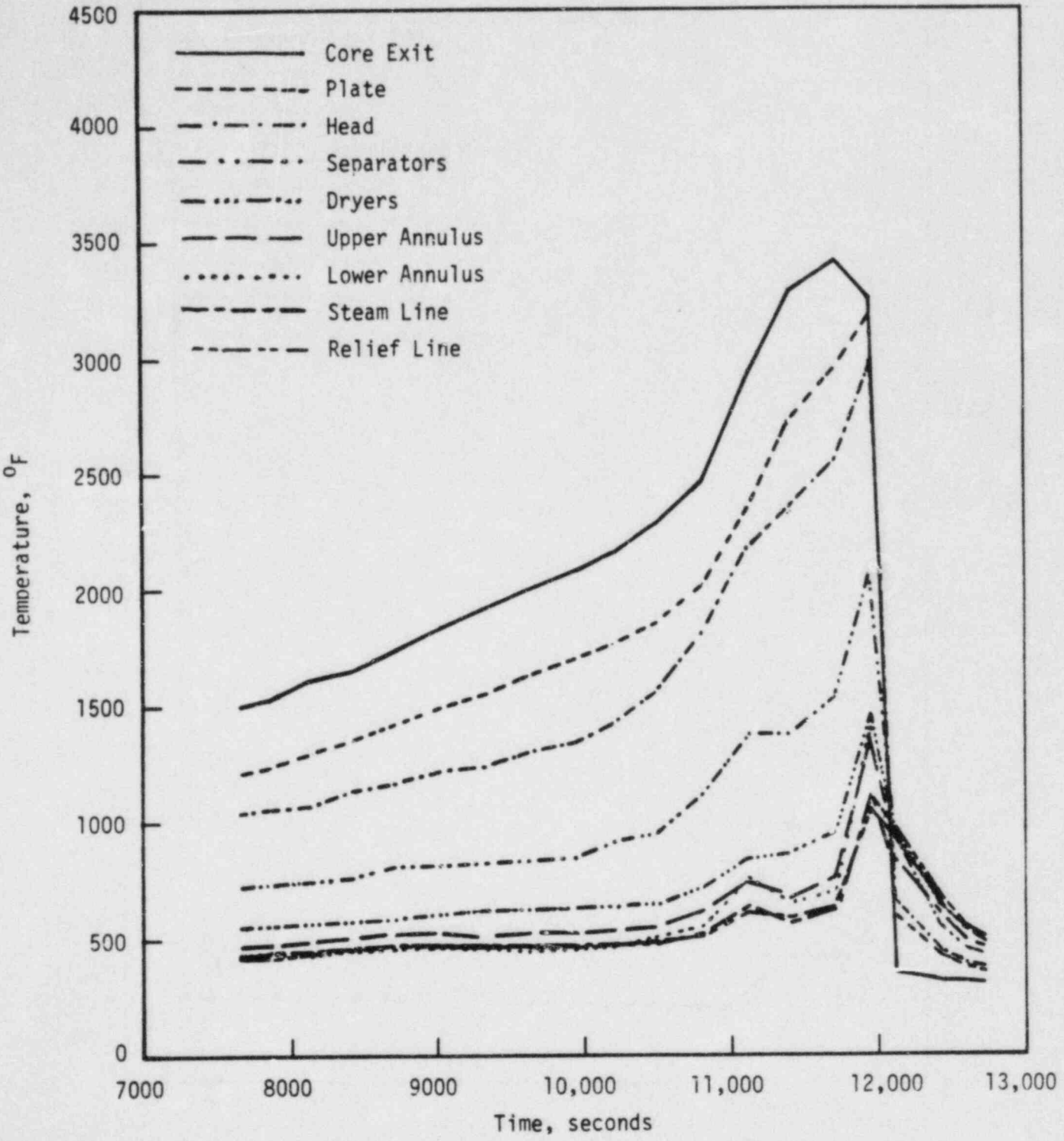

FIGURE 6.23. GAS TEMPERATURES IN RCS VOLUMES - SEQUENCE TW

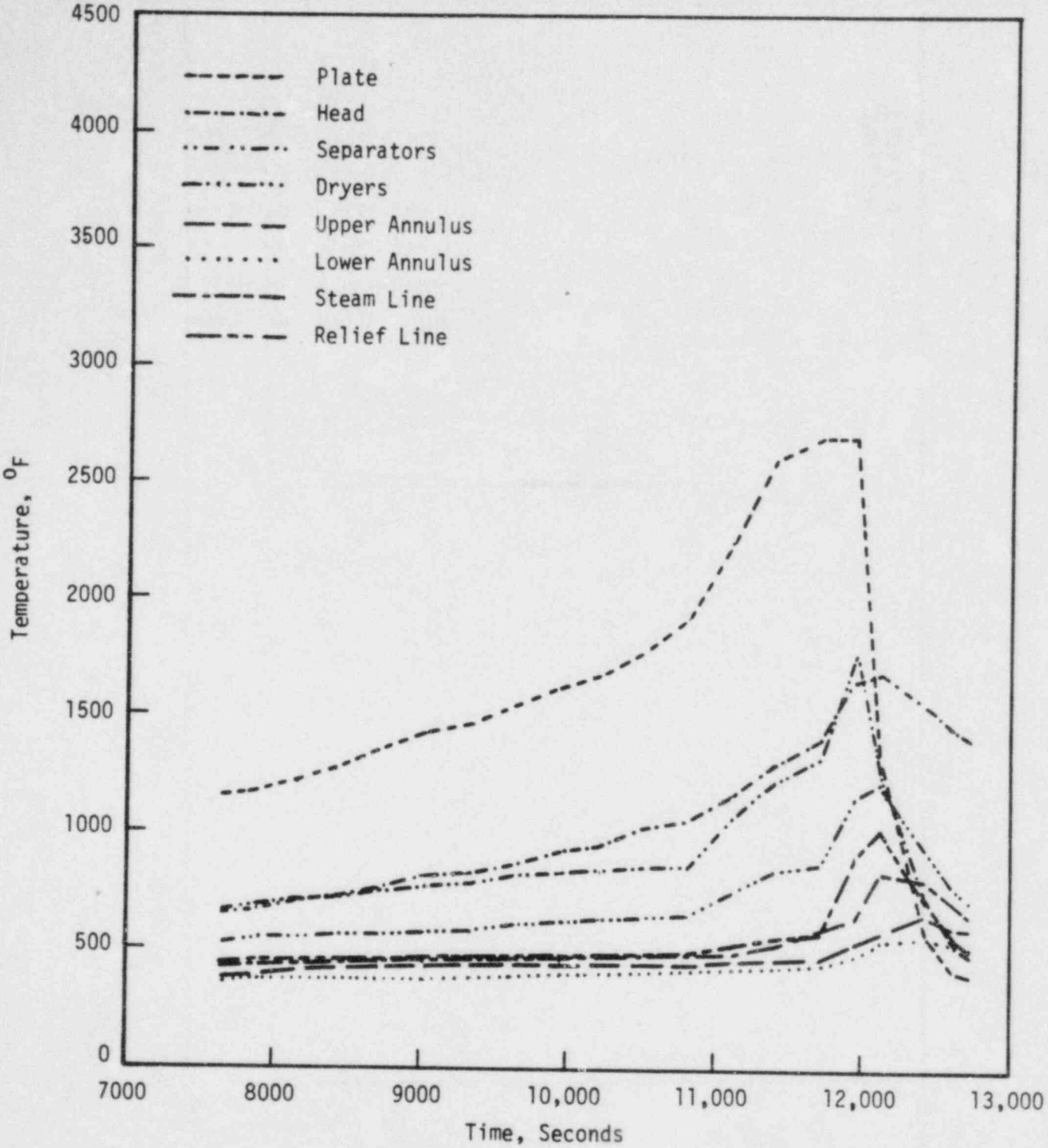

FIGURE 6.24. STRUCTURE TEMPERATURES IN RCS VOLUMES - SEQUENCE TW

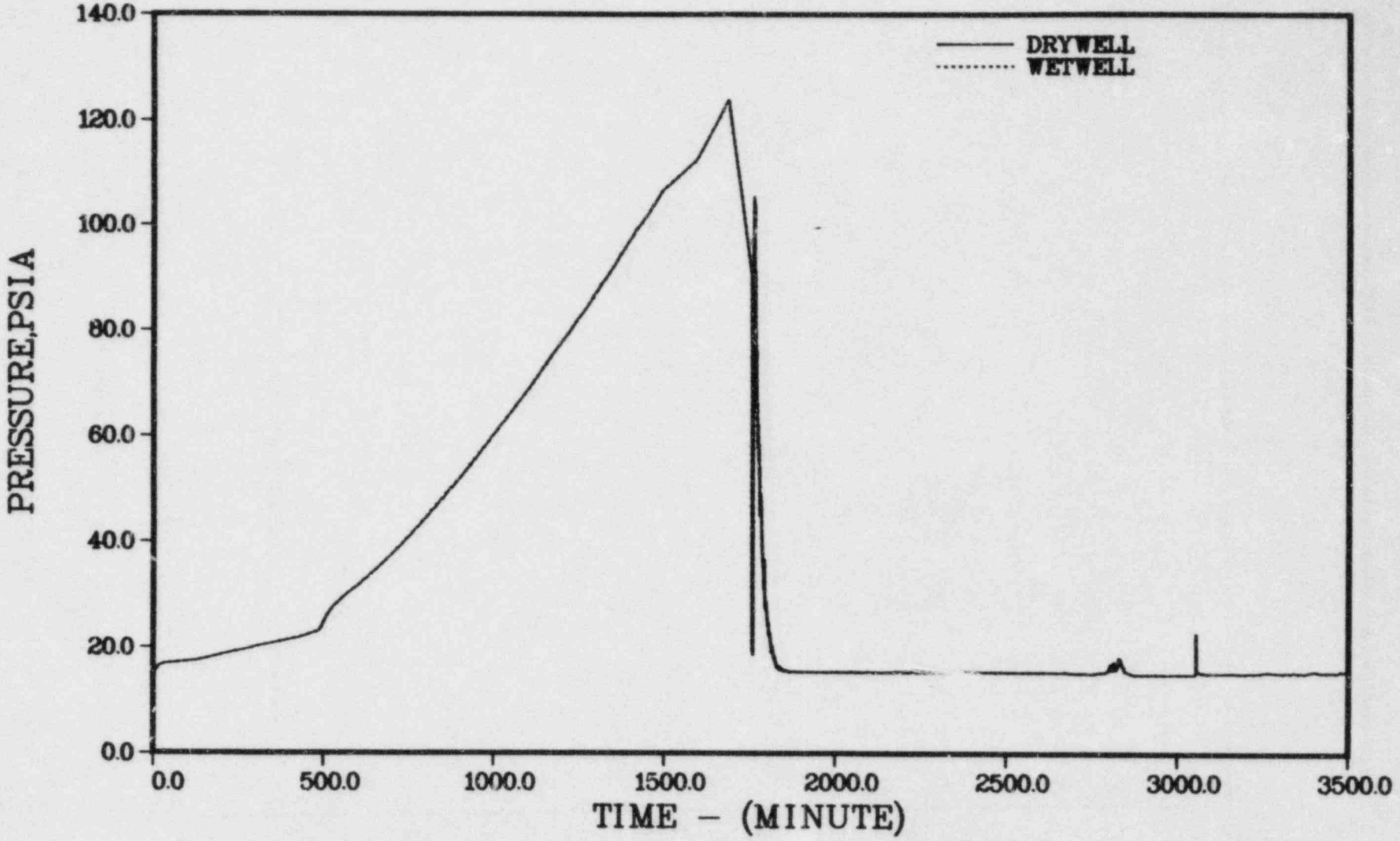

FIGURE 6.25. PRESSURE IN CONTAINMENT VOLUMES - SEQUENCE TW

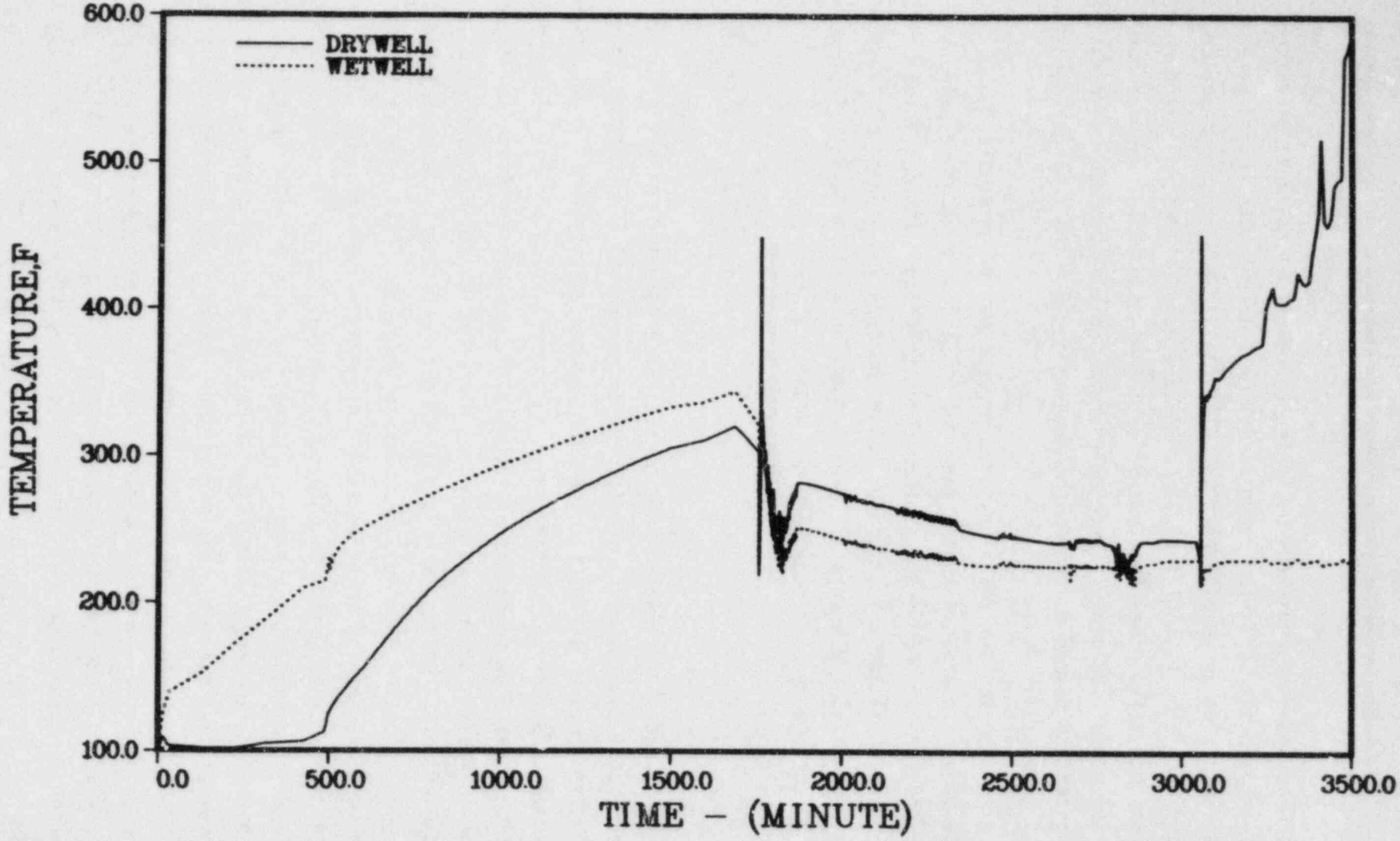

FIGURE 6.26. GAS TEMPERATURES IN CONTAINMENT VOLUMES - SEQUENCE TW

reactor. The computer runs were performed by Oak Ridge National Laboratory in the station blackout study for Browns Ferry Unit 1.[6.2] An actual core loading (Cycle 4) involving seven different types of fuel assemblies are described in Table 6.6. For each type of fuel, two ORIGEN 2 calculations were performed, for the maximum axial power factor and for the minimum axial power factor. The fission product elemental inventories from the high and low power runs were weighted and summed to obtain the inventories for the average power for each type of fuel.

Inventories for each fuel type were summed to determine the total core inventory. In the subsequent analyses of fission product release, the core was treated as homogeneous, rather than ascribing different inventories to different radial and axial zones. The total core inventories of fission products and actinide elements are provided in Table 6.7. Masses of structural materials from the Peach Bottom FSAR are also tabulated.

Release from Fuel

The rates of release from the fuel were computed using the CORSOR code, which utilizes the MARCH predictions of core nodal temperatures as functions of time for each sequence. The MARCH predicted extent of Zr oxidation at each node as a function of time was used in evaluating the Te release from the melting core. The fractions of inventory released prior to vessel dryout and prior to vessel failure are given for each species and each sequence in Tables 6.8 and 6.9. Release from the melting core fragments is calculated up to the point of bottom head failure in these analyses. This results in each of these sequences having emission into a stagnant volume for a portion of each accident sequence, since MARCH predicts vessel dry out to occur prior to head failure by a significant margin. The differences between the values in these two tables indicate that portion of the emission which occurs while the RCS is essentially stagnant. The majority of the volatile species emissions occurs during the period before vessel dryout, though the actual values differ among the sequences examined. The dashes in these tables indicate values less than 0.01. It is clear that only small fractions of the less volatile species are released from the core during the in-vessel melting period of these sequences.

Tables 6.10 through 6.12 contain the mass release rates for cesium, iodine, tellurium, and aerosol particles for the AE, TC, and TW sequences at Peach Bottom. The aerosol particles are considered to be composed of the sum of all the nonfission products, along with fission products other than the noble gases, Cs, Te, and I.

The difference between the releases implied by Table 6.9 and the initial core inventory represents the melt composition as it enters the drywell cavity and becomes a source for fission products within the containment. This 'inventory', which is available for emissions into the drywell is presented for each of the sequences in Table 6.13. More discussion of this aspect of these analyses will be presented in the sections dealing with transport and deposition in the primary system.

Regrouping of Released Species

In order to track the Reactor Safety Study groups independently, an additional CORSOR run was performed for the AE sequence which produced release rates for all groups. A description of the makeup and methodology for release of each group follows.

- Group 1 (Xe, Kr) -- Xe and Kr releases were summed and a release rate computed. This group was not previously computed.

- Group 2 (I, Br) -- Br release was not considered due to an absence of data concerning Br release and its small inventory relative to I (1:16).

- Group 3 (Cs, Rb) -- Thermodynamic and physical properties of Rb justify treating it identically to Cs. As a result, the Rb inventory was lumped into the Cs inventory for treatment by CORSOR. Releases for I and Cs and CsOH were combined to produce release rates for CsI which were the forms assumed to be transporting through the primary system. This assumption is based on the predicted temperatures and gas compositions combined with consideration of the likely chemical thermodynamic equilibrium states.(6.3,6.4)

- Group 4 (Te, Se, Sb) -- Se and Sb were not considered based on their small inventory and lack of data concerning their behavior. Their inclusion

in this group would be further complicated by the dependence of Te release on Zircaloy oxidation.

- Group 5 (Ba, Sr) -- Ba and Sr were released separately and their releases summed to form the release rates for this group. Further, their releases were not included in the aerosol materials sum.

- Group 6 (Rh, Pd, Tc, Ru, Mo) -- Rh, Pd, and Tc inventories were added to the Ru inventory for purposes of release. The releases of Ru and Mo were then summed to produce release rates for this group. The aerosol materials sum does not include Mo or Ru releases.

- Group 7 (La, Y, Eu, Nd, Np, Sm, Pm, Pu, Zr, Ce, Nb, Pr) -- All members of Reactor Safety Study Group 7 with the exception of Zr were treated identically for purposes of release, using UO_2 release rate coefficients. Their release and the release of Zr were summed to produce release rates for this group. Table 6.7.B lists initial inventories of Group 7 members not included in Table 6.7.

- Aerosol Materials (Fe, UO_2, Zr (cladding)), -- The release rate for this group includes only nonfission products.

Table 6.7c lists initial inventories and final CORSOR releases for the Reactor Safety Study groups and compares the results with the "ungrouped" results.

It is necessary to select an initial particle size for those materials forming the aerosol species. It has been shown[5.5] that when significant agglomeration occurs, the initial aerosol size has a negligible effect on subsequent aerosol behavior after agglomeration has proceeded for a very short time. Nevertheless, initial particle sizes were chosen to correspond to the best available information. Numerous reviews of experimental mean aerosol sizes from vaporizing and condensing fuel indicate that the sizes will be from slightly below 0.01 μm to about 0.1 μm with the most likely size being about 0.05 μm.[6.6,6.7] A number median radius of 0.05 μm and a geometric standard deviation of 1.7 were assumed for the primary particles in the current analyses, and a bulk density of 3 g/cc was assumed for the particles.

6.2.2 Sources Within the Containment

Release into the drywell region can come from the primary circuit, the wetwell, or from core-concrete interaction. The pathway from the wetwell has as its original source, materials transported through the suppression pool but which originated within the reactor vessel or resulted from core-concrete interaction. The flow paths among compartments and the timing of events which control the flows were discussed in Chapter 4 and in earlier sections of this chapter. The source within the pressure vessel was discussed in Section 6.2.1. Discussion of the release during the core-concrete interaction follows.

Release from Core-Concrete Interaction

The VANESA code (described in Chapter 5) was used to make predictions of aerosol and gas release rates and compositions as functions of time. Composition of the core materials contacting the concrete was determined with the CORSOR code. These represent the materials remaining in the melt at the time of head melt-through. These compositions for the various sequences are given in Table 6.13. The concrete was taken to be a limestone concrete and the initial temperature of the molten material was as calculated with the MARCH code. The total release rates and composition of the release are given in Tables 6.14, 6.15, and 6.16. These rates and compositions define the source to the drywell after vessel head failure.

Source Term for Volatile Iodides

In a previous section it was noted that the thermodynamics of the cesium-iodine-hydrogen-oxygen system indicate that iodine will be present primarily as a nonvolatile iodide in the primary coolant system. After release from the primary system, a small fraction of the iodine inventory in the containment is believed to be present as volatile iodides.[6.3] The presence of volatile iodide species in containment-type systems has been observed in experiments[6.8] and in the TMI-2 post-accident containment atmosphere.[6.9] At present, the mechanisms responsible for the generation of these volatile iodides are not well understood. Since a theoretical model is not available, an

empirical approach has been selected for the formulation of a source term for volatile iodides. This source term consists of two components. One component represents the fraction of the containment iodine inventory which is present as volatile iodides before containment failure. The second component represents a generation rate for volatile iodides after containment failure. The containment inventory of volatile iodides present prior to containment failure was estimated from levels observed in TMI-2[6.9] and from estimates of the probable detection limits in relevant experiments.[6.10] The volatile iodide generation rate was estimated from a conservative evaluation of the measurements of the airborne iodine levels in the TMI-2 containment over the time period from 100-2000 hours after reactor trip. Based on these estimates it has been assumed for this study that 0.05 percent of the containment iodine inventory will be present as volatile iodides prior to containment failure and after containment failure, additional volatile iodides will be generated at a rate of 2×10^{-7} fraction/hour of the containment iodine inventory.

Of this volatile iodine source, it is believed that a fraction of the iodine inventory in a reactor containment will be present as volatile organic iodides (predominantly CH_3I).[6.3] (Other volatile species may also be present.) Therefore, in the analysis of reactor accidents involving a radionuclide release from the reactor system and containment failure, formation in the containment and subsequent release of organic iodides should be considered. Unfortunately, the mechanism responsible for the generation of organic iodides has not yet been elucidated. As a result, it is not yet possible to establish a definitive source of organic iodides. Early estimates of the organic iodine source terms were based on a conservative interpretation of experimental systems studies.[6.8,6.11] Early thermodynamic studies predicted that organic iodides should be present in much smaller concentrations than observed in experiments.[6.12] These calculations predicted that CH_3I would comprise only 10^{-4} percent of the total gaseous iodine inventory modeled. Experimental data[6.8] and "chemical species specific" measurements of the TMI-2 airborne iodine inventory[6.9] imply that the concentration of organic iodides present in a reactor containment during and following an accident may be higher than the concentrations predicted by thermodynamic calculations for an equilibrium system. Additionally, observations of the airborne iodine behavior at TMI-2[6.9] imply the presence of competing sources and sinks for

volatile iodine species. In light of these data, a kinetic description may be required to adequately quantify the time dependence of the organic iodide concentration in reactor containments during and following reactor accidents. Pending results of studies, such as those which are currently under way,[6.4] use of a general source term for volatile iodides rather than separate source terms for CH_3I, I_2, etc., has been assumed as noted above.

References

(6.1) Groff, A. G., "ORIGEN 2 -- A Revised and Updated Version of the Oak Ridge Isotope Generation and Depletion Code", ORNL-5621 (July, 1980).

(6.2) Wichner, R. P., et al, "Station Blackout at Browns Ferry Unit One -- Iodine and Noble Gas Distribution and Release", NUREG/CR-2181 (August, 1982).

(6.3) Technical Base for Estimating Fission Product Behavior During LWR Accidents, NUREG-0772, (June, 1981).

(6.4) Torgerson, D. F., et al., Fission Product Chemistry Under Reactor Accident Conditions, presented at the International Meeting on Thermal Nuclear Reactor Safety, Chicago, Illinois, U.S.A. (September, 1982).

(6.5) Jordan, H., Schumacher, P. M., and Gieseke, J. A., "Comparison of QUICK Predictions with Results of Selected, Recent Aerosol Behavior Experiments", NUREG/CR-2922, BMI-2089 (September, 1982).

(6.6) Gieseke, J. A., et al, "Aerosol Source Term for Fast Reactor Safety Analysis", BMI-X-637 (August 11, 1972).

(6.7) Nuclear Aerosols in Reactor Safety, CSNI/SOAR No. 1 (June, 1979).

(6.8) Postma, A. K. and Zavodoski, R. W., Review of Organic Iodide Formation Under Accident Conditions in Water-Cooled Reactors, WASH-1233 (1972).

(6.9) Pelletier, C. A., et al., Preliminary Radioiodine Source Term and Inventory Assessment for TMI-2, SAI-139-82-12-RV (September, 1982).

(6.10) Lin, C. C., Chemical Effecs of Gamma Radiation on Iodine in Aqueous Solutions, J. Inorg. Nucl. Chem., 42, pp. 1101-1107 (1980).

(6.11) Reactor Safety Study: An Assessment of Accident Risks in U.S. Commercial Nuclear Power Plants, WASH-1400 (1974).

(6.12) Barnes, R. H., Kircher, J. F., and Townley, C. W., Chemical Equilibrium Studies of Organic Iodide Formation Under Nuclear Reactor Accident Conditions, BMI-1816 (1966).

TABLE 6.1 REACTOR CHARACTERISTICS, CONTAINMENT PARAMETERS, AND MARCH OPTIONS FOR THE BWR MARK I CONTAINMENT

Weight Zircaloy in core:	144,382 lb (65,490 kg)
Weight other metal in core:	15,680 lb (7,112 kg)
Weight UO_2 in core:	351,440 lb (159,410 kg)
Weight of support structures included in debris:	106,238 lb (48,188 kg)
Weight of bottom head:	207, 500 lb (94,120 kg)
Bottom head diameter:	20.9 ft (6.4 m)
Bottom head thickness:	0.576 ft (17.6 cm)

Containment Parameters

Number of compartments: 2

Compartment 1: Drywell

Compartment 2: Wetwell

	Free Volume		Initial Temperature		Initial Pressure	
	ft^3	m^3	°F	°C	psia	MPa
Drywell	159,000	4,503	100	37.8	14.7	0.1
Wetwell	119,000	3,370	100	37.8	14.7	0.1

	Thermal Conductivity		Heat Capacity		Density	
Material	Btu/hr ft F	W/cm C	Btu/lb F	J/kg K	lb/ft^3	kg/m^3
Iron	25.	0.4325	0.113	473.1	487	7801.7
Concrete	0.8	0.01384	0.238	996.5	158	2531.2

	Thickness		Heat Transfer Area	
	ft	m	ft^2	m^2
Wetwell shell	0.053	1.615	17,060	1,584.9
Drywell concrete	1.0	0.305	7,238	672.4
Drywell concrete	1.5	0.457	2,262	210.1
Drywell concrete	3.0	0.914	1,005	93.4
Drywell shell	0.083	2.530	17,700	1,644.3
Misc steel	0.042	1.280	39,180	3,639.8

TABLE 6.1 (Continued)

Steel/concrete interface coefficient: 100 Btu/hr ft^2 F (0.0568 W/cm^2/C)
Initial slab temperature: 100 F (37.8 C)

Concrete Composition

Weight fraction $CaCO_3$:	0.8
Weight fraction $Ca(OH)_2$:	0.15
Weight fraction SiO_2:	0.01
Weight fraction Al_2O_3:	0.01
Weight fraction free H_2O:	0.03
Gm rebar per gm concrete:	0.135

Engineered Safety Systems

	Rated Flow		Pressure	
ECC Pump	GPM	l/s	psig	MPa
High Head	5,000		3,500	24.2
Low Head	40,000		20	0.24

Heat exchanger rated conditions:

Rated Capacity, Btu/hr	7. x 10^7 (2.05 x 10^8 W)
Primary flow, lb/min	83,429 (630.7 kg/s)
Secondary flow, lb/min	37,543 (283.8 kg/s)
Primary inlet, F	165 (73.9 C)
Secondary inlet, F	90 (32.2 C)

TABLE 6.1 (Continued)

ECC Storage and Injection Tanks

	CST	
Weight of water	3.108×10^6 lb	1.41×10^6 kg
Initial pressure	14.7 psia	0.1 MPa
Temperature	80 F	26.7 C

Fractional value of CST to start ECC recirculation: 0.033

Large LOCA Blowdown

	Enthalpy		Blowdown Rate	
Time, min	Btu/lb	J/kg	lb/min	kg/s
0.0	545.5	261,029	1.0194×10^6	7.707×10^3
0.5	545.5	261,029	1.0194×10^6	7.707×10^3

Water remaining in vessel: 132,010 lb

Calculational Model Input

Core heatup section:

Number of radial zones: 10
Number of axial zones: 24
Meltdown model: BOIL Model A

Core slumping starts when lowest node in region is molten.

Core collapse occurs when 75% of core has melted, or core support reaches melting temperature.

Zircaloy-water reaction: Urbanic-Heidrick reaction rate data, steam limited, continues for melted nodes, reaction of Zircaloy with water in bottom head calculated.

TABLE 6.1 (Continued)

Bottom head failure section:	
Head melting temperature:	2800 F (1538 C)
Debris melting temperature:	4130 F (2277 C)
Heat loss from top of debris:	none
Debris thermal conductivity:	8 Btu/hr ft F (0.1384 W/cm C)
Tensile strength of vessel:	σ = min (80,000, 1.49×10^{16} * TEMP$^{-3.9105}$), lb/in^2
Reactor cavity processes, debris fragmentation:	
Particle diameter:	0.125 inch (0.32 cm)
Particle thermal conductivity:	2 Btu/hr ft F (0.0346 W/cm C)
Reactor cavity processes, concrete decomposition:	
Metal-concrete interface heat transfer coefficient:	HIM = 0.01 W/cm^2 K
Oxide-concrete interface heat transfer coefficient:	HIO = 0.01 W/cm^2 K
Top surface emissivity:	E = 0.5
Heat to cover water:	film boiling and radiation
Containment section:	
Atmosphere-wall heat transfer coefficient:	$h = h_c(TSAT - TWALL) + 0.19(T - TWALL)^{4/3}/(T - TWALL)$ h_c = 0 if TSAT < TWALL 2.0 < h_c = Uchida data < 280 Btu/hr ft^2 F
Containment break area:	7.0 ft^2 for overpressure failure (0.65 m^2)
Failure of safety systems:	
Containment failure fails ECP if sump is saturated.	

TABLE 6.2 ACCIDENT EVENT TIMES

Event	Time, minutes
Peach Bottom AEY	
Core Uncover	1.5
Suppression Pool Cooling On	10.0
Start Melt	11.5
Core Slump	20.8
Containment Fail	33.9
Bottom Head Dry	40.0
Core Collapse	65.2
Bottom Head Fail	126.2
Reactor Cavity Dry	126.3
Start Concrete Attack	126.3
End Calculation	727.0
Peach Bottom TCY	
Containment Heat Removal On	10.0
Containment Fail	58.1
ECC Recirculation On	72.4
ECC Off	72.6
Core Uncover	73.0
Start Melt	93.6
Core Slump	124.6
Bottom Head Dry	136.6
Core Collapse	178.9
Bottom Head Fail	216.6
Reactor Cavity Dry	216.7
Start Concrete Attack	216.7
End Calculation	816.9

TABLE 6.2 (Continued)

Event	Time, minutes
	Peach Bottom TWY
Containment Fail	1756.2
Core Uncover	2619.6
Start Melt	2747.9
Start Slump	2817.1
Core Collapse	2818.9
Bottom Head Dry	2829.3
Bottom Head Fail	3055.2
Reactor Cavity Dry	3055.2
Start Concrete Attack	3055.2
End Calculation	3655.4

TABLE 6.3 CORE AND PRIMARY SYSTEM RESPONSE

Accident Event	Time, minutes	Primary System Pressure, psia	Primary System Water Inventory, lbm	Average Core Temperature, F	Peak Core Temperature, F	Fraction Core Melted	Fraction Clad Reacted
			Peach Bottom AEY				
Core Uncover	1.5	51.5	1.31×10^5	1277	2110	0.	0.
Start Melt	11.5	30.3	1.24×10^5	2233	4130	0.00	0.01
Start Slump	26.8	30.0	1.23×10^5	3229	4170	0.24	0.04
Containment Fail	33.9	132.05	6.58×10^4	2558	4130	0.62	0.34
Bottom Head Dry	40.0	24.2	1.13×10^3	1674	5072	0.62	0.36
Core Collapse	65.2	14.8	9.81×10^2	2805	5995	0.75	0.36
Bottom Head Fail	126.2	14.8	2.22×10^4	3784	---	---	0.36
			Peach Bottom TCY				
Containment Fails	58.1	1237	2.40×10^5	727	922	0.	0.
Core Uncover	73.0	1200	1.97×10^5	682	802	0.	0.
Start Melt	93.6	1149	1.75×10^5	1461	4130	0.00	0.01
Start Slump	124.6	1124	1.575×10^5	3400	4499	0.53	0.26
Bottom Head Dry	136.6	1126	1150	2401	4130	0.50	0.47
Core Collapse	178.9	1120	982.6	3073	4130	0.67	0.47
Bottom Head Fail	216.6	1120	2.39×10^4	3517	---	---	0.47

TABLE 6.3 (Continued)

Accident Event	Time, minutes	Primary System Pressure, psia	Primary System Water Inventory, lbm	Average Core Temperature, F	Peak Core Temperature, F	Fraction Core Melted	Fraction Clad Reacted
			Peach Bottom, TWY				
Containment Fail	1756.2	285.5	6.551×10^5	416	420	0.	0.
Core Uncover	2619.6	170.3	3.39×10^5	372	376	0.	0.
Start Melt	2747.9	170.1	2.31×10^5	1212	4130	0.01	0.01
Start Slump	2817.1	172.0	1.90×10^5	3591	4130	0.77	0.60
Core Collapse	2818.9	171.5	1.61×10^5	4130	4130	0.82	0.61
Bottom Head Dry	2829.9	172.3	1765	1588	---	---	0.61
Bottom Head Fail	3055.2	169.9	1191	3655	---	---	0.61

TABLE 6.4 CONTAINMENT RESPONSE

Accident Event	Time, minutes	Compartment Pressure, psia		Compartment Temperature, F		RWST or CST Water Mass, lbm	Suppression Pool Water		Reactor Cavity Water Mass, lbm	Reactor Cavity Water Temp., F	Steam Cond. on Walls lbm/min
		1	2	1	2		Mass, lbm	Temp., F			
					Peach Bottom, AEY						
Core Uncover	1.5	35.0	35.0	246	171		8.88×10^6	121	2.37×10^4	241	3308/0.*
Spray On	10.0	30.3	30.3	231	122		8.93×10^6	123	2.38×10^4	232	160/25
Start Melt	11.5	30.3	30.3	231	122		8.95×10^6	122	2.39×10^4	230	153/22
Start Slump	26.8	30.4	30.4	235	121		8.95×10^6	121	2.39×10^4	227	0/10
Containment Fail	33.9	131.8	131.8	2031	332		9.0×10^6	129	2.32×10^4	197	0/0
Bottom Head Dry	40.0	15.4	15.4	466	124		9.0×10^6	128	2.26×10^4	172	0/0
Core Collapse	65.2	14.8	14.8	385	188		9.0×10^6	128	2.25×10^4	170	0/0
Bottom Head Fail	126.2	15.4	15.4	194	202		9.0×10^6	128	2.25×10^4	169	0/0
Start Debris/ Water Interaction	126.3	29.3	29.3	490	276				2.25×10^4	169	0/0
Cavity Dryout	126.3	31.7	31.7	488	284		9.02×10^6	131	0.	---	0/0
Start Concrete Attack	126.3	31.5	31.5	487	285		9.02×10^6	131	0.	---	0/0
End Calculation	727.0	15.6	15.6	828	181		9.02×10^6	131	0.	---	0/0
					Peach Bottom, TCY						
Containment Heat Removal On	10.0	18.8	18.8	122	167	2.5×10^6	9.04×10^6	169	288	116	0/291
Containment Fail	58.1	132.6	132.6	326	346	6.11×10^5	11.2×10^6	348	2.41×10^4	207	1061/0
ECC Recirc. On	72.4	90.8	90.8	321	321		11.02×10^6	333	2.41×10^4	207	0/0
ECC Off	72.6	90.5	90.5	321	321	9.94×10^4	11.01×10^6	333	2.41×10^4	207	174/0

* Volume 1/Volume 2

TABLE 6.4 (Continued)

Accident Event	Time, minutes	Compartment Pressure, psia		Compartment Temperature, F		RWST or CST Water Mass, lbm	Suppression Pool Water		Reactor Cavity Water Mass, lbm	Reactor Cavity Water Temp., F	Steam Cond. on Walls lbm/min
		1	2	1	2		Mass, lbm	Temp., F			
						Peach Bottom, TCY (Continued)					
Core Uncover	73.0	89.7	89.7	320	320	9.94×10^4	10.94×10^6	326	2.41×10^4	207	0/0*
Start Melt	93.6	48.8	48.8	280	288	9.94×10^4	10.44×10^6	275	2.41×10^4	207	0/0
Start Slump	124.6	21.8	21.8	230	244	9.94×10^4	9.89×10^6	229	2.41×10^4	207	0/0
Bottom Head Dry	136.6	25.9	25.9	242	260	9.94×10^4	9.85×10^6	236	2.41×10^4	207	0/0
Core Collapse	178.9	15.0	15.0	270	255	9.94×10^4	9.60×10^6	213	2.41×10^4	207	0/0
Bottom Head Fail	216.6	27.7	27.7	655	356	9.94×10^4	9.60×10^6	217	2.41×10^4	207	0/0
Start Debris/ Water Interaction	216.6	25.8	25.8	1231	347	9.94×10^4	9.60×10^6	217	2.41×10^4	207	0/0
Cavity Dryout	216.7	29.9	29.9	496	366	9.94×10^4	9.61×10^6	216	0.		0/0
Start Concrete Attack	216.7	32.1	32.1	443	375	9.94×10^6	9.61×10^6	216	29.	254	0/0
End Calculation	816.9	15.3	15.3	746	272	9.94×10^6	9.54×10^6	209	0.	---	0/0
						Peach Bottom, TWY					
Containment Fail	1756.2	130.1	130.1	324	347	1.025×10^5	11.02×10^6	348	2.45×10^4	158	39/13
Core Uncover	2619.6	15.3	15.3	242	225	1.025×10^5			2.45×10^4	158	
Start Melt	2747.9	15.0	15.0	244	226	1.025×10^5	9.49×10^6	213	2.45×10^4	158	0/0
Start Slump	2817.1	16.8	16.8	225	220						
Core Collapse	2818.9	16.3	16.3	223	218		9.44×10^6	211			

* Volume 1/Volume 2

TABLE 6.4 (Continued)

Accident Event	Time, minutes	Compartment Pressure, psia		Compartment Temperature, F		RWST or CST Water Mass, lbm	Suppression Pool Water		Reactor Cavity Water Mass, lbm	Reactor Cavity Water Temp., F	Steam Cond. on Walls lbm/min
		1	2	1	2		Mass, lbm	Temp., F			
				Peach Bottom, TWY (Continued)							
Bottom Head Dry	2829.3	18.2	18.2	234	223						
Bottom Head Fail	3055.2	15.0	15.0	213	231		9.435×10^6	213	2.45×10^4	158	
Start Debris/ Water Interaction	3055.2	17.2	17.2	467	254				2.45×10^4	158	0/0*
Cavity Dryout	3055.2	21.4	21.4	403	292		9.46×10^6	216	0.		
Start Concrete Attack	3055.2	15.2		397					363	236	
End Calculation	3655.4	15.3	15.3	618	229	1.02×10^5	9.42×10^6	211	0.	0	0/0

* Volume 1/Volume 2

TABLE 6.5 CONTAINMENT LEAK RATES

Revised 7/12/83
Peach Bottom

Subsequence	Time, min	Leak Rate[a] v/min	Drywell Pressure MPa	Drywell Pressure psia	Drywell Temp. °F	Drywell Temp. °C	Wetwell Pressure MPa	Wetwell Pressure psia	Wetwell Temp. °F	Wetwell Temp. °C	Remarks
AEY	0.5	6.9×10^{-6}	0.36	52	283	139	0.36	52	258	126	End of blowdown
	0.5-33.9	6.9×10^{-6}	0.44	64	1093	590	0.44	64	211	100	Core heating and melting
	33.9	2.7	0.91	132	2031	1111	0.91	132	332	167	Containment fails
	33.9-40.0	1.8	0.20	29	1170	632	0.20	29	126	52	Reactor vessel dryout
	40.0-66.0	0.03	0.10	15	385	196	0.10	15	183	84	Vessel heatup
	66.0-126.2	0.03	0.11	15.3	341	172	0.11	15.3	188	87	Vessel melting
	126.2	0.35	0.11	15.4	194	90	0.11	15.4	202	94	Bottom head fails
	126.2-156.3	0.6	0.11	16.4	460	238	0.11	16.4	173	78	Initial concrete attack
	156.3-727	0.06	0.11	15.6	796	425	0.11	15.6	180	82	Concrete decomposition
TCY	58.2	1.5	0.92	133	326	163	0.92	133	347	175	Containment fails
	58.2-124.5	1.5	0.46	67	294	146	0.46	67	296	147	Core heating and melting
	124.5-136.6	1.2	0.17	24	245	118	0.17	24	247	119	Reactor vessel dryout
	136.6-180.0	0.4	0.11	15.8	259	126	0.11	15.8	252	122	Vessel heatup
	180.0-216.6	1.8	0.17	24	1093	589	0.17	24	328	165	Vessel melting
	216.6	2.2	0.14	21	1307	708	0.14	21	320	161	Bottom head fails
	216.6-218.3	1.2	0.15	22	346	174	0.15	22	285	141	Initial concrete attack
	218.3-245.5	0.24	0.12	17	366	186	0.12	17	256	125	Concrete decomposition
	245.5-818.0	0.12	0.11	15.4	648	342	0.11	15.4	274	135	Concrete decomposition
TWY (w/ADS)	1756	2.7	0.91	132	326	163	0.91	132	347	175	Containment fails
	1756-2748	0.24	0.10	15.2	242	117	0.10	15.2	225	107	Core heating and melting
	2748-2819	0.6	0.11	16.3	236	113	0.11	16.3	222	106	Core slumping
	2819-3055	0.24	0.10	15.3	244	118	0.10	15.3	229	109	Vessel heating and melting
	3055	0.25	0.10	15.0	213	101	0.10	15.0	218	103	Bottom head fails
	3055-3085	0.06	0.10	15.2	350	171	0.10	15.2	227	108	Initial concrete attack
	3085-3365	0.03	0.11	15.3	409	209	0.11	15.3	230	110	Concrete decomposition
	3365-3657	0.24	0.11	15.4	614	323	0.11	15.4	228	109	Concrete decomposition

(a) Normalized to a drywell free volume of 1.59×10^5 ft^3. Units are volume fraction/min.

TABLE 6.6 FUEL CHARACTERISTICS IN CYCLE 4 AT BROWNS FERRY UNIT 1[6.2]

Fuel Type	Number of Assemblies	Cycle Inserted	Array Size	Initial U Loading (kg)	Enrichment (%)	Initial Gd Loading (g)	Approximate Burnup[a] (MWd/MT)
2	87	1	7 x 7	187.06	2.50	441	30,400
3	127	1	7 x 7	186.93	2.50	547	23,800
4	140	2	8 x 8	183.361	2.74	292	22,900
5	23	2	8 x 8	183.361	2.74	442	24,000
6	87	3	8 x 8	182.52	2.65	355	16,600
7	68	3	8 x 8	182.32	2.65	537	16,900
8	232	4	8 x 8	182.185	2.84	330	8,900

(a) Burnup calculated through 11 months of Cycle 4 operation.

TABLE 6.7. INVENTORIES OF RADIONUCLIDES AND STRUCTURAL MATERIALS FOR PEACH BOTTOM DURING IN-VESSEL PERIOD OF MELTING

Fission Products		Actinides/Structural	
Element	Mass (kg)	Element	Mass (kg)
Kr	25.7	U	138,000
Rb	23.3	Pu	743
Sr	62.7		
Y	36.2	Cr	4,140
Zr	267	Mn	432
Mo	237	Fe	15,150
Tc	58.8	Ni	2,560
Ru	172	Zr	64,100
Rh	33.2	Sn	1,050
Pd	83.2	Gd	287
Te	34.9		
I	16.6		
Xe	387		
Cs	207		
Ba	105		
La	98.3		
Ce	208		
Pr	80.4		
Nd	271		
Sm	53.8		

TABLE 6.7b. INITIAL INVENTORIES OF ADDITIONAL SPECIES INCLUDED IN GROUPED RELEASE CALCULATIONS

Element	Mass (kg)
Eu	14.1
Nb	4.3
Np	41.2
Pm	11.5

TABLE 6.7c. CORSOR RESULTS WITH AND WITHOUT RSS GROUPINGS FOR THE AE SEQUENCE

	Without RSS Grouping		With RSS Grouping	
Group	Initial Inventory (kg)	Final CORSOR Releases (kg)	Initial Inventory (kg)	Final CORSOR Releases (kg)
Xe	413	413	413	412
I	16.7	16.6*	16.7	16.7*
Cs	207	207*	230	230*
Te	34.8	7.7	34.8	6.9
Sr	NA	NA	168	22.6
Ru	NA	NA	584	29.9
La	NA	NA	2612	1.23
Aerosol	219144	890	218300	835

	Not Grouped	Grouped
CsI	34.1	34.1
CsOH	213	239

*CORSOR releases these species in the form of CsI and CsOH.

TABLE 6.8. CORSOR PREDICTIONS OF FRACTION OF INVENTORY EMITTED BY CORE PRIOR TO VESSEL DRYOUT FOR THE THREE ACCIDENT SEQUENCES FOR PEACH BOTTOM

Species	AE	TC	TW	Core Inventory (kg)
Xe	0.79	0.75	0.94	387
Kr	0.79	0.75	0.94	26
I	0.77	0.73	0.92	17
Cs	0.80	0.75	0.95	207
Te	0.10	0.17	0.41	35
Sr	0.01	0.04	0.10	63
Ba	0.06	0.10	0.21	105
Ru	--	--	0.01	172
Mo	0.03	0.04	0.09	237
Zr (FP)	--	--	--	267
UO_2 [a]	--	--	--	138000
Sn [a]	0.22	0.30	0.52	1050
Zr [a] Clad	--	--	--	64100
Fe [a]	0.01	0.01	0.02	15150

(a) Nonfission product species.

TABLE 6.9. CORSOR PREDICTIONS OF FRACTION OF INVENTORY EMITTED BY CORE PRIOR TO VESSEL FAILURE FOR THE THREE ACCIDENT SEQUENCES FOR PEACH BOTTOM

Species	AE	TC	TW	Core Inventory (kg)
Xe	1.00	0.97	1.00	387
Kr	1.00	0.97	1.00	26
I	1.00	0.95	1.00	17
Cs	1.00	0.98	1.00	207
Te	0.22	0.25	0.48	35
Sr	0.07	0.06	0.12	63
Ba	0.17	0.17	0.27	105
Ru	0.01	0.01	0.01	172
Mo	0.12	0.10	0.16	237
Zr (FP)	--	--	--	267
UO_2[(a)]	--	--	--	138000
Sn[(a)]	0.47	0.44	0.63	1050
Zr[(a)] Clad	--	--	--	64100
Fe[(a)]	0.02	0.02	0.03	15150

(a) Nonfission product species.

TABLE 6.10. CORE RELEASE RATES INTO PRIMARY SYSTEM PREDICTED BY CORSOR FOR AE SEQUENCE FOR THE PEACH BOTTOM PLANT

Time (s)	Mass Release Rate (g/s)			
	Cs	I_2	Te	Aerosol
0	0.0	0.0	0.0	0.0
510	50.4	1.9	0.1	5.3
690	24.3	6.1	0.6	80.6
930	114	9.4	1.3	111
1170	112	9.3	2.1	274
1410	93.7	7.8	2.7	342
1650	194	16.1	2.4	306
1890	24.2	2.0	1.0	117
2130	3.8	0.3	3.8	144
2370	20.0	1.7	0.8	81.0
2610	9.2	0.8	0.4	122
2850	8.8	0.7	0.5	124
3870	5.6	0.5	0.2	33.9
5070	14.8	1.2	0.7	60.4
5670	17.4	1.7	1.4	146
6450	0.1	--	2.2	267
6990	0.0	0.0	1.7	236

TABLE 6.11. CORE RELEASE RATES INTO PRIMARY SYSTEM PREDICTED BY CORSOR FOR TC SEQUENCE FOR THE PEACH BOTTOM PLANT

Time (s)	Mass Release Rate (g/s)			
	Cs	I	Te	Aerosol
0	176	6.2	0.2	11.6
120	27.9	2.1	0.2	22.2
360	46.3	3.8	0.5	67.5
600	59.2	4.9	1.0	122
840	74.6	6.0	1.5	184
1080	74.5	6.2	2.0	244
1320	81.8	6.8	2.6	312
1560	79.5	6.6	3.2	375
1800	125.4	10.4	6.3	590
2040	34.2	2.9	2.4	125
2280	0.8	--	2.3	23.2
2520	3.3	0.3	0.9	26.3
2760	4.2	0.3	0.7	29.5
3000	0.8	--	0.2	4.0
3240	0.0	--	0.2	1.3
3480	0.0	0.0	0.2	2.0
3720	0.0	--	0.3	2.8
4380	0.5	--	0.2	10.4
5460	2.2	0.2	0.2	29.1
7380	5.0	0.4	0.7	81.1
9900	23.8	2.1	0.6	45.4

TABLE 6.12. CORSOR PREDICTIONS OF CORE RELEASE RATES INTO PRIMARY SYSTEM FOR THE TW SEQUENCE FOR THE PEACH BOTTOM PLANT

Time (s)	Cs (g/s)	I_2 (g/s)	Te (g/s)	Aerosol (g/s)
0	83.5	3.5	0.1	14.5
180	13.4	0.7	0.1	12.2
540	14.0	1.2	0.2	28.9
900	22.6	1.7	0.4	50.1
1260	24.1	2.0	0.7	80.9
1620	30.6	2.4	1.0	112
1980	33.1	2.7	1.2	139
2340	33.1	2.6	1.5	168
2700	45.8	3.6	1.8	207
3060	55.8	4.6	2.8	271
3420	88.1	7.3	9.0	481
3780	29.7	2.5	9.4	773
4140	131	10.9	11.7	549
4500	7.8	0.6	0.4	37.2
4860	0.0	0.0	0.0	0.3
8040	0.1	--	0.0	0.7
11940	0.7	0.1	0.1	4.6
13740	1.6	0.1	0.2	13.2
16560	1.6	0.1	0.5	59.9
18590	0.0	0.0	0.6	97.1

TABLE 6.13. MELT COMPOSITION AT TIME OF BOTTOM HEAD FAILURE, EXCLUSIVE OF BOTTOM HEAD MOLTEN MASS, DETERMINED FROM CORSOR PREDICTIONS

Species	Inventory After RPV Failure (kg)		
	AE	TC	TW
Cs	.1	5.1	0.1
I_2	--	0.8	--
Xe	0.5	10.0	0.6
Kr	--	0.7	--
Te	29.2	26.3	17.9
Ba	86.7	87.6	76.3
Sr	58.7	59.0	55.7
Mo	209	213	199
Zr	267	267	267
Ru	171	171	170
Sn	554	591	384
Fe	14918	14919	14759
Zr (Clad)	64090	64090	64083
UO_2	137899	137947	137836

TABLE 6.14. AEROSOL COMPOSITION AND TOTAL RELEASE RATE FOR PEACH BOTTOM, AE

Species, %	Time, sec								
	0	1200	2400	3600	4800	6000	7200	8400	9600
FeO	0.12	5.47	11.54	12.26	12.84	13.37	14.18	15.58	16.32
Cr_2O_3	--	2.62	0.19	0.13	0.11	0.096	0.082	0.071	0.059
Ni	0.07	0.03	0	0	0	0	0	0	0
Mo	3×10^{-8}	6×10^{-6}	4×10^{-6}	4×10^{-6}	3×10^{-6}	3×10^{-6}	2×10^{-6}	2×10^{-6}	1×10^{-6}
Ru	2.4×10^{-7}	4×10^{-5}	3×10^{-5}	3×10^{-5}	2.6×10^{-5}	2×10^{-5}	2×10^{-5}	1×10^{-5}	1×10^{-5}
Sn	0.91	2.89	3.73	3.41	3.09	2.78	2.48	2.27	2.06
Te	0.76	0.98	1.32	1.06	0.86	0.71	0.60	0.52	0.45
Mn	4.63	5.38	11.35	12.06	12.63	13.15	11.90	10.15	8.63
CaO	--	6.04	12.75	13.82	14.55	15.12	15.89	17.24	17.89
Al_2O_3	--	4.99	4.52	5.05	4.97	4.51	3.86	2×10^{-4}	2×10^{-4}
Na_2O	--	0.14	0.26	0.32	0.33	0.34	0.35	0.39	0.38
K_2O	--	6.36	11.44	12.30	12.95	13.52	14.35	15.75	16.45
SiO_2	--	11.78	24.83	26.39	27.62	28.76	30.52	33.52	35.12
UO_2	0.89	1.46	1.29	1.03	0.83	0.66	0.51	0.41	0.33
ZrO_2	6×10^{-3}	0.54	0.074	0.063	0.053	0.043	0.034	0.007	0.008
Cs_2O	31.55	0	0	0	0	0	0	0	0
BaO	34.02	13.68	2.61	1.85	1.40	1.10	0.90	0.77	0.65
SrO	22.96	10.15	2.60	1.43	0.90	0.607	0.437	0.34	0.26
La_2O_3	1.8×10^{-4}	10.53	3.57	2.94	2.40	1.903	1.46	1.13	1×10^{-4}
CeO_2	4.22	16.88	7.87	5.88	4.45	3.34	2.46	1.85	1.39
Nb_2O_5	9×10^{-7}	5×10^{-5}	9×10^{-5}	7×10^{-5}	6×10^{-5}	5×10^{-5}	3×10^{-5}	3×10^{-5}	2×10^{-5}
CsI	0.616	0.062	0	0	0	0	0	0	0
Source Rate, g/sec	201	613	336	283	253	230	212	189	176

TABLE 6.14. (Continued)

Species, %	Time, sec						
	T0800	T2000	T3200	T4400	T5600	T6800	T8000
FeO	16.74	17.05	17.33	17.59	19.15	21.08	1.02
Cr_2O_3	0.05	0.04	0.04	0.04	0.035	0.033	0.38
Ni	0	0	0	0	0	0	0
Mo	1×10^{-6}	8×10^{-7}	7×10^{-7}	6×10^{-7}	6×10^{-7}	5.6×10^{-7}	0.002
Ru	8×10^{-6}	7×10^{-6}	6×10^{-6}	5×10^{-6}	5×10^{-6}	4.6×10^{-6}	2×10^{-5}
Sn	1.88	1.75	1.63	1.53	1.53	1.55	27.44
Te	0.38	0.33	0.29	0.25	0.24	0.23	1.08
Mn	7.44	6.54	5.79	5.14	5.00	4.85	22.98
CaO	18.22	18.49	18.72	18.92	20.51	22.50	7.41
Al_2O_3	2×10^{-4}	2×10^{-4}	2×10^{-4}	2×10^{-4}	2×10^{-4}	3×10^{-4}	1.5×10^{-3}
Na_2O	0.39	0.39	0.40	0.39	0.43	0.48	0.13
K_2O	16.81	17.03	17.17	17.25	18.51	19.91	28.63
SiO_2	36.01	36.69	37.29	37.85	33.76	28.77	5.80
UO_2	0.272	0.233	0.202	0.175	0.163	0.154	5.06
ZrO_2	8×10^{-3}	8×10^{-3}	8×10^{-3}	8×10^{-3}	9×10^{-3}	0.096	0.050
Cs_2O	0	0	0	0	0	0	0
BaO	0.54	0.45	0.36	0.29	0.23	0.16	0.018
SrO	0.20	0.16	0.12	0.094	0.073	0.048	4.8×10^{-4}
La_2O_3	1×10^{-4}	1×10^{-4}	1×10^{-4}	9×10^{-5}	1×10^{-4}	1×10^{-4}	5×10^{-4}
CeO_2	1.06	0.83	0.64	0.47	0.35	0.22	1×10^{-3}
Nb_2O_5	1.7×10^{-5}	1.4×10^{-5}	1.3×10^{-5}	1.2×10^{-5}	1.2×10^{-5}	1.3×10^{-5}	2.3×10^{-3}
CsI	0	0	0	0	0	0	0
Source Rate, g/sec	169	164	159	154	134	116	22

TABLE 6.15. AEROSOL COMPOSITION AND TOTAL RELEASE RATE FOR PEACH BOTTOM, TC

Species, %	Time, sec								
	0	1200	2400	3600	4800	6000	7200	8400	9600
FeO	6.03	4.82	8.64	15.38	15.88	16.36	16.86	17.47	17.87
Cr_2O_3	--	3.90	0.17	0.27	0.22	0.18	0.15	0.12	0.096
Ni	0.08	0.84	0.21	1.6×10^{-6}	--	--	--	--	--
Mo	--	1.7×10^{-6}	1.1×10^{-6}	1.6×10^{-6}	1.3×10^{-6}	1.1×10^{-6}	8×10^{-7}	6×10^{-7}	4×10^{-7}
Ru	--	1.3×10^{-5}	8.3×10^{-6}	1.2×10^{-5}	1×10^{-5}	8.2×10^{-6}	6.1×10^{-6}	4.4×10^{-6}	3.3×10^{-6}
Sn	0.14	0.65	0.75	1.49	1.13	1.04	0.92	0.80	0.72
Te	0.22	0.28	0.38	0.61	0.57	0.52	0.57	0.44	0.41
Mn	1.41	4.74	5.58	8.66	7.80	6.97	6.10	5.34	4.76
CaO	--	5.26	9.46	17.04	17.65	18.12	18.50	18.96	19.24
Al_2O_3	--	4.40	7.89	1.70	1.63	1.44	1.18	1.4×10^{-4}	1.5×10^{-4}
Na_2O	--	0.13	0.20	0.40	0.41	0.42	0.42	0.43	0.42
K_2O	--	6.65	11.32	14.56	15.11	15.60	16.08	16.64	16.98
SiO_2	--	10.39	18.63	33.14	34.22	35.26	36.32	37.62	38.47
UO_2	0.08	1.12	0.84	1.10	0.85	0.66	0.43	0.36	0.28
ZrO_2	6×10^{-3}	3.33	0.59	0.043	0.035	0.028	0.022	6.7×10^{-3}	6.7×10^{-3}
Cs_2O	25.92	--	--	--	--	--	--	--	--
BaO	20.65	13.26	0.30	0.012	9×10^{-3}	7×10^{-3}	6×10^{-3}	5×10^{-3}	4×10^{-3}
SrO	17.23	8.94	9×10^{-5}						
La_2O_3	1.5×10^{-5}	14.05	8.28	2.43	1.93	1.50	1.11	0.80	8.5×10^{-5}
CeO_2	2.06	14.95	26.56	3.26	2.39	1.75	1.23	0.86	0.63
Nb_2O_5	8×10^{-7}	1.6×10^{-5}	1.8×10^{-5}	1.1×10^{-4}	8.7×10^{-5}	6.8×10^{-5}	4.9×10^{-5}	3.4×10^{-5}	2.6×10^{-5}
CsI	15.46	1.78	6×10^{-14}	--	--	--	--	--	--
Source Rate, g/sec	219	696	449	225	204	188	178	168	160

TABLE 6.15. (Continued)

Species, %	Time, sec								
	10800	12000	13200	14400	15600	16800	18000	19200	20400
FeO	18.05	18.19	18.32	18.44	18.56	19.86	0.69	0.94	1.22
Cr_2O_3	0.073	0.068	0.060	0.053	0.046	0.042	0.30	0.70	0.78
Ni	--	--	--	--	--	--	--	--	--
Mo	3.5×10^{-7}	2.9×10^{-7}	2.5×10^{-7}	2.1×10^{-7}	1.8×10^{-7}	1.6×10^{-7}	4.2×10^{-4}	3.6×10^{-4}	3.2×10^{-4}
Ru	2.7×10^{-6}	2.3×10^{-6}	1.9×10^{-6}	1.6×10^{-6}	1.4×10^{-6}	1.3×10^{-6}	5×10^{-6}	3.6×10^{-6}	2.3×10^{-6}
Sn	0.66	0.60	0.57	0.53	0.50	0.49	6.82	7.00	7.15
Te	0.377	0.352	0.331	0.311	0.292	0.297	1.29	1.49	1.72
Mn	4.30	3.96	3.67	3.40	3.20	3.16	13.60	14.22	14.64
CaO	19.33	19.40	19.47	19.54	19.59	20.90	4.68	5.42	5.46
Al_2O_3	1.6×10^{-4}	1.6×10^{-4}	1.7×10^{-4}	1.7×10^{-4}	1.8×10^{-4}	1.9×10^{-4}	9×10^{-4}	1.2×10^{-3}	1.7×10^{-3}
Na_2O	0.42	0.42	0.40	0.41	0.41	0.44	0.12	0.23	0.43
K_2O	17.11	17.17	17.19	17.18	17.12	18.03	21.40	26.74	35.36
SiO_2	38.86	39.17	39.44	39.70	39.95	36.51	47.21	39.72	30.06
UO_2	0.230	0.194	0.165	0.141	0.121	0.111	2.98	2.66	2.20
ZrO_2	6.6×10^{-3}	6.6×10^{-3}	6.5×10^{-3}	6.5×10^{-3}	6.5×10^{-3}	6.8×10^{-3}	0.031	0.039	0.048
Cs_2O	--	--	--	--	--	--	--	--	--
BaO	3.4×10^{-3}	2.8×10^{-3}	2.3×10^{-3}	1.8×10^{-3}	1.4×10^{-3}	9.1×10^{-4}	1.6×10^{-4}	1.9×10^{-4}	1.5×10^{-4}
SrO	--	--	--	--	--	--	--	--	--
La_2O_3	7.8×10^{-5}	7.4×10^{-5}	7.4×10^{-5}	6.6×10^{-5}	6.3×10^{-5}	6.4×10^{-5}	2.8×10^{-4}	3.5×10^{-4}	4.4×10^{-4}
CeO_2	0.469	0.357	0.270	0.196	0.133	0.081	6.6×10^{-4}	6.3×10^{-4}	6.1×10^{-4}
Nb_2O_5	2.1×10^{-5}	1.8×10^{-5}	1.6×10^{-5}	1.4×10^{-5}	1.3×10^{-5}	1.4×10^{-5}	1.6×10^{-3}	1.3×10^{-3}	2.7×10^{-6}
CsI	--	--	--	--	--	--	--	--	--
Source Rate, g/sec	157	154	151	147	138	123	26.5	36.4	24.8

TABLE 6.16. AEROSOL COMPOSITION AND TOTAL RELEASE RATE FOR PEACH BOTTOM, TW

Species, %	Time, sec								
	0	1200	2400	3600	4800	6000	7200	8400	9600
FeO	2.14	5.17	9.15	14.21	14.49	14.76	15.61	17.80	18.12
Cr_2O_3	--	3.33	0.111	0.152	0.127	0.108	0.094	0.085	0.069
Ni	0.140	1.00	0.330	--	--	--	--	--	--
Mo	1×10^{-8}	1.6×10^{-6}	1×10^{-6}	1.3×10^{-6}	1×10^{-6}	8×10^{-7}	6×10^{-7}	5×10^{-7}	4×10^{-7}
Ru	1×10^{-7}	1.3×10^{-5}	8.4×10^{-6}	1.1×10^{-5}	9×10^{-6}	7×10^{-6}	5×10^{-6}	4×10^{-6}	3×10^{-6}
Sn	0.113	0.365	0.410	0.584	0.537	0.486	0.440	0.425	0.378
Te	0.232	0.184	0.252	0.352	0.323	0.295	0.277	0.281	0.259
Mn	2.29	4.93	5.66	7.69	6.85	6.06	5.45	5.26	4.67
CaO	20.01	7.51	11.73	17.83	17.81	17.75	18.29	20.36	20.37
Al_2O_3	4×10^{-3}	4.72	8.36	12.97	13.23	13.48	10.52	0.003	0.003
Na_2O	11.14	0.136	0.207	0.370	0.365	0.353	0.368	0.417	0.400
K_2O	--	6.46	10.44	12.75	13.05	13.32	14.09	16.05	16.28
SiO_2	--	11.13	19.71	30.59	31.19	31.78	33.60	38.32	39.01
UO_2	0.029	0.302	0.254	0.329	0.277	0.228	0.186	0.160	0.130
ZrO_2	4×10^{-3}	1.36	0.349	0.015	0.012	0.010	0.008	0.004	0.004
Cs_2O	0.346	--	--	--	--	--	--	--	--
BaO	6.13	14.20	1.96	0.056	0.048	0.041	0.036	0.033	0.026
SrO	5.69	9.59	0.672	0.013	0.011	0.009	0.007	0.006	0.005
La_2O_3	6.6×10^{-5}	12.27	5.60	1.15	0.931	0.730	0.554	0.437	4×10^{-5}
CeO_2	0.752	15.96	24.67	0.78	0.602	0.452	0.331	0.248	0.166
Nb_2O_5	3×10^{-7}	8×10^{-6}	8×10^{-6}	6×10^{-5}	5×10^{-5}	4×10^{-5}	3×10^{-5}	3×10^{-5}	2×10^{-5}
CsI	--	--	--	--	--	--	--	--	--
Source Rate, g/sec	128	649	424	244	224	209	192	165	158

TABLE 6.16. (Continued)

Species, %	Time, sec								
	10800	12000	13200	14400	15600	16800	18000	19200	20400
FeO	19.53	22.79	0.745	1.03	1.27	1.48	1.64	1.71	1.72
Cr_2O_3	0.061	0.048	1.001	1.31	1.43	1.46	1.43	1.22	0.90
Ni	--	--	--	--	--	--	--	--	--
Mo	3×10^{-7}	3×10^{-7}	8×10^{-4}	8×10^{-4}	8×10^{-4}	9×10^{-4}	1×10^{-3}	9×10^{-4}	8×10^{-4}
Ru	3×10^{-6}	3×10^{-6}	1×10^{-5}	9×10^{-6}	9×10^{-6}	8×10^{-6}	7×10^{-6}	5×10^{-6}	3×10^{-6}
Sn	0.367	0.397	5.72	5.86	6.04	6.27	6.52	6.51	6.65
Te	0.256	0.278	1.173	1.181	1.194	1.213	1.242	1.377	1.533
Mn	4.51	4.81	19.74	19.63	19.88	19.90	19.98	20.19	20.08
CaO	21.68	25.10	10.10	9.95	9.83	9.78	9.71	10.78	10.20
Al_2O_3	3×10^{-3}	3×10^{-3}	0.015	0.015	0.016	0.017	0.018	0.022	0.027
Na_2O	0.420	0.352	0.185	0.247	0.296	0.340	0.379	0.448	0.573
K_2O	17.71	18.86	17.86	19.23	20.58	22.07	23.59	28.37	35.31
SiO_2	35.41	26.09	38.84	36.95	34.86	32.87	30.83	25.00	18.33
UO_2	0.117	0.120	3.312	3.06	3.00	2.97	2.96	2.65	2.31
ZrO_2	4×10^{-3}	5×10^{-3}	0.022	0.023	0.024	0.025	0.026	0.032	0.040
Cs_2O	--	--	--	--	--	--	--	--	--
BaO	0.019	0.007	0.004	0.004	0.004	0.004	0.004	0.004	0.004
SrO	3×10^{-3}	1×10^{-3}	2×10^{-5}	2×10^{-5}	2×10^{-5}	2×10^{-7}	3×10^{-7}	3×10^{-7}	4×10^{-7}
La_2O_3	4×10^{-5}	5×10^{-5}	2×10^{-4}	2×10^{-4}	2×10^{-4}	2×10^{-4}	3×10^{-4}	3×10^{-4}	4×10^{-4}
CeO_2	0.108	0.034	7×10^{-4}	6×10^{-4}	6×10^{-4}	5×10^{-4}	5×10^{-4}	5×10^{-4}	5×10^{-4}
Nb_2O_5	2×10^{-5}	4×10^{-5}	2×10^{-3}	2×10^{-3}	2×10^{-3}	2×10^{-3}	2×10^{-3}	2×10^{-3}	2×10^{-6}
CsI	--	--	--	--	--	--	--	--	--
Source Rate, g/sec	145	123	27.3	24.9	21.9	19.3	17.9	25.5	17.9

7. RESULTS AND DISCUSSION

7.1 Introduction

Results of calculations for the transport and deposition of radionuclides are presented and discussed in this section. The plants and sequences selected for consideration were discussed in Chapter 4, the analytical and calculational methods were described in Chapter 5, and the assumptions and bases for the calculations were described in Chapter 6. Results presented in this chapter include the deposition and release from the reactor coolant system of radionuclides leaving the core region. These results are based on TRAP-MELT code calculations. Also included as results are the masses of radionuclides airborne and deposited in the containment and suppression pool, as well as the airborne materials leaked to the environment. These results are based on SPARC calculations for retention in the suppression pool and NAUA-4 calculations for transport in the containment and reactor buildings.

Three accident sequences are considered in the analyses: AE, TC, and TW. In each sequence failure of the primary containment was assumed to result in a direct pathway for the release of radioactivity to the environment. This is the most severe failure mode (referred to as γ') from the viewpoint of the magnitude of fission product source term to the environment. Additionally for the TC sequence, the potential influence of the reactor building was examined by assuming the reactor building maintains its integrity following failure of the primary containment (γ failure mode). Retention in the reactor building is also a possibility for the AE and TW system sequences. No attempt is made in this report to estimate the relative likelihoods of the γ' and γ failure modes.

7.2 Transport and Deposition in Reactor Coolant System (RCS)

The analyses of the transport and deposition within the RCS of materials released from the melting core have been performed using the TRAP-MELT 2 code. The time frame of interest in the RCS for core meltdown accidents such as those considered here spans the period of time starting with the onset of core melting and ending with failure of the bottom head of the RPV. For accidents involving only minor fuel damage, the gap release term, which occurs

prior to melting of fuel, may be the major release and require careful consideration. For the accidents examined here, however, this release term is insignificant in comparison with the melt release and the period immediately prior to the onset of core melting is not considered. Rather, the gap releases calculated by CORSOR are added to the initial material emitted by the melting core.

Releases from the melting core and their behavior in the RCS are evaluated beyond the time of core collapse in these analyses. This differs from the analyses presented in Volume I of this report wherein the source to the RCS was assumed to go to zero when the core slumped into the residual water in the lower plenum. In the analyses of the Peach Bottom sequences presented here, the slumping of the core has been simulated in MARCH on a nodal basis as discussed earlier. This change and the presence of much greater below core structures in the BWR pressure vessel dictate that emission from nodes which have left the core be included in the analyses.

Another significant difference in the RCS phenomenology for the BWR sequences is the prediction of a significant time period between RPV dry out and RPV failure. During this period, the melting core emits fission products into an essentially stagnant RCS, since there is no water available to provide the steam as a carrier. The duration of time between vessel dryout and bottom head failure is predicted by MARCH to be 78, 104, and 225 minutes for the AE, TC, and TW sequences, respectively. This residence time will be seen to result in significant attenuation of the aerosol.

It should be recognized that the uncertainties in the behavior of the molten core in the lower plenum region are quite large. The analyses performed by the MARCH 2 code for this phase of the accident are greatly simplified. The rates of steam production as molten core material enters the lower plenum and the duration of time to failure of the reactor vessel have large associated uncertainties. While the MARCH code is well suited to the exploration of the effects of various assumptions on the overall results, practical considerations have limited the extent of such exploration.

The heatup of the RCS structures downstream of the core is not modeled following dryout of the vessel. This is not expected to be a significant source of error since the surface temperatures in the core region are too high to permit condensation of the volatile species considered in these

analyses prior to this period and there is little subsequent emission of these species from the core.

At the time of bottom head failure, the materials suspended in the RCS are assumed to exit the primary system through the bottom head without further attenuation. This results in a short duration "puff" release of aged material into the drywell at the time of vessel failure. Re-entrainment of previously deposited particles or vapors is not considered to occur during this process.

One further aspect of the time frame of the primary system analyses which should be noted is that the primary system is not considered in the analyses after the molten core has left the RPV. Air ingress into the RPV and deposition of materials evolved during the core-concrete interaction is not considered, nor is the primary system considered as a potential source of fission products due to reevolution of previously deposited materials.

The analyses presented in the following section are subject to a number of uncertainties. Principal among these are the source rates of materials emitted by the core, and the details of the flow patterns in the RCS. An additional aspect of the flow or, more precisely, the lack of flow during these sequences which represents a source of uncertainty is the duration of the "stagnant" phase of in-vessel portion of the melt down.

The results of the analyses of the AE, TC, and TW sequences for the Peach Bottom plant are discussed separately in the following sections. The flow paths, associated geometry, and the timing of the core-melt period in the RCS can be found in Chapter 6.

7.2.1 RCS Transport and Deposition for Sequence AE

This sequence resembles, in several respects, the AB sequence analyzed for the Surry plant in Volume I of this report. The principal similarity between these two is that, due to the location of the assumed large break, the materials released from the melting core transit only a very limited portion of the primary system during their release to the "containment". Here, the notion of "containment" is a bit more involved than was the case for the PWR and this will be discussed at length later in this document. The primary system components of interest here are the core region, the steam separators, and the lower annulus to the intake of the recirculation loop.

Table 7.1 presents the total masses (Total) of the RSS species groups of interest which have been emitted into the RCS as a function of time during the in-vessel portion of the melt. These values, of course, increase monotonically with time, though not linearly due to the nature of the release process. It is interesting to note that, on this time scale, vessel dryout occurs at t = 1710 s. Thus, about 20 percent of the CsI and CsOH are emitted into a stagnant RCS, and over 50 percent of the Te and aerosol are emitted during this period. This table also indicates that the mass of vapor species retained in the RCS first increases, then decreases as surfaces in the system heat up due to the high temperature steam flow out through the break. The aerosol retention does not exhibit any similar behavior since no resuspension mechanisms are included in the TRAP-MELT code. It is interesting to note the fairly dramatic increase in aerosol retention which occurs during the stagnant portion of this sequence. This is due to the agglomeration of the particles to form larger sizes and subsequently enhanced settling of the particles in the RCS. Of course, there is no similar mechanism for the vapor species and their retained amount remains essentially unchanged during this period.

Table 7.2 expresses these results in terms of retention factors (RF) which are simply defined as Ret/Total in Table 7.1. These values pertain to the entire RCS and are integral in nature, so that the final value (i.e., at t = 6360 s, which is the time at which bottom head failure occurs) can be taken to be the RCS retention factor which characterizes the sequence. The values listed under Lower Annulus for CsI, CsOH, and Te indicate the retention factor for that control volume. These values are also based on the total mass of the species emitted from the core and therefore do not represent true efficiencies of retention for the control volume. Figures 7.1 through 7.4 illustrate the masses of each species retained in key volumes of the RCS, and the total amounts emitted by the core as functions of time during the in-vessel period of core melting.

The retention factors for the aerosol in the core and in the steam separators illustrate the basic features of the aerosol behavior. The retention in the core region is well under 10 percent until after vessel dryout occurs. Then, as the aerosol ages and the core continues to inject aerosol mass into the stagnant system, the removal of aerosol mass in the core becomes increasingly effective. This is also indicated by the increase in the aerosol mass median diameter which is calculated from the discrete aerosol size

TABLE 7.1. CORSOR PREDICTIONS OF MASSES OF SPECIES RELEASED FROM THE CORE (TOTAL) AND TRAP-MELT PREDICTIONS OF MASSES RETAINED IN THE RCS (RET) DURING THE AE SEQUENCE FOR THE PEACH BOTTOM PLANT FOR THE RSS SPECIES GROUPS[a]

(Times Measured from Start of Core Melting)

Time (s)	CsI		CsOH		Te		Aerosol	
	Ret (kg)	Total (kg)	Ret (kg)	Total (kg)	Ret (kg)	Total (kg)	Ret (kg)	Total (kg)
500	0.0	1.7	0.4	21.3	0.0	0.1	0.1	7.4
1000	2.7	8.3	20.4	66.2	0.2	0.4	20.7	62.2
1498	9.3	16.9	65.4	124	0.7	1.1	102	189
1997	6.2	25.7	44.4	183	0.6	2.3	110	295
2497	6.3	26.9	42.5	192	0.7	3.1	112	351
3997	6.3	28.8	42.7	204	0.7	3.6	237	465
4994	6.3	30.5	43.3	215	0.7	4.0	264	496
5994	6.3	33.1	44.3	233	0.8	5.1	359	606
6491	6.3	33.9	45.0	238	0.8	6.0	467	719
6990	6.3	34.1	45.6	240	0.9	6.9	584	834

(a) See Table 6.7c.

TABLE 7.2. TRAP-MELT PREDICTIONS OF PRIMARY SYSTEM RETENTION FACTORS (RF) AND VOLUME SPECIFIC RETENTION FACTORS AS FUNCTIONS OF TIME FOR THE AE SEQUENCE FOR THE PEACH BOTTOM PLANT

Time (s)	CsI		CsOH		Te		Aerosol		
	RF	Lower Annulus	RF	Lower Annulus	RF	Lower Annulus	RF	Core	Steam Sep
500	.01	.01	.02	.02	.20	.01	.02	.01	.0
1000	.32	.20	.31	.20	.44	.14	.33	.01	.14
1498	.55	.27	.53	.27	.69	.21	.54	.06	.26
1997	.24	.24	.24	.24	.26	.09	.37	.04	.18
2497	.23	.23	.22	.22	.21	.08	.32	.04	.15
3997	.22	.22	.21	.21	.19	.07	.51	.29	.12
4994	.21	.21	.19	.19	.18	.06	.53	.33	.11
5994	.19	.19	.19	.18	.15	.05	.59	.43	.09
6491	.19	.19	.19	.18	.13	.04	.65	.51	.08
6990	.19	.19	.19	.17	.13	.04	.70	.58	.07

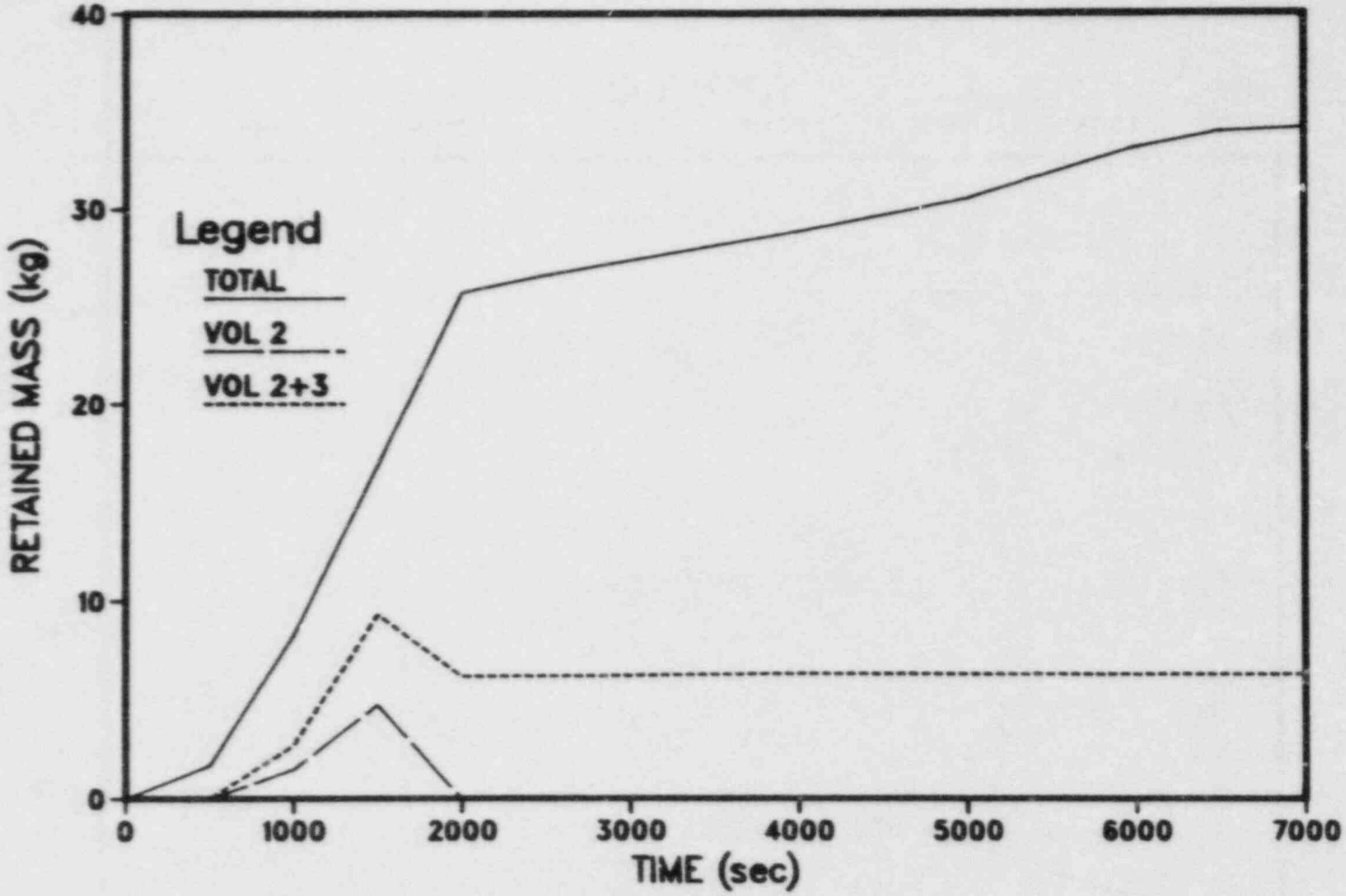

FIGURE 7.1. MASSES OF CsI EMITTED FROM CORE AND RETAINED IN THE RCS CONTROL VOLUMES AS FUNCTIONS OF TIME FOR THE AE SEQUENCE (Vol 1 = Core, Vol 2 = Steam Separators, Vol 3 = Lower Annulus, Vol 4 = Drywell). Times Measured from Start of Core Melting.

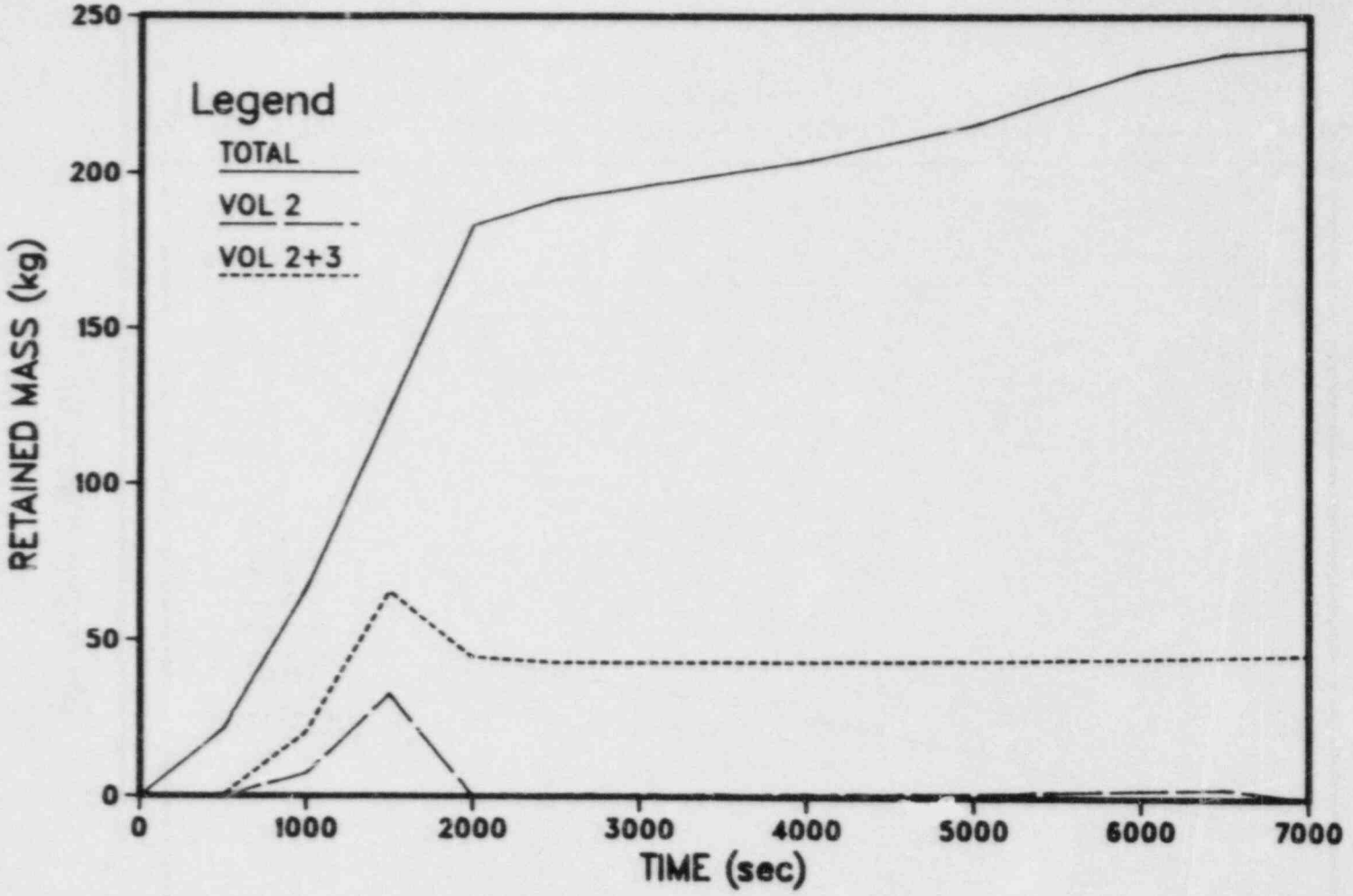

FIGURE 7.2. MASSES OF CsOH EMITTED FROM CORE AND RETAINED IN THE RCS CONTROL VOLUMES AS FUNCTIONS OF TIME FOR THE AE SEQUENCE (Vol 1 = Core, Vol 2 = Steam Separators, Vol 3 = Lower Annulus, Vol 4 = Drywell). Times Measured from Start of Core Melting.

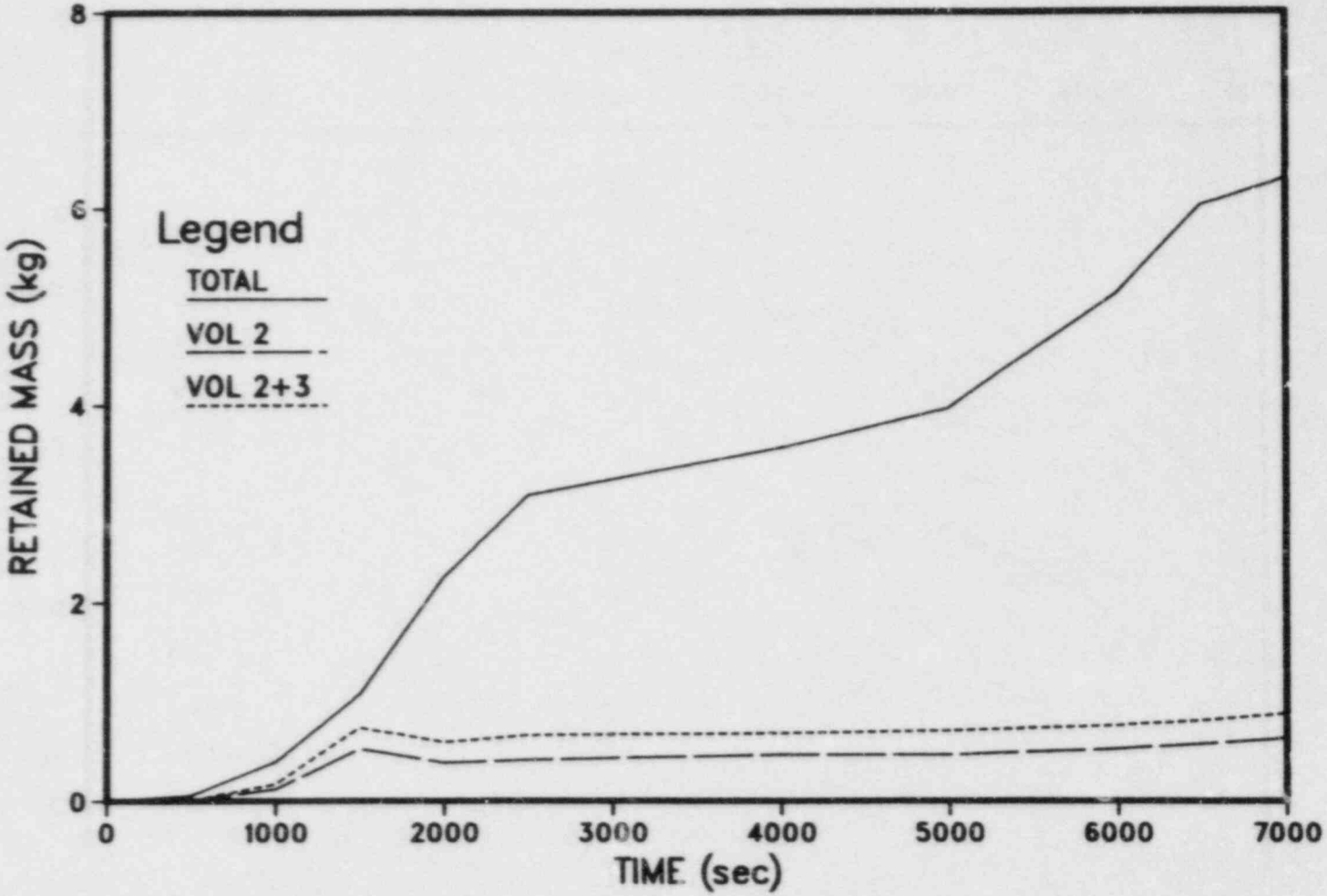

FIGURE 7.3. MASSES OF Te EMITTED FROM CORE AND RETAINED IN THE RCS CONTROL VOLUMES AS FUNCTIONS OF TIME FOR THE AE SEQUENCE (Vol 1 = Core, Vol 2 = Steam Separators, Vol 3 = Lower Annulus, Vol 4 = Drywell). Times Measured from Start of Core Melting.

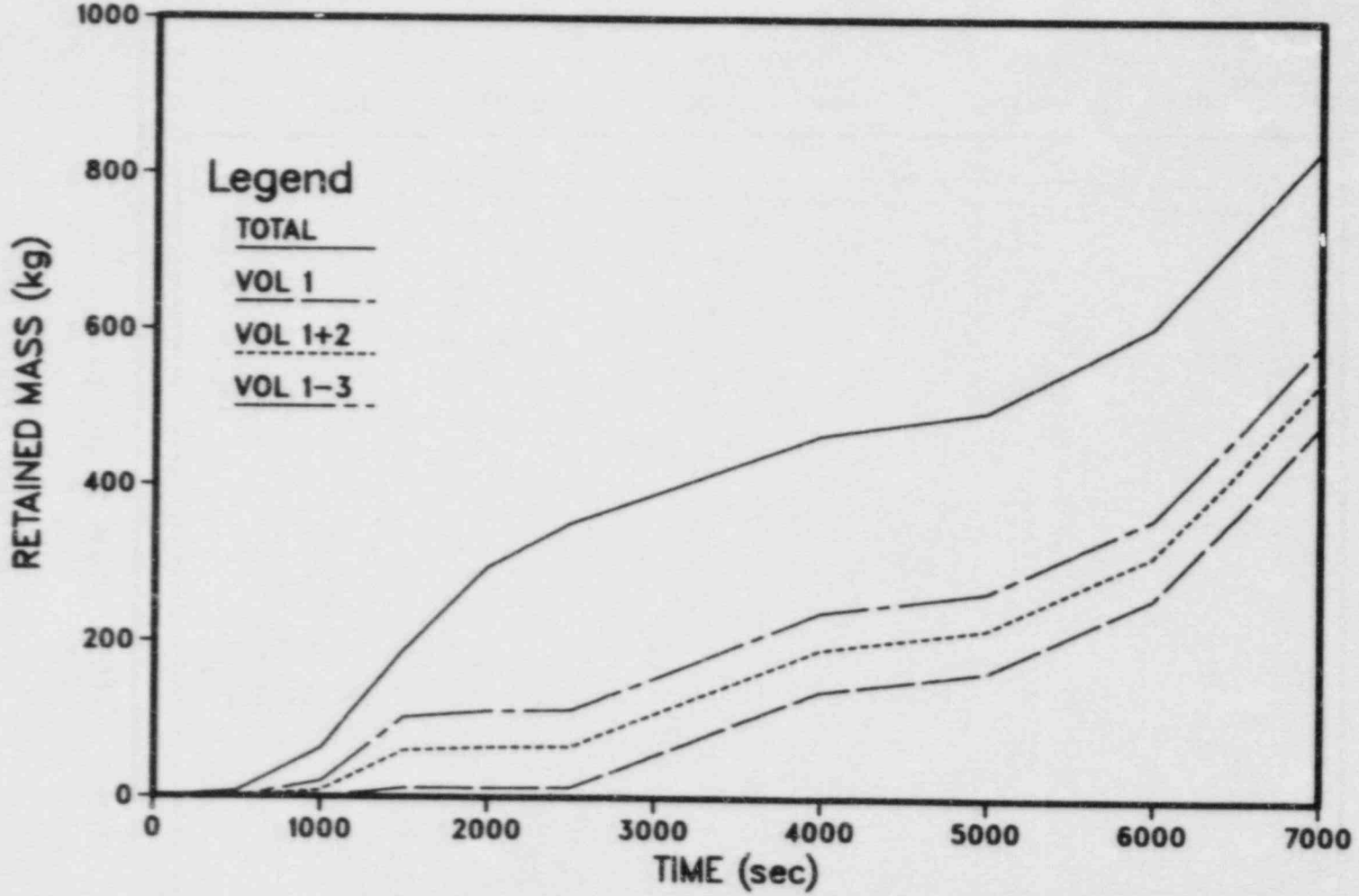

FIGURE 7.4. MASSES OF AEROSOL EMITTED FROM CORE AND RETAINED IN THE RCS CONTROL VOLUMES AS FUNCTIONS OF TIME FOR THE AE SEQUENCE (Vol 1 = Core, Vol 2 = Steam Separators, Vol 3 = Lower Annulus, Vol 4 = Drywell). Times Measured from Start of Core Melting.

distribution followed through the TRAP-MELT calculations. At t = 1800 s, the mass median diameter is 0.188 μm, and by t = 4800 s, it has increased to 2.76 μm, which, of course, leads to an enhanced removal rate for the aerosol via gravitational settling. A further note regarding the aerosol retention values in this table concerns the values of the retention in the steam separator. The decrease evident after t = 1770 should not be misinterpreted to indicate a resuspension of previously deposited aerosol. Rather, it is merely a consequence of the fact that the total aerosol mass emitted by the core has continued to increase while the amount retained in the steam separators is fixed, due to the absence of flow.

The source to the drywell for this sequence can be characterized as a fairly steady injection rate up to the time of vessel dryout. During this period, approximately 30 percent of the CsI, CsOH, and Te passing through the RCS is retained, as is just over half of the aerosol. There is then no source until the bottom head fails, at which time the suspended materials in the RCS are injected into the drywell. No further emissions from the RCS are considered in these analyses.

The simulation of the AE case was performed using TRAP-MELT to track the RCS retention of the WASH-1400 radionuclide groups as described in Chapter 6, and the results are summarized in Table 2a. The retention of groups I, Cs, and Te is consistent with that previously noted for CsI, CsOH, and Te. The Sn and Ru groups closely parallel the retention of the total aerosol throughout the sequence. At various times during the sequence, the La group varies as much as 19 percent from the retention of inert aerosol. However, at the time of bottom head failure, the retention of La is very nearly the same as the other aerosols. This interesting behavior is primarily the result of the timing of releases of various groups with respect to the varying gas flow rate through the RCS.

7.2.2 RCS Transport and Deposition for Sequence TC

In this postulated accident sequence, the RCS is essentially at operating pressure up until bottom head failure, making this sequence somewhat analogous to the TMLB' sequence studied in Volume I for the Surry PWR. During the in-vessel phase of the meltdown the flow pathway exits the RCS through the relief lines which transmit the gases and fission products to the suppression

TABLE 7.2a. CORSOR PREDICTIONS OF RELEASE FROM CORE AND TRAP-MELT PREDICTIONS OF PRIMARY SYSTEM RETENTION OF WASH-1400 GROUPS FOR AE SEQUENCE

Group	Released (kg)	Retained (kg)
I	16.7	3.1
Cs	230.9	43.8
Te	6.9	0.9
Sr	22.6	16.1
Ru	30.0	23.3
La	1.19	0.89

*Groups are defined in Chapter 6.

pool. The flow pathway and relevant geometry were presented in an earlier section, so it is sufficient to simply restate that the flow passes through the steam separators and then splits, with about 85% considered to pass through the steam dryers, and the remainder bypassing the dryers via the outer annulus. These flows then merge at the steam lines and enter the relief lines to the pool.

Table 7.3 presents the total masses of the various species emitted from the core (Total) as functions of time during this sequence, and the mass retained in the RCS at any time. Following from the CORSOR results, these sources to the RCS are only on the order of half what the values for the AE sequence were predicted to be. Vessel dryout for this sequence occurs at t = 3720 on this time scale, by which time the CsI and CsOH emissions are nearly completed. The masses retained in this sequence are considerably less than for AE, partly due to the reduction in the source term for the RCS and partly due to the differing system thermal hydraulics. An interesting feature of this table is the larger retention predicted for CsOH, in comparison with the retention of CsI. The cause of this apparent discrepancy is that the mechanism of CsOH retention is chemical reaction with surfaces, which is not a viable process for CsI. This difference between CsI and CsOH retention is emphasized in Table 7.4, which contains the RCS retention factors, along with several volume specific values as defined above. Figures 7.5 and 7.6 illustrate retained masses of these species.

The relatively large surface area of the steam dryers is reflected in their large contribution to the reaction of the CsOH and Te. These vapors which react are considered to be irreversibly bound to the surface in all sequences examined here. The location of retained Te is indicated in Figure 7.7. The aerosol retention in this sequence exhibits similar behavior to that observed in the AE results, but on a less impressive scale as is shown in Figure 7.8. The increase in aerosol RF from 0.43 just before vessel dryout to 0.51 at the time of bottom head failure is, again, due to the aging of the particles in the stagnant core region of the RCS. That the increase in the RF is not greater than what appears in this table is due to the lower rate of aerosol generation predicted for this sequence.

TABLE 7.3. CORSOR PREDICTIONS OF MASSES OF SPECIES RELEASED FROM THE CORE (TOTAL) AND TRAP-MELT PREDICTIONS OF MASSES RETAINED IN THE RCS (RET) DURING THE TC SEQUENCE FOR THE PEACH BOTTOM PLANT

(Times Measured from the Start of Core Melting)

Time (s)	CsI		CsOH		Te		Aerosol	
	Ret (kg)	Total (kg)	Ret (kg)	Total (kg)	Ret (kg)	Total (kg)	Ret (kg)	Total (kg)
370	0.4	3.3	4.3	27.3	--	0.1	1.5	13.1
740	3.8	8.1	28.2	56.4	0.2	0.4	22.5	55.3
1100	9.3	13.5	62.9	90.0	0.7	0.9	81.6	129
1480	15.2	18.9	99.0	123	1.4	1.6	175	236
2210	1.9	26.8	40.0	171	10.6	11.0	232	648
2580	2.0	27.6	43.0	175	11.4	11.8	240	770
2950	2.0	27.9	44.4	177	11.7	12.1	288	875
3320	2.1	28.0	45.3	178	11.9	12.2	346	978
3690	2.1	28.2	45.9	179	12.0	12.3	402	1081
4430	2.1	28.5	45.9	181	12.0	12.5	624	1284
5900	2.0	29.6	45.6	188	12.0	13.3	833	1454
7380	2.0	32.2	45.5	203	12.0	15.1	887	1520

TABLE 7.4. TRAP-MELT PREDICTIONS OF PRIMARY SYSTEM RETENTION FACTORS (RF) AND VOLUME SPECIFIC RETENTION FACTORS AS FUNCTIONS OF TIME FOR THE TC SEQUENCE FOR THE PEACH BOTTOM PLANT

Time (s)	CsI		CsOH		Te		Aerosol		
	RF	Lower Annulus	RF	Steam Dryers	RF	Steam Dryers	RF	Core	Steam Dryers
370	.13	.01	.16	.06	.46	.01	.11	.03	.02
740	.47	.02	.50	.20	.61	.04	.41	.04	.11
1100	.69	.04	.70	.22	.76	.05	.63	.07	.14
1480	.80	.06	.81	.23	.88	.04	.74	.08	.14
2210	.07	.07	.23	.15	.97	.45	.36	.05	.08
2580	.07	.07	.24	.16	.97	.43	.31	.05	.07
2950	.07	.07	.25	.16	.97	.43	.33	.04	.09
3320	.07	.07	.25	.17	.97	.42	.35	.04	.11
3690	.07	.07	.26	.17	.97	.42	.37	.04	.12
4430	.07	.07	.25	.17	.96	.41	.49	.19	.11
5900	.07	.07	.24	.16	.91	.39	.57	.30	.11
7380	.06	.06	.22	.15	.80	.34	.58	.33	.10

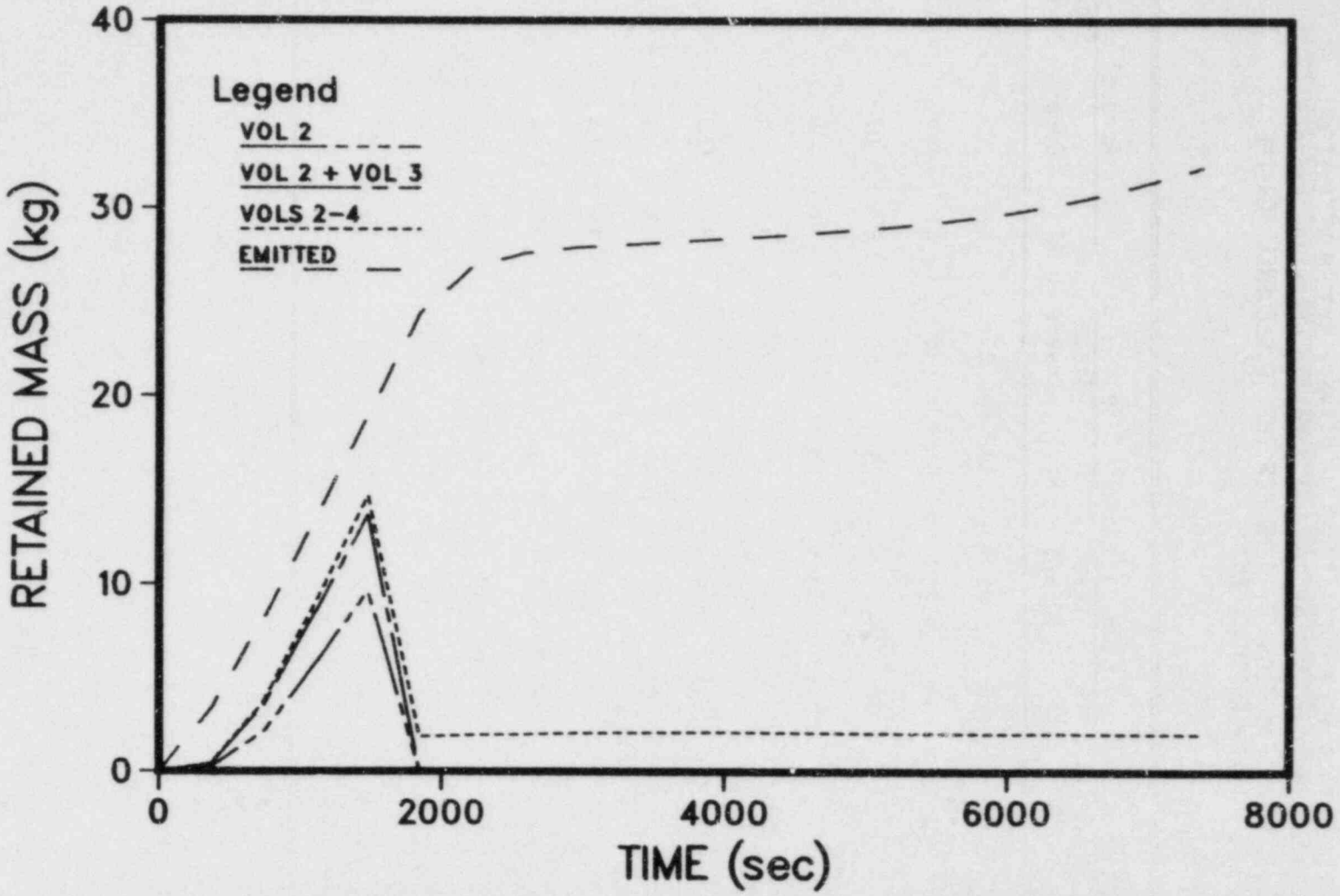

FIGURE 7.5. MASSES OF CsI EMITTED FROM CORE AND RETAINED IN THE RCS CONTROL VOLUMES AS FUNCTIONS OF TIME FOR THE TC SEQUENCE (Vol 1 = Core, Vol 2 = Steam Separators, Vol 3 = Steam Dryers, Vol 4 = Lower Annulus, Vol 5 = Steam Line, Vol 6 = Containment). Times Measured from Start of Core Melting.

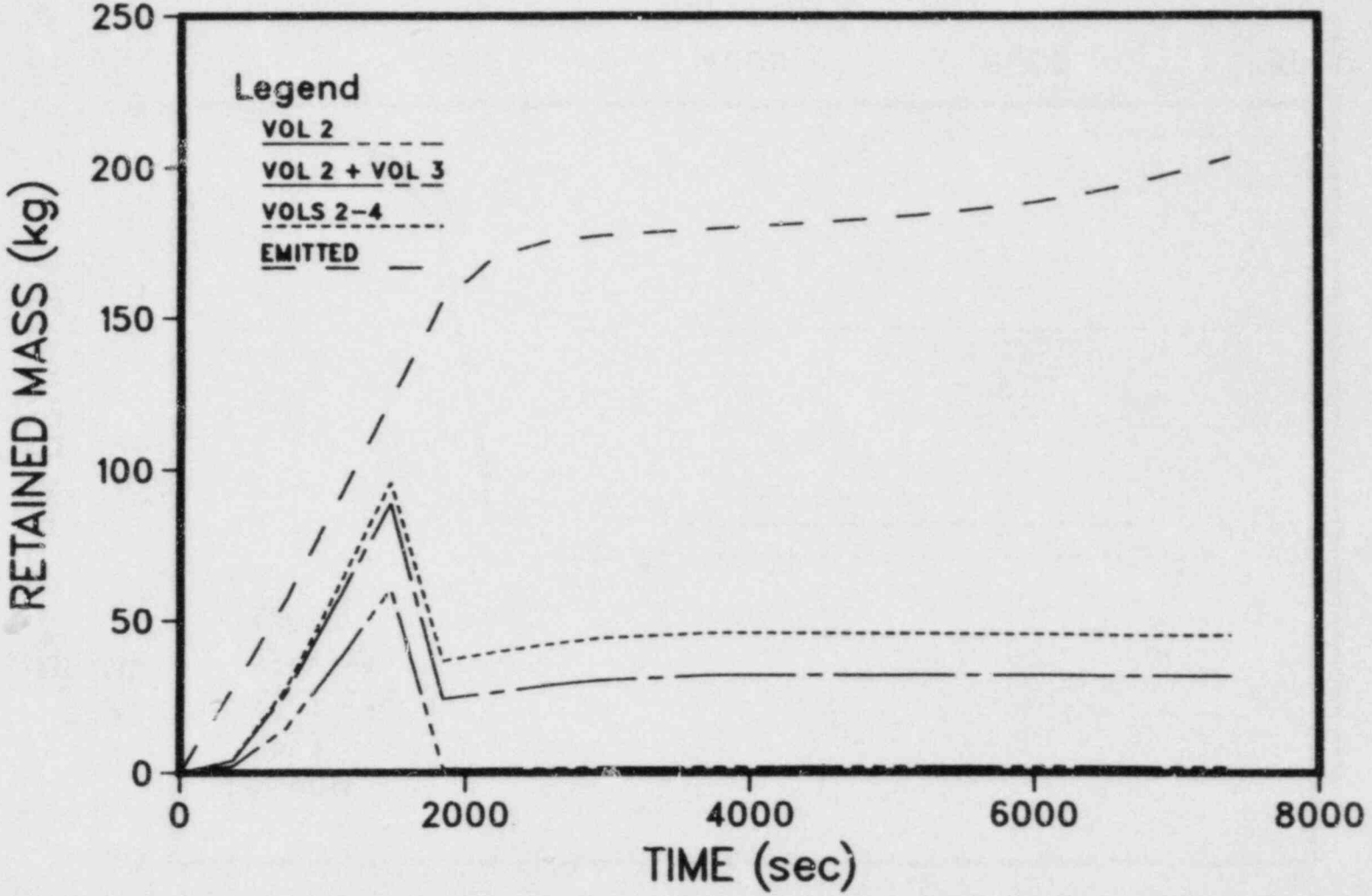

FIGURE 7.6. MASSES OF CsOH EMITTED FROM CORE AND RETAINED IN THE RCS CONTROL VOLUMES AS FUNCTIONS OF TIME FOR THE TC SEQUENCE (Vol 1 = Core, Vol 2 = Steam Separators, Vol 3 = Steam Dryers, Vol 4 = Lower Annulus, Vol 5 = Steam Line, Vol 6 = Containment). Times Measured from Start of Core Melting.

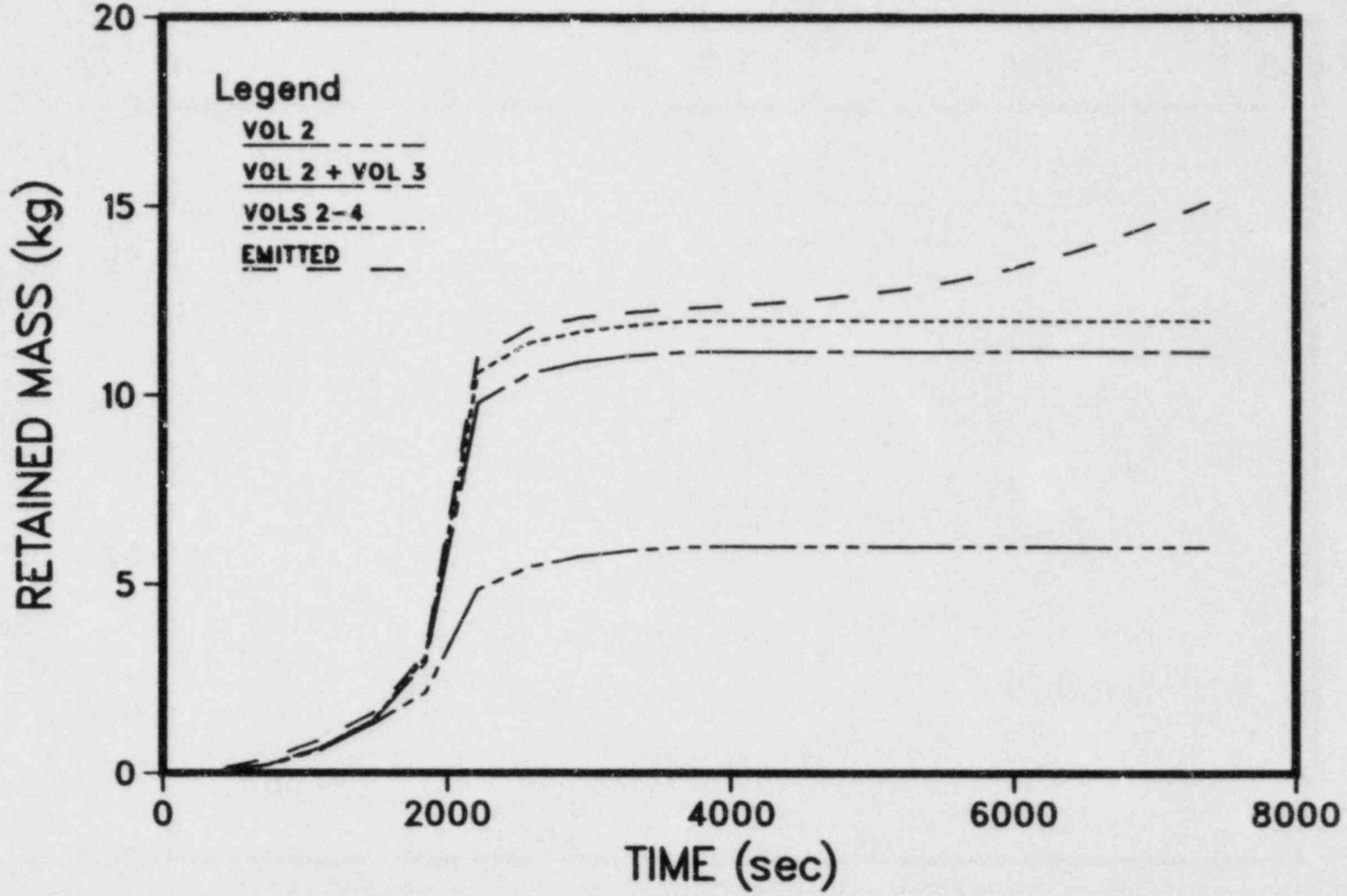

FIGURE 7.7. MASSES OF Te EMITTED FROM CORE AND RETAINED IN THE RCS CONTROL VOLUMES AS FUNCTIONS OF TIME FOR THE TC SEQUENCE (Vol 1 = Core, Vol 2 = Steam Separators, Vol 3 = Steam Dryers, Vol 4 = Lower Annulus, Vol 5 = Steam Line, Vol 6 = Containment). Times Measured from Start of Core Melting.

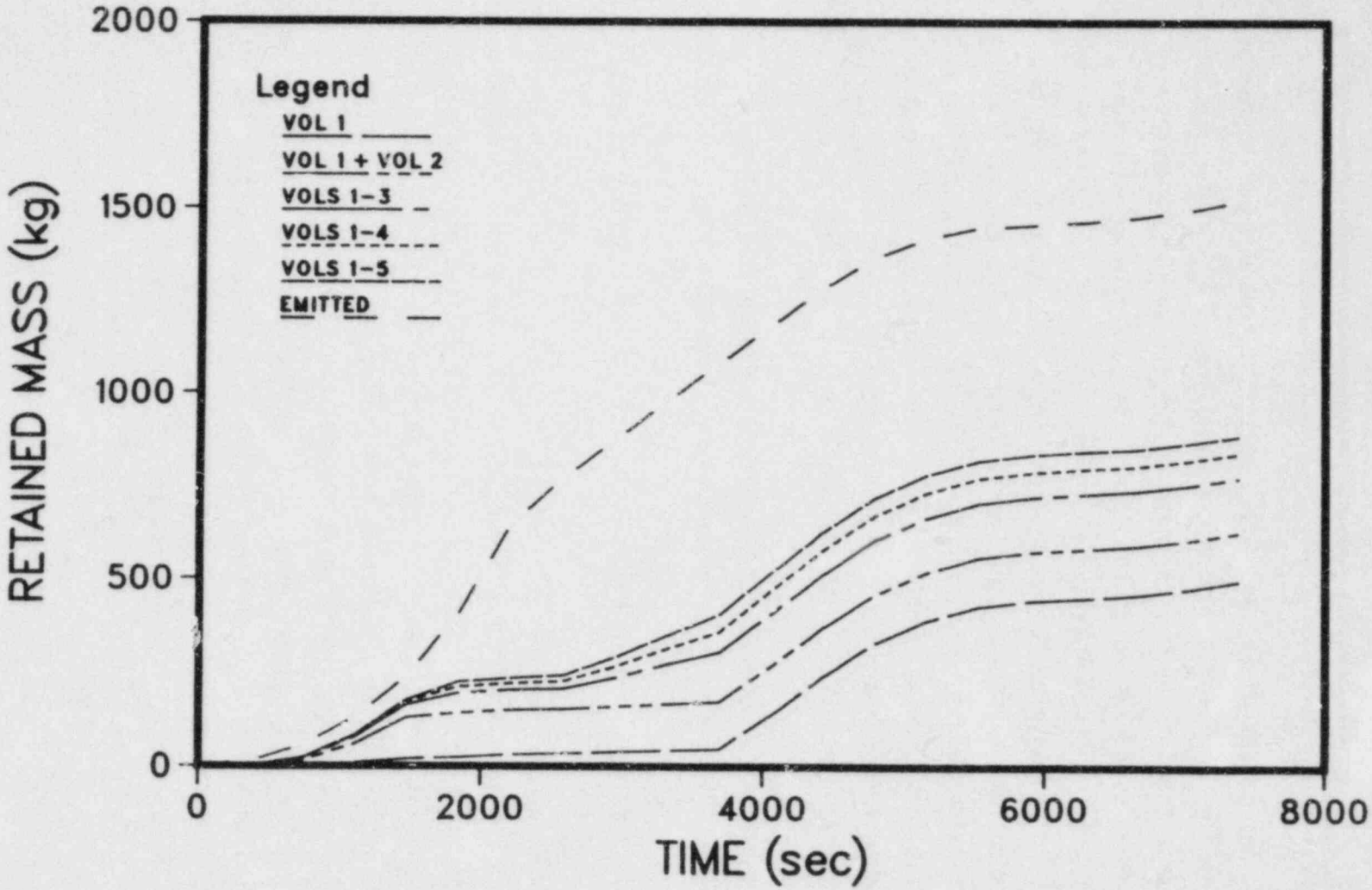

FIGURE 7.8. MASSES OF AEROSOL EMITTED FROM CORE AND RETAINED IN THE RCS CONTROL VOLUMES AS FUNCTIONS OF TIME FOR THE TC SEQUENCE (Vol 1 = Core, Vol 2 = Steam Separators, Vol 3 = Steam Dryers, Vol 4 = Lower Annulus, Vol 5 = Steam Line, Vol 6 = Containment). Times Measured from Start of Core Melting.

7.2.3 RCS Transport and Deposition for TW Sequence

Tables 7.5 and 7.6 present the masses emitted, masses retained and RFs for the various species in the TW sequence. On the time scale given in these tables, vessel dryout occurs at t = 5010 s and bottom head failure is predicted by MARCH to occur at t = 18540 s.

The masses of CsI and CsOH retained in the primary system are seen in Figures 7.9 and 7.10 to increase steadily until t = 3900 s. At some point between this time and 4900 s in these tables the surface temperatures in the volumes where condensation of the vapors has occurred increase sufficiently to drive off the condensed material and permit it to be transported. While cooler surfaces are encountered by these vapors in transit to the "containment", the surface areas and residence times are not large enough to significantly attenuate the flowing vapors. The principal retention mechanism for the CsI and CsOH is the retention of particles upon which these vapors have condensed. The slightly larger retention factor presented in Table 7.6 for CsOH is due to the influence of reactions with the system surfaces--which do not occur for CsI.

Tellurium behavior as exhibited in Figure 7.11 is similar to what has been presented for the other sequences discussed above. Only a portion of the core inventory is released, and of this material, over 80 percent is predicted to be retained in the RCS due to chemical interaction with system surfaces.

Aerosol retention illustrated in Figure 7.12 is again approximately 70 percent for this sequence. Since this is a more prolonged sequence than the others, there is a greater mass of aerosol emitted and a longer residence time is available to the material released from the core region into the RCS. The influence of the long residence time during the stagnant portion of the accident is seen in the increase in the fractional deposition of aerosol particle mass in the core region. Nearly all of the mass released by the melting core during this period is retained in the RCS. There remains, however, a portion of the aerosol emission which is suspended in the RCS at the time of bottom head failure and released as a puff from the RCS.

TABLE 7.5. CORSOR PREDICTIONS OF MASSES RELEASED FROM THE CORE AND TRAP-MELT PREDICTIONS OF MASSES RETAINED IN THE RCS DURING THE TW SEQUENCE FOR THE PEACH BOTTOM PLANT

(Times Measured from Start of Core Melting)

Time (s)	CsI		CsOH		Te		Aerosol	
	Ret (kg)	Total (kg)	Ret (kg)	Total (kg)	Ret (kg)	Total (kg)	Ret (kg)	Total (kg)
490	0.1	1.4	0.7	14.1	0.1	0.1	1.8	8.2
1960	2.8	7.1	18.6	50.9	0.9	1.0	56.5	120
2940	8.2	13.3	53.3	89.9	2.2	2.6	214	295
3420	13.0	18.8	82.9	123	4.5	5.0	344	462
3910	17.6	23.5	111	152	8.8	9.5	588	781
4890	4.7	31.8	32.8	202	14.0	14.3	693	1038
6360	4.7	31.8	32.8	202	14.0	14.3	694	1039
7830	4.7	31.8	32.8	202	14.0	14.3	694	1040
10760	4.7	31.9	32.8	203	14.0	14.4	698	1045
13700	4.7	32.4	32.8	206	14.0	14.6	714	1065
15170	4.7	32.8	32.8	208	14.0	15.0	745	1100
16630	4.7	33.2	32.8	211	14.0	15.7	811	1170
18540	4.7	33.5	32.8	212	14.0	16.8	960	1323

TABLE 7.6. TRAP-MELT PREDICTIONS OF PRIMARY SYSTEM RETENTION FACTORS (RF) AND VOLUME SPECIFIC RETENTION FACTORS AS FUNCTION OF TIME FOR THE TW SEQUENCE FOR THE PEACH BOTTOM PLANT

(Times Measured from Start of Core Melting)

Time (s)	CsI			CsOH			Te		Aerosol			
	RF	Steam Dryers	Relief Lines	RF	Steam Dryers	Relief Lines	RF	Steam Sep	RF	Core	Steam Dryers	Relief Lines
490	.05	.01	.03	.05	.02	.03	.81	.73	.21	.19	.01	.02
1960	.39	.22	.07	.36	.20	.07	.85	.79	.47	.11	.22	.06
2940	.62	.32	.06	.59	.30	.06	.87	.82	.72	.15	.29	.04
3420	.69	.36	.06	.67	.34	.06	.92	.85	.74	.12	.33	.05
3910	.75	.38	.06	.73	.37	.06	.92	.85	.75	.16	.34	.05
4890	.15	--	.05	.16	.01	.05	.98	.73	.67	.08	.30	.05
6360	.15	--	.05	.16	.01	.05	.98	.73	.67	.08	.30	.05
7830	.15	--	.05	.16	.01	.05	.98	.73	.67	.08	.30	.05
10760	.15	--	.05	.16	.01	.05	.97	.73	.67	.09	.30	.05
13700	.15	--	.05	.16	.01	.05	.95	.72	.67	.10	.30	.05
15170	.14	--	.05	.16	.01	.05	.93	.70	.68	.13	.29	.05
16630	.14	--	.05	.16	.01	.05	.89	.67	.69	.17	.27	.05
18540	.14	--	.05	.15	.01	.05	.83	.62	.73	.27	.24	.04

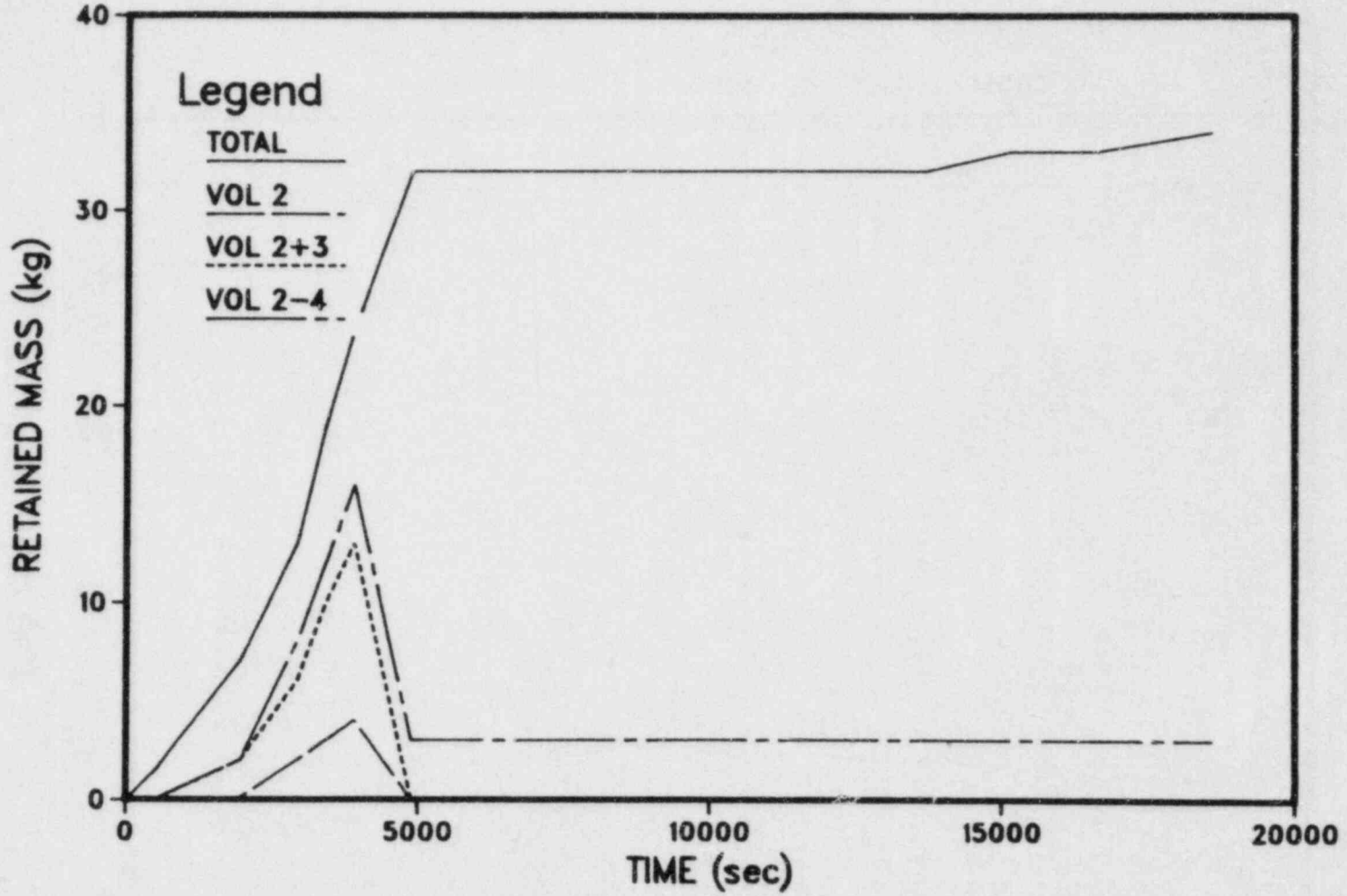

FIGURE 7.9. MASSES OF CsI EMITTED FROM CORE AND RETAINED IN THE RCS CONTROL VOLUMES AS FUNCTIONS OF TIME FOR THE TW SEQUENCE (Vol 1 = Core, Vol 2 = Steam Separators, Vol 3 = Steam Dryers, Vol 4 = Lower Annulus, Vol 5 = Steam Line, Vol 6 = Containment). Times Measured from Start of Core Melting.

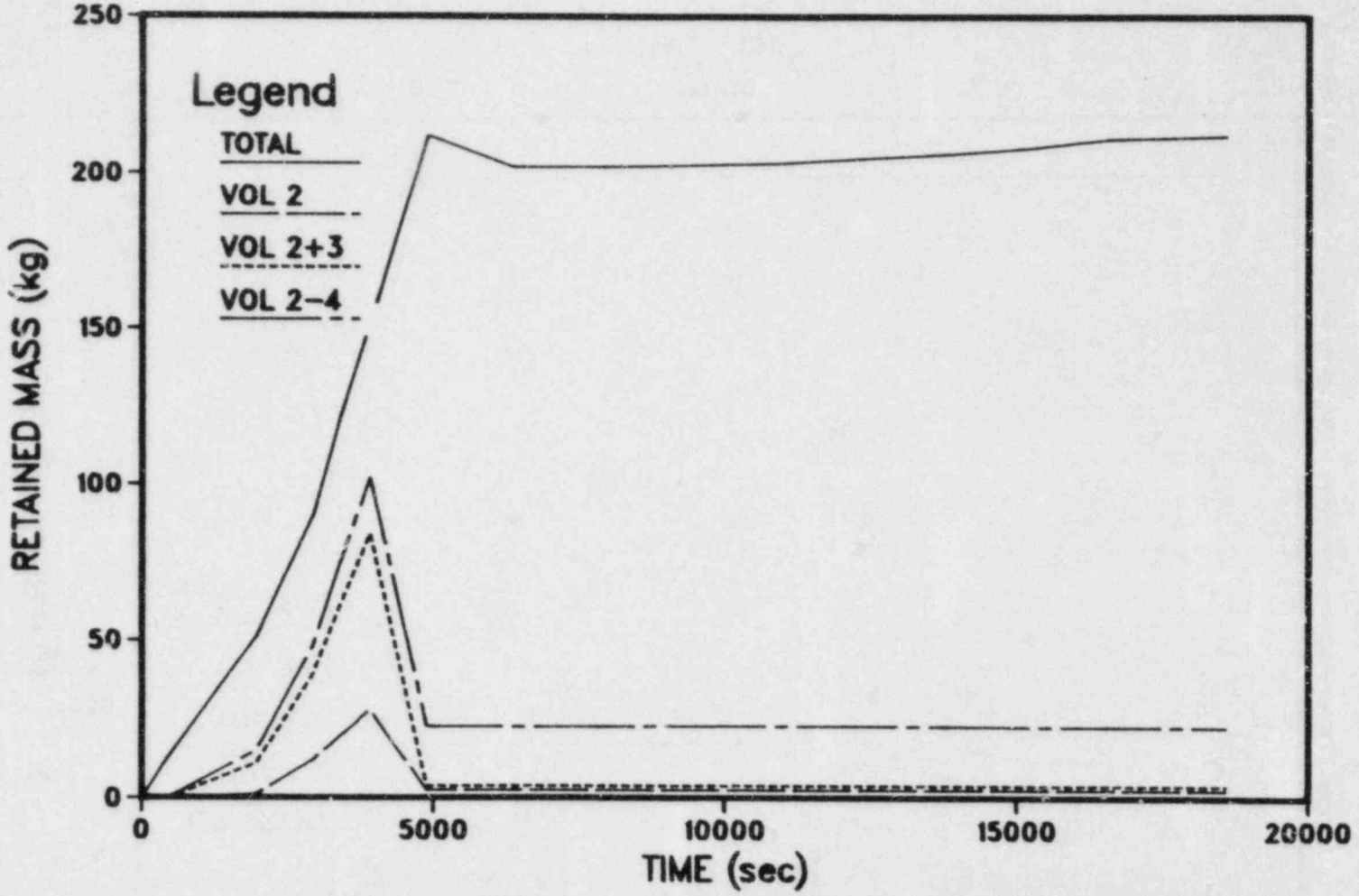

FIGURE 7.10. MASSES OF CsOH EMITTED FROM CORE AND RETAINED IN THE RCS CONTROL VOLUMES AS FUNCTIONS OF TIME FOR THE TW SEQUENCE (Vol 1 = Core, Vol 2 = Steam Separators, Vol 3 = Steam Dryers, Vol 4 = Lower Annulus, Vol 5 = Steam Line, Vol 6 = Containment). Times Measured from Start of Core Melting.

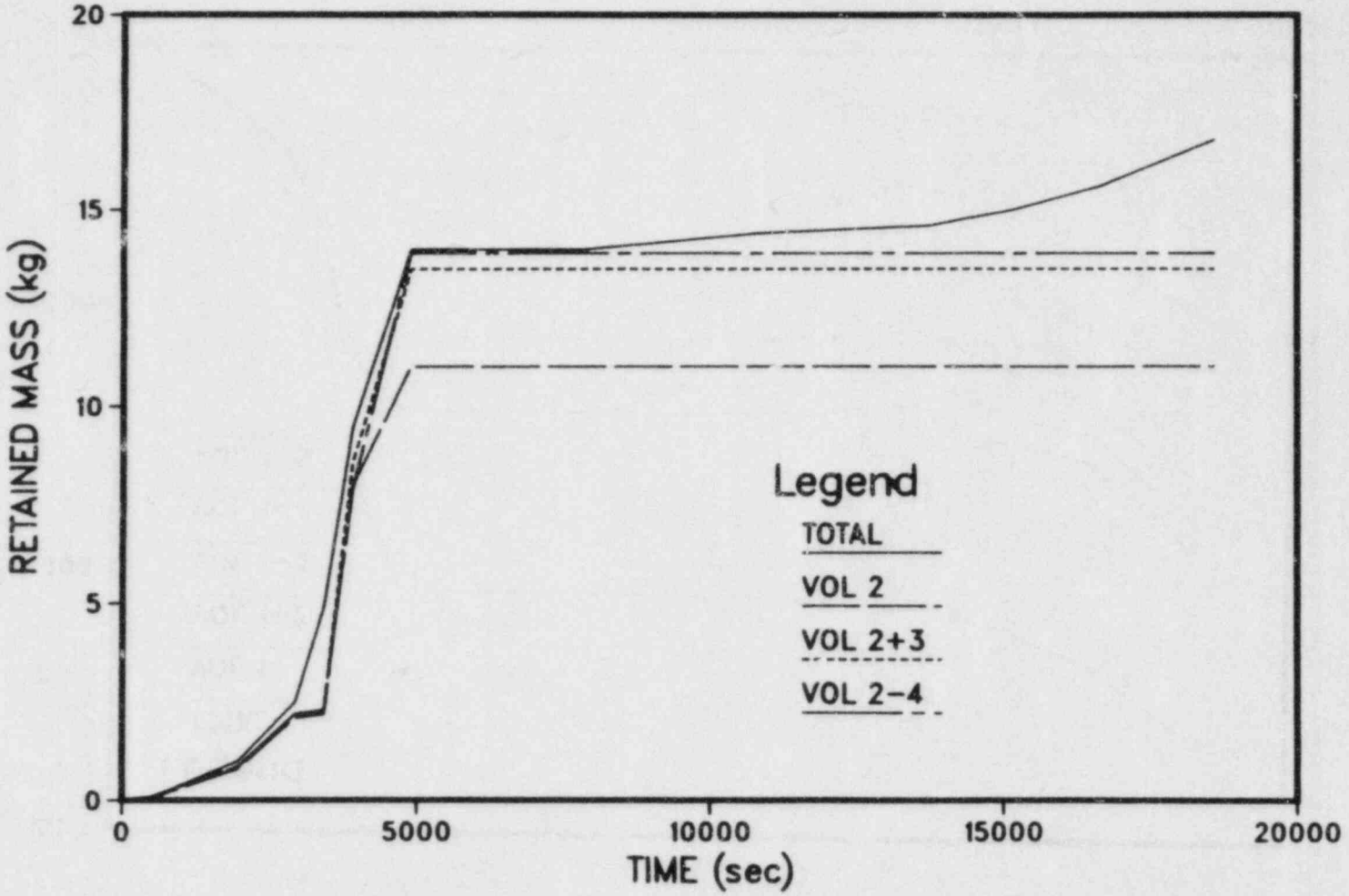

FIGURE 7.11. MASSES OF Te EMITTED FROM CORE AND RETAINED IN THE RCS CONTROL VOLUMES AS FUNCTIONS OF TIME FOR THE TW SEQUENCE (Vol 1 = Core, Vol 2 = Steam Separators, Vol 3 = Steam Dryers, Vol 4 = Lower Annulus, Vol 5 = Steam Line, Vol 6 = Containment). Times Measured from Start of Core Melting.

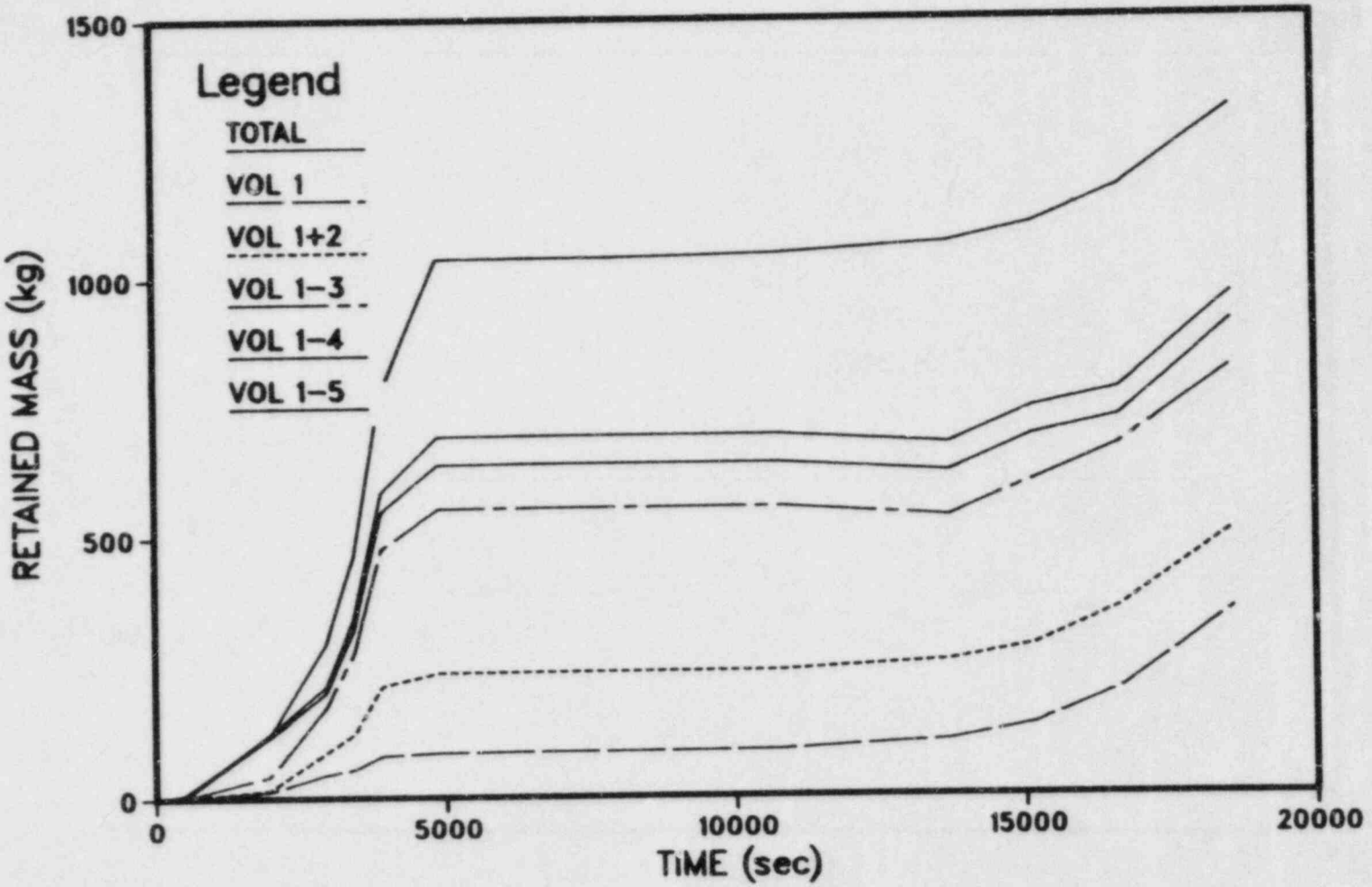

FIGURE 7.12. MASSES OF AEROSOL EMITTED FROM CORE AND RETAINED IN THE RCS CONTROL VOLUMES AS FUNCTIONS OF TIME FOR THE TW SEQUENCE (Vol 1 = Core, Vol 2 = Steam Separators, Vol 3 = Steam Dryers, Vol 4 = Lower Annulus, Vol 5 = Steam Line, Vol 6 = Containment). Times Measured from Start of Core Melting.

7.3 Transport of Fission Products Through Containment

Results are presented in this section for analyses performed for the transport and retention of various fission products that leave the reactor coolant system. The various compartments of the reactor considered for these analyses include the suppression pool, the wetwell, the drywell, and the reactor containment building. The NAUA code that calculates transport of fission products in particulate form was utilized for the mentioned compartments except that the SPARC code was utilized for calculating the retention of fission product in the suppression pool.

Results from the MARCH, TRAP-MELT, and VANESA calculations were utilized to provide the required input for the NAUA and SPARC calculations. Three species, CsI, CsOH, and Te, were distinguished in the calculations and all the other species were treated as one group. All species in this additional group were assumed to exist in the particulate form once they escape the reactor coolant system.

Dimensions of the compartment volumes were based on geometric data provided in the Peach Bottom 2 FSAR. The largest cross sectional area of a volume was used to estimate the floor area. This area directly affects the removal rate for particle sedimentation. For example, the cross sectional area of the spherical section based on a diameter of 67 ft (20.4 m) was used for the drywell calculation.

Three different accident sequences, AE, TC, and TW, were considered in the present calculations.

7.3.1 AE_{γ}' Sequence

This sequence involves a large pipe break accident resulting in loss of reactor coolant. The fission products released from the reactor coolant system enter the drywell through the lower annulus section and subsequently are allowed to enter the suppression pool to reach the wetwell. As the drywell fails due to the pressure built up by the release of gases from the reactor coolant system, the fission products released to the drywell no longer enter the suppression pool but are released to the failed reactor building or environment. Due to this event-dependent flow path of the fission product involving several physically separate compartments, the analyses for the AE sequence

were performed sequentially as depicted by Figure 7.13 and this is briefly described as follows.

First, the NAUA code was utilized to calculate the behavior of particulates in the drywell. The calculation was suspended as the containment failure time was reached. The results of this NAUA calculation were then used with the SPARC code for calculating the scrubbing of fission products in the suppression pool. A separate NAUA calculation was performed to describe the behavior of the fission products in the wetwell air space. The input for this was the output of the SPARC calculation. To cover the accident time beyond the containment failure time, the NAUA calculation that had been suspended was reactivated for the drywell. The source terms used for this resumed calculation are the TRAP-MELT calculation results, the separate NAUA calculation results for the wetwell, and the VANESA calculation results. Figure 7.14 shows the suspended mass concentration of particulates in the drywell. It is seen that the amount of the suspended particulate increases rapidly as the core starts melting at 12 minutes and the highest concentration results at a time of 34 minutes when the drywell fails. It should be realized that during this time period, a considerable amount of particulate enters the suppression pool and is captured. Distribution of the total particulate at various locations and at various times is listed in Table 7.7. As the drywell fails, the gas in the dry well is directed toward the environment and the particulate concentration in the drywell decreases rapidly due to this new leakage flow path. As the time elapses further and the head finally fails, the particles released through the bottom head cause the airborne particulate concentration to increase again and the amount leaked to the environment builds up (see Table 7.7). At a time of 1200 minutes (20 hours), the particulate released during the accident is located in the drywell, the suppression pool, and in the environment each with the amounts listed in Table 7.7.

The particle size distribution of aerosol suspended in the drywell at selected times is shown in Figure 7.15. It is noted that the mass median particle size of the aerosol ranges from 0.1 to 1.2 μm before the drywell fails. As will be discussed shortly, scrubbing of particulates by the suppression pool depends substantially on the size of particles that enter the pool. Combined with a particle density of 3 g/cc which was used in the present analysis, an aerosol with the above range of mass median diameter is found to be removed rather effectively by the suppression pool.

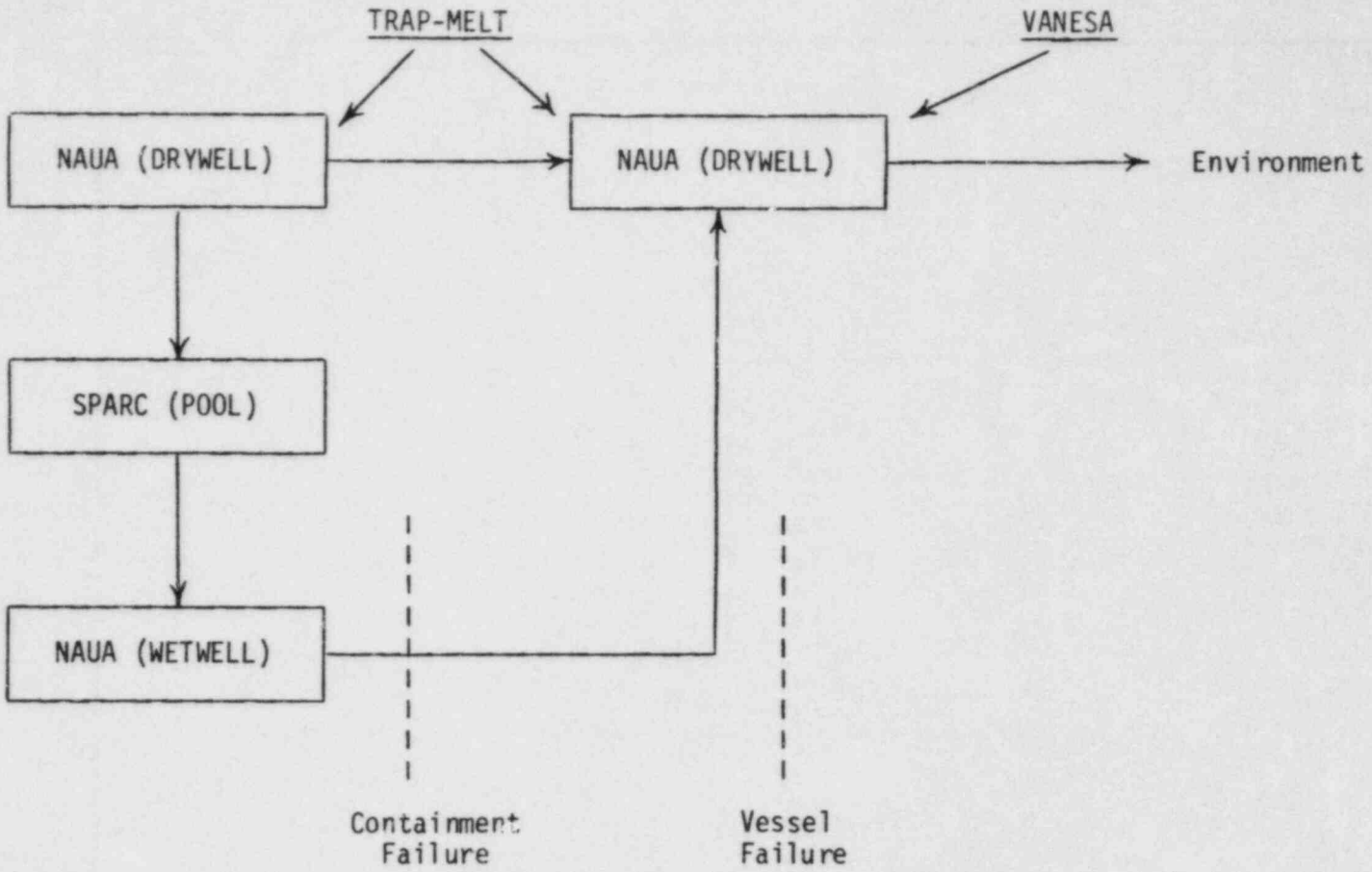

FIGURE 7.13. NAUA AND SPARC CALCULATION PATHS USED FOR PERFORMING ANALYSES OF AE SEQUENCE

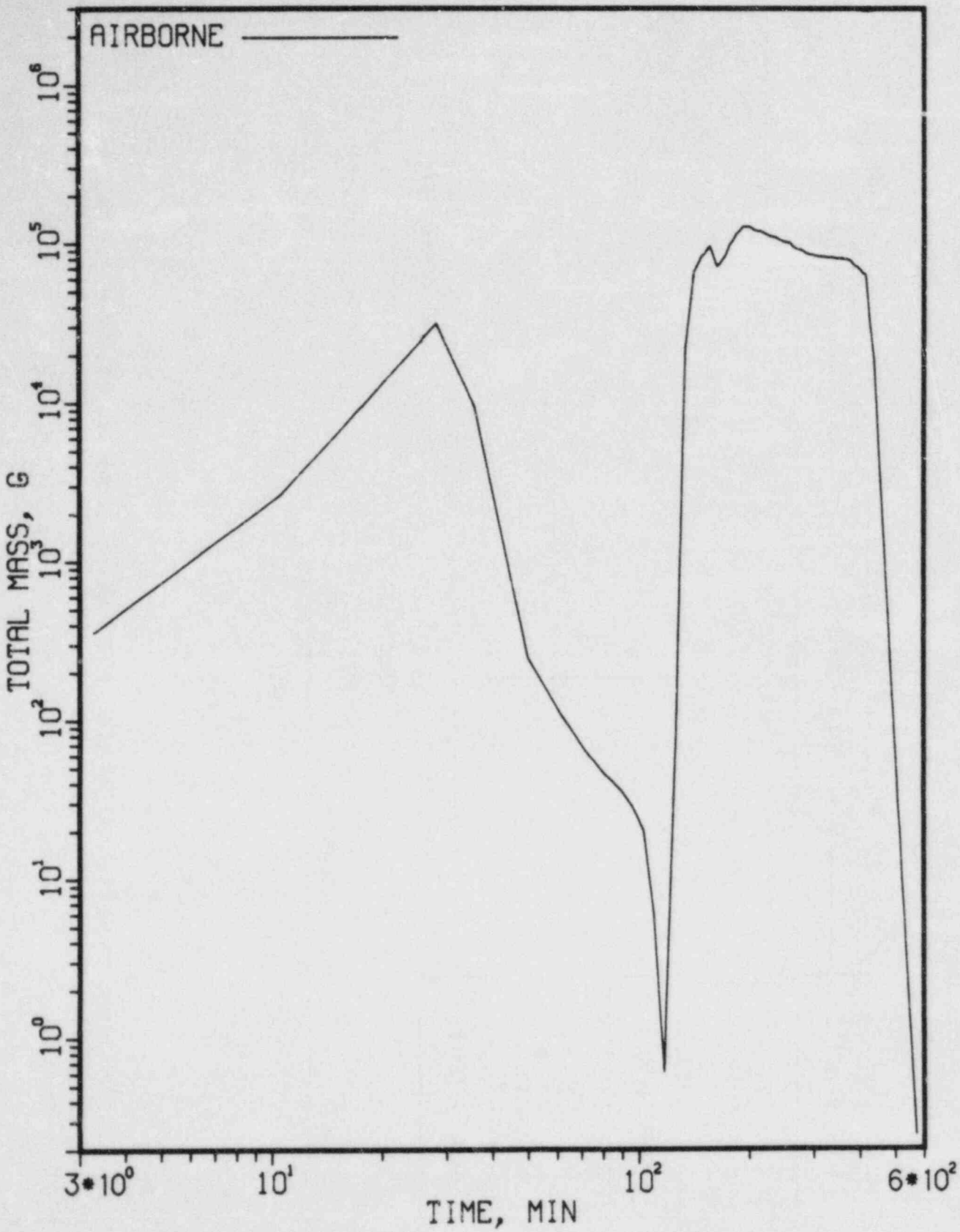

FIGURE 7.14. AIRBORNE CONCENTRATION IN THE DRYWELL AS A FUNCTION OF TIME, AE

TABLE 7.7. DISTRIBUTION OF TOTAL SOLID PARTICULATE MASS (KG) AT VARIOUS TIMES, AE

Time (min)	Event	Drywell		Pool Captured	Wetwell	Environment
		Suspended	Deposited			
12	Melt start					
20		17.0	11.9	0.09	0.001	0
34	Cont fails	46.3	22.1	218	18.1	0
35		16.1	22.5	218	14.4	49.4
40	Vessel dry					
50		0.25	23.9	218	10.9	129
58	Core collapse					
80		0.15	24.2	218	10.4	129.3
118	Head fails					
120		28	40.9	228[(a)]	~0[(a)]	157.6
420		51	1458	228	~0	2682
1200	End of accident	~0	1485	228	~0	2729

(a) Wetwell mass being added to pool captured mass.

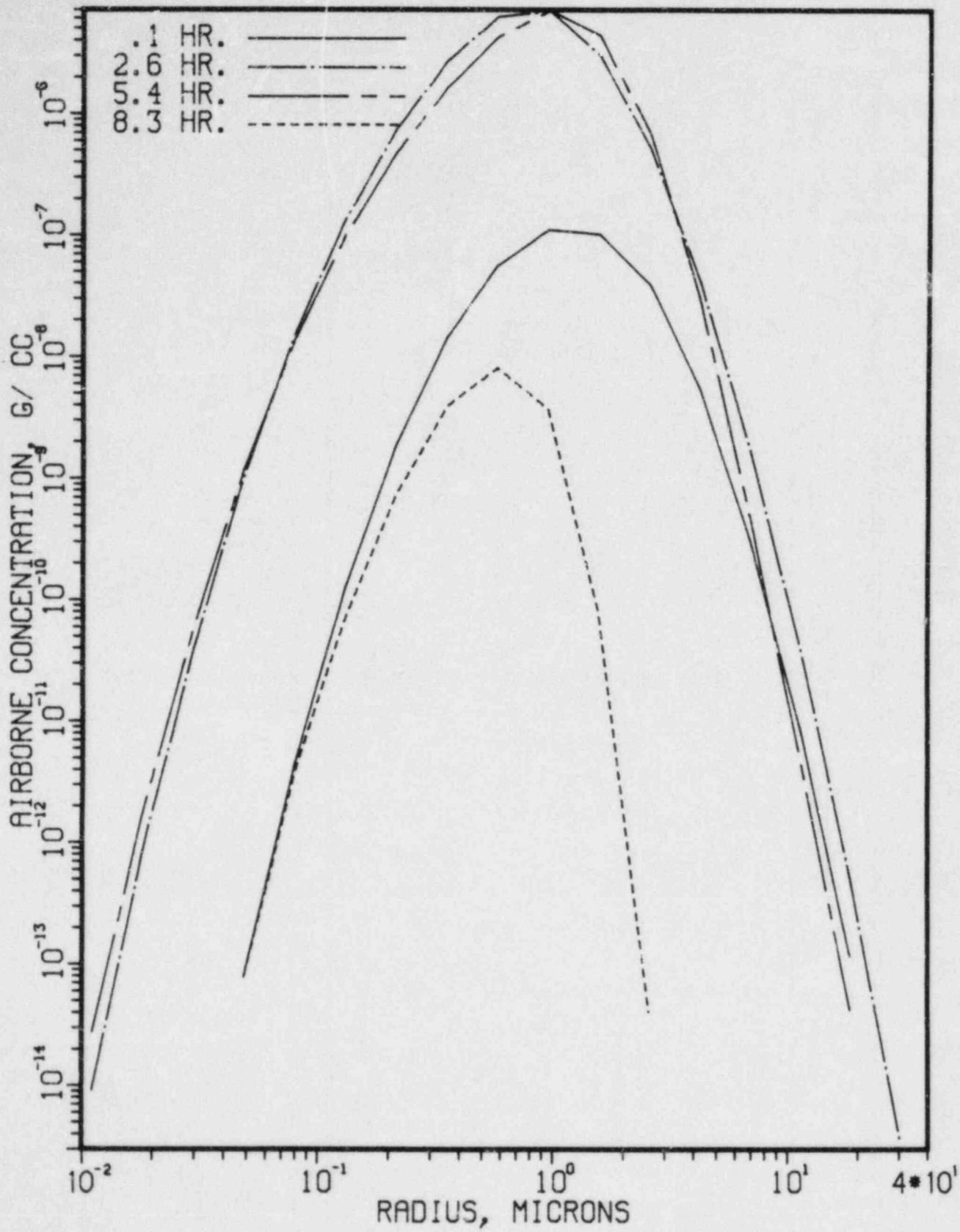

FIGURE 7.15. PARTICLE SIZE DISTRIBUTION OF AEROSOL SUSPENDED IN THE DRYWELL, AE

Since the release timing of individual fission product species may be different than that for the total particulate, the time-dependent amounts of CsI, CsOH, and Te were distinguished in the present calculation. Table 7.8 shows the calculated fractions of the core inventory of each species found to reach various locations at the end of the accident. It is interesting to see that significant fractions of CsI and CsOH are captured by the suppression pool. As a result, about 30 percent is seen to escape the drywell to reach the environment.

The MARCH calculation results indicated that between the core melting period and the containment failure, the thermal hydraulic conditions are such that there is little supersaturation of water vapor in the drywell. The NAUA calculation also shows that the diffusiophoresis of fission products onto surfaces is not significant.

Collection in the suppression pool as calculated by the SPARC code indicated that the pool is indeed an effective means for scrubbing particulates. The SPARC code considers removal of particulates by sedimentation, inertial deposition, diffusion, and diffusiophoresis inside bubbles. In addition, particulates are allowed to grow by steam condensation, thus enhancing gravitational sedimentation and the inertial deposition. It has been speculated that particulates would be removed by an additional impaction mechanism just after the gas is discharged from a vent pipe for AE or from quencher holes for TC and TW into the pool water forming an impaction regime. For modeling this type mechanism, an existing theory for an impactor was added to the SPARC code.

The SPARC code calculation results showed that depending upon the size of particles, decontamination factors over a wide range can be obtained. Typical decontamination factors obtained from SPARC calculations are listed in Table 7.9.

7.3.2 TCγ' Sequence

This accident represents the sequence in which the containment fails first and the fission products released from the relief valve enter the suppression pool through the T quencher, pass through the wetwell and reach the drywell before being released to the environment. As the reactor vessel fails, the fission products enter directly into the drywell and are then released to the failed reactor building or environment. The sequential use of various computer

TABLE 7.8. DISTRIBUTION OF SPECIES AT 20 HOURS AFTER ACCIDENT, AE

Species	Fraction of Core Inventory				
	RCS	Pool	Drywell	Wetwell	Environment
CsI	0.19	0.35	0.12	0	0.34
CsOH	0.19	0.34	0.14	0	0.33
Te	2.9×10^{-2}	3.2×10^{-3}	0.32	0	0.65

TABLE 7.9. DECONTAMINATION FACTORS CALCULATED AS A FUNCTION OF PARTICLE SIZE AND OF TIME FOR AE SEQUENCE

Time (min)	Particle Diameter, μm					DF Based on Total Mass
	0.1	0.7	1.2	5	8.4	
14.3	1.2	3.3×10^2	$10^{5(a)}$	10^5	10^5	1504
18.9	1.2	2.9×10^2	10^5	10^5	10^5	1400
27.4	1.2	51	2.5×10^4	10^5	10^5	25
33.3	1.3	5.4	69	10^5	10^5	4.1

(a) A decontamination factor larger than 10^5 is assumed to be 10^5.

Pool depth: 4 ft
Bubble diameter: 0.75 cm
Aspect ratio: 1:3

codes for calculating the transport of fission products in this accident sequence is shown in Figure 7.16.

Since the first volume fission products encounter after being released from the RCS for the TC sequence is the suppression pool, the SPARC code was utilized to calculate the retention of fission products by the pool. The decontamination factors calculated are listed in Table 7.10. This table shows a particle size dependency that is similar to that shown previously for the AE sequence. Time variations of the calculated decontamination factor for 0.1 and 0.7 μm particles are, of course, due to the difference in the thermal hydraulic condition that prevail at the corresponding times.

Figure 7.17 is the suspended aerosol mass as a function of time for the drywell. Sharp increases in the mass concentration as shown in Figure 7.17 represent the initial core melting time and the bottom head failure time, respectively. Figure 7.18 is the accumulated mass leaked outside the drywell shown by species. Figure 7.19 is the geometric number median radius of the aerosol mass suspended in the drywell. It is interesting to note that due to the presence of the suppression pool, which removes predominantly large particles, the particle size during the time up to bottom head failure is relatively small, while the size becomes large thereafter.

Table 7.11 is the calculated distribution of the CsI, CsOH, and Te that are located in the RCS, the suppression pool, the drywell, and the wetwell. The last column indicates that fractions of core inventory of these species between 0.21 to 0.37 are released to the environment. It is also noted that fractions of 0.69 for CsI and 0.56 for CsOH are captured in the suppression pool. The reason why the amount of Te captured by the suppression pool is low is because it is released predominantly during the core-concrete interaction phase of the accident and thus does not pass through the pool.

7.3.3 TCγ Sequence

This accident sequence is similar to the TCγ' sequence except that the fission products released from the drywell are assumed to pass through the secondary containment (reactor building). Therefore, an additional calculation has been made simulating fission product behavior in the secondary containment. The flow path of fission products from the secondary containment is partly directly to the environment and partly through the Standby Gas Treatment System

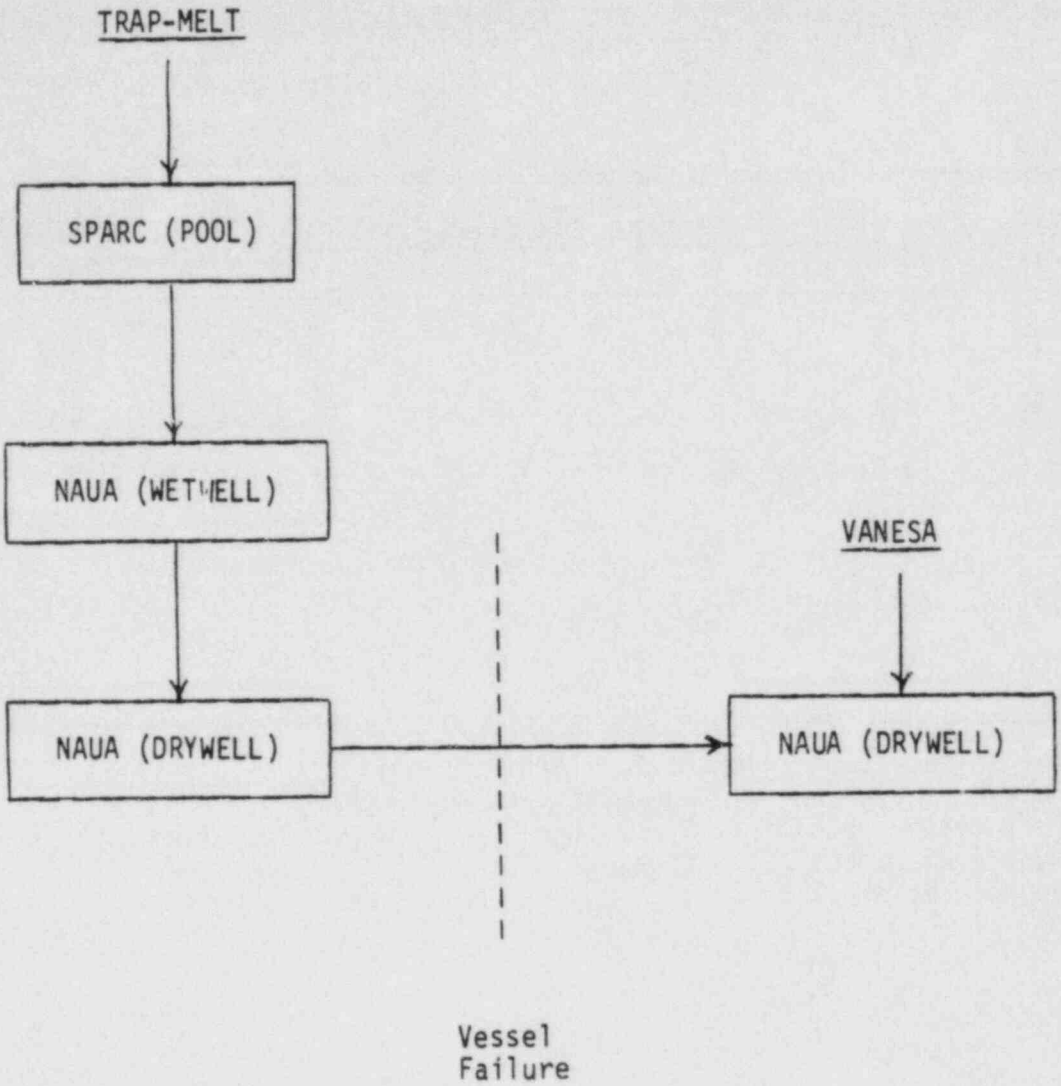

FIGURE 7.16. NAUA AND SPARC CALCULATION PATHS USED FOR PERFORMING ANALYSES OF TC AND TW SEQUENCES

TABLE 7.10. DECONTAMINATION FACTOR CALCULATED AS A FUNCTION OF PARTICLE SIZE AND OF TIME FOR TC

Time (min)	Particle Diameter, μm					DF Based on Total Mass
	0.1	0.7	1.2	5.1	8.4	
96.2	1.3	1.08×10^3	10^5(a)	10^5	10^5	3690
99.2	5.2	98	10^5	10^5	10^5	2850
104	3.0	45	10^5	10^5	10^5	2166
121.7	1.1	15.8	1.87×10^3	10^5	10^5	7.7
131.5	1.2	4.5	41	10^5	10^5	298
156.3	1.2	4.0	32	10^5	10^5	600

(a) A decontamination factor larger than 10^5 is assumed to be 10^5.

Pool depth: 6.5 ft (198 cm)
Bubble diameter: 0.75 cm
Aspect ratio: 1:3

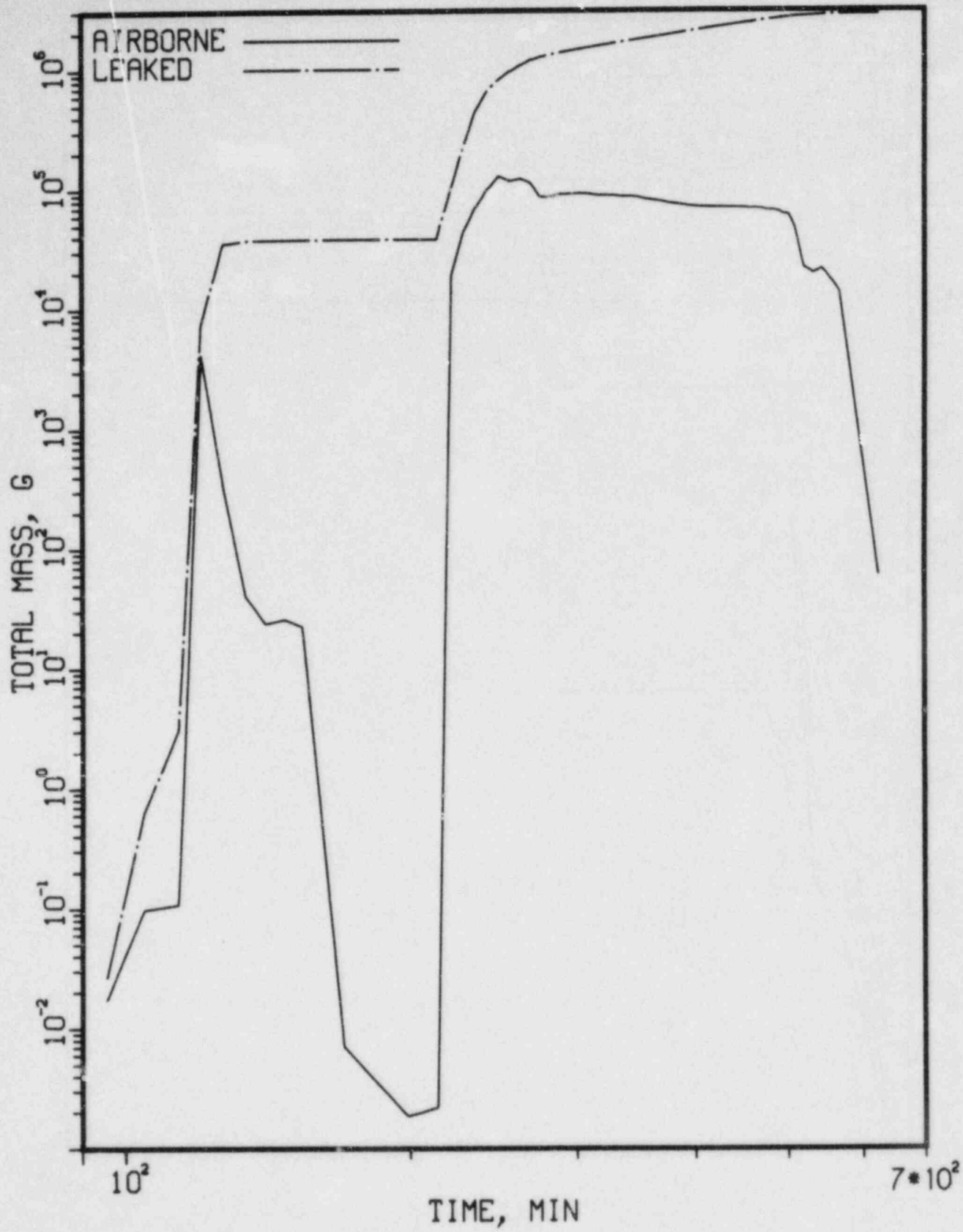

FIGURE 7.17. AIRBORNE AND LEAKED AEROSOL MASS FOR THE DRYWELL AS A FUNCTION OF TIME, TC-γ'

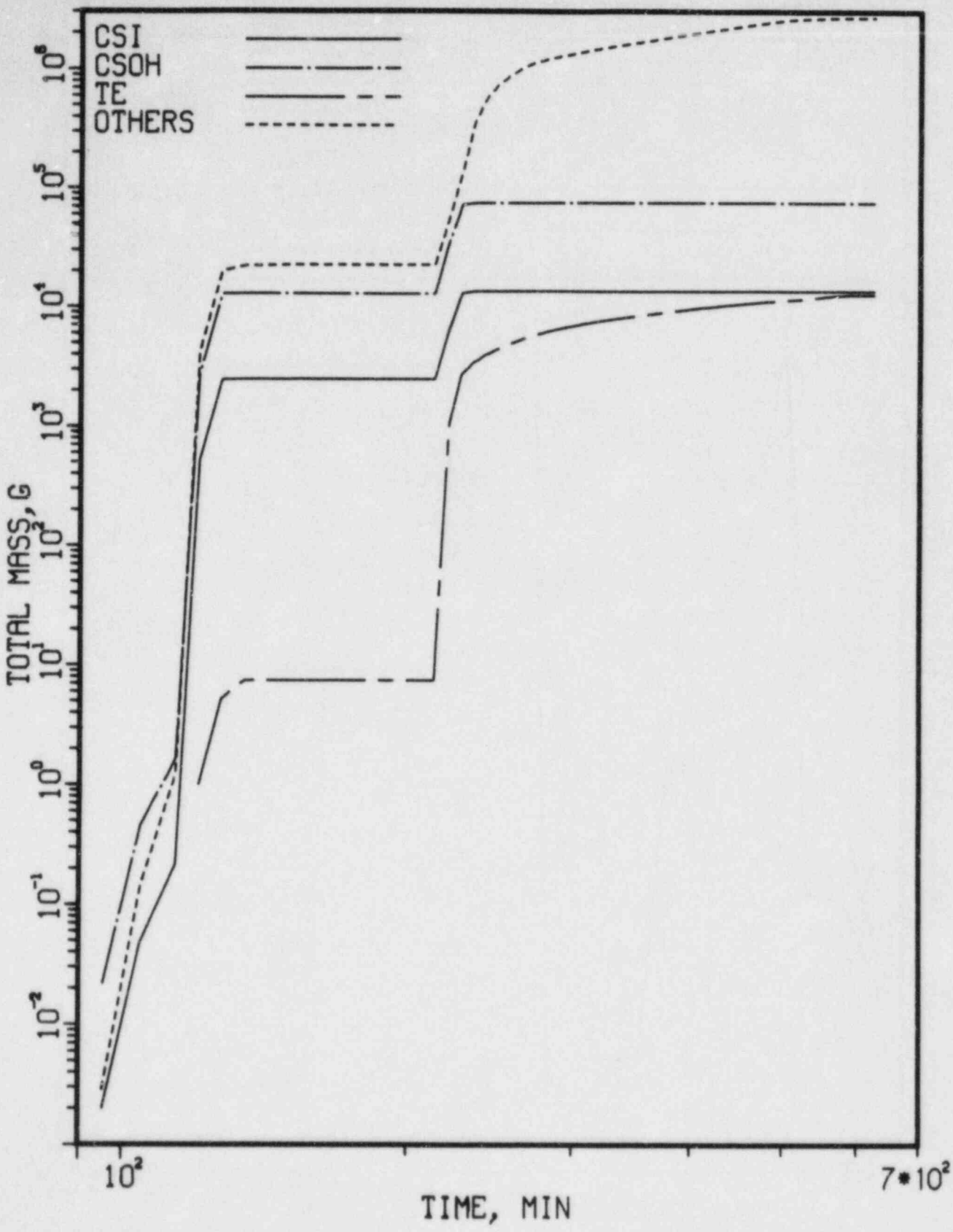

FIGURE 7.18. ACCUMULATED MASS LEAKED INTO ENVIRONMENT FOR VARIOUS SPECIES, TC-γ'

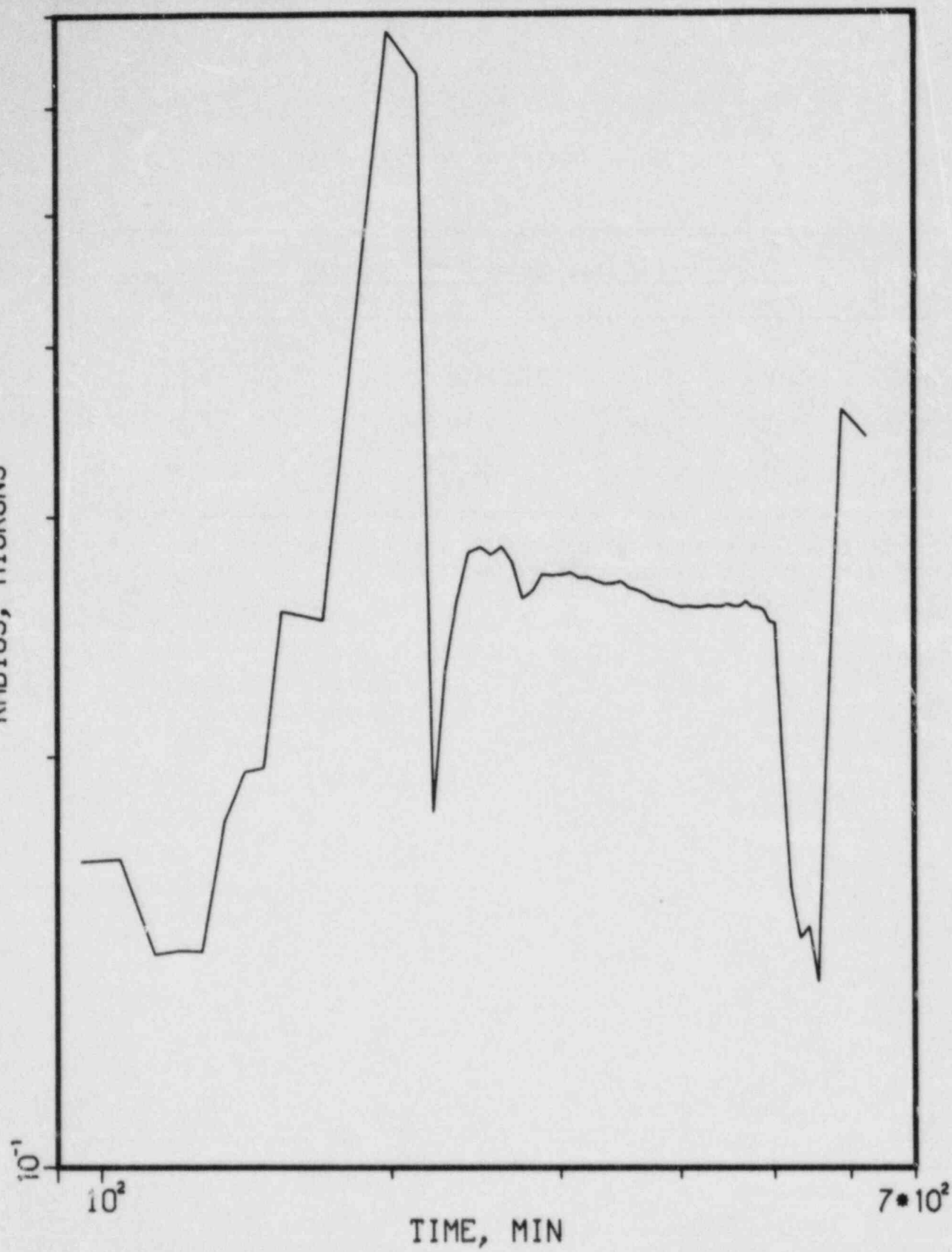

FIGURE 7.19. GEOMETRIC MEAN PARTICLE RADIUS IN DRYWELL, TC-γ'

TABLE 7.11. DISTRIBUTION OF SPECIES AT 20 HOURS AFTER ACCIDENT, TC-Y'

Species	Fraction of Core Inventory				
	RCS	Pool	Drywell	Wetwell	Environment
CsI	0.06	0.69	1.5×10^{-2}	0	0.24
CsOH	0.22	0.56	1.4×10^{-2}	0	0.21
Te	0.34	7.9×10^{-3}	0.29*	0	0.37

*This includes a fraction of 0.13 for Tc that is found not to be released from the core-concrete interaction.

(SGTS) which consists of High Efficiency Particulate Air (HEPA) filters. The operation and the effectiveness of the SGTS are described in Appendix A. It was assumed in the present calculation that a constant volumetric flow rate of 25,000 cfm through the SGTS is maintained during the accident. A collection efficiency of 99.99 percent, regardless of particle size, was utilized. However, the filter banks were assumed to fail after 108 kg of particulate matter was collected as specified in the analyses in Appendix A.

Figure 7.20 is the airborne mass plotted as a function of time for the secondary containment. As expected, a time dependency of the airborne mass very similar to that for the drywell as depicted by Figure 7.17 is seen to occur in the secondary containment.

Table 7.12 shows the distribution of the CsI, CsOH, and Te as calculated by the NAUA code. It is interesting to find that compared with Table 7.11 a fraction of core inventory ranging from 0.12 for Te to 0.14 for CsI is retained in the secondary containment and in the filter.

7.3.4 TW Sequence

This sequence is similar to the TC' sequence in that the flow paths for fission products are the same and that the containment fails before core meltdown takes place. However, the time scale for the present sequence is much more extended than that for the TC' sequence. The key accident events and containment conditions used in the TW analysis are given in Section 6.1.3.

Generally a calculation procedure similar to that adopted for the TC sequence was taken. The sequential use of various computer codes depending upon the accident events is shown in Figure 7.16. The decontamination factors calculated by the SPARC code are listed in Table 7.13. It is shown in the table that the overall decontamination factor of the suppression pool ranges from 326 at 2818 minutes to 10^5 at 2827 minutes after the accident commences. The calculated decontamination factor depends not only upon the thermal hydraulic conditions in the suppression pool but upon the particle size distribution of the aerosol entering the pool. For example, at 2815 minutes, the mass median particle size entering the suppression pool is found to be about 0.66 μm causing the overall decontamination factor at that time to become as high as 352.

Figure 7.21 is the calculated airborne mass as a function of time for the drywell and Figure 7.22 is accumulated mass leaked out to the atmosphere.

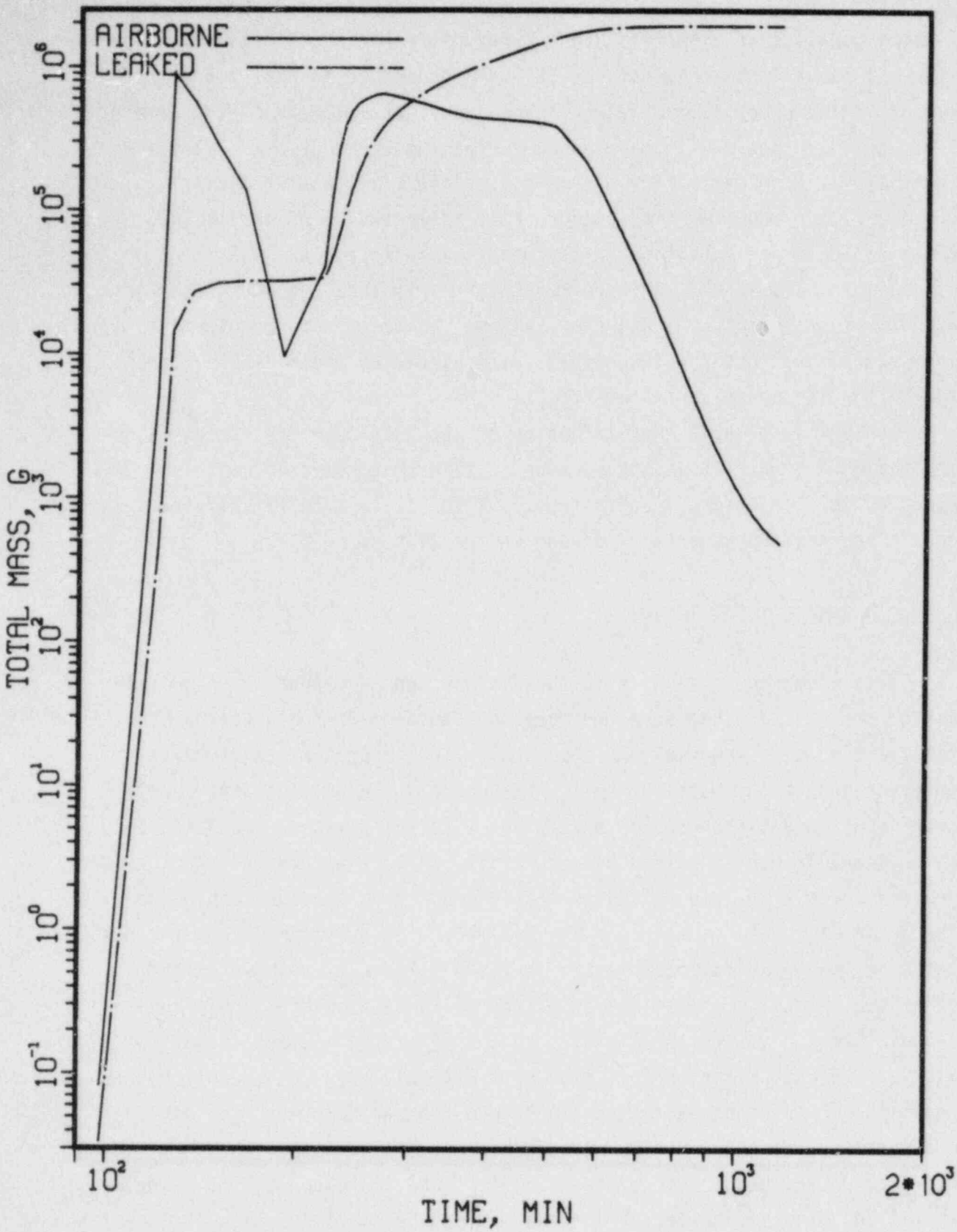

FIGURE 7.20. AIRBORNE MASS FOR THE SECONDARY CONTAINMENT AS A FUNCTION OF TIME, TC-Y

TABLE 7.12. DISTRIBUTION OF SPECIES AT 20 HOURS AFTER ACCIDENT, TC-Y

Species	Fraction of Core Inventory						
	RCS	Pool	Drywell	Wetwell	Reactor Bldg	SGTS	Environment
CsI	0.06	0.69	1.5×10^{-2}	0	6.9×10^{-2}	6.8×10^{-2}	0.10
CsOH	0.22	0.56	1.4×10^{-2}	0	6.1×10^{-2}	5.8×10^{-2}	9.1×10^{-2}
Te	0.34	7.9×10^{-3}	0.29*	0	0.11	1.3×10^{-2}	0.25

*This includes a fraction of 0.13 for Te which is found not to be released from the core-concrete interaction.

TABLE 7.13. DECONTAMINATION FACTORS CALCULATED AS A FUNCTION OF PARTICLE SIZE AND OF TIME FOR TW SEQUENCE

Time (min)	Particle Diameter, μm					DF Based on Total Mass
	0.2	0.5	1.0	4	10	
2756	1.9	18	1.17×10^4	10^5(a)	10^5	257
2777	1.4	9.4	2.51×10^3	10^5	10^5	576
2801	1.2	10.5	3.8×10^3	10^5	10^5	408
2811	1.1	10.4	2.2×10^3	10^5	10^5	865
2815	1.1	11.7	3.5×10^3	10^5	10^5	352
2818	10.3	60	9.9×10^3	10^5	10^5	326
2820	2.3×10^3	7.2×10^3	1.7×10^4	110^5	10^5	1336
2827	10^5	10^5	10^5	10^5	10^5	10^5

(a) A decontamination factor larger than 10^5 is assumed to be 10^5.

Pool depth: 6.5 ft (198 cm)
Bubble diameter: 0.75 cm
Aspect ratio: 1:3

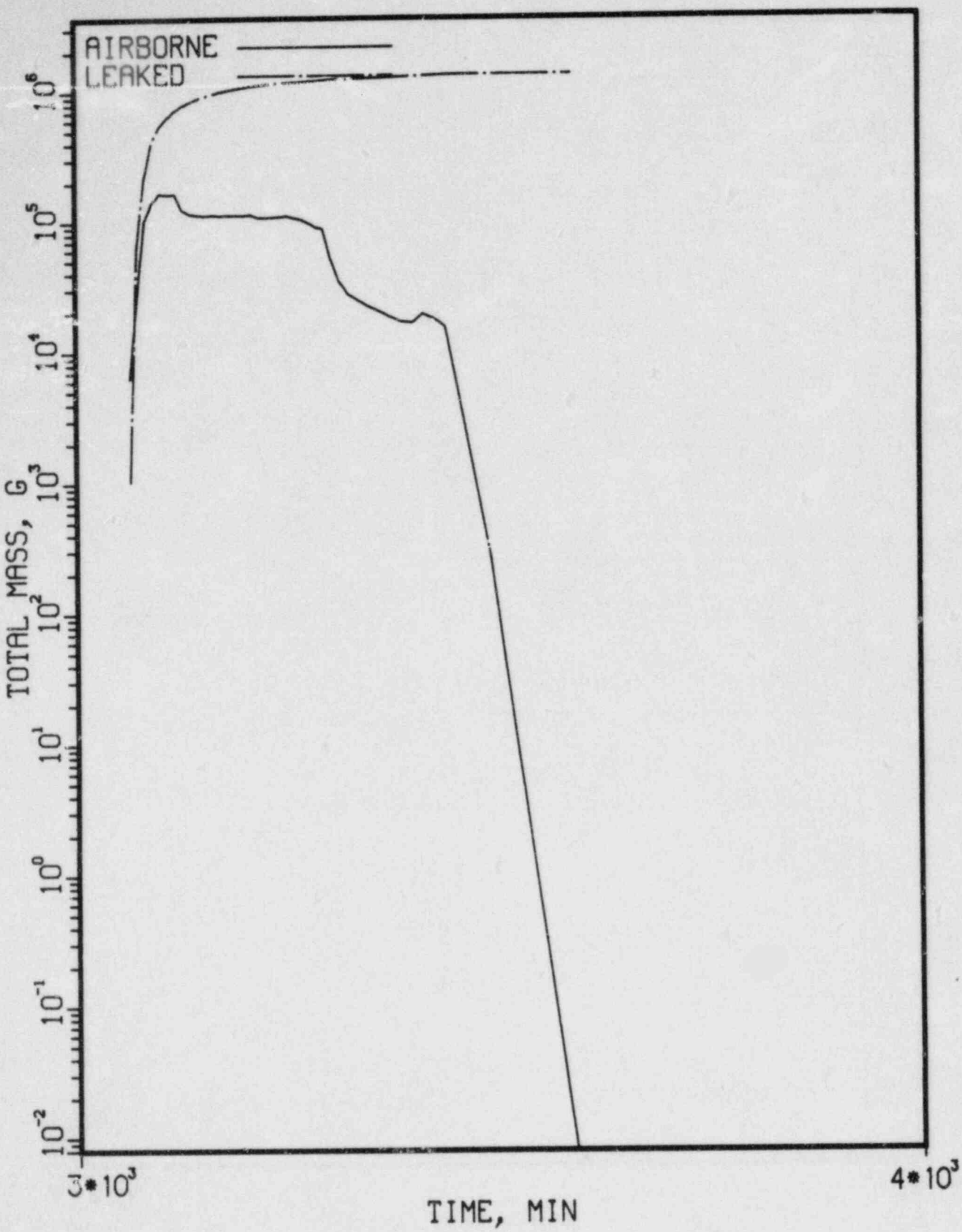

FIGURE 7.21. AIRBORNE AND LEAKED AEROSOL MASS FOR THE DRYWELL AS A FUNCTION OF TIME, TW-Y'

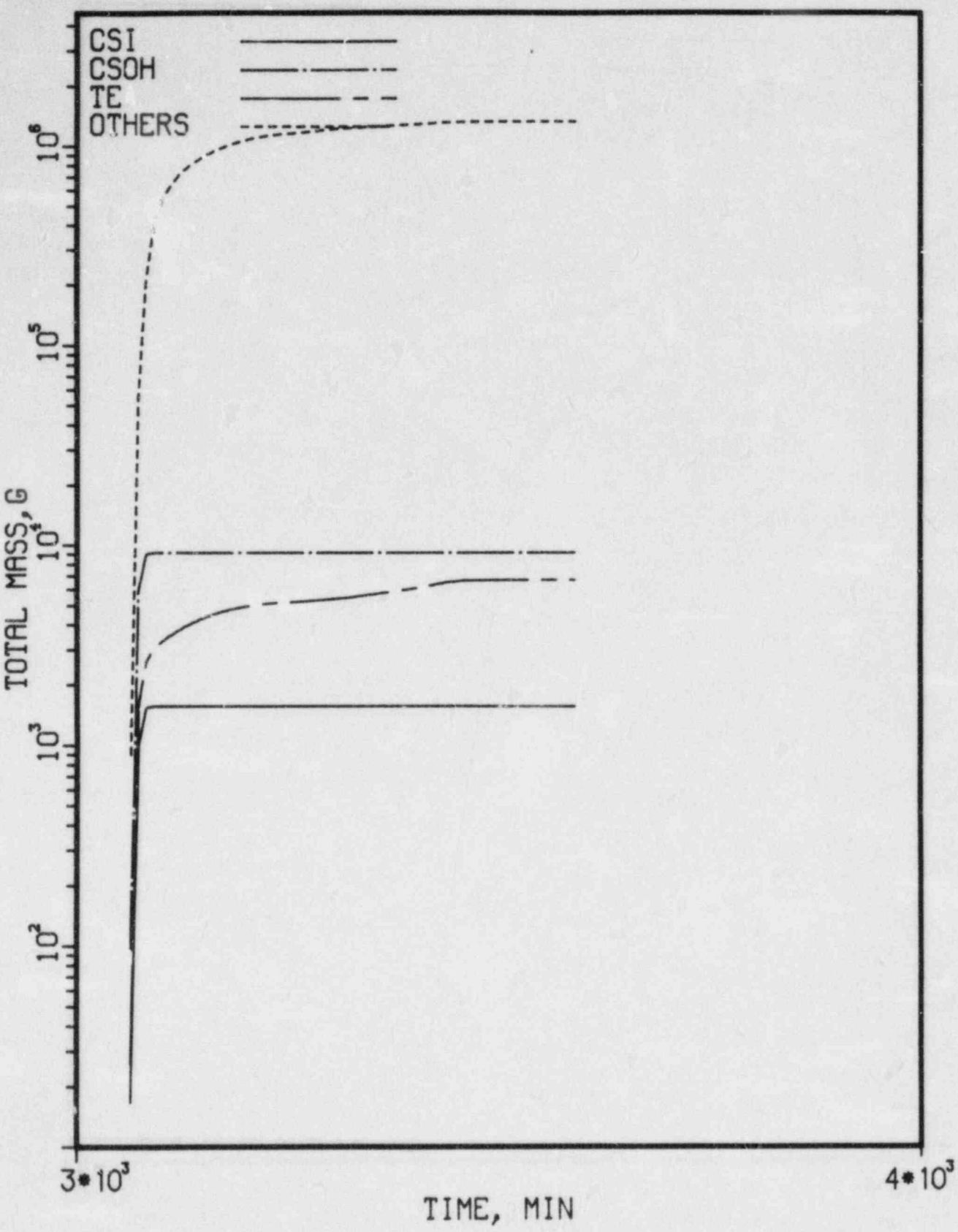

FIGURE 7.22. ACCUMULATED MASS LEAKED INTO ENVIRONMENT FOR VARIOUS SPECIES, TW-γ'

Table 7.14 is the distribution of solid particulate mass at various containment locations and at various times. Recognizing that the flow path of fission products for an accident time up to the vessel failure time (3055 minutes) is from RCS through the suppression pool and wetwell and finally to the drywell, approximately 1.2 kg of particulate is calculated to be released to the environment during this period of time while about 540 kg is retained in the suppression pool. After the reactor vessel fails, fission products are released directly into the drywell and transported to the atmosphere. From Table 7.14 it is seen that about 2000 kg of particulate is retained in the drywell primarily by the gravitational settling coupled with the particulate growth mechanism while 1350 kg reaches the atmosphere.

Table 7.15 is the locational distribution of various species as fraction of core inventory. It should be noted that a very small amount of core inventory fraction was found to be retained in the wetwell at the time the vessel failed. Considering that the assumed "floor" area of the wetwell is the water surface of the suppression pool, the amount calculated to settle in the wetwell was added to the amount retained in the suppression pool. For this reason, distribution of particulates beyond the vessel failure time is shown to be nil both in Tables 7.13 and 7.14. In general, about one-fifth of CsI and CsOH is seen to be released to the environment in Table 7.15 when compared with the results for TCγ' (Table 7.11). Nearly one-half of Te escapes from the reactor in TWγ' compared to TCγ'.

7.3.5 Results for Release of Reactor Safety Study Groups

An additional calculation for the AEγ' sequence was carried out to obtain information for transport and retention of fission products in the containment for WASH-1400 fission product groups. As was discussed in Chapter 6, six groups were identified: I (Group 2), Cs (Group 3), Te (Group 4), Sr (Group 5), Ru (Group 6), and La (Group 7). Xe and Kr, which are members of Group 1, do not appear in the containment calculation because they are not deposited in the containment and are in gaseous form and not treated in the aerosol codes. For Groups 2 through 7, results from TRAP-MELT calculations were adopted as the sources to the containment in addition to the core-concrete interaction source from VANESA. Other than Cs, I, and Te, VANESA calculations

TABLE 7.14. DISTRIBUTION OF TOTAL SOLID PARTICULATE MASS (KG) AT VARIOUS TIMES, TW

Time (min)	Event	Drywell		Pool Captured	Wetwell	Environment
		Suspended	Deposited			
2737	Melt start					
2786		0.15[a]	~0[a]	55	0.01	~0[a]
2815	Slump starts	0.42[a]	~0[a]	203	0.131	~0[a]
2822	Core collapse	1.18[a]	~0[a]	491	0.148	~0[a]
2825		1.21[a]	~0[a]	511	0.032	~0[a]
2827	Vessel dry					
2900		~0	0[a]	540	~0	1.22[a]
3055	Head fails					
3062		25.8	3.8	540	~0	56.3
3120		116	677	540	~0	835
3400		16.3	1990	540	~0	1325
3600		~0	1997	540	~0	1338
3660	Accident ends					

(a) Estimated.

TABLE 7.15. DISTRIBUTION OF SPECIES AT 60 HOURS AFTER ACCIDENT, TW$_Y$'

Species	Fraction of Core Inventory				
	RCS	Pool	Drywell	Wetwell	Environment
CsI	0.14	0.80	5.4×10^{-3}	0	4.8×10^{-2}
CsOH	0.15	0.79	5.0×10^{-3}	0	4.5×10^{-2}
Te	0.40	8.6×10^{-3}	0.40*	0	0.19

*This includes a fraction of 0.20 for Te that is found not to be released from the core-concrete interaction.

supplied the release rates for Mo, Ru (Group 6), Ba, Sr (Group 5), La, Ce, and Nb (Group 7). Using Cs to represent Group 3, Mo and Ru to represent Group 6, and La, Ce, and Nb to represent Group 7, scaling factors were used to obtain the respective total group release rates. Scaling factors are defined as the elemental inventory for each entire group divided by the sum of the inventories of the elements representing the group.

Table 7.16 shows the fraction of fission products released to the environment for this calculation of release by group. Compared to Table 7.8, the release fraction of Group 2 is the same as the CsI release fraction, and the release fraction of Group 3 is the same as the CsOH release fraction. This is because all of the iodine is included in CsI and the major portion of Cs is included in CsOH. For the release rate of Group 4, nothing is modified from the previously calculated release rates for Te due to the small inventories for Se and Sb, which are two of the three members in Group 4. Therefore the release fraction for Te in Table 7.8 is identical to the release fraction for Group 4 in Table 7.16. Since the scaling factor for Group 7 is 5.9, the uncertainty in the release fraction for Group 7 could be considerable. The release fraction for Group 6 is the smallest because the low fraction released from the fuel for this group.

7.4 Discussion

In WASH-1400, the TW and TC system sequences dominated the predicted risk to the public for this reactor design. This dominance was a result of the estimated likelihood for these sequences as well as their consequences. The estimated mean core melt frequency for each sequence was 1×10^{-5} yr^{-1}. This was compared with a median frequency of 5×10^{-7} yr^{-1} for the TQUV system sequence which had the next highest frequency. The estimated median frequency for the AE sequence was 1×10^{-7} yr^{-1}. Thus, the TW and TC system sequences were more than an order of magnitude higher in estimated frequency than the next most likely sequence and were two orders of magnitude more likely than the background of remaining sequences. This perspective on the importance of the TW and TC sequences has not changed substantially in the intervening years and is reflected in the results of the Accident Sequence Evaluation Program.

For the BWR sequences only four fission product release categories were used for core meltdown sequences as opposed to the seven categories used

TABLE 7.16. FRACTION OF CORE INVENTORY RELEASED TO THE ATMOSPHERE FOR GROUPS OF REACTOR SAFETY STUDY (AE)

Time (hr)	I Group 2	Cs Group 3	Te Group 4	Sr Group 5	Ru Group 6	La Group 7
0.5	0	0	0	0	0	0
1	0.19	0.19	3.6×10^{-2}	1.2×10^{-2}	2.7×10^{-3}	9.9×10^{-5}
2	0.25	0.24	6.6×10^{-2}	1.3×10^{-2}	3.6×10^{-3}	1.0×10^{-4}
4	0.34	0.33	0.51	0.64	4.6×10^{-3}	0.44
7	0.34	0.33	0.64	0.68	4.6×10^{-3}	0.49
10	0.34	0.33	0.65	0.68	4.6×10^{-3}	0.49
15	0.34	0.33	0.65	0.68	4.6×10^{-3}	0.49

for the PWR. The time-integrated release fractions are shown in Table 7.17 for each of the release categories. Categories BWR 1 and 2 involve very large fractions for the volatile fission products and are comparable in severity. The comparatively large release of ruthenium in the BWR 1 sequence is the result of fuel fragmentation, dispersal, and oxidation following a steam explosion that fails the primary containment.

All of the in-vessel steam explosion failure sequences, α, were assigned to the BWR 1 category. Because of the low probability of steam explosions leading to containment failure (10^{-2}), this failure mode was not a major risk contributor in WASH-1400.

In general, the overpressure failure sequences with direct release to the environment, γ', were assigned to Category BWR 2 and the overpressure failure sequences with deposition in the reactor building, γ, were assigned to Category BWR 3. This category is less severe than BWR 2, but would still result in major public health consequences. Since 25 percent of overpressure sequences were assigned to γ', the relative probabilities of the sequences in Category 2 and Category 3 in WASH-1400 were approximately in the ratio 1:3. An important exception to the assignment of failure modes to release categories was the treatment of the system sequence TC. The analyses performed for TC in WASH-1400 indicated that core meltdown would precede containment failure and that some retention of fission products would occur in the suppression pool. For this reason, TCγ and TCγ' were both assigned to Category 3, increasing its relative importance.

The final core melt release category, BWR 4, involves significantly reduced release fractions. At this level of in-plant attenuation, the actual values for the release fractions for the volatile fission products are not particularly important because the public health consequences would be dominated by the noble gases. The principal sequences in this release category involved isolation failures in which the small leakage rate from the primary containment could be treated by the SGTS prior to release to the environment. The likelihood of this mode of containment isolation failure was estimated to be small. The combination of low probability and low consequences made the contribution of Category BWR 4 to the public risk negligible. Thus, Categories BWR 2 and BWR 3 were the important risk contributors.

In Table 7.18 the release fractions for sequences TWγ', TCγ', and AEγ' are compared with the WASH-1400 values. The lower release fractions are

TABLE 7.17. WASH-1400 RELEASE CATEGORIES

Release Category	Fraction of Core Inventory Released						
	Xe-Kr	I	Cs-Rb	Te-Sb	Ba-Sr	Ru	La
BWR 1	1.0	0.4	0.4	0.7	0.05	0.5	5×10^{-3}
BWR 2	1.0	0.9	0.5	0.3	0.1	0.03	4×10^{-3}
BWR 3	1.0	0.1	0.1	0.3	0.01	0.02	3×10^{-3}
BWR 4	0.6	8×10^{-4}	5×10^{-3}	4×10^{-3}	6×10^{-4}	6×10^{-4}	1×10^{-4}

TABLE 7.18. COMPARISON OF SEQUENCES ASSIGNED TO BWR 2

Sequence	Fraction of Core Inventory Released			
	Xe-Kr	I	Cs-Rb	Te-Sb
BWR 2	1.0	0.9	0.5	0.3
AEY'	1.0	0.2	0.2	0.7
TCY'	1.0	0.3	0.3	0.3
TWY'	1.0	0.3	0.3	0.2

the result of predicted retention in the reactor coolant system and in the suppression pool. Because of the high temperatures in the reactor coolant system, the predicted retention for the volatile species is limited. The retention of the less volatile species as aerosols is more effective. In the transport of fission products through the suppression pool, it is assumed that all radionuclides other than the noble gases are in the form of aerosols. For the AE$_\gamma$' sequence, the decontamination factor is rather large for material carried into the pool prior to containment failure. After containment failure the flow path would no longer include the suppression pool.

In the TC$_\gamma$' and TW$_\gamma$' sequences, the release pathway is through the pool until the time of reactor vessel melt-through. The pool of water is saturated during this time period so the amount of decontamination is not as great as for the AE system sequence. As discussed earlier, the decontamination factor for the saturated pool is very sensitive to the size distribution of the aerosols and the resulting uncertainty in the release fractions in Table 7.18 is large.

The TC$_\gamma$ sequence was analyzed in order to examine the potential effectiveness of the reactor building and SGTS in further mitigating the consequences of an accident when the structural integrity of the reactor building is maintained following failure of the primary containment. The results for this sequence are compared with the release fractions for Category BWR 3 in Table 7.19. The effect of the reactor building systems can be determined by comparing the results for the TC$_\gamma$ and TC$_\gamma$' sequences directly. The quantities of fission products, other than noble gases, that do escape to the environment are primarily the result of outleakage from the reactor building. The TC$_\gamma$ sequence analyzed did not consider the effect of the fire sprinkler system on further reducing the fission product source term if it were activated by the hot steam during blowdown of the primary containment. The sprinkler system would be expected to lead to a significant additional reduction in the source term both due to washout of airborne aerosols and due to steam condensation which would result in a net air in-leakage to the building. Eventually the mixing of air and hydrogen in this sequence would probably result in flammable conditions with the potential of destroying the reactor building. The consequences of the sequence would be very sensitive to the timing of the hydrogen burning event.

TABLE 7.19. COMPARISON OF SEQUENCES ASSIGNED TO BWR 3

Sequence	Fraction of Core Inventory Released			
	Xe-Kr	I	Cs-Rb	Te-Sb
BWR 3	1.0	0.1	0.1	0.3
TCY	1.0	0.2	0.2	0.2

The analyses performed for the Peach Bottom 2 reactor indicate that the WASH-1400 release fractions in the high consequence BWR 2 category are overestimated for iodine, cesium, and the involatile fission products. The specific scenario analyzed to compre to the BWR 3 category resulted in comparable but slightly higher releases than in WASH-1400. Slight variations in modeling assumptions would have led to substantial additional retention, however. The implications of these results to the WASH-1400 perspective on risk depend on the relative likelihoods of the γ and γ' failure modes. If the reactor building were expected to withstand blowdown forces from the failure of the primary containment with a high degree of confidence, the risk could be reduced substantially. The uncertainties in the thermal, hydraulic, and structural response of the primary containment structure and the reactor building are very large, however. The scope of the current effort was oriented at developing an understanding of the consequences of given accident scenarios rather than estimating the likelihoods of alternative scenarios.

The results presented in this report are referred to as best-estimate results. Sensitivity studies will be performed later in the program to provide perspective on the ranges of the uncertainties associated with the best-estimate values. In each phase of release and transport, important uncertainties exist. Changes in assumptions and models could affect the prediction of the environmental source term substantially.

In calculating the initial period of core heatup, the MARCH 2 code has been demonstrated to have reasonable accuracy. After fuel melting and slumping begins, the MARCH 2 code models very complex phenomena with very simple models. The maximum fuel temperature is probably underpredicted by MARCH 2 and the time at temperature is quite uncertain. As a result, the timing of release of volatile fission products and the magnitude and timing of release of less volatile fission products from the fuel could be affected by thermal hydraulic modeling deficiencies.

Thermal hydraulic modeling uncertainties also have a major impact on uncertainties in the transport of fission products in the reactor coolant system, primary containment and the reactor building. The temperatures and flows in the reactor coolant system directly influence the extent of retention. Indeed, the MARCH 2/MERGE results indicate temperatures that are just high enough to limit the retention of the volatile species CsI and CsOH. The predicted time, location, and mode of failure of the primary containment

building also have a major influence on the predicted environmental source term. The predicted failure of the primary containment prior to pressure vessel melt-through, coupled with failure in the drywell region, resulted in a large fraction of the fission products bypassing the suppression pool in the AE sequence. The rate of generation of hydrogen, failure pressure for the primary containment, and location of failure (drywell versus wetwell) are sufficiently uncertain that the actual accident scenario could follow a pathway that could result in substantially greater attenuation in the suppression pool. Similarly for the TC and TW sequences, failure of the primary containment in the wetwell region could result in substantially less retention in the suppression pool.

The decontamination factor for the pool is itself quite uncertain even with well specified input thermal hydraulic conditions. The decontamination factor predicted by SPARC is very sensitive to aerosol size. A small shift in the predicted size distribution could change the results of the calculated aerosol retentions substantially.

Finally, the reactor building potentially has the capability to significantly reduce the environmental source term depending on its response to failure of the primary containment. The associated technical questions will be extremely difficult to resolve.

In conclusion, the reader should be careful not to assign greater significance to the single-valued best-estimate source terms that are provided in this report than warranted by the uncertainties in the underlying assumptions and methods of analysis.

APPENDIX A

STANDBY GAS TREATMENT SYSTEM OPERATION AND EFFECTIVENESS UNDER SEVERE ACCIDENT CONDITIONS: PEACH BOTTOM AND GRAND GULF NUCLEAR STATIONS

APPENDIX A

STANDBY GAS TREATMENT SYSTEM OPERATION AND EFFECTIVENESS UNDER SEVERE ACCIDENT CONDITIONS: PEACH BOTTOM AND GRAND GULF NUCLEAR STATIONS

Introduction

In the unlikely event that a severe accident should actually occur at a Boiling Water Reactor (BWR) facility, the primary containment would eventually fail. Fission products would pass from the primary containment into the secondary containment and from there to the atmosphere by way of the Standby Gas Treatment System (SGTS). It is the function of the SGTS to mitigate the fission product release by means of exposure of the exhaust flow to filters and activated charcoal. The operation and effectiveness of the SGTS at the Peach Bottom and Grand Gulf nuclear stations under severe accident conditions are discussed in this report. Most of the design information has been obtained from the respective Final Safety Analysis Reports (FSARs). Information concerning filter train effectiveness has been taken from "Analysis of a Small-Break LOCA Outside Containment at Browns Ferry Unit One --Iodine, Cesium, and Noble Gas Distribution and Release", NUREG/CR-2672 Volume 2 (to be published).

Peach Bottom

System Design and Description

In the BWR MK-I containment design employed for Units 2 and 3 at the Peach Bottom Station, the primary containment comprises the drywell and wetwell. In each unit the primary containment is surrounded by a reactor building which includes two ventilation zones, the areas above and below the refueling floor. During routine operation, the

reactor building is kept at a pressure just below atmospheric by the normal building ventilation system.

Under accident conditions*, the normal ventilation system for the affected reactor building is automatically shut down and the SGTS is automatically started. The SGTS is designed to minimize the escape to the environment of radioactive material released to the reactor building of either unit from its primary containment. The SGTS filters the exhaust, exposes it to charcoal absorption, and provides an elevated release through the 500-ft plant stack. A schematic drawing of the system is provided in Figure A-1.

The SGTS comprises suction ducts, two parallel filter trains, three full-capacity (10,500 cfm) exhaust blowers, and the exhaust ducting to the plant stack. The filter trains and blowers are located in an underground shielded room in the basement of the radwaste building. The suction ducts connect with the normal ventilation system exhaust piping and duct work of each of the reactor buildings. The normal ventilation system exhaust ducts are provided with fast-acting (3-5 sec) cylinder-operated butterfly valves for rapid isolation when an accident signal occurs. The isolation signal also actuates the SGTS; both parallel filter trains go into operation with suction from all three blowers.

The volumetric flow from the affected reactor building would be about 25,000 cfm with all three blowers running, but the operator would be expected to shut off two of the blowers to reduce the flow to the SGTS design value of 10,500 cfm. A vacuum relief system is provided to prevent the differential pressure between the outside atmosphere and the interior of the reactor building from exceeding 1/2-inch H_2O. The total flow into the SGTS is taken approximately equally from the two ventilation zones above and below the refueling floor.

*Signaled for an affected unit by high radiation in the exhaust duct, low reactor vessel water level, or high drywell pressure.

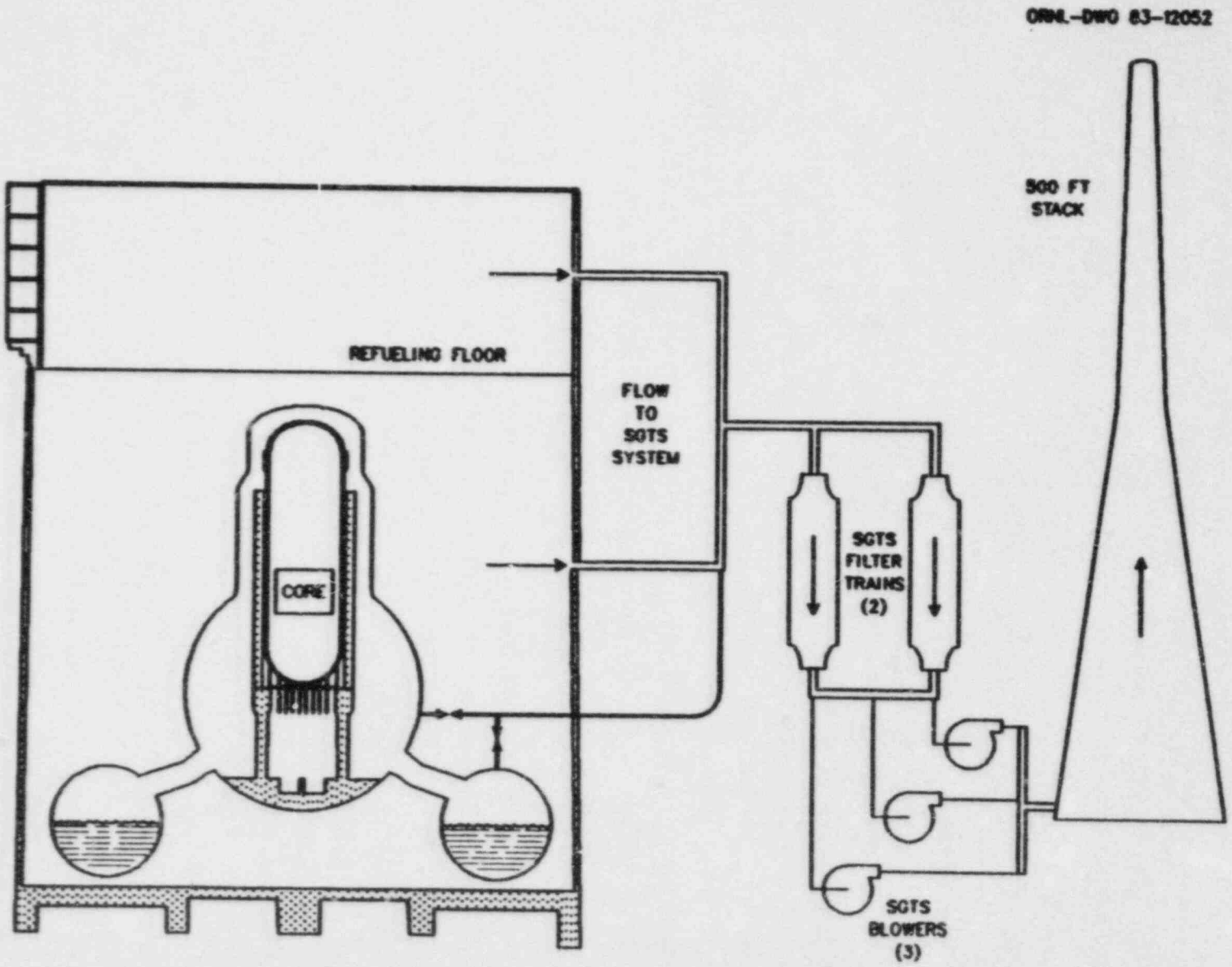

FIGURE A-1. SCHEMATIC DRAWING OF PEACH BOTTOM STANDBY GAS TREATMENT SYSTEM. AS SHOWN, PROVISION IS MADE FOR EXHAUST FROM THE PRIMARY CONTAINMENT DURING NITROGEN INERTING OR UNDER ACCIDENT CONDITIONS.

Each SGTS train comprises six elements. The first is a moisture separator designed to remove 99.9 percent of the moisture particles 2 microns or larger and 30 percent of the 1-micron particles. The separated moisture is collected in a sump and pumped to the radwaste building.

Just after the moisture separator, an electric heater (energized with the startup of the SGTS) is provided to reduce the relative humidity of the mixture of steam and other gases in the flow. The heater will cut off automatically on low flow or if the temperature of the flow exceeds a set value. Thus, the relative humidity of a flow at a temperature greater than the set value would not be reduced.

A water resistant prefilter (roughing filter) designed to remove large particulates and thereby protect the downstream High Efficiency Particulate Assembly (HEPA) filters is installed just after the moisture separators and heater. The prefilter actually serves as a backup to the moisture separator, which also acts as a good prefilter.

The fourth element in each filter train is a bank of nine 2-ft^2 High Efficiency Particulate Assembly (HEPA) 1000 cfm filter cells, which will remove 99.97 percent of particulates 0.3 micron and larger. The HEPA cells have water retardant glass fiber media, aluminum separators, and cadmium-plated steel frames with rubber base adhesives and neoprene gaskets and have a design temperature capability of 250 F (200 F for continuous service).

Exposure to radiation during a severe accident might reduce the efficacy of the HEPA filters. Radiation testing of HEPA filters coordinated at the Naval Research Laboratory for exposures as high as 10^8 rads has shown some reduction in the tensile strength of the filter media and some deterioration of the rubber adhesive and the neoprene gasket. The gasket, although brittle, continued to seal. Thus the filter media, adhesives, and gaskets should remain satisfactory for continued filtration and normal pressure losses with exposures as high as 10^8 rads.

The fifth element in each filter train is an activated charcoal bed containing a minimum of 1,320 lb of charcoal. The bed consists

of individual rigid, welded, leaktight, stainless steel rectangular canisters. The canisters are filled with impregnated charcoal with an ignition temperature of 640 F. Each canister contains about 50 lb of charcoal. The charcoal canisters are mounted in dual tray module drawers. Each train has 27 drawers arranged in a single bank of nine horizontal rows with each row being three drawers wide. The flow is vertical through a 2-inch thick layer of charcoal, and is equally distributed across all of the canisters. The canisters are sealed to the bulkhead frame with continuous gaskets and are held in place by individual clamps. Water sprays are provided to prevent overheating of the charcoal filter if the air flow should be totally lost while a large radioactive iodine inventory is present.

According to the Peach Bottom FSAR, the carbon absorber unit is capable of removing at least 85 percent of methyl iodide (CH_3I) and 99.9 percent of elemental iodine (I_2) under entering conditions of 70 percent relative humidity of 190 F. It should be noted that the Browns Ferry FSAR claims a 95 percent removal efficiency for methyl iodide for a similar charcoal bed.

The sixth element in each filter train is a second HEPA filter, identical in characteristics to the first HEPA filter.

HEPA Filter Behavior

HEPA Filter Efficiency. Individual 1000 cfm HEPA filter units usually have an efficiency of 99.99 percent when tested with dioctyl-pthalate (DOP) smoke. An assembly of these filters might show a lower average efficiency because of gasket leakage or minor damage to the filter medium during installation. Filtration of accident-generated aerosols should occur with efficiencies similar to those found for DOP aerosols. When both HEPA filter banks (in front of and behind the charcoal absorber units) are intact, the combined efficiency can safely be assumed to be 99.99 percent or greater.

HEPA Filter Plugging and Rupture. Large amounts of aerosol will be collected in the SGTS units during a severe accident sequence. Calculations show that the amount collected can result in a pressure drop across the HEPA filters sufficient to cause rupture of the filters. The pressure differential required for filter failure is uncertain, but it is reasonable to assume that a differential pressure equivalent to 12-inch water will cause rupture. With this assumption, the flow conditions at the time of filter failure are illustrated in Figure A-2, which is a pressure drop-flow diagram for a single 9000 cfm SGTS train which has nine filters in-parallel in each bank. According to this diagram, the initial clean system flow is 9000 ft^3/min with a pressure drop across the system of 13.3-inch water. (Each clean HEPA filter bank has a pressure differential of 1.0-inch water.)

As aerosol particles are collected on the nine filters in the first HEPA bank, the pressure drop across these filters increases and the system flow decreases following the characteristic curve of the blower. When the first HEPA filter bank reaches a pressure drop of 12-inch water, the system flow will have decreased to 3300 ft^3/min and it is reasonable to assume that one or more of the nine HEPA filter units in this bank would fail with openings large enough to decrease both pressure drop and filtration efficiency to zero. In addition, it is reasonable to assume that the second HEPA filter bank is not damaged, and that the aerosol particles passing through the charcoal absorber unit do not affect the adsorption of iodine species. Granular charcoal beds are poor filters of particulates, and it can be assumed that no aerosol deposition occurs in the charcoal beds.

The behavior of the second HEPA filter bank can be assumed to duplicate that of the first with respect to buildup of pressure differential and rupture at 12-inch water. The overall filtration efficiency would drop to 99.9 percent since only one filter bank is in operation.

As previously stated, the exact conditions that result in massive filter failure are unknown. New filters are required to withstand 10-inch water while the filters are exposed to a moist

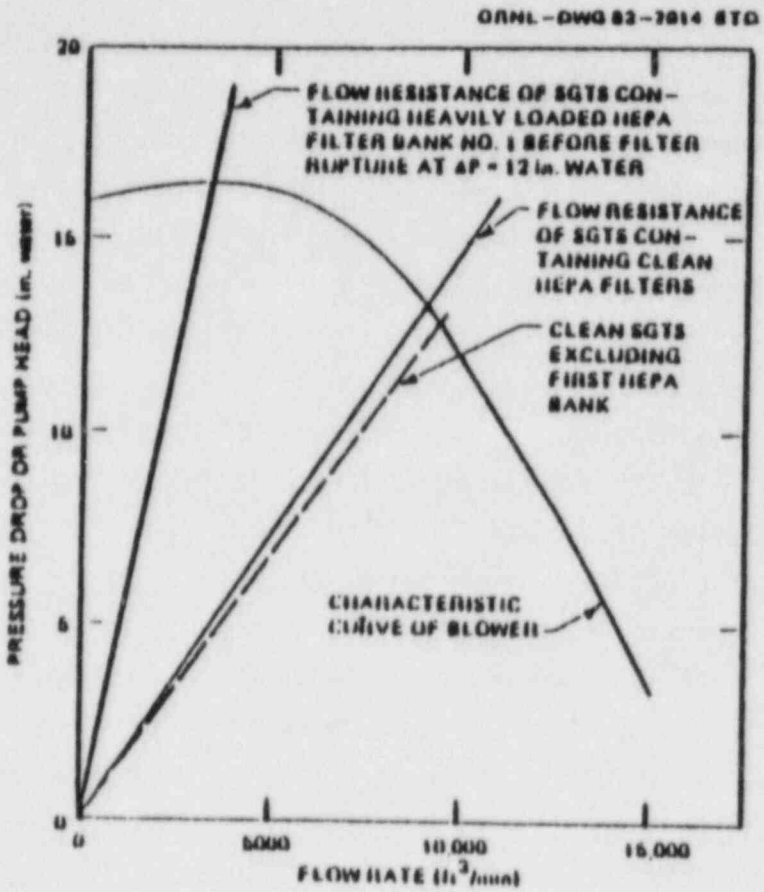

FIGURE A-2. FLOW CHARACTERISTICS OF A SINGLE SGTS TRAIN

atmosphere.[A-1] The flow conditions corresponding to the assumption of filter failure at other pressure differentials can be obtained from Figure A-2. For 10-inch water, the system flow would be 4600 ft^3/min; for 12-inch, 3300 ft^3/min; for 15-inch, 800 ft^3/min; and for failure threshold above 16-inch water the filters would not fail.

No data are available for pressure buildup on HEPA filters caused by accident-produced aerosols. In severe accident sequences, most of the aerosol would result from core melt-concrete interaction. Pressure buildup data in the literature are mainly from natural atmospheric aerosols, and these tests are usually terminated when the pressure drop reaches 3- or 4-inch water. An average for seven such tests is 4-inch water pressure drop for an accumulation of 1.2-kg atmospheric aerosol particles on a 1000 ft^3/min HEPA filter.[A-2] This is equivalent to 10.8 kg on a nine filter SGTS bank. Similar behavior was observed with five tests of various HEPA filter types when operated at design flow conditions.[A-3]

A best estimate of pressure drop across the first bank HEPA filters as a function of accident-produced aerosol collected in one 9-filter SGTS train is shown in Figure A-3. The mass shown is that collected in all parts of the SGTS: ductwork, demisters, prefilters, and HEPA filters. It should be emphasized that the pressure drop shown in Figure A-3 is for the full flow conditions; reduced flow and pressure drop would occur in a real SGTS system as suggested in Figure A-2.

As an illustration, the HEPA filter behavior assumed for the computer simulation of the Browns Ferry Scram Discharge Volume Break (SDV) accident sequence is shown in Table A-1. Flow reduction through the SGTS resulting from aerosol collection was not considered. This results in faster collection of the amount of aerosol required for obstruction and consequent rupture of the HEPA filters. However, the time difference would not be very great since the high pressure drop and flow reduction occurs to a significant extent only with the last 10 or 20 percent of the aerosol collected.

If we had chosen 15-inch water as the rupture criterion, the flow reduction would probably have been enough to allow the reactor

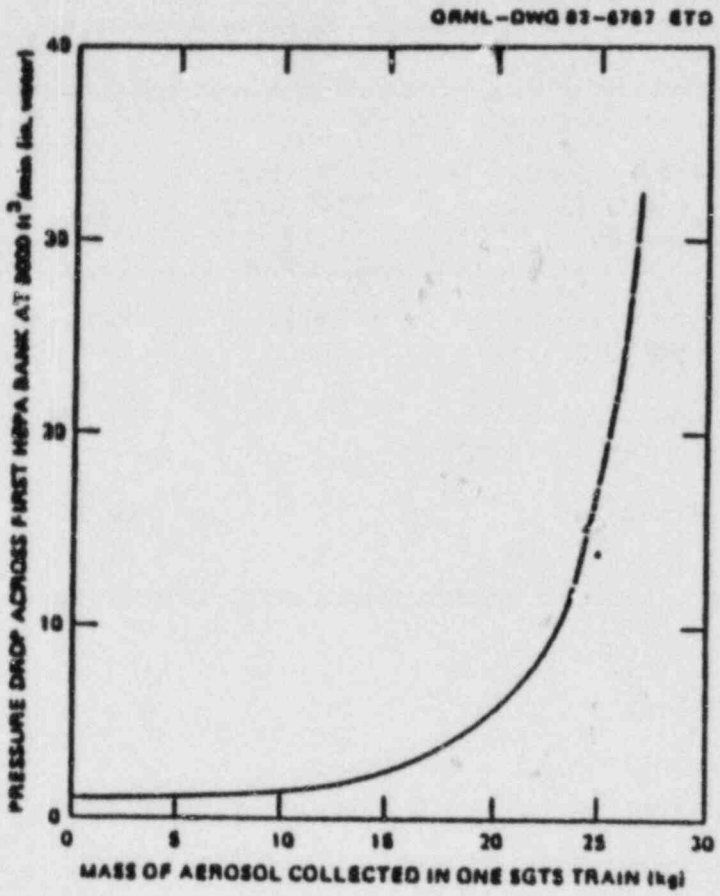

FIGURE A-3. PRESSURE DROP ACROSS A HEPA FILTER BANK

TABLE A-1. HEPA FILTER BEHAVIOR FOR THE SDV BREAK ACCIDENT CALCULATION FOR BROWNS FERRY

Interval (Determined by Aerosol Load)	Aerosol Load in SGTS (kg)	Aerosol Filtration Efficiency (%)	Flow Rate
First	0-27 per train (0-81 per 3 trains)	99.99	Normal: no reduction
Second	27-54 per train (81-162 per 3 trains)	99.9	Normal: no reduction
Third	54 per train (>162 per 3 trains)	0	Normal

building to become positive in pressure so that some of the aerosol and iodine vapor species would have leaked out without filtration. Leakage directly from the building would also occur if no HEPA filter rupture had been assumed. The low flow rates concomitant with the 15-inch water rupture and no-rupture scenarios would result in elevated charcoal bed temperatures, enhanced iodine desorption, and possible charcoal ignition.

Charcoal Adsorber Efficiency

The tray type charcoal adsorber system described previously provides a face (superficial) velocity through the bed of 40 ft/min which is typical for American nuclear reactor adsorber systems. The 2-inch deep beds result in a stay-time of ~0.25 s.

Charcoal Adsorber System Efficiencies -- General. Charcoal adsorbers in nuclear reactor ventilation systems are designed to trap two chemical forms of radioactive iodine: molecular iodine (I_2), and organic iodides (mostly CH_3I). Molecular iodine is easily adsorbed from gases by activated charcoal, but the charcoal must be treated with special additives (impregnants) in order to efficiently trap and retain radioactive iodine in the organic iodide form. Even with very high quality impregnants, charcoals are normally significantly lower in efficiency for collecting organic iodides. Once the radioiodine from the organic iodide is trapped, either by isotopic exchange with the excess of nonradioactive iodine in the impregnant (as with a KI or KI_3 type impregnant) or by direct chemical reaction with the impregnant (triethylenediamine, TEDA, for example), the radioactive iodine from the organic iodide becomes indistinguishable from that originating as radioactive I_2. No significant desorption of trapped radioiodine will occur unless the charcoal temperature rises above ~150 F.

Charcoal efficiencies are usually determined by subjecting small representative quantities of a commercial lot to laboratory tests as specified in ANSI N510 and ASTM D3803. If the charcoal meets these

requirements and is installed in a properly built and leak-tested system, it is assumed to be able to function with I_2 and organic iodide trapping efficiencies somewhat lower than the test results show.

Adsorption efficiencies and desorption rates (at elevated temperatures) can be calculated for nonstandard conditions by using conventional correlations for gas-to-solid mass transfer in packed beds. An example is the correlation of Chu, et al.(A-4-A-6) The parameters of importance are particle size, void fraction, gas velocity, density, viscosity, diffusion coefficient (I_2 or CH_3I in the bulk gas), temperature, and bed depth. At elevated temperatures desorption must be accounted for by including an absorption/desorption isotherm that specifies the pressure or concentration of iodine in the gas phase in equilibrium with iodine sorbed on the charcoal.

Tests results from the standard tests must be used to adjust the mass transfer correlation for the inherent properties of the charcoal. This can be done by means of a term that specifies what fraction of the charcoal grain surface is available for active adsorption, isotopic exchange, or chemical reaction. "Poisoning" of the charcoal surface by adsorbed or reacted contaminants, or the presence of adsorbed water will reduce the surface area available for trapping I_2 and CH_3I trapping. The effective surface area available for CH_3I trapping is less than that for I_2 sorption because the impregnants are not perfect in their surface coverage and chemical action.

Radiation Effects on Charcoal Adsorber Behavior. The first radiation effect investigated was the temperature increase that would occur from the decay of adsorbed radioiodine(A-7,A-8). It was determined that normal air flow rates would supply sufficient cooling. Tests using only heat from the decay of highly radioactive iodine (up to 2000 Ci $^{130}I/cm^2$ adsorber face area) showed that charcoal ignition from decay heat could occur but that the heat released by oxidation of the charcoal as the temperature rose past ~392 F would exceed the decay heat.(A-4,A-5)

Radiation effects on the retention of iodine sorbed on charcoal were first conducted using ^{60}Co gamma rays.(A-9) Organic iodides were formed that were released unless impregnants were present to trap them. A small decrease in iodine retention was observed even with good quality impregnated charcoal.(A-10) A radiation intensity saturation effect was observed at about 10^7 rad/h ^{60}Co gammas. The opposite effect was also observed. It was necessary to add the iodine to the charcoal immediately after placing the apparatus in the ^{60}Co facility because preliminary irradiation of the charcoal improved its performance.(A-11)

Tests with highly radioactive iodine as the radiation source(A-4,A-5) (<200 Ci $^{130}I/cm^2$ adsorber bed face area) showed a low desorption rate <110 C and that even at high temperatures desorption was slow enough at reduced air flow rates that several hours time would be available to correct the abnormal air flow occurrence. Tests with service-aged charcoals were included.

Recent tests with ^{60}Co and accelerator irradiations showed that irradiation of old, poisoned charcoals before adding iodine rejuvenated the charcoal.(A-12) Tests with ^{60}Co irradiations of charcoal containing sorbed iodine have been initiated.

In summary, both beneficial and detrimental effects of radiation have been observed. The magnitude of the effects were not large when compared to others. Exposure of iodine on charcoal at 80 C to ^{60}Co gamma irradiation for 4 hours resulted in an iodine fractional release rate of $\sim 10^{-4}$/h. The released iodine was easily trapped by impregnated iodine on charcoal in moist air released iodine at a rate of $\sim 5 \times 10^{-6}$ fraction/h. The released iodine was not collected efficiently by any of the impregnated charcoals or silver-exchanged zeolites tested.

Operating Conditions During the Browns Ferry SDV Break Accident. Calculations for the analysis of a hypothetical accident sequence at Browns Ferry Unit One will be described for illustrative purposes. There are three SGTS filter trains at Browns Ferry, each similar to

the filter trains used at Peach Bottom. A heating system with a humidity sensor built into the charcoal adsorber system assures that the charcoal will be initially at equilibrium with air containing a maximum of 70 percent relative humidity. For the accident sequence studied, the SGTS began operating at the time of the SDV break. By the time that radioactive material began being transported to the SGTS, the air inlet temperature to the charcoal bed was 180 F because of the combined effect of warm air entering the SGTS and temperature control by the heaters in the SGTS. The relative humidity of the air entering the charcoal bed oscillated between 70 and 100 percent. Following the failure of the drywell and actuation of the reactor building fire protection sprinkler system, the relative humidity of the air entering the SGTS was 100 percent, but the lowered temperature of this air, ~140 F, enabled the preheaters to warm the air entering the charcoal bed to 154 F so that the relative humidity in the adsorber system was 70 percent.

Collection Efficiency for Radioactive Iodine During the SDV Accident. Typical iodine collection efficiencies expected for the Browns Ferry charcoal bed are listed in Table A-2. As described in the previous section, the relative humidity was above 70 percent initially and decreased to 70 percent following start of the fire protection sprays. The efficiencies shown in Table A-3 are those deemed to be most representatives of the accident conditions. The delayed change to the higher efficiency is a result of the slow dryout of moisture from charcoal.(A-6)

Desorption of Radioiodine from the Charcoal Bed. A large amount of iodine will desorb if the charcoal temperature increases and air flow is maintained. Since the SGTS was expected to continue operation throughout the SDV break accident sequence (the HEPA filters were assumed to plug and then immediately tear), the charcoal temperature was not expected to increase significantly during this sequence.

TABLE A-2. TYPICAL ADSORPTION EFFICIENCIES FOR 2-INCH DEEP CHARCOAL BEDS

Species	Relative Humidity (%)	New Charcoal State of Art (%)	Reg Guide 1.52[a] New Charcoal (%)	Reg Guide 1.52[a] Old Charcoal (%)	Browns Ferry FSAR
I_2	95	99.99	99.9	99	99
CH_3I	95	99	95	90	95
I_2	70	99.999			
CH_3I	70	99.9	99.5	99	

(a) Charcoal tested in the laboratory at design temperature and velocity.

TABLE A-3. BEST-ESTIMATE EFFICIENCIES FOR BROWNS FERRY SDV ACCIDENT CHARCOAL BED

Iodine Species	Radioactive Iodine Collection Efficiency (kg)	
	Before Fire Sprays + 3 h[a]	3 h after Fire Sprays Start and Thereafter[b]
I_2	99.9	99.95
CH_3I	95	99.0

(a) Charcoal temperature 180 F (82.2 C), relative humidity 70 to 100 percent.

(b) Charcoal temperature 154 F (68 C), relative humidity 70 percent.

Ordinarily, the air flow through a charcoal bed must be reduced well below normal to cause a significant increase in charcoal temperature since air flow is the cooling medium that removes decay heat. At high temperatures, the captured radioiodine will move slowly toward the outlet end of the bed at a speed which increases with bed temperature and air flow rate, much as with material in a gas chromatograph. In tests with highly radioactive iodine on charcoal,(A-4,A-5) this movement of iodine was monitored continuously. A computer program named DESORB was used to convert the rate of movement into linear adsorption isotherm coefficients as a function of charcoal temperature. The linear coefficient assumed that the iodine partial pressure in equilibrium with the iodine sorbed on the charcoal was directly proportional to the concentration of sorbed iodine plus impregnant iodine. This model was in good agreement with data from the five different types of charcoal tested.

Although the model for desorption is simple, it requires a cmoputer program to follow desorption since the radioactive iodine is distributed nonuniformly through the bed. A second version of DESORB was used to calculate desorption that would occur during the Browns Ferry SDV break accident sequence. It was found that the desorption rate would be negligible because of the low charcoal temperatures. The continued supply of methyl iodide would result in more penetration of methyl iodide during adsorption than the desorption of both I_2 and methyl iodide.

Figure A-4 shows the result of DESORB calculations for various combinations of gas velocity, flow time, and bed temperatures. (These combinations did not occur in the case of the Browns Ferry SDV break accident sequence but are intended to show what is required for massive desorption to occur.) Note that the penetration experienced at the time of initial adsorption is calculated separately.

The plotted line in Figure A-4 for 70 C and 20 cm/s is close to that expected for the charcoal bed conditions following initiation of the fire protection spray system. Extrapolation of that line to 1-week operation would indicate ~1.5 percent desorption. Note that the

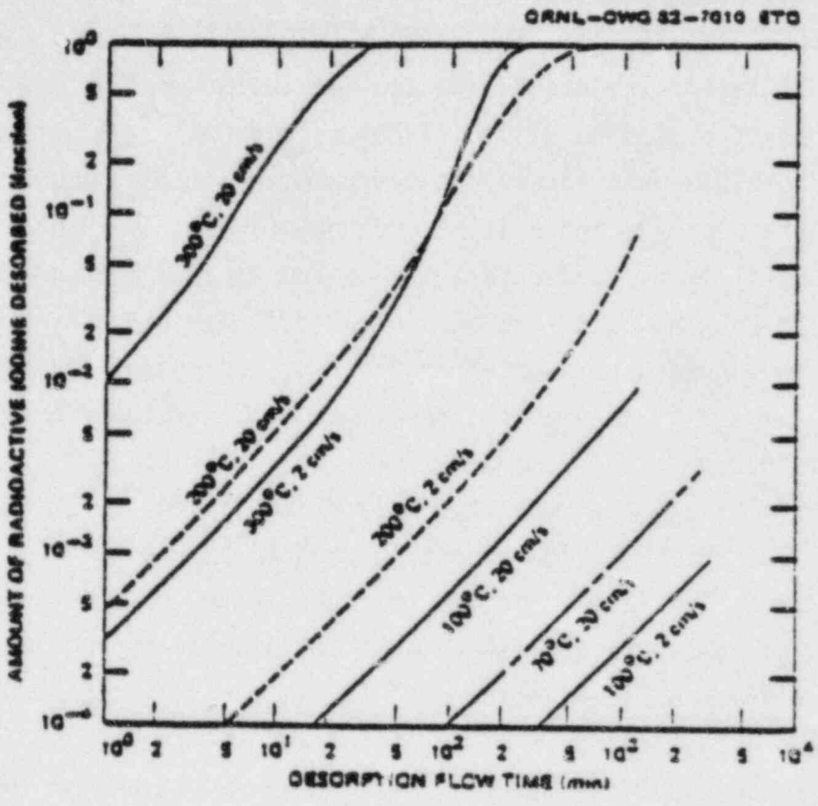

FIGURE A-4. DESORPTION FROM A 2-INCH DEEP CHARCOAL BED

approximately 10^{-4} fraction per hour release rate measured at 80 C in a ^{60}Co gamma field extrapolates to approximately 1.7 percent desorption in 1 week. This good agreement is fortuitious since both calculations involve extrapolation of short-term test data. The true amounts could differ as much as by a factor of 10.

The calculation results shown in Figure A-4 are for a bed with an initial adsorption efficiency of ~99 percent. A bed with higher adsorption efficiency would desorb at a lower rate, especially initially. These desorption curves are calculations for radioactive iodine existing on the bed at time zero. Iodine adsorbed later as will occur with CH_3I must be accounted for separately. The program DESORB is written for simultaneous adsorption and desorption.

Conclusions Regarding SGTS Behavior in the Browns Ferry SDV Break Accident Sequence. With the reasoning and the assumptions previously discussed, the HEPA filters in the SGTS trains were predicted to plug with aerosols, then immediately tear shortly after drywell failure. The ability to remove aerosols by filtration was assumed lost after the filters were torn, but the blowers were assumed to continue to operate so that charcoal bed iodine adsorption efficiency would be maintained.

Other SGTS failure modes are conceivable and the choice of an alternate scenario might have a major impact on the calculated fission product transport. For example, if the HEPA filters did not tear after plugging, flow through the SGTS would cease, the secondary containment would pressure, and the only pathway from the interiors of the reactor building and refueling bay to the surrounding atmosphere would be via exfiltration through the exterior walls. In addition, the SGTS charcoal beds might overheat, and plastic and organic sealants of the ducting in the portions of this system not exposed to the reactor building fire protection system sprays might fail by overtemperature.

The estimated SGTS train aerosol filtration efficiencies for the period when both the upstream and downstream HEPA filters are effective and for the period when the upstream filter has torn and only the

downstream filter is effective are listed in Table A-3. The absorption efficiencies for I_2 and organic iodide actually used in the Browns Ferry SDV fission product release calculation are those listed under "Browns Ferry FSAR" in Table A-2 (99 percent for I_2 and 95 percent for organic iodide). These efficiencies are assumed to be effective for the entire sequence.

Summary of Recommended Reasonable Assumptions Concerning SGTS Operation During Severe Accident Sequences at Peach Bottom

With the exception of Station Blackout, the SGTS should operate continuously during at severe accident sequence at Peach Bottom. Although positive pressure pulses just after reactor vessel bottom head failure or drywell failure might cause rupture of the reactor building blowout panels, the SGTS blowers are of sufficient capacity to maintain the building pressure at a slight vacuum during most of the accident sequence. Fission product transport would be from the primary containment into the lower portion of the reactor building and from there directly into the SGTS or up into the volume above the refueling floor and from there into the SGTS.

It seems reasonable to expect that sufficient aerosols would be generated from the core-concrete reaction on the drywell floor to plug the HEPA filters in each of the twso SGTS filter trains. This should result in filter destruction by tearing when about 3 kg of aerosol has accumulated on each 1000 cfm filter face or 27 kg for each bank of nine in-parallel filters. The upstream filter bank would tear first, and because the charcoal bed is not effective in removing aerosols, the downstream HEPA filter bank would subsequently fail. Since the differential pressure between the atmosphere and the reactor building would not significantly change during the accident sequence, the flow through the filter train should remain at a constant value between 10,500 cfm and 25,000 cfm depending on the number of blowers operated. After the upstream and downstream HEPA filter banks have torn, the efficiency for particulate removal should be about zero, but a

significant efficiency for the removal of iodines by the charcoal bed would remain.

Grand Gulf

System Design and Description

The BWR 6 - Mark III containment design employed at the Grand Gulf nuclear station provides that the drywell and pressure suppression pool are located in a primary containment. The primary containment structure consists of a reinforced concrete cylinder and hemispherical dome, lined with welded steel plates to form a continuous intenral membrane.

The secondary containment at Grand Gulf consists of an auxiliary building and an enclosure building. The auxiliary building is a reinforced concrete structure which completely surrounds the lower cylindrical portion of the primary containment with a free volume of about 3×10^6 ft^3. The enclosure building is a metal-sliding structure with a free volume of about 6×10^5 ft^3 which completely surrounds the uppermost cylindrical portion and the hemispherical dome portion of the primary containment above the auxiliary building roofline. The secondary containment is at atmospheric pressure during normal reactor operation.

The SGTS does not operate during normal plant operation but is automatically started in response to an accident signal.* The SGTS is designed to limit the release to the environment of fission products that might leak from the primary containment, the fuel handling area, ECCS systems, main steam isolation valve leakage control systems, and other sources to the secondary containment region under accident conditions. The system recirculates the atmosphere within the secondarycontainment while continually exhausting a relatively small portion of the recirculation flow to the outside atmosphere through a charcoal and HEPA filter train.

*Signaled for an affected unit by high radiation in the exhaust ducts, low reactor vessel water level, or high drywell pressure.

Each Grand Gulf unit has its own SGTS. Each SGTS comprises two completely redundant (including ductwork) systems. The components of each system include: a 17,000 cfm enclosure building recirculation fan, a charcoal filter train with a 4000 cfm centrifugal blower, and the associated sets of ductwork, dampers, and controls.* The enclosure building recirculation fans are located at elevation 208' and the charcoal filter trains are located at elevation 138' in the auxiliary building. Each system is designed to maintain a 1/4-inch wg negative pressure in the secondary containment under accident conditions, with a minimum mixing ratio of enclosure building air to auxiuliary building air of 8:1 for the design long-term exhaust flow of 2300 cfm. The recirculation fan draws air from the auxiliary building and the enclosure building, mixes this air by the turbulent flow conditions in the ductwork, and returns most of the mixed air to the enclosure building. A portion of the recirculation fan discharge is drawn into the charcoal and HEPA filter train and exhausted via the centrifugal blower to the atmosphere. A schematic drawing of one of the two redundant systems is provided in Figure A-5.

The elements of the charcoal and HEPA filter trains are similar to those previously discussed for the Peach Bottom SGTS trains. The first two elements are a demister to remove entrained water followed by an electric heater, sized to reduce the humidity of 4000 cfm of air from 100 percent to 70 percent. The third element is a prefilter whose function is to remove large particulate matter from the flow. The fourth element is a set of parallel HEPA filters to remove fine particulate matter. The fifth element is the charcoal adsorber to remove gaseous elemental iodine and organic iodides, and the sixth element is a second HEPA filter bank to collect any charcoal fines carried over from the charcoal adsorber bed. The design features of these components are provided in Tables A-4, A-5, and A-6.

*It should be noted that the Grand Gulf SGTS incorporates a recirculation system and thereby differs significantly from the Peach Bottom SGTS.

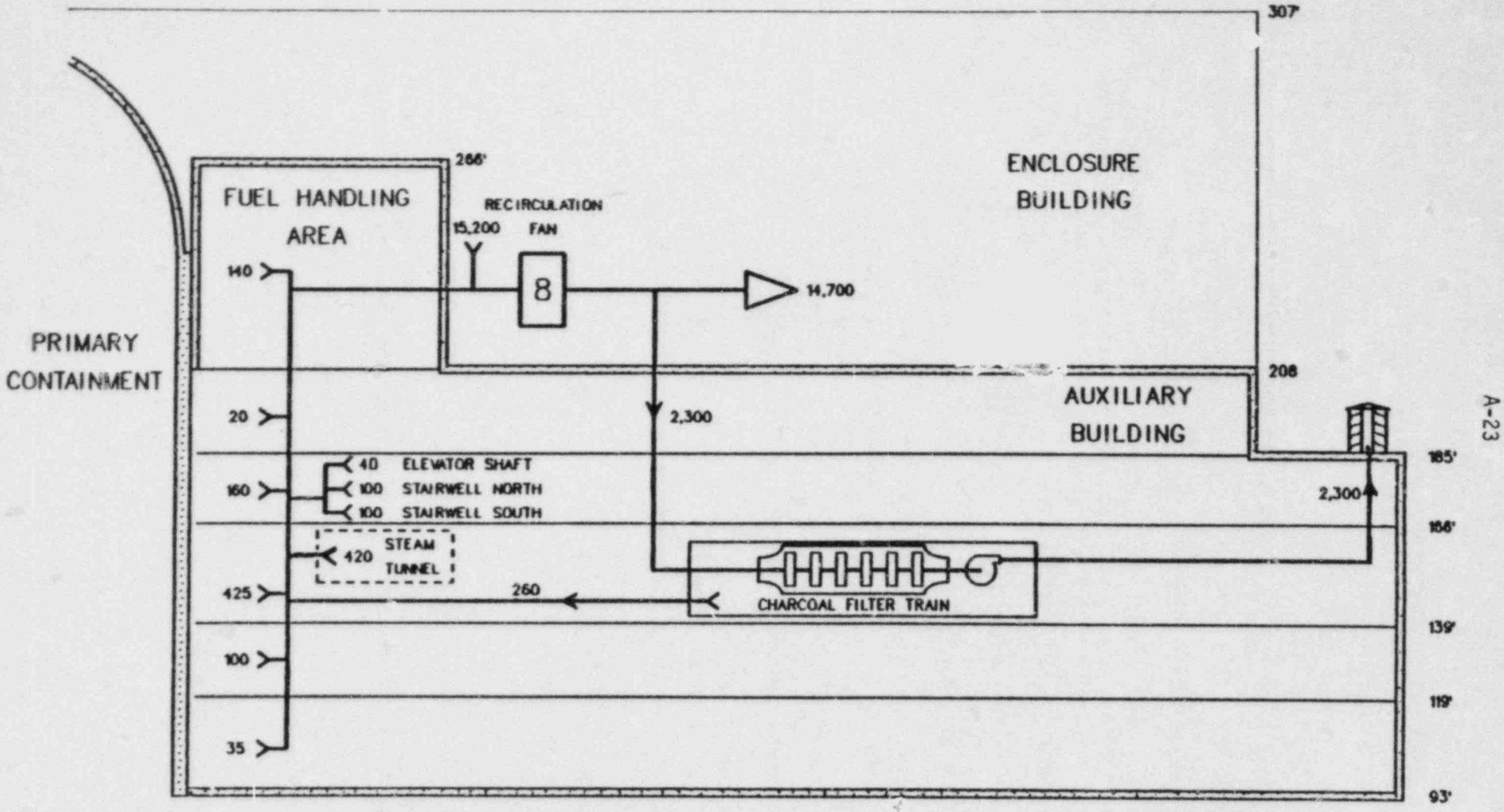

FIGURE A-5. SCHEMATIC DRAWING OF ONE OF THE STANDBY GAS TREATMENT SYSTEMS AT GRAND GULF. THE OTHER SYSTEM IS SIMILAR. THE INDICATED FLOWS ARE FOR POST-DRAWDOWN SINGLE-SYSTEM OPERATION. BUILDING ELEVATIONS ARE GIVEN IN FEET.

TABLE A-4. ELEMENTS IN THE GRAND GULF SGTS CHARCOAL FILTER TRAIN

Component	Units Installed	Unit Capacity	Units Required for Operation
Filter units	2		1
Fans, per filter unit:	1		1
capacity ft^3/min, drawdown/long term		4300/2300	
total pressure, in. wg.		13.0	
motor, hp		20	
Prefilters, per filter unit:	4		4
capacity, ft^3/min		1,000	
HEPA filters, per unit:	8		8
capacity, ft^3/min		1,000	
Demisters, per filter unit:	4		4
capacity, ft^3/min		1,000	
Electric heaters, per unit:	1		1
capacity, kW		18	
Charcoal (8") per filter unit, lb	2746		2746

TABLE A-5. GRAND GULF SGTS CHARCOAL FILTER TRAIN COMPONENT DESCRIPTION

Demister (each train)	
Type	Woven mesh pads
Capacity, cfm	4000 per bank
Pressure drop, clean, in. wg.	0.5
Electric Heater (each train)	
Type	Electric, finned tube
Quantity	1
Capacity, kW	18
Prefilters (each train)	
Type	Dry
Quantity	1 bank
Capacity, cfm	4000 per bank
Efficiency, %	90 ASHRAE 52
Pressure drop, clean, in. wg.	0.5
HEPA Filters (each train)	
Type	High efficiency
Quantity	2 banks
Capacity, cfm	4000 per bank
Efficiency, %	99.97, DOP
Pressure drop, clean, in. wg.	1.0
Charcoal Adsorber (each train)	
Type	Deep bed
Capacity, cfm	4000
Media	Impregnated coconut shell
Efficiency credit, %	99, elemental iodine and organic iodide
Depth of bed, in.	8 nominal
Charcoal volume, ft^3	70.0 minimum
Face velocity, fpm	40
Residence time, sec	1.0

TABLE A-5. (Continued)

Charcoal Adsorber (each train) (Cont'd)	
Pressure drop, clean, in. wg.	4.5
Iodine desorption temp range, F	250-300
Charcoal ignition temp, F	640 approx
Charcoal density, gm/cc	0.3 to 0.55
Impregnant content, % by weight	5 maximum
Charcoal size distribution	8 x 16 Tyler mesh nominal
Charcoal surface area, m^2/gm	1000 minimum
Charcoal moisture content efficiency, %	3 maximum
Charcoal ash content, %	6 maximum
Exhaust Fan (each train)	
Type	Centrifugal SWSI
Quantity	1
Capacity, cfm, drawdown/long term	4300/2300

TABLE A-6. MATERIALS USED IN GRAND GULF SGTS CHARCOAL FILTER TRAIN COMPONENTS

Demister	
Media	Fiberglass
Casing	304 stainless steel
Heater	
Sheath	Steel
Prefilter	
Media	Fiberglass
Casing	Chromized steel
Separators	Aluminum
HEPA Filters	
Media	Fiberglass
Casing	Chromized steel
Face guard	Galvanized steel
Mounting frame	304 stainless steel
Charcoal Filters	
Media	Impregnated, activated coconut shell charcoal
Casing	304 SS
Frame	304 SS
Unit Housing	
Shell	Carbon steel, A36 Mobil Val-Chem Hi-build epoxy, 89 Series, 5-7.0 mils DFT, over Mobilizinc 7, 1-3 mils DFT
Exterior coating	Mobil Val-Chem Hi-build epoxy, Series 89, 5-7 mils DFT, over Mobil 13-R-56, 1-3 mils DFT, underside coated with Koppers Bitumastic Black Solution or Gaco Neoprene Asphalt NA-62, by Gates Engineering Co.
Door gaskets	Neoprene

The Grand Gulf SGTS uses approximately four times as much charcoal per volumetric flow rate as do the Peach Bottom and Browns Ferry systems. This improves the charcoal filter efficiency to a marked degree. For a given form of iodine such as CH_3I, the absorption efficiency might increase from 95 percent to greater than 99.99 percent. Such an increase is no usually observed in practice because of gasket leaks and the presence on formation of other more penetrating forms of iodine.

SGTS Operation

Following an accident signal (high drywell pressure, low reactor vessel water level, or high radiation in the secondary containment exhaust ducting), both enclosure building recirculation fans and both charcoal filter train centrifugal blowers automatically start and all normal ventilation penetrations through the secondary containment are automatically closed.

SGTS flows are controlled by modulating inlet vanes on the charcoal and HEPA filter train centrifugal blowers and by two-position flow control dampers installed in the recirculation fan suction ducts from the various regions of the secondary containment. Upon system statup, the inlet vanes and control dampers are fully open and the centrifugal blowers operate at full capacity (4300 cfm) until the secondary containment has been drawn down to the design negative pressure of 1/4-inch wg. This requires 101 seconds if only one train is in operation and somewhat less time in the more likely event that both trains are operable.

After the secondary containment has been drawn down, two-position motor-operated dampers located in the SGTS ductwork automatically throttle the exhaust flow so that the volume of air being exhausted is equal to the volume of air infiltrated at the 1/4-inch wg negative pressure. Subsequent flow through the charcoal and HEPA filter train is controlled by the centrifugal blower motor-operated inlet vanes, which respond automatically to a pressure controller as necessary

to maintain a 1/4-inch wg negative pressure in the secondary containment for the long-term operation. The required long-term flow is expected to be 2300 cfm; however, if necessary, the modulating inlet vanes will automatically open to establish a system flow up to 4000 cfm (per train) as needed to maintain a negative pressure of 1/4-inch wg.

When the desired negative pressure has been achieved in the secondary containment, the operator is alerted that one recirculation fan and one charcoal filter train centrifugal blower can be shut down and placed in a standby mode. The system in a standby mode will automatically restart in response to a low flow signal from the operating enclosure building recirculation fan or from the charcoal and HEPA filter train centrifugal blower, or in response to an insufficient negative pressure in the secondary containment.

The air flow to the suction of the enclosure building recirculation fans is taken from corridors and general areas within the auxiliary building rather than from specific rooms. These areas communicate through stairwells, an elevator shaft, and several equipment hatches. For long-term operation with one SGTS in operation, a flow of 1640 cfm is taken from the auxiliary building and mixed with 160 cfm from the fuel handling area and 15,200 cfm from the enclosure building in the suction ducts to the enclosure building recirculation fans.* Of the 17,000 cfm passing through the recirculation fans, 2300 cfm is drawn into the suction ducting for the charcoal and HEPA filter train and 14,700 cfm is released back into the enclosure building atmosphere.

*With the negative pressure maintained by the SGTS, the enclosure building, by design, has a much higher in-leakage rate from the atmosphere than does the auxiliary building.

Recommended Reasonable Assumptions Concerning Severe Accident Sequences at Grand Gulf

Each system of the SGTS is completely redundant and provided with a 100 percent capacity filter train, centrifugal exhaust blower, recirculation fan, ductwork, and associated instrumentation and controls. Any accident signal automatically starts both of the SGTS systems. During long-term operation, one of the systems is manually placed in a standby mode. The standby system would automatically start in the event of a major component failure, degradation of performance of the operating system, or failure of electrical power to the operating system. Component malfunctions that result in startup of the standby system are summarized in Table A-7.

In certain severe accident sequences, sufficient core-concrete reaction aerosols might reach the secondry containment to plug the HEPA filters in the charcoal filter trains. However, this is less likely in the Grand Gulf Mark III containment design than for the Peach Bottom Mark I design because the Mark III design provides that flow from the drywell must pass through the pressure suppression pool on its way to the secondary containment. From the information in Table A-4, there are four 1000 ft^3/min capacity HEPA filters in parallel in the HEPA filter bank upstream of the charcoal bed and a similar arrangement for the downstream HEPA filter bank. As noted in Table A-7, the operator would be alerted to a high differential pressure across the upstream HEPA filter bank and would probably switch the standby SGTS system.

In the Peach Bottom SGTS filter train, it was assumed that the HEPA filters would tear at a differential pressure of 12 inches of water. Available experimental data indicate that this would occur when 3 kg of aerosol had entered the filter train for each HEPA filter arranged in parallel across the flow. Since there are nine 1000 cfm HEPA filters in parallel for a 9000 cfm flow, a total accumulation of 27 kg was estimated necessary to cause filter tearing at Peach Bottom.

TABLE A-7. GRAND GULF SGTS FAILURE MODES AND EFFECTS ANALYSIS

Component	Malfunction	Comment
Enclosure building recirculation fan	Fan failure resulting in loss of air flow	Low flow switch will automatically shift to redundant train and fan.
Filter train exhaust fan	Fan failure resulting in loss of air flow	Low flow switch will automatically shift to redundant train and fan.
Electric heater	Heater failure resulting in inability to reduce air stream to 70 percent RH	High humidity will give alarm in control room, operator may switch to redundant train.
	Heater failure resulting in overheating	Heater is equipped with thermal overload cutout switches.
Filter train	Failure resulting in high differential pressure across HEPA or charcoal sections	High differential pressure is alarmed in control room. Operator may switch to redundant train.
	Failure resulting in high temperature in charcoal bed	High temperature is alarmed in control room. High-high temperature is alarmed in control room and initiates deluge system. Initiation of deluge system is alarmed in control room, and operator may switch to redundant train.
Ductwork fan inlet vanes	Duct failure:	Redundant ductwork is provided.
	Fail closed	Low air flow automatically starts redundant train.
	Fail open	High air flow causes excessive negative pressure in building which actuates an alarm. Upon alarm actuation, the control room operator can determine which system has failed (A or B) and remove it from service, allowing the other train to continue to operate.

TABLE A-7. (Continued)

Component	Malfunction	Comment
Pressure sensor/ transmitter/ controller instruments	Instrument failure	Redundant instruments provided.
Positioning dampers	Fail closed	Redundant train achieves negative pressure. If second train is in standby mode when failure occurs, loss of air flow or low negative pressure starts redundant train.
	Fail open	Loss of low negative pressure signal opens filter train fan inlet vanes.

At Grand Gulf, each filter train is designed for 4000 cfm and there are four 1000 cfm HEPA filters arranged in parallel. Therefore, for 4000 cfm flow the required accumulation to cause tearing would be 4/9 x 27 or 12 kg of aerosols. However, as described previously, the train is operated at 2300 cfm and therefore a larger aerosol deposition would be required in order to develop 12 inches of water pressure drop at the lower flow. Thus, a reasonable estimate might be 16 kg of accumulated aerosol within a filter train to cause rupture of the upstream HEPA filter bank and an additional equal amount for rupture of the downstream filter bank.

For Grand Gulf, the presence of aerosols in the secondary containment during the course of a severe accident sequence should affect the operation of the SGTS as follows. Aerosols would deposit on the upstream HEPA filter bank of the operating SGTS system. When about 9 kg have deposited, a high differential pressure alarm would sound in the control room and the operator would shift to the standby system. When about 16 kg has accumulated on the upstream HEPA filter bank of this system, the upstream filter bank would tear and when an additional 16 kg of aerosols has entered the system and deposited on the downstream HEPA filter ban, it also would tear. After this, the efficacy for particulate removal by the system would be about zero but a significant efficiency for the removal of iodines by the charcoal bed would remain.

As in the case of Peach Bottom and Browns Ferry, other SGTS failure modes are conceivable and the choice of an alternate scenario could very well have a major impact on the calculated fission product transport. At Grand Gulf, the SGTS charcoal and HEPA filter trains and the recirculation fans are located within the auxiliary building and therefore are subject to the hazards of an accident environment within the building.

If the HEPA filters plugged did not tear, flow through the operable SGTS charcoal and HEPA filter train to the atmosphere would cease, the building pressure would rise above atmospheric and fission products would be released to the surrounding atmosphere only by way

of exfiltration through the walls of the auxiliary building within the building.

The efficacy of the SGTS at Grand Gulf must be considered to be accident-sequence dependent. The system should not be simply ignored, yet there are accident sequences in which its beneficial effect would be diminished. The SGTS should be recognized as a very important fission product release mitigation system whose function or loss should be evaluated in every accident sequence, i.e., on a case-by-case basis.

References

(A-1) Military Specification MIL-F-51068, Filter, Particulate, High Efficiency, Fire Resistant.

(A-2) First, M. W. and Price, J. M., "Performance of 1000- and 1800-cfm HEPA Filters on Long Exposure to Low Atmospheric Duct Loadings, III", Proceedings of the 17th DOE Nuclear Air Cleaning Conference (in preparation).

(A-3) Gunn, C. A. and McDonough, J. B., "Survey of Loading Performance of Currently Available Types of HEPA Filters Under In-Service Conditions", Proceedings of the 16th DOE Nuclear Air Cleaning Conference, CONF-801038, Vol 1, 667-668 (February, 1981).

(A-4) Lorenz, R. A., Martin, W. J., and Nagao, H., "The Behavior of Highly Radioactive Iodine on Charcoal", in Proceedings of the 13th AEC Air Cleaning Conference, CONF-740807, 707-735 (March, 1975).

(A-5) Lorenz, R. A., Manning, S. R., and Martin, W. J., "The Behavior of Highly Radioactive Iodine on Charcoal in Moist Air", in Proceedings of the 14th ERDA Air Cleaning Conference, CONF-760822, 323-352 (February, 1977).

(A-6) Shiomi, H., et al, "A Parametric Study on Removal Efficiency of Impregnated Activated Charcoal and Silver Zeolite for Radioactive Methyl Iodide", presented at the 17th DOE Nuclear Air Cleaning Conference, August 2-5, Denver, Colorado.

(A-7) Shields, R. P., "Ignition of Charcoal Adsorbers by Fission Product Decay Heat", Proceedings of the 11th AEC Air Cleaning Conference, Hanford, Washington, August 31-September 3, 1970, CONF-700816.

(A-8) Shields, R. P. and Siman-Tov, M., "The Effect of Iodine Decay Heat on Charcoal Adsorbers", US AEC Report ORNL-4602 (April, 1971).

(A-9) Evans, A. G. and Jones, L. R., "Confinement of Airborne Radioactivity", progress report, January-June, 1971, DP-1280 (October, 1971).

(A-10) Evans, A. G., "Effect of Intense Gamma Radiation on Radioiodine Retention by Activated Carbon", in Proceedings of the 12th AEC Air Cleaning Conference, CONF-720823, Vol 1, 401-416 (January, 1973).

(A-11) Personal communication from A. G. Evans, March, 1973.

(A-12) Deitz, Victor R., "Charcoal Performance Under Simulated Accident Conditions", NRL Memorandum Report 4760 (NUREG/CR-2660) (June, 1982).

*U.S. GOVERNMENT PRINTING OFFICE : 1984 0-421-297/4046

UNITED STATES
NUCLEAR REGULATORY COMMISSION
WASHINGTON, D.C. 20555